Synthesis and Application of Novel Adsorbents for Wastewater Treatment

A Thesis
Submitted in Partial
Fulfillment of the Requirements for the Degree of

DOCTOR OF PHILOSOPHY

by

J. Anandkumar

Centre for the Environment
Indian Institute of Technology Guwahati
Guwahati – 781039, Assam, India

August 2012

Dedicated

To

My family and my mentors

Centre for the Environment
Indian Institute of Technology Guwahati
India-781039

CERTIFICATE

It is certified that the work contained in this thesis entitled **"Synthesis and Application of Novel Adsorbents for Wastewater Treatment"** submitted by **Mr. J. Anandkumar** for the award of the degree of Doctor of Philosophy has been carried out in Centre for the Environment, Indian Institute of Technology Guwahati under my supervision and this work has not been submitted elsewhere for the award of any other degree or diploma.

This thesis in my opinion, has reached the standard fulfilling the requirements for the award of the degree of Doctor of Philosophy in accordance with the regulations of the institute.

(Dr. Bishnupada Mandal)
Associate Professor
Department of Chemical Engineering
IIT Guwahati, India-781039

Vitae

J. Anandkumar

Permanent Address

S/o S. Jayapal
No: 26 Thullukanam Street
Pernambut
Vellore District
Tamil Nadu-635810

Email

jpanandkumar.env@gmail.com
jpanandkumar@yahoo.com

Date of birth 05/02/1981

Education

- ***Ph.D Student (Research Scholar)***
  Centre for the Environment
  Indian Institute of Technology Guwahati
  Guwahati, Assam, India.
  (2007-2012)
- ***M.E (Environmental Engineering)***
  (First Class)
  Anna University, Chennai, India
  (2004-2006)
- ***B.Tech (Chemical Engineering)***
  (First Class)
  University of Madras, Chennai, India
  (1999-2003)

Achievements

- *School First in SSLC (10th Std)*
- *NCC 'A' Certificate*
- *Qualified in GATE 2003*

PUBLICATIONS

Published/Accepted Articles in International Refereed Journals

1. **Anandkumar, J** and Mandal, B. Removal of Cr(VI) from aqueous solution using Bael fruit (*Aegle marmelos correa*) shell as an adsorbent. ***Journal of Hazardous Materials,*** 168 (2009), 633-640 **(Elsevier)**.
2. **Anandkumar, J** and Mandal, B. Adsorption of chromium(VI) and rhodamine B by surface modified tannery waste: Kinetic, Mechanistic and Thermodynamic Studies. ***Journal of Hazardous Materials*****,** 186 (2011), 1088-1096 **(Elsevier)**.
3. **Anandkumar, J** and Mandal, B. Single, binary and ternary metal adsorption using acid treated *Aegle marmelos correa* shell: Kinetic, mechanistic and thermodynamic Study. ***Asia-Pacific Journal of Chemical Engineering*****,** 7 (2012) 928-939 **(Wiley)**.

Communicated/Under Review in Refereed International Journals

4. **Anandkumar, J** and Mandal, B. Single and multi-contaminant adsorption of Cr^{6+}, phenol and rhodamine B using activated carbon: Kinetic, mechanistic and thermodynamic approach. ***Journal of Environmental Engineering*** **(under review).**
5. **Anandkumar, J** and Mandal, B. Systematic preparation of high surface area activated carbon from *Aegle marmelos correa* shell. ***Journal of Porous Materials*** **(under review).**
6. **Anandkumar, J** and Mandal, B. Single and multi contaminant adsorption of strontium, *o*-cresol and methylene blue from aqueous solution using activated carbon. ***Journal of Environmental Management*** **(under review).**
7. **Anandkumar, J** and Mandal, B. Adsorption of Cr^{6+}, *o*-cresol and rhodamine B using activated tannery sludge: Kinetic and Mechanistic study. ***Clean Technologies and Environmental Policy*** **(under review).**

Conference Presentations (National and International)

1. **Anandkumar, J** and Mandal, B. (2012). Multi contaminant adsorption behaviour of activated carbon: Kinetic and mechanistic approach. ***"International Conference on Environmentally Sustainable Urban Ecosystems"*** **(ENSURE-2012)**, February 24-26, IIT Guwahati, Guwahati, INDIA.
2. **Anandkumar, J** and Mandal, B. (2011). Effect of different chemical treatments on the adsorption of strontium from synthetic wastewater. ***"International Conference on Sustainable Water Resource Management and Treatment Technologies"*** **(Water 2011 - NEERI)**, January 19-21, Nagpur, INDIA.
3. **Anandkumar, J** and Mandal, B. (2009). *Utilization of Aegle Marmelos Correa* Fruit Shell as a Novel Sorbent for Methylene Blue Adsorption. ***"Spring National Meeting of "The American Institute of Chemical Engineers"*** **(AIChE-2009)**, April 26-30, Tampa (FL), USA, North America.
4. **Anandkumar, J** and Mandal, B. (2008). Study on the Preparation of Cashew Husk Adsorbents and Biosorption of Cr^{6+} from Aqueous Solution. ***"International Congress on Environmental research"*** **(ICER-2008)**, December 18-20, Goa, INDIA.
5. **Anandkumar, J** and Mandal, B. (2010). Removal mechanism of Cr(VI) and Rhodamine B from aqueous solution using HCl treated adsorbent. ***"The Indian Chemical Engineering Congress"*** **(CHEMCON-2010)**, Dec 27-29, Annamalainagar, INDIA.
6. **Anandkumar, J** and Mandal, B. (2009). Equilibrium and kinetic modeling of Malachite green and Cu (II) adsorption by surface enhanced Aegle marmelos correa shell. ***"The Indian Chemical Engineering Congress"*** **(CHEMCON-2009)**, Dec 27-30, Visakhapatnam, INDIA.
7. **Anandkumar, J** and Mandal, B. (2008). Adsorption of chromium (VI) from aqueous solution using Bael fruit (Aegle marmelos correa) shell as an adsorbent. ***"The Indian Chemical Engineering Congress"*** **(CHEMCON-2008)**, Dec 26-30, Chandigarh, INDIA.

ACKNOWLEDGEMENTS

I express my sincere thanks to my research supervisor **Dr. Bishnupada Mandal** for his valuable guidance towards the completion of my research work. His continuous support towards research and given me enough freedom to think, plan and execute my ideas towards my work, which has provided a good basis for the present thesis. I would like to thank him for spending his precious time for discussion by which i have gained immense skills of knowledge in terms of research. I am also indebted to Dr. Bishnupada Mandal for instilling in me a craving for perfection. I believe, it will always remain with me in my future life. It has really been a notable working experience with him.

Besides my supervisor, I would like to thank my doctoral committee members, **Prof. A.K. Ghoshal, Dr. P. Saha,** Department of Chemical Engineering and **Dr. P.K. Ghosh,** Department of Civil Engineering, for their valuable suggestion and effort which made my thesis successful. I am also grate full to my present and former **HOC's** and **Staffs** of Centre for the Environment for providing me necessary facilities.

My special thanks to **Dr. G. Pugazhenthi** of Chemical Engineering Department for his continuous encouragement and helping nature in several ways of my Ph.D life. I should thank **Dr. P. Saravanan** of University of Malaya for his continuous encouragement and help in XPS analysis.

I am very much grateful and infact lucky to get **Mr. Lukumoni Borah** and **Mr. Kaustavmoni Deka (JTS)** of Chemical Engineering Department for their timely help both technical and personal, without any hesitation have been invaluable. I would like to thank my seniors **Dr. Sivasankar** (NIT-Trichy), **Dr. Suresh Pandian** (ISM Dhanbad) and **Dr. Badabrata Saha** for their friendly support and timely assistance whenever needed.

I acknowledge with thanks to the **Central Instruments Facility**, Department of **Chemistry, Chemical** and **Civil Engineering** of IIT Guwahati for providing me the necessary instrument facility which has been very important in this research work.

I was fortunate enough to get excellent and close friends like **Santhi Raju**, **Design Ravi Anna**, **Someswaran, Shravan, Kannan** and **Sengodan** for their friendly support and helping nature during my stay in IITG.

I would like to thank all my **seniors**, **juniors**, **friends** and other **well-wishers** whoever making my stay in IITG memorable.

Finally, I express my gratitude to my beloved **parents, brothers, uncles (Chithappas)** and my wife **Biju** for showering their love, care, sacrifice and encouragement which have made it possible for me to come so for.

J. Anandkumar

August, 2012

.

TABLE CONTENTS

LIST OF FIGURES

LIST OF TABLES

ABSTRACT

Adsorptive removal of certain tannery wastewater pollutants and other industrially important heavy metals, using newly synthesized adsorbents from waste Bael shell (BS) and Tannery residual biomass (TB), is the main theme of this thesis. Adsorptive removal has been advocated to be a better option to eliminate organic and inorganic pollutants both single and multiple forms with high efficiency as compared to other popular methods for wastewater treatment. Cr^{6+}, phenol, *o*-cresol, rhodamine B and methylene blue have been identified as critical inorganic and organic contaminants that are found in various industrial effluents especially in tannery effluent. In addition to this, Pb^{2+}, Ni^{2+} and Sr^{2+} are few other important heavy metals present in the effluents which are used for fabrication many of commercial products in industries. Although, past researchers have mostly studied the adsorption of organic or inorganic pollutants only in single form using commercially available and other biosorbents, but these pollutants are usually exist together in industrial wastewater. It has been studied and reported in this thesis that the above mentioned/targeted organic and inorganic pollutants are successfully removed with high adsorption capacity both in single and mixed form using synthesized novel adsorbents. Hence, to prepare this novel multiple usage adsorbents from the locally available industrial waste materials (BS and TB), three activation methods such as thermal, chemical and thermochemical activation were employed in this thesis. The utilization of these industrial waste materials as useful adsorbents may helpful to reduce the cost of solid waste disposal and recycle for their own and other industrial wastewater treatment.

Initially, synthesized adsorbents of BS and TB at various conditions were employed for BET surface area optimization followed by preliminary performance evaluation test (PPET) with the targeted pollutants to identify the potential adsorbent for the particular pollutant removal. BET results of synthesized adsorbents revealed that thermochemically activated BS and TB using H_3PO_4 had high surface area of 1954 and 892 m^2/g. However, PPET results showed that thermochemically activated BS and TB using H_3PO_4 (BSAC and TBAC), chemically activated BS and TB using H_2SO_4 (SBS and STB) and TB using HCl (HTB) had high adsorption capacity with targeted pollutants. Therefore, BSAC, TBAC, SBS and HTB were chosen as best adsorbents for elaborate adsorption studies with the selected contaminants from the PPET.

Batch mode adsorption experiments of Cr^{6+}, Sr^{2+}, phenol, *o*-cresol, rhodamine B (RB) and methylene blue (MB) dye from aqueous solution using Bael shell activated carbon (BSAC) was carried out in single and multi-contaminant system with various operating conditions. The solution pH and temperature experiment showed that they have considerable impact on the adsorption capacity of the BSAC. The maximum adsorption capacities of Cr^{6+}, Sr^{2+}, phenol, *o*-cresol, RB and MB dye were observed at pH 2.0, 6.7, blank (6.2), blank (6.3), 3.5 and 7.0, respectively. The presence of (NH_4^+, Ca^{2+}, F^-, and I^-) ions significantly reduces the Cr^{6+} and Sr^{2+} uptake but marginal enhancement in the phenol and *o*-cresol removal was observed when NH_4^+ and NO_2^- ions were present in the solution at high concentrations. The equilibrium data fitted satisfactorily with the Langmuir model and monolayer sorption capacity obtained as 222.2, 113.4, 304, 243.3, 434.8 and 476.2 mg/g for Cr^{2+}, Sr^{2+}, phenol, *o*-cresol, RB and MB dye at 30ºC, respectively. The phenol and *o*-cresol adsorption was enhanced by RB and MB dye, respectively when they were present in the binary and ternary contaminant system. The sorption kinetics was found to follow the pseudo-second-order kinetic model for Cr^{6+}, phenol and RB dye contaminants. The increase in adsorption capacity for Cr^{6+}, RB and MB dye with increase in temperature indicates that the uptake was endothermic in nature. But, the negative ΔH^o value of phenol, *o*-cresol and Sr^{2+} indicate the exothermic nature of adsorption. The adsorption-coupled reduction, monomeric adsorption and π-π interaction mechanisms were responsible for the adsorption of Cr^{6+}, RB dye and phenol, respectively. The BSAC is characterised using scanning electron microscope (SEM), Fourier transform infrared spectroscopy (FT-IR), energy dispersive X-ray spectroscopy (EDX), before and after adsorption.

In batch adsorption study using SBS, the maximum adsorption capacities of Pb^{2+}, Ni^{2+}, Sr^{2+}, RB and MB dye were observed at pH 5.2, 5.8, 6.8, 3,5 and 7.2, respectively. Presence of other ions (Na^+, K^+, Ca^{2+} and NH_4^+) significantly reduces the metal uptake when they were present at high concentrations in the metal solution and no impact on dye adsorption. The equilibrium data fitted satisfactorily with the Langmuir model and monolayer sorption capacity was obtained as 122.7, 70.18, 80.73, 221.2 and 330 mg/g for Pb^{2+}, Ni^{2+}, Sr^{2+}, RB and MB dye at 30ºC, respectively. The binary and ternary metal effect on SBS was found to be antagonistic behaviour. The sorption kinetics was found to follow the pseudo-second-order kinetic model. The decrease in adsorption capacity of both Pb^{2+} and Sr^{2+} with increase in temperature indicates that the uptake was exothermic in nature. But, the positive value of $\Delta H°$ and the increase in uptake with increase in solution temperature indicates the endothermic reaction for Ni^{2+}, RB and MB dye adsorption. Inter molecular binding

(ion-dipole) of $Pb^{2+}$and Sr^{2+} and inter-molecular binding coupled intra-molecular binding of Ni^{2+} was responsible for metal binding with cellulosic and lignin function groups.

The batch removal of Cr^{6+}, RB and MB dye using HTB was carried under different experimental conditions. Presence of other ions (Na^{+}, Ca^{2+} and NH_4^{+}) significantly reduces the Cr^{6+} uptake and no impact on RB and MB dye removal was observed. The equilibrium data fitted satisfactorily with the Langmuir model and monolayer sorption capacity obtained as 177-217, 213-250 and 480.8-518.1 mg/g for Cr^{6+}, RB and MB at 30-50ºC, respectively. The sorption kinetics was found to follow the pseudo-second-order kinetic model. The increase of adsorption capacity for both metal and dye with increase in temperature indicates that the uptake was endothermic in nature.

Adsorption of Cr^{6+}, *o*-cresol and RB dye was conducted in the batch mode study using TBAC. Maximum removal of Cr^{6+}, *o*-cresol and RB occurred at pH 3.5, 6.0 and 3.5, respectively. NH_4^{+} ions considerably enhanced the *o*-cresol adsorption on TBAC when it was simultaneously present with *o*-cresol at higher concentration. The sorption data fitted satisfactorily with Langmuir isotherm model. Evaluation using Langmuir equation gave the monolayer sorption capacity as 1698.9, 200 and 373.1 mg/g. Cr^{6+} (adsorption-coupled reduction), *o*-cresol (H-bond formation) and RB dye (monomeric pore penetration) uptake by TBAC was best described by pseudo-second-order kinetic model. The negative ΔG^{o} confirmed the spontaneous nature and positive ΔH^{o} value showed the endothermic nature of both Cr^{6+} and RB dye sorption onto TBAC.

Continuous flow packed-Bed study was performed for RB dye using BSAC by changing the flow rate, RB dye concentration and bed height. The maximum removal of RB dye in a packed-bed adsorption column was found to be 179.8 mg/g at pH 3.5, at an initial adsorbate concentration of 200 mg/l, flow rate of 5 ml/min and bed height of 10 cm. From the regression coefficient analysis, it was found that the experimental data well fitted to the Yoon-Nelson model compared to BDST and Thomas model.

The results obtained in this research work provide a new insight for developing efficient high potential multiple usage adsorbents from industrial solid wastes to remove the above studied organic and inorganic contaminants both single as well as multiple forms from the aqueous solution including industrial wastewater.

CHAPTER 1

INTRODUCTION TO WASTEWATER TREATMENT AND LITERATURE REVIEW

This chapter presents an introductory discussion on water pollution. It discusses about three major sources of pollutants such as heavy metals, phenolic derivatives and dye as well as their impacts on aquatic and human life. It also describes the features of different currently available wastewater treatment techniques and the necessity of the alternative technique based on the elaborate review of the literatures. End of this chapter, the importance and objectives of this work has been made and painted according to the current demand in the field of wastewater treatment technologies. Organization of this thesis is highlighted in simple form in this chapter as well.

1.1 INTRODUCTION

All living organisms depend on air, water and food for their growth and survival. Today, the living conditions of human being have been certainly improved due to scientific and technological development towards the elevation of standard living. Hence, the generation of gaseous, liquid and solid wastes are unavoidable due to the various human activities such as rapid growth of population, industrial proliferations, urbanizations, agricultural and domestic activities. However, the environmental impact of these activities must be minimized to ensure the secured life of human beings and ecosystem. A sustainable balance among environmental, economic, and social systems is the key to sustaining the quality of life for all of earth's inhabitants.

Among the various environmental resources water is one of the most important commodities which need special attention. That's why water has been aptly described as "Blue Gold" by our ancestors. Earth surface is covered by 70.9% of water, mainly in the form of salty water in the oceans. However, only 0.6-0.7% of land surface water is available for human utilization in the form of rivers, lakes and ponds (Wollmann, 1962). Today, these water resources are mostly exploited and polluted mainly by the industrial sectors. More than half of the world has no adequate access to clean drinking water. It is estimated that by year 2025 more than half of the population in the world will be facing water based vulnerability (Kulshreshtha, 1998). Water pollution has been very damaging to aquatic ecosystems, and may consist of agricultural, urban, and industrial wastes containing contaminants such as sewage, fertilizer, and heavy metals that have proven to be detrimental to aquatic habitats and species. Water toxicity due to industrial effluents is one of the major factors of environmental pollution. Generally industrial effluents are a heterogeneous mixture of several components, many of which are organic and inorganic compounds of varying composition and surface activity. Industrial effluents are having two main category of pollutants and its derivatives such as aromatic components (Colouring agents**:** Methylene blue, Malachite green, Acid yellow, Congo red etc. and Phenolic components: Phenol, Cresol, Chloro phenol etc.) and toxic heavy metals (Arsenic, Chromium, Copper, Lead, Nickel etc.).

Therefore, the real challenge before the scientific society is as follows:

- Consideration of water as an endangered source

- Water conservation and management begins at the local level with policies and practices to sustain natural water resources.
- Protection of all water bodies from pollution.
- Treatment of available water by cost effective methods.
- Development of new environmental friendly technologies.

Elaborate discussions of each category of pollutants are discussed below:

1.2 HEAVY METAL POLLUTION

The term "heavy metal" is defined based on many factors such as metal density, atomic number, atomic weight and chemical properties or toxicity. Based on density aspect, the metallic elements having density greater than or equal to 6.0 g cm^{-3} are referred as heavy metals (Barrera *et al.,* 2006). The most familiar heavy metals are Cadmium (8.65 g cm^{-3}), Chromium (7.19 g cm^{-3}), Cobalt (8.90 g cm^{-3}), Copper (8.95 g cm^{-3}), Lead (11.34 g cm^{-3}), Mercury (13.53 g cm^{-3}), Nickel (8.91 g cm^{-3}) and Zinc (7.14 g cm^{-3}). From environmental toxicity point of view, heavy metals can be generally defined as group of elements which are toxic even at trace concentration and that lies on periodic table between chromium and lead with atomic weights of 51.99 and 207.20, respectively and specific gravity greater than 4.0.

Environmental contamination and exposure to heavy metals such as mercury, cadmium and lead etc. is a serious growing problem throughout the world. Human exposure to heavy metals has risen dramatically in the last 50 years as a result of an exponential increase in the use of heavy metals in industrial processes and products. Many occupations involve daily heavy metal exposure. In the modern world, there is no way for human beings to get away entirely from the exposure of toxic chemicals and metals. Heavy metal or toxic metal pollution has posed a serious threat to the aquatic environment through the discharge of industrial wastewater. Moreover, heavy metals are non biodegradable and their presence at high concentrations in streams, lakes and other water bodies lead to bioaccumulation through food chain in living organisms, causing health problems in animals, plants and human beings (Argun and Dursun, 2008; Li *et al.,* 2009). However, they are virtually present in every area of modern consumerism from construction materials to cosmetics, medicines to processed foods; fuel sources to agents of destruction; appliances to personal care

products. It is very difficult for anyone to avoid exposure to any of the many harmful heavy metals that are so prevalent in our environment.

1.2.1 Sources of Heavy Metals

Heavy metals resources can be identified as natural and anthropogenic sources. Naturally heavy metals have been often released into soil, water and air through chemical and physical weathering of igneous, metamorphic rocks and soils. They are also generally associated with volcanic activities, wind erosion, forest smoke fire and fossil fuels. The level of metals of such natural origin is usually harmless to human and environment. Secondly, human's exploitation of world mineral resources and technological activities disperse the chemicals particularly metallic elements into the environment in unprecedented quantities and concentrations. The extreme rate of dispersion of metals is categorized under anthropogenic source such as industries. Anthropogenic source of heavy metals are much higher than that of natural source (Goel, 1997). For example, the concentration of arsenic in soil and in the earth's crust is in between 0.1-8,000 mg/kg and 1.5-5 mg/kg, respectively (Ergican *et al.,* 2005) whereas human activity contributes 80,000 tonnes of arsenic per year. Generally the primary anthropogenic sources of heavy metals are industrial sectors, which discharge a huge amount of wastewater contaminated with the highly toxic metal substances. The major industries that discharge wastewater containing heavy metals include mines, foundries, smelters, electroplating, tanneries, coal-burning power plants etc. as well as diffuse sources such as combustion by-products and vehicle emissions. The distribution of heavy metals in manufacturing industries is given in Table 1.1.

1.2.2 Toxicological Aspects of Heavy Metals

Heavy metals are found naturally in the earth's crust and can enter into the living organisms in very small amounts through the food, water and air. They are important as trace minerals for metabolic functions but, at greater amounts through biomagnification, they can lead to poisoning. Due to their mobility in aquatic ecosystems and they are toxic to higher life forms, heavy metals in surface and groundwater supplies have been considered as major inorganic contaminants in the environment even at very low concentrations.

1.2.2.1 Effects of Heavy Metals on Human Health

Some heavy metals are naturally found in the body and are essential to human health. The human body need many friendly trace heavy metal elements. For example, iron prevents anemia, and zinc is a cofactor in over 100 enzyme reactions. Magnesium and copper are other familiar metals that, in minute amounts, are necessary for proper metabolism to occur. Other metals are *xenobiotics*, i.e., they have no useful role in human physiology (and most other living organisms) and, even worse, as in the case of Arsenic, Cadmium, Lead, Mercury and Nickel etc. may be toxic to the enzyme systems and metabolism of the human body even at trace levels of exposure. These heavy metals are taken into the body at very low concentrations via inhalation, ingestion, and skin absorption. They tend to accumulate in the food chain and in the body and can be stored in soft (e.g., kidney) and hard tissues (e.g., bone). When heavy metals are accumulated in human body tissue faster than the body's detoxification pathway will build-up these toxins gradually in the human body. Being metals, they often exist in a positively-charged form and can bind on to negatively-charged organic molecules to form complexes. Overload of heavy metals in the adrenal glands reduce the production of hormones, which cause early aging, stress, decreased sex drive and aggravation of menopausal symptoms. Heavy metal overload can lead to unresponsiveness of diabetics to their medication and neurological diseases such as depression and loss of thinking power. It can also aggravate conditions such as osteoporosis and hypothyroidism. For obvious reasons, removing metals from the body safely has been a concern of physicians for many years. Even minute levels of toxic elements have negative health consequences, affecting nutritional status, metabolic rate and the integrity of detoxification pathways. The biological half-lives for heavy metals are generally long; the half-life for cadmium in the kidney is decades. Most heavy metals are readily transferred across the placenta, found in breast milk, and are well known to have serious detrimental effects on behaviour, intellect and the developing nervous system in children. For adults, silent symptoms of chronic, low level heavy metal accumulation in tissues can progress from a steady decline in energy, productivity and quality of life to accelerated cardiovascular disease, premature dementia and total debilitation. Details of toxic response on human due to some important heavy metals ions are presented in Table 1.2.

1.2.2.2 Effects of Heavy Metals on Aquatic Organisms

Aquatic organisms are adversely affected by heavy metals in the environment. The toxicity is largely a function of the water chemistry and sediment composition in the surface water system. The metals are mineralised by microorganisms, which are taken up by plankton and further by the aquatic organisms. Finally, the metals which are bio accumulated by aquatic organisms are several times biomagnified by fish and this fish is taken by human from metal contaminated water. Slightly elevated metal levels in natural waters may cause the following sub lethal effects in aquatic organisms:

- Histological or morphological change in tissues;
- Changes in physiology, such as suppression of growth and development, poor swimming performance, changes in circulation;
- Change in biochemistry, such as enzyme activity and blood chemistry;
- Change in behaviour; and
- Changes in reproduction (Connell *et al*., 1984).

Many organisms are able to regulate the metal concentrations in their tissues. Fish and crustacean can emit essential metals, such as copper, zinc, and iron that are present in excess. Some can also emit non-essential metals, such as mercury and cadmium, although this is usually met with less success (Connell *et al*., 1984). Research has shown that aquatic plants and bivalves are not able to successfully regulate metal uptake (Connell *et al*., 1984). Thus, bivalves tend to suffer from metal accumulation in polluted environments. In estuarine systems, bivalves often serve as biomonitor organisms in areas of suspected pollution (Kennish, 1992).

In comparison to freshwater fish and invertebrates, aquatic plants are equally or less sensitive to cadmium, copper, lead, mercury, nickel, and zinc. Thus, the water resource should be managed for the protection of fish and invertebrates to ensure aquatic plant survivability (USEPA, 1987). Metal uptake rates will vary according to the organism and the metal in question. Phytoplankton and zooplankton often assimilate available metals quickly because of their high surface area to volume ratio. The ability of fish and invertebrates to adsorb metals is largely dependent on the physical and chemical characteristics of the metal (Kennish, 1992). With the exception of mercury, little metal bioaccumulation has been observed in aquatic

organisms (Kennish, 1992). Metals may enter the systems of aquatic organisms via three main pathways:

i. Free metal ions that are absorbed through respiratory surface (e.g., gills) can readily diffused into the blood stream.
ii. Free metal ions that are adsorbed onto body surfaces can also passively diffused into the blood stream.
iii. Metals which are adsorbed onto food and particulates may be ingested from free metal ion bearing water bodies (Connell *et al.*, 1984). For example: Chromium is not known to accumulate in the bodies of fish but high concentrations of chromium due to the disposal of metal products in surface waters can damage the gills of fish that swim near the point of disposal.

1.2.3 Guidelines for Heavy Metals

The quality of drinking water may be controlled through a combination of protection of water sources, control of treatment processes and management of the distribution and handling of the water. The guidelines are intended to support the development and implementation of risk management strategies that will ensure the safety of drinking water supplies through the control of hazardous constituents of water (Kanamadi *et al.,* 2006). For effluents, these standards restrict the quantity of pollutants in the effluents that set the desired degree of treatment. The establishment of minimum standards of quality for wastewater discharge and for public water supply is of fundamental importance in achieving this objective. The Indian standards and the WHO guidelines for some of the heavy metals for drinking water and the effluents are given in Table 1.3.

1.2.4 Need for the Removal of Heavy Metals

Continuous discharge of industrial, domestic and agricultural wastes in rivers and lakes causes deposit of pollutants in sediments. Such pollutants include heavy metals, which endanger public health after being incorporated in food chain. Heavy metals cannot be destroyed through biological degradation, as is the case with most organic pollutants. Incidence of heavy metal accumulation in fish, oysters, mussels, sediments and other components of aquatic ecosystems have been reported from all over the world (Naimo, 1995; Sayler *et al.,* 1975).

Excessive amounts of some heavy metals can be toxic through direct action of the metal or through their inorganic salts or via organic compounds from which the metal can become easily detached or introduced into the cell. Exposure to different metals may occur in common circumstances, particularly in industrial setting. Accidents in some environments can result in acute, high level exposure. Some of the heavy metals are toxic to aquatic organisms even at low concentration. The problem of heavy metal pollution in water and aquatic organisms including fish, needs continuous monitoring and surveillance as these elements do not degrade and tend to biomagnify through food chain in human body. Hence there is a need to remove the heavy metals from the aquatic ecosystems.

Research and development, therefore focuses on sector-specific methods and technologies to remove heavy metals from different kinds of waste streams. In view of the above toxicological effects of heavy metals on environment, animals and human beings, it becomes imperative to treat these toxic compounds in wastewater effluents before they are discharged into freshwater bodies.

1.2.5 Treatment Techniques for Heavy Metal Removal

Over the last few decades, several methods have been devised for the treatment and removal of heavy metals. Numerous industries (see Table 1.1) discharge a variety of toxic metals into the environment. The various common methods exists for the removal of heavy metal ions from aqueous system include chemical precipitation, lime coagulation-flocculation, ion exchange, membrane filtration, biological and electrochemical treatment (Kurniawan *et al.,* 2006; Anandkumar and Mandal, 2008). The advantages and disadvantages associated with each method are listed in Table 1.4. The simple process description of each method is presented below.

The most widely used method of removing heavy metals from solution is to increase the pH of the effluent, thus converting the soluble metal into an insoluble form (i.e., its hydroxide). Ion exchange is the second most widely used method for heavy metal removal from aqueous streams (Shukla *et al.,* 2002). During removal, recovery, or processing of metals, ion exchange acts as a concentrator of metals. The chemistry of the influent stream becomes very important to the success of the ion exchange application. Coagulation–flocculation can also be employed to treat wastewater laden

with heavy metals wherein the coagulation process destabilizes colloidal particles by adding a chemical agent (coagulant) and results in sedimentation (Wang *et al.,* 2004). Coagulation is followed by flocculation of the unstable particles in order to increase their size and form into bulky floccules which can be settled out. Flotation is employed to separate solids or dispersed liquids from a liquid phase using bubble attachment (Wang *et al.,* 2004). Adsorptive bubble separation is used to separate the metal impurities through foaming technique. Ion flotation, precipitate flotation and sorptive flotation are the main flotation process mechanisms for removal of metal ions from solution. Membrane filtration has received considerable attention for the treatment of inorganic effluent, since it is capable of removing not only suspended solid and organic compounds, but also inorganic contaminants such as heavy metals.

Amongst all the available treatment processes, adsorption using sorbents is one of the most popular and effective processes for the removal of heavy metals from wastewater. The adsorption process offers flexibility in design and operation and in many cases produces treated effluent suitable for reuse, free of colour and odour. In addition, regeneration of adsorbent is also possible for multiple usages of adsorbents with the help of suitable eluents through desorption process for economical operation

Activated carbon adsorbents are used widely in the removal of organic contaminants and to lesser extent heavy metal contaminants in product purification and pollution control. Carbon is converted to activated carbon by heating in the absence of air. The activation process results in the creation of a network of fine pores in the carbon particles. The vast areas (300–4000 m^2/g) of the walls within the pores account for the most of the total surface area of the carbon (Namasivayam and Kavitha, 2002). In spite of its prolific use, activated carbon remains an expensive material and the higher the quality of activated carbon, the higher its cost. Also, in practice activated carbon is employed more frequently for adsorption of organic compounds rather than heavy metal ions.

1.3 DYE POLLUTION

A dye is a coloured substance that can be applied in the solution or dispersion to substance and giving it a coloured appearance. Usually the substance is a textile fiber but it may be paper printing, leather, colour photography, pharmaceutical, food stuff,

fur, plastic materials wax, cosmetics and other industrial products (Demirbas *et al.,* 2008). Dyes are another group of pollutants that are increasingly causing pollution in fresh water bodies. Different types of dyes are utilized to colour the substances, but the fact that thousands of dyes are in use may seem excessive. Dyes are classified based on many factors such as solubility in water, ionic charge, chemical structure, chemical properties or toxicity, their origin and application. Based on ionic charge aspect, dyes can be classified as anionic, cationic and non-ionic dyes (Fu and Viraraghavan, 2002). Anionic dyes are acid dyes which are brightly coloured, water-soluble reactive and their removal from wastewater is highly problematic (Mishra and Tripathy, 1993; Willmott *et al.,* 1998). Cationic dyes are the brightest class of basic soluble dyes mostly used by textile industries as their tinctorial value is very high (Sureshkumar and Namasivayam, 2008). Non-ionic dyes refer to disperse dyes because they do not ionise in an aqueous medium. However, dye classifications vary from country to country though there are some fundamental categories that are common to all. There are more than 100000 commercial dyes available worldwide (Zollinger, 1987). The release of considerable amounts of these dyes to the environment has posed challenges to environmental scientists apart from increased public concern and legislation.

1.3.1 Sources of Dye Pollution

The change in the colour of water and wastewater is due to many phenomenons and resources such as natural and synthetic dyes. The natural colorants derived from plants (roots, berries, bark, leaves, wood and other organic resources) and mineral sources of soils are not being used a lot in these days, except for handicraft**.** Synthetic dyes are now replaced the traditional natural dyes, because it's cost is much less, has purer consistency and there are more varieties of new colours to choose for utilization. Synthetic dyes are extensively used in many fields of up-to-date technology e.g., in various branches of the textile industry (Gupta *et al.,* 1992; Shukla and Gupta, 1992 and Sokolowska-Gajda *et al.,* 1996), of the leather tanning industry (Tünay *et al.,* 1999 and Kabadasil *et al.,* 1999) in paper production (Ivanov *et al.,* 1996), in food technology (Bhat and Mathur, 1998), in agricultural research (Cook and Linden, 1997 and Kross *et al.,* 1996), in light-harvesting arrays (Wagner and Lindsey, 1996), in photoelectrochemical cells (Wrobel *et al.,* 2001), and in hair

colourings (Scarpi *et al.,* 1998). Moreover, synthetic dyes have been employed to control the sludge generation in sewage (Morgan-Sagastume *et al.,* 1997) and wastewater treatment (Hsu and Chiang, 1997 and Orhon *et al.,* 1999) compare to usage of natural dyes (Sorensen and Wakeman, 1996; Field *et al.,* 1995), etc.

According to the central pollution control board (CPCB), India there are about one million known dyes and dye intermediates out of which 5,000 are produced commercially. Based on their application 14 groups of dyes are used by Indian industries that are presented in Table 1.5. India produces 64,000 tonnes of dyes, 2% of which i.e., 7,040 tonnes are directly discharged into the environment. With the Indian dyestuff industry growing by over 50% during the last decade, India is now the second largest producer of dyes and intermediaries in Asia. The production is estimated to be around 60,000 tonnes or about 6.6 percent of the world production. There are around 700 varieties of dyes and dye intermediates produced in India. In India only one third of the dyestuff producing industries are in organised sector. The rest come from the unregulated small-scale sector, which produces more than half of India's aggregate volumes. Worldwide also high level of production and extensive use of dyes especially textile industries generates more coloured wastewaters which causes environmental pollution. The textile industry utilizes about 10,000 different dyes and pigments. These dyes are invariably left in the industrial wastes after the use. Especially, the textile finishing industry has a specific water consumption (approx. 1L/kg of product), part of which is due to dying and rinsing processes (Garg *et al.,* 2004a). The worldwide annual production of dyes is over 7×10^5 tonnes (Aksu and Tezer, 2005; Daneshwar *et al.,* 2005). Out of the current world production of dyestuffs of about 10 million kg/year between 1 and 2 million kg of active dye enter the biosphere either dissolved or suspended form every year (Allen *et al.,* 2003).

1.3.2 Toxicological Aspects of Dyes

The anionic and non-ionic dyes are mostly azo groups or anthroquinone types. The reductive cleavage of azo linkages is responsible for the formation of toxic amines in the effluent. Anthraquinone based dyes are more resistant to degradation due to their fused aromatic ring structures and thus remain coloured in the wastewater. Reactive dyes are typically azo-based chromophore combined with different types of reactive group's e.g., vinyl sulphone, chlorotriazine, trichloropyrimidine, difluorochloro-

pyrimidine. They differ from all other dyes in that they bind to textile fibers like cotton to form covalent bonds. They are used extensively in textile industries regarding favourable characteristics of bright in colour, water soluble and simple application techniques with low energy consumption. Water soluble reactive and acid dyes are problematic since they can pass through the conventional treatment system. Hence, their removal is also of great importance (Robinson *et al.,* 2001; Hu, 1992; Juang *et al*., 1997; Karcher *et al*., 1999; Sumathi and Manju, 2000; Aksu and Tezer *et al.,* 2000; O'Mahony *et al.,* 2002; Moran *et al.,* 1997).

Basic dyes have high brilliance and intensity of colours and are highly visible even in very low concentration (Clarke and Anliker, 1980; Banat *et al*., 1996; Fu and Viraraghavan, 2001; Mittal and Gupta, 1996; Chu and Chen, 2002; Fu and Viraraghavan, 2002). Metal complex dyes are mostly chromium based, which is carcinogenic (Clarke and Anliker, 1980; Banat *et al*., 1996; Mishra and Tripathy, 1993; Gupta *et al*., 1990). Disperse dyes do not ionize in an aqueous medium and some disperse dyes have also been shown to have a tendency to bioaccumulation (Banat *et al*., 1996). It has been reported that dyes can cause effects of carcinogenesis, mutagenesis, chromosomal fractures, teratogenecity and respiratory toxicity. McGeorge *et al*. (1985) studied the mutagenic activity of textile wastewater effluents using the salmonella/microsome assay and reported the highest percentage (67%) of mutagenic effluents. Costan *et al*. (1993) found that a textile effluent ranked second in toxicity, among eight industrial sectors represented, by using a series of bioassays assessing the acute, sublethal and chronic toxicity at various trophic levels.

Estimation of LC_{50} values of many commercial dyes at different time intervals on fish was done earlier by Clarke and Anliker, (1980). Srivastava *et al*. (1995a) also observed changes in LC_{50} values of malachite green in a fresh water catfish. Malachite green has been shown recently to be linked to an increased risk of cancer. It is highly cytotoxic to mammalian cells and also acts as a liver tumour enhancing agent (Rao, 1995). Over 90% of some 4000 dyes tested in an ETAD (Ecological and Toxicological Association of the Dyestuffs Manufacturing Industry) had LD_{50} values greater than 2×10^3 mg/kg. The highest rates of toxicity found amongst basic and diazo direct dyes (Shore, 1996).

Sub–chronic exposure (13 week) to benzidine-based dyes resulted in hepatocellular carcinomas and hepatic neoplastic nodules in rats (National Cancer Institute 1978) and carcinomas in very short duration (National Institute for Occupational Safety, 1980). Histopathological changes in the testes of textile wastewater exposed rats (sub-chronic) showed a reduction in the number of germ and Leydig cells, resulting in impaired spermatogenesis (Mathur *et al*., 2003).

A number of studies have demonstrated mutagenic activity in effluents from textile and dye related industries (Mcgeorge *et al*. 1985). Dyes also can cause severe damage to human beings, such as dysfunction of kidney, reproductive systems, liver, brain and central nervous system (Kadirvelu *et al.,* 2003). The occupational exposure of workers in the textile industry is linked to a higher bladder cancer risk.

Dyes may affect the photosynthetic activity in aquatic life due to reduced light penetration and may also be toxic to some aquatic life due to the presence of aromatics, metals, etc. in them (Clarke and Anliker 1980; Zollinger 1987; Mishra and Tripathy 1993; Banat *et al.,* 1996; Fu and Viraraghvan, 2001; Robinson *et al.,* 2001).

1.3.3 Guidelines and Need of Dye Removal

Due to the commercial importance of dyes, their impact (Guaratini and Zanoni, 2000) and toxicity (Tsuda *et al*., 2001) when released in the environment have been extensively studied during the last decade. Dyes and colour pigments contain metals such as copper, nickel, chromium, mercury and cobalt. Moreover, the unused dyes and colour released in effluent from dyeing vats interferes with the transmission of light in the water bodies that receives the effluent. This in turn inhibits the photosynthesis activity of aquatic biota besides direct toxic effects on biota. Several textile and food dyes have been linked to carcinogenicity, such as dye intermediaries like benzidines. Hence the ubiquitous colour needs to be regulated.

The new drinking water standards prescribed by the Bureau of Indian Standards (IS 10500) set colour standards at five colour units as the desirable limit and 25 colour units as the permissible limit in the absence of alternate source. Government legislation is becoming more and more stringent regarding the removal of dyes from industrial effluents. But removing the colour from effluents is extremely difficult.

Various techniques have been employed for the removal of dyes from wastewaters (Choy *et al.,* 1999; Gupta and Bhattacharrya, 1985; Khattri and Singh, 2000; Kun-She *et al.,* 2000; Liversidge *et al.,* 1997; McKay *et al.,* 1985; Mittal and Gupta, 1996; Perineau *et al.,* 1982; Singh *et al.,* 1984). Their advantages and disadvantages are listed in Table 1.6.

Traditional wastewater treatment technologies have proven to be markedly ineffective for handling wastewater of synthetic textile dyes because of the chemical stability of these pollutants. Thus, it has been reported that of the 18 azo dyes studied 11 compounds passed through the activated sludge process practically untreated, 4 (Acid Blue 113, Acid Red 151, Direct Violet 9, and Direct Violet 28) were adsorbed on the waste activated sludge and only 3 (Acid Orange 7, Acid Orange 8, and Acid Red 88) were biodegraded (Shaul *et al*., 1991). Decolouration of textile dye effluent does not occur when treated aerobically by municipal sewerage systems (Willmott *et al.,* 1998).

1.3.4 Treatment Techniques of Dye Removal

The industrial dyes are mostly synthetic origin and complex aromatic molecular structures, which make them more stable and more difficult to be biodegraded. Thus the conventional primary and secondary systems are not suitable to treat these effluents (Gürses *et al.,* 2004). Therefore, removal of dyes from the industrial effluents in an economic fashion remains a major challenge (Figueiredo *et al.,* 2000). Generally, dye wastewater is treated by physical or chemical-treatment process. These include physical-chemical flocculation combined with flotation, electroflotation, flocculation with Fe (II)/$Ca(OH)_2$, membrane-filtration, electrokinetic coagulation, precipitation, ozonation and Katox treatment method involving the use of activated carbon and air mixtures (Fu and Viraraghavan, 2001). Robinson *et al.* (2001) have done a review on the widely used methods of dye removal from dye-containing industrial effluents. The methods have been categorized in three categories, which are chemical, biological, and physical.

1.3.4.1 Chemical Methods

Fenton's reagent is suitable for treating wastewaters which are resistant to biological treatment or is poisonous to live biomass (Slokar and LeMarechal, 1997). Chemical

separation uses the action of sorption or bonding to remove dissolved dyes from wastewater and has been shown to be effective in decolourising both soluble and insoluble dyes (Pak and Chang, 1999).

- In ozonation, the use of ozone was first pioneered in the early 1970s, and it is a very good oxidising agent due to its high instability (oxidation potential, 2.07) compared to chlorine, another oxidising agent (1.36), and H_2O_2 (1.78). Oxidation by ozone is capable of degrading chlorinated hydrocarbons, phenols, pesticides and aromatic hydrocarbons (Lin and Lin, 1993; Xu and Lebrun, 1999).
- Photochemical oxidation method degrades dye molecules to CO_2 and H_2O (Yang *et al.,* 1998; Peralto-Zamora *et al.,* 1999) by UV treatment in the presence of H_2O_2. Degradation is caused by the production of high concentrations of hydroxyl radicals. UV light may be used to activate chemicals, such as H_2O_2, and the rate of dye removal is influenced by the intensity of the UV radiation, pH, dye structure and the dye bath composition (Slokar and Le Marechal, 1997).
- Sodium hypochloride (NaOCl) method attacks at the amino group of the dye molecule by the Cl. It initiates and accelerates azo bond cleavage. This method is unsuitable for disperse dyes.
- Electrochemical destruction is a relatively new technique, which was developed in the mid 1990s. It shows efficient and economical removal of dyes and a high efficiency for colour removal and degradation of recalcitrant pollutants (Ogutveren and Kaparal, 1994; Pelegrini *et al.,* 1999).

1.3.4.2 Physical Methods

- Adsorption techniques have gained favour recently due to their efficiency in the removal of pollutants. Adsorption produces a high quality product, and is a process which is economically feasible (Anandkumar and Mandal, 2011). Decolourisation is a result of two mechanisms: adsorption and ion exchange (Slokar and Le Marechal, 1997), and is influenced by many physio-chemical factors, such as, dye/sorbent interaction, sorbent surface area, particle size, temperature, pH, and contact time (Gad and El-Sayed, 2009). The

commercially available activated carbon and silica gel are frequently used for higher removal.

- The membrane separation technique has the ability to clarify, concentrate and, most importantly, to separate dye continuously from effluent (Mishra and Tripathy, 1993; Xu and Lebrun, 1999). Reverse osmosis is suitable for removing ions and larger species from dye bath effluents.
- In ion-exchange method, wastewater is passed over the ion exchange resin until the available exchange sites are saturated. Both cation and anion dyes can be removed from dye-containing effluent using this technique.
- Sufficient quantities of dissolved oxygen are required for organic substances to be broken down effectively by Irradiation. The dissolved oxygen is consumed very rapidly and so a constant and adequate supply is required (Hosono *et al.,* 1993).
- In Electro kinetic coagulation, the addition of ferrous sulphate and ferric chloride is making excellent removal of direct dyes by coagulation and flocculation from wastewaters. This method does not work well for acid dyes.

1.3.4.3 Biological Methods

1.3.4.3.1 Decolourisation by white-rot fungi

White-rot fungi are able to degrade dyes using enzymes, such as lignin peroxidases (LiP), manganese dependent peroxidases (MnP). Other enzymes used for this purpose include H_2O_2-producing enzymes such as glucose-1-oxidase and glucose-2-oxidase, along with laccase, and a phenoloxidase enzyme (Archibald and Roy, 1992; Thurston, 1994; Schliephake and Lonergan, 1996; Kirby, 1999). These are the same enzymes used for the lignin degradation (Lonergan, 1992; Barr and Aust, 1994; Reddy, 1995). Other fungi such as *Hirschioporus larincinus, Inonotus hispidus, Phlebia tremellosa* and *Coriolus versicolor* have also been shown to decolourise dye-containing effluent (Banat *et al.,* 1996; Kirby, 1999).

1.3.4.3.2 Other microbial cultures

Mixed bacterial cultures from a wide variety of habitats have also been reported to decolourise the diazolinked chromophore of dye molecules in 15 days (Knapp and Newby, 1995; Nigam and Marchant, 1995 and Nigam *et al.,* 1996). In this, a mixture of dyes were decolourised by anaerobic bacteria in 24±30 h using free growing cells

or in the form of bio films on various support materials. Ogawa and Yatome (1990) also demonstrated the use of bacteria for azo dye biodegradation. Yeasts such as *Klyveromyces marxianus* are capable of decolourising dyes. Banat *et al.* (1999) showed that *K. marxianus* was capable of decolourising Remazol Black B by 78 to 98%. Zissi *et al.* (1997) reported that *Bacillus subtilis* could be used to break down p-aminoazobenzene, a specific azo dye. Further research using *mesophilic* and *thermophilic* microbes have been also reported to degrade and decolourize dyes (Banat *et al.,* 1997).

1.3.4.3.3 Adsorption by living/dead microbial biomass

The accumulation or uptake of dyes by death microbial mass such as bacteria, yeast and fungi has been termed biosorption (Hu, 1992, 1996; Tsezos and Bell, 1989; Kumar *et al.,* 1998). Dyes vary greatly in their chemistries, and therefore their interactions with micro-organisms depend on the chemistry of a particular dye and the specific chemistry of the microbial biomass (Polman and Brekenridge, 1996).

1.3.4.3.4 Anaerobic dye bioremediation systems

In this method azo and other water-soluble dyes can be decolourised. This decolourisation involves an oxidation/reduction reaction with hydrogen rather than free molecular oxygen in aerobic systems. Typically, anaerobic breakdown yields methane and hydrogen sulfite (Carliell *et al.,* 1996). Azo dye acts as an oxidising agent for the reduced flavin nucleotides of the microbial electron chain and thus decolourised concurrently with reoxidation of the reduced flavin nucleotides. In order to occur this, additional carbon is required in order for decolourisation to proceed at a viable rate. This additional carbon is converted to methane and carbon dioxide, releasing electrons. These electrons cascade down the electron transport chain to a final electron acceptor, in this case, the azo-reactive dye. The electrons react with the dye reducing the azo bonds, and ultimately causing decolourisation (Carliell *et al.,* 1996).

Although, some of these techniques have been shown to be effective, they have limitations. Among these are: excess amount of chemical usage, or accumulation of concentrated sludge with obvious disposal problems; expensive plant requirements or operational costs; lack of effective colour reduction; and sensitivity to a variable

wastewater input. Some of the advantages and disadvantages of existing treatment methods are listed in Table 1.6.

1.4 PHENOLIC POLLUTION

Phenols or phenolics or carbolic acids are variety of chemical compounds containing hydroxyl (-OH) bonded aromatic hydrocarbon. Halogenated phenols such as chlorophenol and bromophenol are made up by one or more of the chlorine or bromine atoms from water that are attached to the benzene ring of phenol. Alkylation of phenols gives many branched phenols for many industrial applications. Phenol and cresol are the two most important phenolic compounds that are present in wastewater discharged from the industries (Yan *et al.,* 2006). Phenol and cresol are characteristic pollutants in wastewater from crude oil refineries, ceramic plants, steel plants, coal conversion processes, manufacturing units of phenolic resins, pesticides and explosives, *etc*. These chemicals are toxic and hazardous even at low concentrations. The generation of such phenolics and their major adverse effects are reported by many researchers (Hill and Robinson, 1975; Li and Humphrey, 1989; Kumaran and Paruchuri, 1996**;** Kar *et al.*, 1997; Monteiro *et al.*, 2000; Kim *et al.*, 2002; Murialdo *et al.*, 2003; Kumar *et al.*, 2005; Rodriguez *et al.*, 2006; Bai *et al.,* 2007; Feng *et al.*, 2007). The harmful characteristics of phenolic compounds lie in concentrations level they present (García *et al.*, 2000), which are very inferior to toxic concentrations, and contribute a disagreeable smell and taste to chlorinated water. Normally, the taste cannot be detected in concentrations if they are present in the range of 0.1 to 0.01 mg/L. Phenols are considered toxic to most of the aquatic life forms and the ingestion of 1 g of phenol can have fatal consequences in humans. They are toxic to human beings and aquatic biota (Kumaran and Paruchuri, 1996; Monteiro *et al.,* 2000). For the last two decades, rigorous pollution control and legislation in many countries have resulted in an intensive search for new and more efficient water treatment technologies.

1.4.1 Sources of Phenolic Compounds

Phenols are used by petroleum refineries, petrochemicals, textile, dye manufacturing, phenolics resin and polymers manufacturing, paper and pulp, varnish industries, explosives, phosphor-organic insecticides, pesticides, and wood preservative etc.

(Rhee *et al.,* 2003; Howe *et al.,* 2005; Nuhoglu and Yalcin, 2005; Juang and Tsai, 2006; Hassenklo¨ver *et al.,* 2006; Yan *et al.,* 2006; Bai et al., 2007; Uhnáková *et al.,* 2009). Currently, phenol is produced at a rate of about 6 million tons/year worldwide, with a significantly increasing trend (Buscaa *et al.,* 2008). Its methylated derivative cresol has been detected not only in leachate from creosote sites, raising the pollution of groundwater (Lin and Juang, 2009), but also in a huge range of industrial effluents (Hussain *et al.,* 2008). The cresols have wide applications in the phenolic resin, explosive, petroleum, photographic as well as paint and agricultural industries. They are ingredients of many household disinfecting solutions. Cresol is also an additive to lubricating oils and a component of degreasing compounds and paintbrush cleaners. *M*-cresol is a textile scouring agent. *O*-cresol is used in tanning, fibre treatment and metal degreasing. *P*-cresol is a solvent for wire enamels and an agent used in metal cleaning, ore flotation, synthetic flavouring and perfumes. The worldwide production of o-Cresol is approximately 37000-38000 tons/annum. Some of the important applications of phenols and its derivatives are given below:

- ***Plastics, resins and plasticizers*:** Phenol is used above all in the production of plastics and phenol-formaldehyde resins. In addition, cresols are used in the making of tricresyl phosphate, which is a plasticizer useful for cellulose acetate, nitrocellulose, ethane thiol cellulose and vinyl plastics.
- ***Preserving agent for wood, disinfectants and insecticides*:** Creosote oil, a distillation obtained from the process of coal-making at high temperatures, is used for preserving wood in addition to being a source of cresylic acid. Cresols are also used as disinfectants and insecticides.
- ***Vegetable hormones and detergents*:** Phenol is directly used for the production of these compounds.
- ***Medicines*:** A clear example of a derivative of phenol is acetylsalicylic acid - a compound from which aspirin is obtained.
- ***Dyes, photography and explosives*:** These industries have many usages of phenol although the total consumption is not very high. Some aminophenols are used as dyes and photographic developers. Trinitrophenol, for example, is used as a dye and as an explosive.

All these above said industries discharge phenolics in their wastewaters. Hence, it is advocated for efficient treatment methods to reduce phenol concentration in

wastewater to acceptable levels. Following is a short account on the state-of-the-art wastewater treatment methods.

1.4.2 Toxicological Aspects and Guidelines of Phenolic Compounds

Phenol and cresol are considered to be hazardous contaminants due to their toxicity for human being, animals and aquatic life (Shourian *et al.,* 2009; Naas *et al.,* 2009). Due to their high solubility and toxicity, they can easily contaminate the water sources (Mollaei *et al.,* 2010). These two can fastly penetrate in skin and that may cause irritation and respiratory tract. Therefore, human exposure to phenol and cresol by ingestion or inhalation may cause severe liver and kidney damage as well as cardiac depression. Ingestion of more than 1 mg/l of phenol is reported as harmful to human health (Nuhoglu and Yalcin, 2005).

Phenol and phenolic compounds have detrimental effects on the aquatic micro-flora and fauna at a very low concentration of 5 mg/l (Santos *et al.,* 2009). But the concentration of phenol in wastewater generally varies from 0.5 mg/l to 300 mg/l. Phenol may exert its toxic effect by reducing enzyme activity or even lethal to fish at relatively low levels of 5-25 mg/l. Phenol and cresols, even at a very low concentrations of 2 µg/l imparts objectionable taste and odour to drinking water (Chung *et al.,* 2003).

Due to their potential toxicity, the United States Environmental Protection Agency (US-EPA) has defined phenols, cresols and its derivatives as priority pollutants and set a water purification level concentration less than 1 µg/l in the inland surface waters (Keith and Telliand, 1979). The WHO has set their guideline of 1 µg/l to regulate the phenol concentration in drinking water. Also, a limit of 0.5 µg/l has been directed by the European Council Directive for regulating phenol concentration in the drinking water (Tziotzios *et al.,* 2005). The Indian Standard specifications have set the maximum allowable limit of phenol 0.001 mg/l for drinking water and 1 mg/l industrial effluent discharge into surface water (Mukherjee *et al.,* 2007; Vasu, 2008), whereas, 0.35 µg/l of effluent phenol concentration is fixed for petroleum oil refineries by Central Pollution Control Board (CPCB), India.

1.4.3 Treatment Techniques of Phenolic Wastewater

The removal of phenolics to sufficiently low levels in wastewater is mandatory. Appropriate strategies of wastewater treatment have to be employed in order to counterbalance the growing environmental problems. For the last two decades, rigorous pollution control and legislation in many countries have resulted in an intensive search for new and more efficient water treatment technologies. Important wastewater treatment technologies that have come up in recent times, include but are not limited to flocculation, precipitation, adsorption on granular activated carbon, reverse osmosis, combustion and advanced oxidation process (AOP) *viz*., photo fenton, photocatalysis and sonication. Some of these are briefly discussed below:

1.4.3.1 Air Stripping

It involves the transfer of volatile organics from liquid phase to the air phase by greatly increasing the air/water contact area. Typical aeration methods include packed towers, diffusers, trays and spray aeration. It is a well established and more widely understood technology than chemical oxidation (Metcalf and Eddy, 2003).

1.4.3.2 Adsorption

This is a separation method in which the contaminants, dissolved in water phase, are transferred to the surface of active carbon, the most commonly used adsorbent, where it is accumulated for subsequent extraction or destruction of the contaminants. The application of adsorption process includes but is not limited to control of color and odors, removal of organic compounds or trihalomethanes precursors, removal of chlorine *etc*. Numerous literatures have been reported regarding the treatment of phenolics on activated carbon (Calleja *et al.*, 1993; Dargaville *et al.*, 1996; Viraraghavan and Alfaro, 1998; Przepiórski, 2006; Vázquez *et al.*, 2007). Phenol was found to be a well adsorbable compound onto activated carbon, but only in low concentrations.

1.4.3.3 Electrochemical Oxidation

The use of electrochemical oxidation for the destruction of organic compounds in water solutions has been tried on bench and pilot plant scale operation (Boudenne *et al.*, 1996; Brillas *et al.*, 1990; Brillas *et al.*, 1998). The electrochemical oxidation of organic compounds is thermodynamically favoured against the competitive reaction

of oxygen production by oxidation of water. However, the kinetics of oxidation of water is much faster than the kinetics of oxidation of the organic compounds, among other reasons because of its higher concentration. The mechanism of the electrochemical processes involves three stages: electrocoagulation, electrofloatation and electrooxidation (Boudenne *et al.*, 1996; Brillas *et al.*, 1998).

1.4.3.4 Advanced Oxidation Processes (AOP)

It refers specifically to processes in which oxidation of organic contaminants occurs primarily through reactions with hydroxyl radicals (Glaze *et al.*, 1995). It involves two stages of oxidation: (1) the formation of strong oxidants (*e.g.*, hydroxyl radicals) and (2) the reaction of these oxidants with organic contaminants in water (Alnaizy and Akgerman, 2000). In water treatment applications, AOPs usually refer to a specific subset of processes that involve O_3, H_2O_2, and/or UV light.

1.4.3.5 Ozonation/UV

The O_3 system is one of the AOP for the destruction of organic compounds in wastewater. Basically, aqueous systems saturated with ozone are irradiated with UV light of 253.7 nm. The extinction coefficient of O_3 at 253.7 nm is 3300 L mol/cm, much higher than that of H_2O_2 (18.6 L /mol/cm). The decay rate of ozone is about a factor of 1000 higher than that of H_2O_2 (Guittonneau *et al.*, 1991). The AOP with UV radiation and ozone is initiated by the photolysis of ozone. The photodecomposition of ozone leads to two hydroxyl radicals, which do not act as they recombine producing hydrogen peroxide (Peyton and Glaze, 1988).

1.4.3.6 Ultrasonication

Implosion of cavity bubbles in sonicated water containing dissolved gases results in formation of hydrogen and hydroxyl radicals by fragmentation of water molecules. These radicals in turn combine and generate other oxidative species such as peroxy and super oxide radicals ($^{\bullet}OH$) as well as hydrogen peroxide; the quantities of each depend on the ambient conditions and the operating parameters. Such $^{\bullet}OH$ radicals are used for the degradation of the organic compounds (Kidak and Ince, 2006).

1.4.3.7 Solar Photocatalytic Oxidation

It is based on the use of UV light and a semiconductor. Many catalysts have been tested, although titanium dioxide (TiO_2) in the anatase form seems to possess the most

interesting features, such as high stability, good performance and low cost (Fox and Dulay, 1993; Legrini *et al*., 1993; Hoffmann *et al*., 1995; Bahnemann., 2004). TiO_2 has become the most studied and used photocatalyst, because it is easily available, chemically robust and durable. It can be used to degrade, *via* photocatalysis, a wide range of organic compounds (Leyva *et al.*, 1998; Robert and Malato, 2002; Hincapié *et al.*, 2005; Herrmann *et al.*, 2007). Photocatalytic degradation of phenolic compounds by employing Degussa P-25® in presence of sunlight has been successfully studied by many researchers (Minero *et al*., 1994).

1.4.3.8 Biodegradation

The process of biodegradation of exploits the ability of microorganisms (such as bacteria, fungi and algae) to convert the phenolic compounds to water, carbon oxide and biomass under aerobic or anaerobic condition. Phenol and cresol can be degraded either aerobically or anaerobically depending upon the specific growth conditions of the microorganisms. Pseudomonas putida bacteria and other members of Pseudomonas genus are the most widely investigated bacteria with higher removal efficiency of phenolic compounds (Naas *et al.,* 2009).

1.5 REQUIRMENT OF ALTERNATIVE TREATMENT TECHNIQUE

The existing conventional treatment processes which are discussed in each section of heavy metals, dyes and phenols are having some of the benefits and many of its own disadvantages. These processes are usually expensive when pollutants are present in moderate concentrations. Moreover, all the aforementioned treatment techniques are mostly applicable for the removal particular single pollutant not for the treatment of different category of components like heavy metal, phenols and dyes. This characteristic kindles the technical peoples especially in the developing countries like India to search for the usage of alternative wastewater treatment techniques which are having less cost, high efficiency and lower aggressiveness to the environment. Hence, more economical means such as adsorptive removal of industrial wastewater pollutants have been sought for heavy metals, industrial dyes and phenolic compounds treatment. However, in adsorption there is a need to search an effective low-cost adsorbent for economical wastewater treatment rather than commercially

available adsorbents. In recent years, more attention has been paid on the development of surface modified adsorbents with superior adsorption capacity from locally and abundantly available plant based waste materials. Biosorbents are attractive since those are naturally occurring materials and can be effectively used in the wastewater treatment. Biosorption is a rapid phenomenon of passive metals/dyes/phenols sequestration by the non-growing biomass/adsorbents. The biosorption process involves a solid phase (sorbent or biosorbent; adsorbent; biological material) and a liquid phase (solvent, normally water) containing a dissolved species to be sorbed (adsorbate, metals/dyes/phenols). Due to the higher affinity of the adsorbent for the adsorbate species, the latter is attracted and bound there by different mechanisms. The process continues till equilibrium is established between the amount of solid-bound adsorbate species and its portion remaining in the solution. The degree of adsorbent affinity for the adsorbate determines its distribution between the solid and liquid phases. There are many types of adsorbents such as earth's forests and plants, ocean and freshwater plankton, algae and fish, all living creatures, that including animals are all "biomass/adsorbents". The binding capacities of certain biomass/adsorbents are comparable with the commercial synthetic activated carbons and cation exchange resins. Some of the recently reported literature biosorbents for the removal of various heavy metals, dyes and phenols are listed in the Table 1.7-1.10. The renewable character of biomass that grows, fuelled directly or indirectly by sunshine, makes it an inexhaustible pool of chemicals of all kinds. Biosorption has advantages compared with conventional techniques (Anandkumar and Mandal, 2011). Some of these are listed below:

- **Cheap:** the cost of the biosorbent is low since they often are made from locally available abundant or waste material.
- **Metal/Dye/Phenolic Selective:** the metal/dye/phenol adsorption performance may be less or more for different types of adsorbents based on the selectivity. This selectivity is depends on various factors such as type of biomass, mixture in the solution, type of biomass preparation and physicochemical treatment.
- **Regenerative:** biosorbents can be reused after the metal or phenol or dye removal.
- **No Sludge Generation:** no secondary problems with sludge occur with biosorption, as is the case with many other techniques, for example, precipitation.

- **Metal/Dye/Phenolic Recovery Possible:** In case of metals, it can be recovered after being sorbed from the solution.
- **Competitive Performance:** biosorption technique is highly competitive and comparable with most other similar techniques, for example: ion exchange treatment. As mentioned above, ion exchange is more costly than low-cost biosorption technique using biosorbents.
- Biosorbents intended for bioremediation environmental applications are waste biomass of plant materials, crops, algae, fungi, bacteria, etc. which are the naturally abundant. Numerous chemical groups have been suggested to contribute to biosorption. The review results of biosorption of various heavy metals, dyes and phenols by biomass based adsorbents are presented in Table 1.7-1.10.

1.6 IMPORTANCE AND OBJECTIVES OF THE PRESENT STUDY

After the detailed review analysis of heavy metals, phenols and dyes as well as their treatment techniques, it has been found that the removal and remediation of these pollutants from contaminated wastewater/industrial effluent is expensive. This is mainly due to the major treatment cost associated with the imported technologies and chemicals. Advances in water and wastewater treatment technology need spur for the development of technologies that may be more effective and less costly. Therefore, it is important to improve the current conventional wastewater treatment systems to obtain higher efficiency. The indigenous invention of treatment techniques and chemicals locally, or use of locally available non-conventional materials to treat pollutants seems to be the solution to the increasing problem of effluent treatment. In this regard, there has been a focus on the use of appropriate low-cost technology for the treatment of wastewater in developing countries in recent years. But this process should have ease of operation with effectiveness so that the rural people can use it with least technical knowledge.

Adsorption is universally accepted as the latest method of treating industrial wastewaters bearing variety of organic and inorganic based pollutants for the removal of soluble toxic components. In this regard, technically feasible and economically viable pretreatment procedures with suitable biomaterials based on better

understanding of the adsorbate biosorbent mechanism(s) are gaining importance. Biosorbents and activated carbons of agricultural waste products as low-cost adsorbents have been reported till now. However, there is weakness in the adsorption effiency and an additional cost involved in the processing of solid waste generation after the single usage of the agricultural materials, which is posing economic difficulties necessitating research on alternate adsorbents with high potential and reuse capability. In practical situation, industrial effluents are heterogeneous mixture of several components, many of which are organic and inorganic compounds of varying composition and surface activity. Most of the literature reported activated carbons and other biomass based adsorbents failed to adsorb/remove such type of mixed contaminants and high concentration pollutants. In adsorption process, a detailed understanding of adsorbate binding mechanisms with active sites facilitates to determine the rate-limiting step. This information can then be used for the rational design and optimization of the adsorbents and adsorption conditions. However, very little research has focused on the role of surface chemistry and the adsorption mechanism using adsorbent materials.

Therefore, keeping all the environmental, ecological, societal health issues and other unexplored research directions in view, it is considered necessary to find novel adsorbents which will provide easy, feasible and economical solution for the removal of certain industrially important heavy metals, phenols and cationic dyes both in single and mixed forms. The present research work has been undertaken to achieve the above goals with the following objectives:

- Development of high potential adsorbents from industrial wastes (Bael fruit shell and Tannery residual biomass).
- Characterization of laboratory synthesized adsorbents for its optimization of surface morphology and valuable absorbable properties such as BET and ChemiSorb surface area analysis, FT-IR, Zeta-potential, XPS, FESEM, SEM and EDX.
- Find out the optimum operating parameters such agitation/equilibrium time, pH and effect of adsorbent at different initial adsorbate concentrations as well as the maximum adsorption capacity of targeted heavy metals (Cr^{6+}, Pb^{2+}, Ni^{2+}

and Sr^{2+}), phenols (phenol and *o*-cresol) and cationic dyes (rhodamine B and methylene blue) in both single and mixed form using synthesized adsorbents.

- Desorption of adsorbates from adsorbate loaded adsorbents by suitable eluents to check the reusability.
- Find out the performance of continuous fixed bed column mode studies using high capacity adsorbent with adsorbate.
- Development of appropriate thermodynamic, kinetic and equilibrium isotherm model to analyze the adsorbate-adsorbent interaction.
- Finding the possible adsorbate binding mechanisms of synthesised adsorbents with the help of surface chemistry.

1.7 THESIS OUTLINE

From the discussion in the previous section, it is apparent that the development of novel adsorbent has immense industrial significant and there is huge scope of research work. The present work has been divided into eight chapters.

Chapter 1:

Chapter 1 presents a general discussion on water and wastewater pollution. It also discusses the sources of various industrial pollutants, their impacts on environment structure and the available treatment techniques. This chapter also describes the results of other similar components and potentiality from the recent reported literatures which supports to make the objectives and importance of this research work at the end of this chapter.

Chapter 2:

Chapter 2 describes the detailed method of synthesis and optimization of adsorbents from bael fruit shell and tannery residual biomass. This chapter also discusses the performance evaluation test results of each synthesized adsorbents with each studied heavy metals, phenols and dyes.

Chapter 3:

Chapter 3 elaborates the detailed adsorption studies of selected heavy metals, phenols and dyes using H_3PO_4 followed by thermal treated bael shell activated carbon (BSAC) in batch mode operations. This chapter also describes the adsorption

isotherm and kinetic model fittings with experimental data, possible adsorption mechanisms and thermodynamic studies in detail.

Chapter 4:

Chapter 4 presents the complete adsorption studies of selected heavy metals and cationic dyes using only H_2SO_4 treated bael shell activated adsorbent (SBS) in batch mode operations. The adsorption isotherm and kinetic model fittings with experimental data, possible adsorption mechanisms and thermodynamic studies are also described in detail.

Chapter 5:

Chapter 5 presents the detailed batch mode adsorption studies of selected heavy metals and cationic dyes by HCl activated tannery residual biomass (HTB). In this chapter the various kinetic and isotherm model fittings, thermodynamic studies and the adsorption mechanisms of the pollutants with adsorbent are described elaborately.

Chapter 6:

Chapter 6 presents the elaborate batch mode adsorption studies of selected heavy metals and cationic dyes by H_3PO_4 followed by thermal activated tannery residual biomass (TBAC). In this chapter the various isotherm model fittings, thermodynamic studies and the adsorption mechanisms of the adsorbates with adsorbent are presented in detail.

Chapter 7:

Chapter 7 presents the packed-bed continuous mode adsorption studies at different experimental conditions using high performance adsorbent (BSAC) with a highly adsorbed adsorbate (RB). Furthermore, experimental data are analysed with various available mathematical models for their validation.

Chapter 8:

Chapter 8 draws summary and appropriate conclusion based on the previous results and discussion. This chapter also provides some useful recommendations for future research in the relevant field.

A part of the work in this thesis has been published or accepted for publication in different international journals, International and National conference proceedings, and some more papers would be communicated in due course of time. The details of papers published/ accepted, to be communicated and conference presentations have been appended at the beginning.

1.8 SUMMARY

Liquid and solid waste generations are always increasing the problems in the industries and environment. From the literature citation, it is clear that there is a need to find a low-cost process for the removal of toxic heavy metals, dyes and phenolic contaminants from its wastewater. The treatment process is also simple and convenient. One of the most popular ways of dealing with local solid waste is its use as a raw material for the production of activated adsorbents that can be subsequently employed for the removal of the aforementioned pollutants from the wastewater. Keeping in view the importance of removal of heavy metals, dyes and phenolic compounds from the contaminated industrial wastewaters, the objectives of present study is made to utilize or recycle two locally available solid waste materials to prepare the environment friendly low-cost novel adsorbents for single and contaminant removal.

Chapter 1
Figures & Tables

Table 1.1 Distribution of heavy metals in the particular industrial effluents

Heavy metals	Industries	References
Arsenic (Ar)	Pesticides (including wood preservatives), paints, desiccants, glass, alloys, electronic components (semiconductors), pigments, and pharmaceuticals	Thomas *et al.*, 2007
Cadmium (Cd)	Electroplating, batteries, smelting, pigments, plastic, iron and steel, mining and mineral processing, non-ferrous metal industry, printing and photographic, paints.	Matheickal *et al.*, 1999.
Chromium (Cr)	Electroplating, tanning and leather, textile, pigments, plastic and dye.	Gang *et al.*, 2000; Park *et al.*, 2005
Cobalt (Co)	Mining, electronics, metallurgical, electroplating and paint industries	Krishnan and Anirudhan, 2008
Copper (Cu)	Electroplating, electricals, pipes and tubes, automobile, paper and pulp, paint, textile, fertilizer, petroleum.	Aksu *et al.*, 1991; Figueira *et al.*, 2000
Lead (Pb)	Battery, paper and pulp, mining, electroplating, lead smelting, metallurgical finishing industries, paints and pigments, metal dye, electricity and petroleum.	Noeline *et al.*, 2005; Ucun *et al.*, 2003
Mercury (Hg)	Mining, combustion of fossil fuels, pulp and paper, paints, oil refinery, plastic, battery manufacturing, electrical equipment, leather tanning, metal finishing, petroleum refinery, agriculture, smelters, chlorine and chloroalkali manufacturing processes.	Jeon and Ho¨ll, 2003
Nickel (Ni)	Paint industry, metal finishing, mineral processing, silver refineries, hydrometallurgical industry, leather tanning, electroplating, zinc base casting, storage battery industries, and steam-electric power plants	Dizgea *et al.*, 2009
Strontium (Sr)	Nuclear power plants, research applications, power remote weather stations, navigational buoys, fireworks, and satellites applications.	Chegrouche *et al.*, 2009
Zinc (Zn)	Metals, chemicals, pulp and paper manufacturing, steel works with galvanizing lines, zinc and brass plating, viscose rayon yarn and fiber production industries.	Mohan *et al.*, 2002

Table 1.2 Toxic response of heavy metal ions on human (US Department of Health and Human Services, 1991)

Heavy metals	Toxicological effects on human health	References
Arsenic (Ar)	Skin cancer, hyper pigmentation, carcinogen and mutagen, dermatitis, skin damage or problems with circulatory systems, and may have increased risk of getting cancer.	Thomas *et al.*, 2007
Cadmium (Cd)	Kidneys and respiratory disorders; carcinogenic, long-term-concentrations will affect liver, kidneys, pancreas, and thyroid; hypertension suspected effect.	Matheickal *et al.*, 1999
Chromium (Cr)	Skin and respiratory disorders; Cr(VI) is carcinogenic and corrosive on tissue; Long-term-skin sensitization and kidney damage.	Gang *et al.*, 2000; Park *et al.*, 2005
Cobalt (Co)	Lungs, pneumonia, wheezing and including asthma problems.	Krishnan and Anirudhan, 2008
Copper (Cu)	Long-term exposure to copper can cause irritation of the nose, mouth, eyes, headaches, stomachaches, dizziness, vomiting and diarrhea; High uptakes of copper may cause liver and kidney damage and even death.	Aksu *et al.*, 1991; Figueira *et al.*, 2000
Lead (Pb)	Long term exposure may cause brain nervous, kidney and damage; birth effects; disruption of the biosynthesis of hemoglobin and anemia; Declined fertility of men through sperm damage.	Noeline *et al.*, 2005; Ucun *et al.*, 2003
Mercury (Hg)	Vapour inhalation can cause nerve, brain, kidney damage; lung and eye irritation; Skin rashes, vomiting and diarrhea.	Jeon and Ho¨ll, 2003
Nickel (Ni)	Uptake of excess quantity will cause lung cancer, nose cancer, larynx cancer and prostate cancer; Respiratory failure, birth defects, asthma and chronic bronchitis.	Al-Asheh and Duvnjak, 1997; Kadirvelu, 1998
Strontium (Sr)	Strontium chromate is known to cause lung cancer, cause problems with bone growth and radioactive effects.	Chegrouche *et al.*, 2009
Zinc (Zn)	Zinc poisoning can cause desiccating muscles, imbalance of electrolytes, stomach ache, vertigo and disharmony.	Mohan *et al.*, 2002

Table 1.3 Guidelines of heavy metals for drinking water and industrial effluents

Heavy Metals	Permissible limit (mg/l) of industrial effluent as per CPCB*, India			Allowable drinking water standards (mg/l)	
	Inland surface water	Public sewer	Irrigation water	BIS**	WHO***
Arsenic (As)	0.2	0.2	0.2	0.01	0.01
Cadmium (Cd)	2.0	2.0	-	0.01	0.003
Chromium (Cr)	0.1	2.0	-	0.05	0.05
Copper (Cu)	3.0	3.0	-	1.5	2.0
Iron (Fe)	3.0	3.0	-	0.3	0.2
Manganese (Mn)	0.1	0.3	-	0.05	0.05
Mercury (Hg)	0.01	0.01	-	0.001	0.001
Nickel (Ni)	3.0	3.0	-	-	0.02
Lead (Pb)	0.1	1.0	-	0.05	0.01
Selenium (Se)	0.05	0.05	-	-	0.01
Zinc (Zn)	5.0	15.0	-	5.0	3.0

** Central Pollution Control Board (CPCB), India; ** Bureau of Indian Standards (BIS); *** World Health Organisation (WHO).*

Table 1.4 Advantages and disadvantages of existing heavy metal treatment techniques

Treatment	Advantages	Disadvantages	Heavy Metals	References
Chemical Precipitation	Process simplicity; Not metal selective; Inexpensive capital cost	Not suitable for mixed metals; Large amount of sludge containing metals; High sludge disposal cost; High maintenance costs.	Cd^{2+}, Cr^{6+}, Cu^{2+}, Fe^{3+}, Pb^{2+}, Sn^{2+} & Zn^{2+}	Patterson *et al.*, 1975;
Ion exchange	Withstand at shock loading; Metal selective; Limited pH tolerance; High regeneration	Fouling of bed by organic components; Plugging of resin bed by suspended solids; Resins requires regeneration or disposal; High initial capital cost; High maintenance cost.	Cr^{3+}, Cu^{2+}, Fe^{3+}, Pb^{2+} & Ni^{2+}.	Groffman *et al.*, 1992
Membrane Filtration	Good removal; Low solid waste generation; Low chemical consumption; Small space requirement; Possible to be metal selective.	Requires extensive pretreatment; High initial capital cost; High maintenance and operation costs; Membrane fouling; Limited flow-rates.	Cr^{6+}, Pb^{2+}, Fe^{3+}, Ni^{2+}, Cu^{2+} & Zn^{2+}.	Pyrzynska, 2006
Electrochemical Treatment	Rapid process and effective for certain metal ions; Can treat effluent > 2000 mg/l.	High energy costs and formation of by products; High initial capital cost and production of H_2 (in some processes); Filtration process for flocs.	Cr^{6+}, Pb^{2+}, Fe^{3+}, Bi^{2+}, Cu^{2+} & Zn^{2+}.	Dikusar et al., 1993;
Biological Treatment	Low cost; Effective for many metals.	Treatment not yet to be established and commercialized	Cd^{2+}, Cu^{2+}, Pb^{2+}, Ni^{2+} & Zn^{2+}.	Sheng et al., 2004; Holan and Volesky, 1994, 1995
Adsorption (CAC)	Wide variety of target pollutants; High capacity; Fast kinetics; Possibly selective depending on adsorbent	Performance depends on type of adsorbent; Require chemical regeneration to improve its sorption capacity.	Cd^{2+}, Cu^{2+}, Pb^{2+}, Hg^{2+} & Ni^{2+}.	Crini, 2005; Connell *et al.*, 2008
Coagulation & Flocculation	Bacterial inactivation capability; Good sludge settling and dewatering Characteristics.	High chemical consumption; Increased sludge volume generation	Bi^{+}, Fe^{3+}, Zn^{2+}, Sb^{2+} & Cr^{6+}.	Dikusar et al., 1993; Connell *et al.*, 2008

Table 1.5 Classification of dyes based on their use

Types of dyes	Industrial application	
	According to CPCB[1]	According to world Bank[2]
Acid dyes	Wool, silk, nylon	Animal fibres
Azo dyes	Cotton	Cotton
Basic dyes	Acrylic	Paper
Direct dyes	Cotton, leather, paper and synthetics	Cotton wool or cotton silk
Disperse dyes	Polyster	-
Food dyes	Food, cosmetics	-
Metal complexes	Cotton	-
Mordant dyes	Wool	-
Whitening agent	Plastics, paper, soap	-
Pigment dyes	Paints and plastics	Paints and inks
Reactive dyes	Wool and cotton	-
Solvent dyes	Synthetics	-
Sulphur dyes	Cotton and Synthetics	-
Vat dye	Cotton and Synthetics	-

Note: [1]Anon 2002, Effluent toxicity status in water polluting industries, Part 1 – Dye and dye intermediate, bulk drugs and textile industries, Central Pollution Control Board, Ministry of Environment and Forests, Government of India, p7.

[2]Pollution prevention and abatement handbook, World Bank, p 298.

Table 1.6 Advantages and disadvantages of existing dye treatment techniques

Treatment methods	Advantages	Disadvantages	References
Fenton's reagent	Effective decolourisation of both soluble and insoluble dyes	Sludge generation	Raghavacharya, 1997 Pak and Chang, 1999
Ozonation	Applied in gaseous state: no alteration of volume	Short half-life (20 min)	Ince and Gonenc, 1997 Xu and Lebrun, 1999
Photochemical	No sludge production	Formation of by-products	Yang *et al.,* 1998
NaOCl	Initiates and accelerates azo-bond cleavage	Release of aromatic amines	Banat *et al.,* 1999
Cucurbituril	Good sorption capacity for various dyes	High cost	Karcher *et al.,* 1999b
Electrochemical destruction	Breakdown compounds are non-hazardous	High cost of electricity	Ogutveren and Kaparal, 1994; Pelegrini *et al.,* 1999
Activated carbon	Good removal of wide variety of dyes	Very expensive; disposal problem	Gad and Sayed, 2009
Membrane filtration	Removes all dye types	Sludge production; Need high pressures; expensive, Incapable of treating large volumes.	Mishra and Tripathy, 1993; Xu and Lebrun, 1999
Ion exchange	Regeneration: no adsorbent loss	Not effective for all dyes; Economic constraints.	Slokar and Le Marechal, 1997
Irradiation	Effective oxidation at lab scale	Requires a lot of dissolved O_2	Hosono *et al.,* 1993
Electro-kinetic coagulation	Economically feasible	High sludge production	Gahr *et al.,* 1994
Biodegradation	Efficient for specific dyes	Slow process, need to create an optimal favourable environment, maintenance and nutrition requirements	Banat *et al.,* 1996; Kirby, 1999

Table 1.7 Literature reported waste material based adsorbents for different heavy metal adsorption

Activated Carbon	Heavy metal	pH	Equilibrium time/Concentration	Adsorption capacity (mg/g)	References
Comingled waste Commercial Norit	Cr(III)	-	500 mins (8 hour)/ 200 mg/L of Cr(III)	1.09 1.02	Lyubchik *et al.*, 2004
Coconut Commercial FS-100	Cr(VI)	3	5 days	73.90 50.30	Hu *et al.*, 2003
Waste tyre Sawdust	Cr(VI)	2	120 mins / 40-100 mg/L of Cr(VI)	58.47 24.65	Hamadi *et al.*, 2001
Hevea Brasilinesis	Cr(VI)	2	300 mins/ 50-200 mg/L of Cr(VI)	44.05	Karthikeyan *et al.*, 2005
Tree fern	Cu(II)		120 mins	11.7	Ho, 2003
Herbaceous peat	Cu(II)	5.5	150 min/ 6×10^{-4} M of Cu(II)	4.8	Gündogan *et al.*, 2004
Bagasse fly ash	Cd(II)	6	60 mins/ Cd(II) of 14 mg/L	1.18	Gupta *et al.*, 2003
Peanut husk	Cd(II) Pb(II)	-	2 hour/ 0.15 mmol of Cd(II) and Pb(II)	50.58 113.96	Ricordel *et al.*, 2001
Coconut shell	Pb(II)	4.5	2 hour for initial Pb(II) of 10- 50 mg/L	26.51	Sekar *et al.*, 2004
Furfural	Hg(II)	5.5	60 mins	174.00	Yardim *et al.*, 2003
Sago waste	Hg(II)	5	120 mins/ 50 mg/L of Hg(II)	55.60	Kadirvelu *et al.*, 2004
Fruit shell of *terminalia catappa*	Hg(II)	5–6	720 mins	94.43	Inbaraj and Sulochana, 2006
Grafted silica	Pb(II); Cu(II)	5.5- 6	90 mins	38; 16.40	Chiron *et al.*, 2003
Cellulose grafted copolymers	Cu(II) Cd(II)	-	2 hours	12.96 13.26	Okieimen *et al.*, 2005
Wheat bran	Cr(III); Hg(II) Pb(II); Cd(II);	6	10 mins	93; 70 62; 21	Farajzadeh *et al.*, 2004

Table 1.8 Literature reported biosorbents for different heavy metal adsorption

Biosorbent	Heavy metals	pH	Adsorption capacity (mg/g)	Functional group	References
Biomass of *Rhizopus arrhizus* (Immobilized)	Cr(VI)	2	23.88	Chitin and chitosan takes more than 8 h to achived equlibrium	Prakasham *et al.*, 1999
Fungal biomass *Neurospora crassa*	Cr(VI)	1	15.85	–NH, hydroxyl, carboxylate anions, carbonyl groups and phosphate group	Tunali *et al.*, 2005
Marine algae	Cd(II)	5	112.4	Carboxylic	Matheickal *et al.*, 1999
Dead Sargassum	Cd(II)	3- 6	120	Carboxyl and guluronic acids	Cruz *et al.*, 2004
Papaya wood	Cd(II) Cu(II) Zn(II)	5	17.35 19.99 14.44	Protein, lignin and cellulose	Saeed *et al.*, 2005
Sugar beet pulp	Cu(II)	4	28.5	Carboxylate and some weaker acidic groups	Aksu *et al.*, 2005
Peat	Cu(II)	2	14.3	Cellulose, pentose and lignin	Ho and McKay, 2003
Grape stalks	Cu(II)	5-6	10	Lignin and C–O bond	Villaescusa *et al.*, 2004
Maize bran	Pb(II)	6.5	98.4	Metal oxides	Singh *et al.*, 2006
Ulva lactuca	Hg(II)	7	149.25	Algal cell sites	Zeroual *et al.*, 2003
Macroalga *Cystoseira baccata*	Hg(II)	7	178	Acid algal sites	Herrero *et al.*, 2005

Table 1.9 Literature reported biosorbents for different dye adsorption

Activated Carbon	Dye	References
Bamboo dust, coconut shell, groundnut shell, rice husk	Methylene blue	Kannan and Sundaram, 2001
Silk cotton hull, coconut tree sawdust, sago waste, maize cob	Rhodamine-B, Congo red, methylene blue, methyl violet, malachite green	Kadirvelu *et al.,* 2003
Parthenium hysterophorus	Methylene blue, malachite green	Rajeshwarisivaraj and Subbaram, 2002
Rice husk	Malachite green	Guo *et al.,* 2005
Coir pith	Acid violet, acid brilliant blue, methylene blue, Rhodamine-B	Namasivayam *et al.,* 2001; Namasivayam and Kavitha, 2002
Indian Rosewood, Prosopis cineraria	Malachite green	Garg *et al.,* 2003, 2004.
Groundnet shell powder	Basic, direct and disperse dyes	Malik *et al.,* 2007.
Banana and orange peels	Methyl orange, methylene blue, Rhodamine-B, Congo red, methyl violet, acid black 10B	Annadurai *et al.,* 2002.
Giant duckweed	Methylene blue	Waranusantigul *et al.,* 2003
Wheat straw, corn cob, bark husk	Cibacron yellow C-2R, Cibacron red C-2G, Cibacron blue C-R, Remazol black B, Remazol	Robinson *et al.,* (2002)
Orange peel	Congo red, Rhodamine-B, Procion orange	Kadirvelu *et al.,* 2003
Carbonized coir pith	Acid violet, Rhodamine-B	Namasivayam *et al.,* 2001
Activated sludge biomass	Basic blue 3, basic violet 3, basic red 18, basic yellow 24, basic red 29, basic blue 47, basic blue 54	Chu and Chen, 2002
Fly ash	Acid orange 7, acid yellow 23, disperse blue 79, basic yellow 28, direct yellow 28.	Mall and Upadhyay, 1998

Table 1.10 Literature reported adsorbents for different phenolic adsorption

Activated Carbon	Phenolic component	Adsorption Capacity (mg/g)	Reference
Parthenium hysterophorous Activated carbon	p-cresol	62.91	Singh *et al.*, 2008
Rattan sawdust activated carbon	Phenol	149.25	Hameed and Rahman, 2008
Coconut shell activated carbon	Phenol	205.8	Din et al., 2009
Sugarcane bagasse fly ash	Phenol	23.83	Srivastava, 2006
Rice husk & its char	Phenol *p*-Nitrophenol *p*-Chlorophenol	4.508 & 7.91 15.31 & 39.21 14.36 & 36.23	Ahmaruzzaman and Sharma, 2005
Samla coal & Petroleum coke	Phenol *p*-Nitrophenol *p*-Chlorophenol	13.28 & 6.009 51.54 & 11.061 50 & 9.337	Ahmaruzzaman and Sharma, 2005
Fresh Coal , Demineralized coal & Oxidized coal	o-crssol	5.9, 9.0 & 5.6	Giirses *et al.*, 1992
M-bentonite Al-bentonite CTAB-bentonite T-bentonite	Phenol	9.9 8.7 8.4 8.2	Al-Asheh *et al.*, 2003
Wood Fly Ash	m-cresol & p-cresol	34.5 & 52.5	Ahmaruzzaman, 2010
Fly Ash	p-cresol	6.7	Hadjar *et al.*, 2011
Rice husk activetd carbon	m-cresol	8.2-10.3	John Kennedy *et al.*, 2007

CHAPTER 2

SYNTHESIS AND OPTIMIZATION OF ADSORBENTS

This chapter presents the various methods of synthesis of adsorbents which are used in this research work to achieve the objectives that are highlighted in chapter 1. This chapter is divided into four sections such as (i) collection of materials, (ii) synthesis of adsorbent, (iii) optimization of adsorbents by BET surface area analysis and (iv) optimization of adsorbents by preliminary performance evaluation test (PPET) with synthesized adsorbents

2.1 COLLECTION OF PRECURSOR

Two plants based industrial waste materials such as **Bael fruit** (Botanical name: *Aegle marmelos correa*) **shell (BS)** and **Tannery residual biomass (TB)** were used as precursor for the synthesis of various activated adsorbents for the removal of many industrial organic and inorganic wastewater pollutants from aqueous solution.

The Bael fruit (Figure 2.1a) is an indigenous ayurvedic medicinal fruit used in India and many other South-Asian countries. It belongs to Rutaceae family and available throughout Southeast Asian countries. The peel of Bael fruit (Figure 2.1b) is a very hard shell (about 30% of total fruit weight) and considered to be a waste by-product after the usage in ayurvedic medicinal industries across the country. These waste shells are not put to any use furthermore and available at low or zero prices. Hence, we collected sufficient amount of this waste Bael fruit shells as a precursor from nearby industrial locality in Guwahati at Assam, India.

Tannery residual biomass (Figures 2.2a and 2.2b) used in this study is a sludge and solid waste generated from the vegetable tanning section of the Indian tannery industry. In tanneries, plants based tannin rich materials such as babul bark, chestnut, myrobalan and cashew husk testa etc. are widely used to treat the hides or animal raw skins in vegetable tanning process to produce the tanned leather. After the tanning process, this tannin extracted plant based materials become a huge amount of unwanted solid waste material in Indian tanneries. This waste sludge is creating the solid waste disposal problem in the tanneries. We collected the cashew husk testa based tannery residual biomass as second precursor for this work from Amjad Finished Leather Company at Pernambut, Vellore in India after the vegetable tanning processes.

2.2 SYNTHESIS OF ADSORBENTS

The adsorption capacity of any adsorbent towards the particular adsorbate depends on many factors of the adsorbent such as nature of the adsorbent (acidic/ basic functional groups), surface area, pore size distribution, carbon content and hydrophobicity. These parameters vary based on the synthesis method of adsorbents. On the other hand, adsorption also depends on the hydrophobicity, polarity, and size of the adsorbate molecule. In order to prepare efficient adsorbents to remove targeted heavy

metals, dyes and phenols from the aqueous solution using two industrial solid waste materials (precursors) such as **Bael fruit shell** and **Tannery residual biomass** following three methods were employed in this study.

1) Thermal (carbonization) activation (at various temperatures)
2) Chemical activation (with acids and base)
3) Thermochemical or chemical followed by thermal activation (at various temperatures with acids and base treatment)

Initially, the two targeted precursors such as Bael fruit shell and Tannery residual biomass were washed thoroughly with sufficient amount of tap water to remove water-soluble impurities and surface-adhering particles. Then, the washed shells were dried in sunlight and shredded into the small pieces using ball mill. Thereafter, various above said activation methods were employed to synthesis different adsorbents. The detailed procedures of each activation method are discussed as below:

2.2.1 Thermal Activation

The thermal activation was the single step process which involves calcination of the precursor (BS and TB) at various desired temperatures and dwelling time in absence of inert gas atmosphere in the closed digital muffle furnace. The temperatures were varied depending on the thermal stability of the raw material and the weight loss of the final adsorbent. The activation temperatures and time were chosen only in the range of 200^{o}C to 600^{o}C and 0.5 to 2.0 hr to avoid the higher oxidation and weight loss of precursor material in absence of inert gas atmosphere. The thermal activation protocol is shown in Figure 2.3.

2.2.2 Chemical Activation

This process involves only single step in which the desired concentration and quantity of acid/base was mixed with precursor (BS and TB) in various impregnation ratios to activate the material. Three acids such as 88% ortho phosphoric acid (H_3PO_4), 98% sulphuric acid (H_2SO_4) and 36% hydrochloric acid (HCl) as well as one base i.e., potassium hydroxide (KOH) were used to activate the precursors based on the recent reported literatures. Chemical activation of BS and TB was carried out by proper mixing of particular concentration of desired quantity of acid/base precursors. Then

the mixtures were kept in the air-tight glass vessel under the sunlight for 2–3 days. The protocol of each chemical (acid/base) treatment is shown in the Figures 2.4-2.7.

2.2.3 Thermochemical Activation

This is two steps process. Initially, chemical activation of precursor (BS and TB) was carried out with various concentrations of acids and then the thermal activation (calcination) was done at various desired temperatures and activation time in absence of any inert gas atmosphere in the closed muffle furnace. The activation temperatures and times were varied depending on the nature of raw material (temperature stability) and the weight loss of the final adsorbent. The activation temperatures and calcination time after chemical treatment with HCl, H_2SO_4 and KOH were chosen in the range of 200^oC to 400^oC and 1 hr, respectively to avoid the huge weight loss. The chemical with thermal activation protocol for HCl, H_2SO_4 and KOH is shown Figure 2.8. But, H_3PO_4 treatment with thermal activation was carried out for BS at various temperatures, H_3PO_4 concentration and activation time due to the stability nature of acid and BS mixer as well as lower weight loss of adsorbent compare to other acids/base. The chemical (H_3PO_4) with thermal activation protocol is shown in Figure 2.9. Due to the crisp nature of precursor, activation of thermochemically activated TB using H_3PO_4 was carried out at optimum activation time (1.5 hr) of BS at various temperatures to avoid the huge adsorbent weight loss as well as acid wastage. The overall activation layout of thermal, chemical and thermochemical activation is shown in Figure 2.10.

Absorbents synthesized by chemical activation and thermochemical activation were soaked in 2% $NaHCO_3$ to remove the residual acid that was left on the adsorbent. Then all the thermal, chemical and thermochemical activated adsorbents were washed thoroughly with distilled water to remove the ash content and residual chemicals until the washed water reaches its natural pH. Subsequently, adsorbents were dried at 110^oC in a hot air oven and sieved in the size range of 600–860 mm using mesh sizes 25–18 (GEOSYN Test Sieves, BSS 410). Finally, the adsorbents were dried again at 110^oC for 24 hr and cooled inside a dessicator until further use.

2.3. SURFACE AREA OPTIMIZATION OF ADSORBENTS

Optimization of synthesized adsorbents was carried out by BET surface area measurement using Beckman Coulter (SA 3100) and ChemiSorb (2720/2750) surface area analyzer. The Beckman Coulter was used for high surface area adsorbent to measure the surface area and porosity of solids based on multi-point surface area technique. But the ChemiSorb was used to find out the lower surface area of adsorbent by single point surface area measurement.

2.3.1 Optimization of thermal activated BS and TB

The surface area optimization of thermal activated of BS and TB was carried out using ChemiSorb surface area analyzer due the low surface area of thermal activated BS and TB adsorbents and the obtained results are presented in the Table 2.1 and 2.2. Carbonization temperature and time have considerable effect on the surface area. When carbonization temperature was 200^{o}C, pyrolysis reaction of both adsorbents had just commenced, thereby producing very small BET surface area of BS and TB. The maximum BET surface area of BS (25.81 m^2/g) and TB (21.26 m^2/g) adsorbent was obtained at 300^{o}C of 1.5 hr and 400^{o}C of 1.5 hr activation time. Beyond this temperature limits BET surface area of both the adsorbents were decreased. Hence, the BS and TB adsorbents produced at 300^{o}C for 1.5 hr and 400^{o}C for 1.5 hr were chosen as optimized adsorbents for the application of targeted wastewater contaminant removal.

2.3.2 Optimization of chemical activated BS and TB

Surface area optimization of different chemical activated adsorbents was carried out using single point surface area method using ChemiSorb. BET surface area values of various concentrations of H_3PO_4, H_2SO_4, HCl and KOH activated BS and TB at particular impregnation ratio are presented in the Table 2.3, 2.4, 2.5 and 2.6, respectively. BET results of BS and TB shows that surface area increases with increase in concentrations of H_3PO_4, H_2SO_4, HCl and KOH. These phenomena may be due to more reaction between concentrated chemicals and adsorbent cell wall elements for the formation of high surface area. The maximum BET surface area of H_3PO_4 (66%), H_2SO_4 (98%) and KOH (0.75 M) activated BS and TB was 12.62 and 9.327 m^2/g, 34.28 and 21.35 m^2/g, 13.44 and 12.61 m^2/g, respectively. Similarly, maximum BET surface area of BS (6.871 m^2/g) and TB (10.42 m^2/g) was achieved

for HCl activation at 1:3 (w/v) impregnation of precursor and acid. Chemical activated high surface area adsorbents were used to remove targeted wastewater contaminants.

2.3.3 Optimization of thermochemical activated BS and TB

Due to the high surface area, H_3PO_4 followed by thermal activated BS and TB were optimized using Beckman Coulter surface area analyzer and rest of the thermochemical activated adsorbents such as (H_2SO_4 + thermal), (HCl + thermal) and (KOH + thermal) activated BS and TB were analysed using Chemisorb analyzer. After chemical treatment of BS and TB with HCl, H_2SO_4 and KOH, activation temperature and time were chosen in the range of 200°C to 400°C and 1 hr, respectively to avoid the huge weight loss. The BET surface area of HCl, H_2SO_4 and KOH treated followed by thermal activated BS and TB adsorbents are presented in Table 2.7 to 2.12. However, thermochemical activation of BS using H_3PO_4 was carried out at various temperatures, concentration of acid and activation time since the temperature stability of (BS + H_3PO_4) mixer and the BET results of the adsorbents are presented in Table 2.13. To avoid the huge adsorbent weight loss as well as acid wastage, thermochemical activation of TB using H_3PO_4 was carried out at the optimum activation time of BS with various action temperatures and concentration of acid and the results are provided in the Table 2.14. The maximum BET surface area of thermochemical activated BS (1954 m^2/g) and TB (893 m^2/g) using 44% H_3PO_4 was obtained at 400°C of 1.5 hr activation time. The high BET surface area adsorbents of thermochemical activated BS and TB were selected for the removal targeted wastewater contaminants.

2.4 PRELIMINARY PERFORMANCE EVALUATION TEST (PPET)

The interaction and the binding capacity of any adsorbent with particular contaminant/adsorbate are not only depending on surface area that includes many other factors such as surface charge and surface groups, depends on the original raw material and the way of activation. Hence, this test was conducted to identify the potentiality and suitability of all high surface area adsorbents which are synthesized by three activation methods with targeted pollutants before starting detail adsorption

study. The PPET results of each synthesized BS and TB adsorbents with targeted pollutants such heavy metals (Cr^{6+}, Pb^{2+}, Ni^{2+} and Sr^{2+}), phenolics (phenol and *o*-cresol) and cationic dyes (rhodamine B and methylene blue) are provided in the Table 2.15, 2.16 and 2.17. Output of the PPET is highlighted below:

- PPET result reveals that thermal, H_3PO_4, KOH, (HCl + thermal) and (KOH + Thermal) activated BS and TB has less adsorption capacity with the targeted metals and phenols.
- HCl treated tannery residual biomass (HTB) has good interaction with Cr^{6+}, rhodamine B and methylene blue.
- H_2SO_4 treated bael shell (SBS) and TB (STB) has higher adsorption capacity with Pb^{2+}, Ni^{2+}, Sr^{2+}, rhodamine B and methylene blue dye when compare to its thermochemically treated (H_2SO_4 + thermal) BS and TB adsorbent.
- H_3PO_4 treated followed by thermal treated bael shell (BSAC) and TB (TBAC) gives the high adsorption capacity with Cr^{6+}, Sr^{2+}, phenol, *o*-cresol, rhodamine b and methylene blue.
- Other optimized high surface area adsorbents have considerable adsorption capacity with only cationic dyes not with targeted metals and phenols.

Due to the work and time limitation, TB (HTB), H_2SO_4 treated BS (SBS) and H_3PO_4 treated followed by thermal activated BS (BSAC) and TB (TBAC) adsorbents were only chosen for further elaborative adsorption studies with selected contaminants in the PPET.

Chapter 2
Figures & Tables

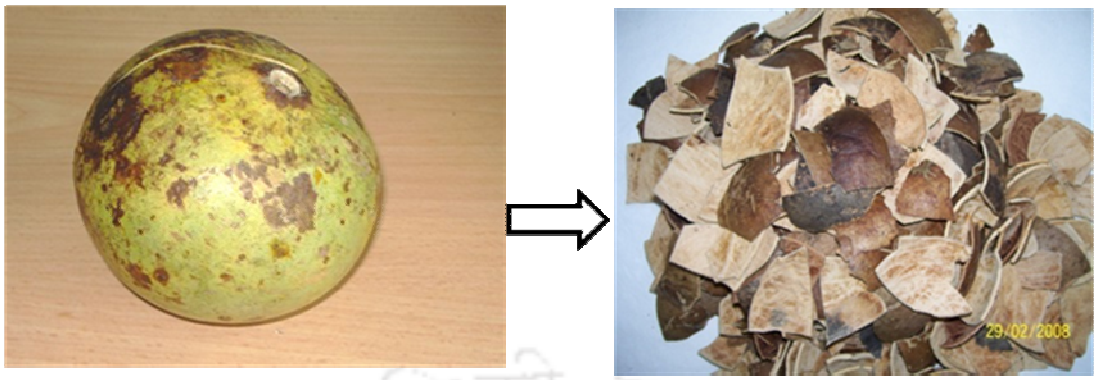

Figure 2.1 (a) Bael fruit (*Aegle marmelos correa)* (b) Shredded Bael Fruit shell

Figure 2.2 (a) Tannery residual biomass (b) Shredded tannery residual biomass

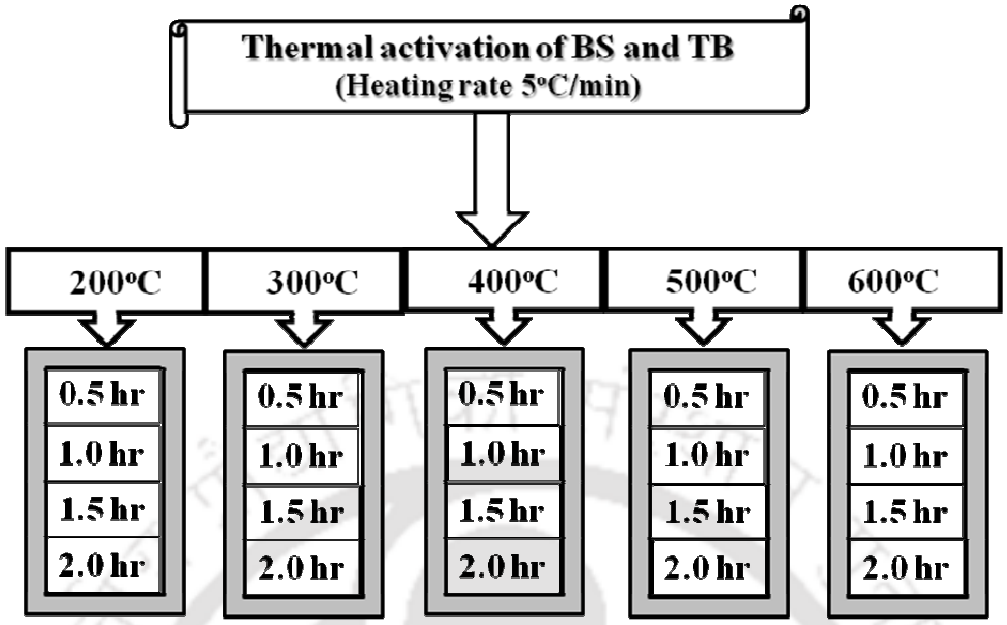

Figure 2.3 Thermal activation method for adsorbents synthesis

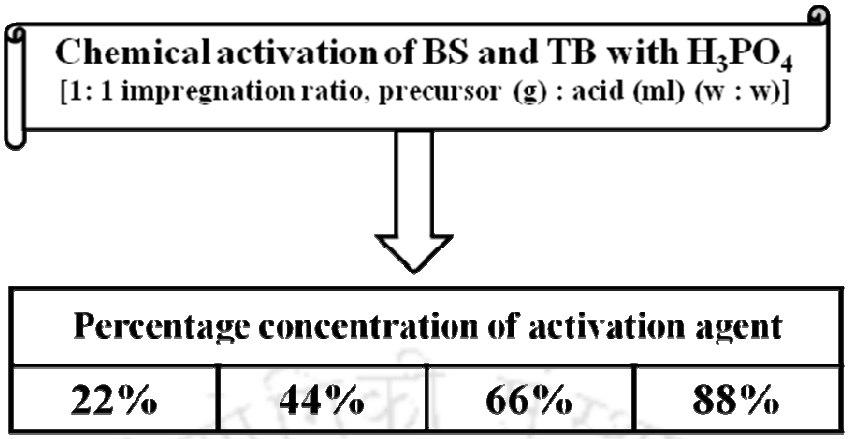

Figure 2.4 H_3PO_4 activation method for adsorbents synthesis

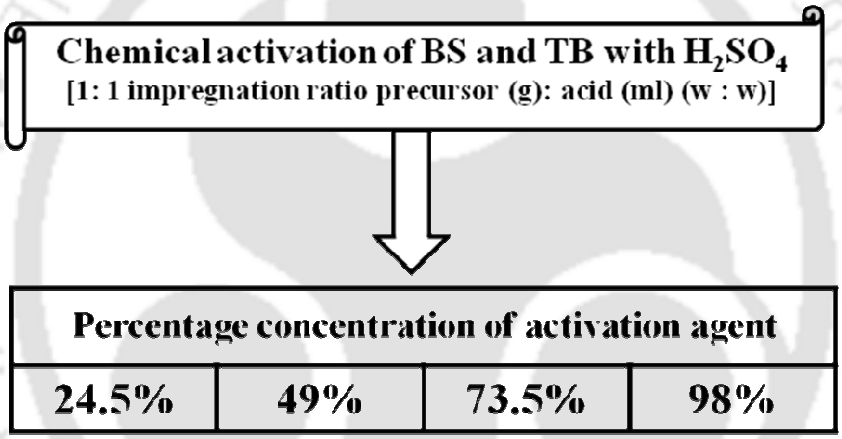

Figure 2.5 H_2SO_4 activation method for adsorbents synthesis

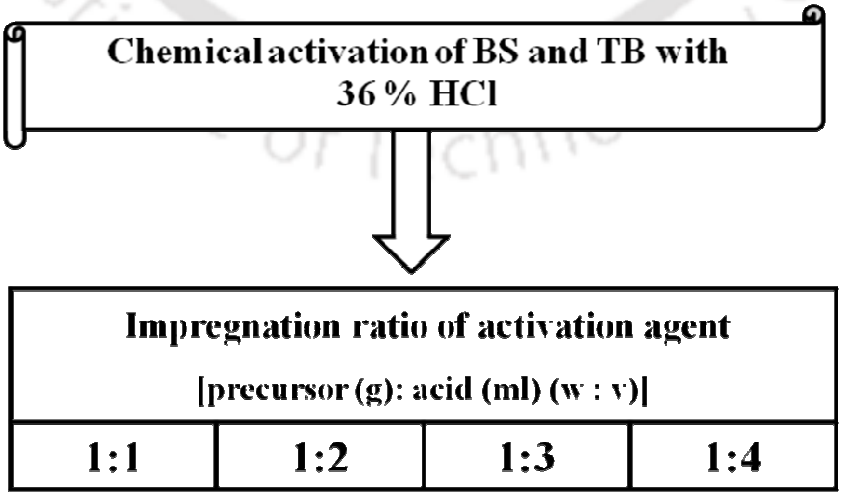

Figure 2.6 HCl activation method for adsorbents synthesis

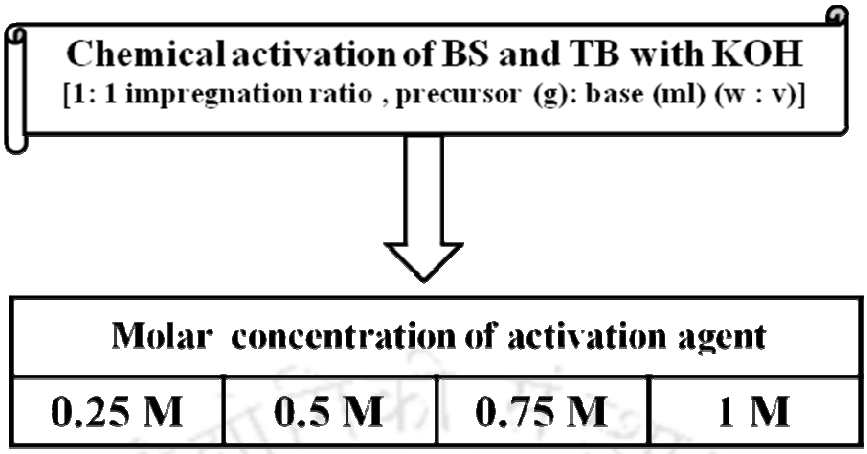

Figure 2.7 KOH activation method for adsorbents synthesis

Chemicals	Different concentrations/ impregnation ratios (IR) of activation agents			
HCl 36% acid	1:1 (IR = w:v)	1:2 (IR = w:v)	1:3 (IR = w:v)	1:4 (IR = w:v)
H_2SO_4 IR = 1:1 (w:w)	24.5%	49%	73.5%	98%
KOH IR = 1:1 (w:v)	0.25 M	0.5 M	0.75 M	1 M
	Thermal activation temperature and time			
	200 to 400°C & 1.0 hr	200 to 400°C & 1.0 hr	200 to 400°C & 1.0 hr	200 to 400°C & 1.0 hr

Figure 2.8 Thermochemical activation method for BS and TB adsorbent synthesis using HCl, H_2SO_4 and KOH

% of H_3PO_4 acid used for activation [impregnation ratio (precursor (g): acid (g)) = 1:1 (w:w)]															
22%				44%				66%				88%			
Activation temperature and time (hr)															
0.5	1.0	1.5	2.0	0.5	1.0	1.5	2.0	0.5	1.0	1.5	2.0	0.5	1.0	1.5	2.0
300 to 400°C				300 to 400°C				300 to 400°C				300 to 400°C			

Figure 2.9 Thermochemical activation method for BS and TB adsorbent synthesis using H_3PO_4

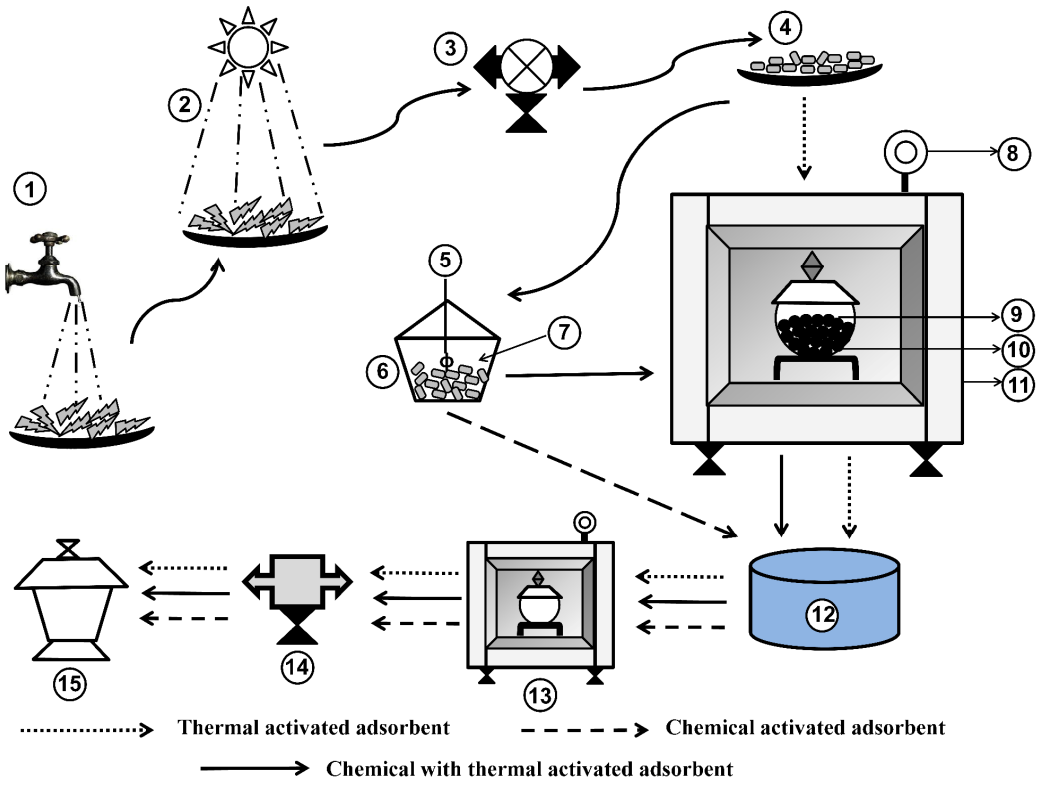

Figure 2.10 Thermal, chemical and thermochemical activation layout

1. Tap water washing 2. Sunlight drying 3. Ball mill 4. Shredded precursor 5. Stirrer 6. Glass-vessel 7. Acid addition 8. Temperature indictor 9. Precursor 10. Crucible 11. Muffle furnace 12. Washing bath 13. Hot-air oven 14. Hammer mill with screen 15. Decicator

Table 2.1

BET surface area of thermal activated BS

BS Adsorbent	BET Surface area at various temperature and time			
	0.5 hr	**1 hr**	**1.5 hr**	**2 hr**
200°C	3.272	5.829	8.722	9.272
300°C	8.56	17.37	25.81	23.72
400°C	11.23	18.72	24.26	24.34
500°C	12.37	20.17	23.42	25.53
600°C	9.724	25.73	23.68	24.73

Table 2.2

BET surface area of thermal activated TB

TB Adsorbent	BET Surface area at various temperature and time			
	0.5 hr	**1 hr**	**1.5 hr**	**2 hr**
200°C	1.676	3.762	6.376	6.742
300°C	2.826	5.741	8.863	9.671
400°C	4.622	12.73	21.26	18.37
500°C	7.723	20.35	20.73	19.63
600°C	9.331	15.73	17.48	16.83

Table 2.3

BET surface area of H_3PO_4 activated BS and TB

Adsorbent	BET Surface area at various concentrations of H_3PO_4			
	22%	44%	66%	88%
BS	3.371	7.316	12.62	12.49
TB	2.421	4.567	8.219	9.327

Table 2.4

BET surface area of H_2SO_4 activated BS and TB

Adsorbent	BET Surface area at various concentrations of H_2SO_4			
	24.5%	49%	73.5%	98%
BS	17.61	21.39	28.45	34.28
TB	4.652	10.32	18.53	21.35

Table 2.5

BET surface area of HCl activated BS and TB

Adsorbent	BET Surface area at various impregnation ratios [Precursor (g) / HCl (ml)]			
	1:1	1:2	1:3	1:4
BS	2.351	3.517	6.643	6.871
TB	3.844	5.868	10.42	9.977

Table 2.6

BET surface area of KOH activated BS and TB

Adsorbent	BET Surface area at various concentrations of KOH			
	0.25 M	0.50 M	0.75 M	1.0 M
BS	5.124	7.481	13.44	12.16
TB	1.683	4.161	12.61	9.37

Table 2.7

BET surface area of thermochemically (HCl + thermal treatment) activated BS

BS Adsorbent	BET Surface area at various impregnation ratios [Precursor (g) / HCl (ml)]			
	1:1	**1:2**	**1:3**	**1:4**
200°C	9.681	11.42	39.68	39.42
300°C	17.38	213.4	322.2	287.2
400°C	25.41	69.42	153.2	172.3

Table 2.8

BET surface area of thermochemically (HCl + thermal treatment) activated TB

TB Adsorbent	BET Surface area at various impregnation ratios [Precursor (g) / HCl (ml)]			
	1:1	**1:2**	**1:3**	**1:4**
200°C	6.708	12.49	17.62	26.37
300°C	16.42	15.41	12.59	13.16
400°C	9.619	7.468	5.868	3.437

Table 2.9

BET surface area of thermochemically (H_2SO_4 + thermal treatment) activated BS

BS Adsorbent	BET Surface area at various concentrations of H_2SO_4			
	24.5%	**49%**	**73.5%**	**98%**
200°C	2.453	6.709	10.07	17.61
300°C	12.41	13.16	26.37	25.41
400°C	18.63	10.07	8.431	6.709

Table 2.10

BET surface area of thermochemically (H_2SO_4 + thermal treatment) activated TB

TB Adsorbent	BET Surface area at various concentrations of H_2SO_4			
	24.5%	**49%**	**73.5%**	**98%**
200°C	6.471	9.872	17.61	12.54
300°C	12.49	16.83	16.72	9.432
400°C	12.30	10.06	6.652	4.468

Table 2.11

BET surface area of thermochemically (KOH + thermal treatment) activated BS

TB Adsorbent	BET Surface area at various concentrations of KOH			
	0.25 M	**0.50 M**	**0.75 M**	**1.0 M**
200°C	13.37	18.28	20.22	19.36
300°C	21.62	39.73	38.14	35.72
400°C	20.52	35.17	36.62	31.51

Table 2.12

BET surface area of thermochemically (KOH + thermal treatment) activated TB

TB Adsorbent	BET Surface area at various concentrations of KOH			
	0.25 M	**0.50 M**	**0.75 M**	**1.0 M**
200°C	12.76	19.34	23.52	23.18
300°C	11.42	16.47	22.82	19.53
400°C	14.38	19.93	20.18	17.11

Table 2.13

BET surface area of thermochemically (H_3PO_4 + thermal treatment) activated BS

Concentration of H_3PO_4	Activation time (hr)	BET Surface area at various temperatures of BS			
		300°C	400°C	500°C	600°C
22%	0.5	57.35	109	164	151
	1.0	148.7	252	283.2	264
	1.5	273	427	539	547
	2.0	462	567	496	542
44%	0.5	423	754	986	1050
	1.0	721	1514	1740	1372
	1.5	1049	1954	1795	1662
	2.0	1184	1444	1589	1548
66%	0.5	251	332	671	723
	1.0	641	742	1043	1096
	1.5	1206	1690	1721	1285
	2.0	1520	1806	1716	1071
88%	0.5	183	277	447	599
	1.0	507	687	862	1071
	1.5	1066	1179	1609	1080
	2.0	1503	1560	1402	1372

Table 2.14

BET surface area of thermochemically (H_3PO_4 + thermal treatment) activated TB

TB Adsorbent	BET Surface area at various concentrations of H_3PO_4			
	22%	44%	66%	88%
300°C	164.28	513.46	557.4	767.41
400°C	508.48	892.57	883.41	854.23
500°C	888.13	792.45	761.72	527.65
600°C	775.66	508.48	648.1	204.58

Table 2.15 Preliminary performance evaluation test (PPET) for the adsorption capacity of BS and TB by thermal activation

Thermal Activated Adsorbents	Heavy Metals (mg/g)				Phenols (mg/g)		Cationic Dyes (mg/g)	
	Cr^{6+}	Pb^{2+}	Ni^{2+}	Sr^{2+}	Phenol	*O*-cresol	RB	MB
Bael Shell	3.1	4.64	1.72	2.83	8.31	6.34	34	41
Tannery Residual Biomass	19.2	6.17	3.37	4.31	9.37	7.82	26	31

Table 2.16 Preliminary performance evaluation test (PPET) for the adsorption capacity of BS and TB by various chemical activations

Chemical Activated Adsorbents	Heavy Metals (mg/g)				Phenols (mg/g)		Cationic Dyes (mg/g)	
	Cr^{6+}	Pb^{2+}	Ni^{2+}	Sr^{2+}	Phenol	*O*-cresol	RB	MB
HCl								
Bael Shell + HCl	18.52	3.27	0.95	4.61	0	0	64	77
Tannery Residual Biomass + HCl	**93.03**	9.61	3.37	6.51	0	0	**89.3**	**100**
H_2SO_4								
Bael Shell + H_2SO_4	28.43	**81.6**	**52.89**	**69.95**	14.7	11.5	**97.1**	**99.43**
Tannery Residual Biomass + H_2SO_4	23.62	**44.55**	**27.28**	**31.27**	11.2	16.4	**92.26**	**94.7**
H_3PO_4								
Bael Shell + H_3PO_4	6.35	0.37	2.05	3.11	2.4	3.2	46.2	51.7
Tannery Residual Biomass + H_3PO_4	8.38	9.61	3.37	4.63	1.5	2.7	41.7	44.5
KOH								
Bael Shell + KOH	0	0.63	0.26	1.24	3.1	1.4	17.65	19.53
Tannery Residual Biomass + KOH	0	2.28	0.27	2.11	2.7	2.4	16.37	21.7

Table 2.17 Preliminary performance evaluation test (PPET) for the adsorption capacity of BS and TB by various thermochemical activations

Chemical + Thermal activated Adsorbents	Heavy Metals (mg/g)				Phenols (mg/g)		Cationic Dyes (mg/g)	
	Cr^{6+}	Pb^{2+}	Ni^{2+}	Sr^{2+}	Phenol	*O*-cresol	RB	MB
HCl								
Bael Shell + HCl + Heat Treatment	7.2	3.27	0.95	4.61	7.01	8.67	39.2	44.2
Tannery Residual Biomass + HCl + Heat Treatment	33.2	7.22	4.17	7.15	8.36	6.2	31.5	35.82
H_2SO_4								
Bael Shell + H_2SO_4 + Heat Treatment	8.7	31.2	**22.19**	**39.05**	18.7	16.5	**86.27**	**87.71**
Tannery Residual Biomass + H_2SO_4 + Heat Treatment	13.63	37.55	**21.72**	**28.11**	17.38	13.3	**79.6**	**81.3**
H_3PO_4								
Bael Shell + H_3PO_4 + Heat Treatment	**63.57**	**26.97**	17.62	**47.11**	**71.36**	**80.21**	**99.95**	**99.08**
Tannery Residual Biomass + H_3PO_4 + Heat Treatment	**60.98**	13.42	6.37	**41.23**	**75.31**	**77**	**98.28**	**97.71**
KOH								
Bael Shell + KOH + Heat Treatment	0	2.51	1.17	3.43	0	0	17.2	21.6
Tannery Residual Biomass + KOH + Heat Treatment	0	1.47	0.82	2.91	0	0	23.1	27.3

Note: C_o = 100 mg/l (all metals, phenol, o-cresol, RB and MB dye), W = 0.05 g, V = 50 ml, T = 30°C, t = 24 hr (dyes), 8 hr (metals) and 6 hr (phenol and *o*-cresol), R = 180 rpm.

CHAPTER 3

ADSORPTION OF SELECTED CONTAMINANTS ON THERMOCHEMICALLY ACTIVATED BAEL SHELL

This chapter presents the elaborative batch adsorption studies of highly removable heavy metals, phenols and cationic dyes which are identified in the preliminary performance evaluation test (PPET) using high surface area Bael shell activated carbon obtained by H_3PO_4 treated followed by thermal activation. In chapter 2, from PPET it was identified that Cr^{6+}, Sr^{2+}, phenol, o-cresol, rhodamine B (RB) and methylene blue (MB) had high interaction with BSAC compare to other activated Bael adsorbents. Therefore, the detailed adsorption studies which were carried out with aforementioned components using BSAC are reported and the results also discussed elaborately in this chapter. It also describes various kinetic and isotherm model fittings as well as thermodynamic parameters.

3.1 INTRODUCTION

Industries such as textile, paper and pulp, cosmetics, paint and pigments, pesticide, pharmaceutical, petroleum and leather tanning produce large amount of colored effluent and considerable amount of phenolic components along with toxic metals (Anandkumar and Mandal, 2011; Liu *et al.,* 2010). Discharge of such effluents in ecosystem results the aesthetical and toxicological problems. Hexavalent chromium (Cr^{6+}), Sr^{2+}, phenol, *o*-cresol, rhodamine B (RB) dye and methylene blue (MB) dye are widely used in the above industries especially in tanneries. In this chapter, results of batch adsorption experiments which were carried out in single, binary and ternary contaminant systems of Cr^{6+}, Sr^{2+}, phenol, *o*-cresol, rhodamine B (RB) dye and methylene blue (MB) dye using high surface area BSAC are presented and discussed in detail. The significant parameters that influence the adsorption process such as solution pH, temperature, presence of other co-ions and effect of binary and ternary contaminant systems were monitored in this study to optimize the sorption process. Moreover, the detailed adsorption mechanism of each component has been derived with the help of surface chemistry and characterization of adsorbent.

3.2 EXPERIMENTAL METHODS

3.2.1 Preparation of Synthetic Solution

A stock solution of Cr^{6+}, Sr^{2+}, phenol, *o*-cresol, rhodamine B (RB) and methylene blue (MB) dye (1000 mg/l) was prepared by dissolving appropriate quantity of $K_2Cr_2O_7$, $SrCl_2.6H_2O$, phenol, *o*-cresol (Merck, India), RB and MB dye (C.I. 45170 and 52015, LOBA Chemie, India) in Millipore water, respectively. The chemical structure of RB and MB is illustrated in Appendix 1. The stock solution was mixed thoroughly for 10 min at 180 rpm to obtain complete dissolution and then suitably diluted with water to get the required initial concentrations (50 to 300 mg/l of Cr^{6+} and Sr^{2+}, 100 to 600 mg/l of phenol and *o*-cresol, and 100 to 600 mg/l of RB and MB dye). The pH of the solution was adjusted using 0.1 N HCl or 0.1N NaOH before mixing the adsorbent. The pH of the solution was measured by pH meter (Eutech, model: 510).

3.2.2 Experimental Protocol

In order to study the nature of interaction of BSAC with Cr^{6+}, Sr^{2+}, phenol, *o*-cresol RB and MB dyes, initially the effect of pH on adsorption capacity was carried out under batch mode experiment. Then further experiments on the effect of other co-ions and solution temperature were conducted in single contaminant system using fixed doses (0.05 g per 50 ml) of BSAC at 180 rpm in an incubating shaker (LabTech, Model LSI-1005R) at optimum pH. The pH of each Cr^{6+}, Sr^{2+}, phenol, *o*-cresol, RB and MB dye solution was adjusted using 1N HCl (or) 1N NaOH before mixing the adsorbent. Consequently, the effect of binary and ternary system was conducted at various favourable pH. In binary and ternary system, the concentration range of one contaminant was changed at a time while others were maintained constant for Cr^{6+}, phenol and RB dye system. However, for Sr^{2+}, *o*-cresol and MB dye system concentrations of mixed components were maintained constant in each combination.

Samples at predefined time intervals were withdrawn and the supernatant of Cr^{6+} and Sr^{2+} solution was separated by filtration using Whatman filter paper no. 42. Final residual metal concentrations were directly measured by flame atomic absorption spectrophotometer (AAS) (Varian spectra, AA240) with an air–acetylene flame. Similarly, the supernatant of RB dye, MB dye, phenol and *o*-cresol solutions were separated by centrifuge (5000 rpm) and the filtrate of dyes were analyzed for the residual dye concentrations using UV–visible spectrophotometer (Perkin-Elmer, model: Lambdas 45) at the maximum wavelength (λ_{max} = 555 nm for RB and 667 nm for MB) of the dyes. The final residual concentration of phenol and *o*-cresol was analyzed by HPLC (ProSTAR, Varian) equipped with a UV-vis detector and C18 column (particle size: 5 µm, length 15 cm, diameter 4.6 mm) at room temperature with a mobile phase of acetonitrile (80%): water (20%) at a flow rate of 0.8 ml/min. An aliquot of 20 µl of the sample was injected and analyzed using a UV-vis detector at a wavelength of 280 nm. Three replicates per sample were done and the average results are taken for calculation.

For desorption experiment, 50 ml eluent solution was added in a conical flask with adsorbate adsorbed BSAC of 0.1 g. This was subjected to an incubating shaker at 180 rpm agitation speed for 24 hours. Then it was again filtered or centrifuged and desorbed concentrations of adsorbate were determined from the filtrate. In this study,

before desorption 100 mg/l of Cr^{6+} and Sr^{2+}, 200 mg/l of phenol, *o*-cresol, RB and MB dye was used for adsorption purpose. The eluents of 0.1 M HCl, 0.1 M HNO_3, 0.1 M CH_3COOH, 0.01 M EDTA and hot distilled water were used for desorption.

Adsorption/desorption percentage and the adsorption capacity/desorption capacity of adsorbent was calculated using the calculations provided in the Appendix 2.

3.2.3 Adsorbent Characterization

The surface texture and porosity of four different prospect of BS such as raw precursor, overall porous structure, one particular pore after treatment and surface structure after the adsorption was observed using Scanning electron microscopy (SEM) (Leo, 1430 vp, Carl Zeiss, German) characterisation. Energy dispersive X-ray spectroscopy (EDX) analysis was employed for further confirmation of metal binding. The morphological properties of BSAC were measured in Beckman-Coulter Surface area analyser (SA™ 3100) using nitrogen adsorption/desorption isotherms at −196°C. The samples were degassed using Helium at 200°C for 2 h before measurement. The surface area was calculated using a multipoint Brunauer-Emmett-Teller (BET) model. The pore size distribution was obtained through the Barrett, Joyner and Halenda (BJH) model using the desorption isotherms and the total pore volume was estimated at a relative pressure of 0.98, assuming full surface saturation with nitrogen. To resolve the functional groups of BSAC, spectra analysis was recorded on a KBr translucent sample disk, which contains 5% sample by weight, using a Fourier transform infrared spectrometer (FT-IR) (Perkin Elmer, PE-RXI) in the range of 500–4000 cm^{-1}. Zeta potential of BSAC was measured using Beckman Coulter zeta potential analyzer (Delsa™ Nano C) at various pH based on the laser Doppler electrophoresis technique. X-ray photoelectron spectroscopy (XPS) (Zetasizer Nano, Malvern Instruments Ltd UK) analysis was done to analyze the oxidation states of chromium at Cr2p orbital core region.

3.3 RESULTS AND DISCUSSION

3.3.1 Characterization of Activated Carbon

3.3.1.1 SEM Analysis

Figure 3.1a depicts that the BS precursor (before activation) having irregular surface with no pores on it, whereas after activation (Figure 3.1b) BSAC having well

developed honeycomb structured pores on the surface. Figure 3.1c (i.e., zooming of single pore) reveals the branch of interior mesopores and micropores of each outside macro pores. The pore formation of BS is mainly attributed to the addition of H_3PO_4 which causes the BS to swell and it opens the surface structure. During activation, phosphoric acid acts as a stabilizer, H_3PO_4 fills up the cavities of the cellulose structure and then due to high temperature during carbonization H_3PO_4 evaporates out of those cavities forming various pores with active sites on the surface of BS (Girgis *et al.,* 2002; Serrano *et al.,* 2004; Mohanty *et al.,* 2005). Figures 3.1d to 3.1f shows the SEM morphology of BSAC after Cr^{6+}, RB and MB dye adsorption. There is a clear indication of adsorbed chromium, RB and MB dye on BSAC as a newly bulky coated layer over the surface and some have occupied inside the pores of BSAC after adsorption.

3.3.1.2 Energy Dispersive X-ray Spectroscopy (EDX) Analysis

Previous investigations reported that natural adsorbents bear many oxygen surface groups such as acidic character (carboxylic and lactonic), non-acidic (ether, quinine and carbonyl), phenol group and anhydride (Serrano et al., 2004). It has been found from Figure 3.2a that BSAC having the carbon, oxygen and phosphorous elements on its surface before interaction with Cr^{6+} and Sr^{2+} ions, whereas in Figures 3.2b and 3.2c new chromium and strontium peaks were observed with the surface bearing groups of carbon, oxygen and phosphorous, which confirmed the chromium and strontium adsorption on BSAC.

3.3.1.3 BET Surface Area Analysis

The nitrogen adsorption/desorption isotherms and pore size distribution of the BSAC is shown in Figures 3.3a and 3.3b, respectively. It is observed from Figure 3.3a that adsorption isotherm is close to type IV of the BDDT classification typical of mostly mesoporous carbon material. The nitrogen adsorption isotherm of this activated carbon also show a H4 type hysteresis loop, characteristic of the slit-shaped pores where the adsorption and desorption branches are parallel (Murillo *et al.,* 2004). The main adsorption characteristics of the activated carbon are summarized in Table 3.1. The pore size distribution was calculated using the Barrett–Joyner–Halenda (BJH) model applied to the adsorption branch of the isotherm, assuming cylindrical pore geometry. Figure 3.3b shows that majority of the pore sizes lie within the mesoporous

range. The total distribution curve is not available due to limitation of the instrument to measure pore size below 3 nm (Monash and Pugazhenthi, 2009). However, summery of BET report (Table 3.1) shows that the synthesized BSAC has considerable amount of micro pore volume and surface area. The total surface area of BSAC is 1954 m^2/g, of which 17% is contained in micropores and rest in meso as well as macropores. The total pore volume of BSAC is 1.2658 ml/g of which 9% is contained in micropores.

3.3.1.4 Fourier Transform Infrared (FT-IR) Analysis

The FT-IR spectra of BS (Figure 3.4a) and BSAC (Figure 3.4b) were recorded to acquire the information regarding wave number changes on the functional groups in the range of 500–4000 cm^{-1}. Table 3.2 presents some of the basic band frequencies of BS and BSAC. The band frequency around 3421 cm^{-1} indicates the existence of hydroxyl (-OH) groups and its significant shift from 3421 to 3421 cm^{-1} reveals the formation of active (-OH) sites for adsorption. At low pH (2.0), H^+ ions neutralize (protonation) the surface bearing -OH groups and then it turns to $-OH_2^+$ site and hence it enhanced the negative $HCrO_4^-$ ion adsorption (Uysal and Ar, 2007; Dakiky *et al.*, 2002).

$$OH_2^+ + HCrO_4^- \leftrightarrow OH_2^+(HCrO_4^-) \quad (3.1)$$

Similar observation has been reported by Mohanty *et al.* (2006) for *Eichhornia crassipes* with chromium binding (peak shifting from 3419 to 3405 cm^{-1}). However, when reaction pH increased from acid to neutral and then alkaline pH, RB and MB dye molecules, Sr^{2+}, *o*-cresol and phenol ions were binded with –OH sites through electrostatic attraction.

The band 2923 and 2924 cm^{-1} is assigned to the stretching vibrations of C-H groups, 1535 and 1554 cm^{-1} is an identification of COO, C=O groups, 1103 and 1054 cm^{-1} is the stretching vibrations of C-O-C, $-OCH_3$ (lignin structure in BS). Also, the absorption peak at 2850 cm^{-1} is assigned to –CH stretching (Li *et al.*, 2008). The amino groups (2347 and 2374 cm^{-1}) that exist ($-NH_3^+$ and $-NH^+$) in positive form is predominantly responsible for interaction with ($HCrO_4^-$) and phenolate ($C_6H_5O^-$) anions in acidic pH and that cannot coordinate with reduced Cr^{3+}, RB and MB

molecules (Li *et al.,* 2008). In Figure 3.4b there is little change in each BSAC absorption peaks compare to BS, this might be due to the creation of active sites on the cell wall functional groups. It has also been suggested that the oxidative treatment of adsorbent with H_3PO_4 would introduce more acidic C=O groups on the surface of adsorbent. This would enhance the electrostatic interaction between adsorbent surface groups and $HCrO_4^-$. The other bending vibrations below 545 cm^{-1} were the finger print zones that indicated the phosphate functional groups (Mohan and Sreelakshmi, 2008).

3.3.1.5 Point of Zero Charge (pH_{pzc}) Analysis

The change in solution pH also alters the charge of the adsorbent surface due to protonation and deprotanation reaction with excess H^+ and OH^- ions. Figure 3.5 shows the measured zeta potential as a function of solution pH for BSAC. The zeta potential results in Figure 3.5 reveals that the positive charge of the BSAC decreases with increase in solution pH. The pH in which the zeta value of BSAC is zero is calculated as point of zero charge (pH_{pzc}) and hence the net charge on the BSAC at pH_{pzc} is zero. In this analysis, pH_{pzc} of BSAC was 3.23. After pH_{pzc}, the surface of BSAC became negative charge and thus favoured for positive Sr^{2+}, MB and RB dye and phenolics ion adsorption.

3.3.2 Effect of pH

The pH of the solution plays an important role to alter the net surface charges of activated carbon and the degree of ionization of the adsorbate (Liu *et al.,* 2010; Subramanyam and Das, 2009). The effect of pH on adsorption capacity of chromium onto BSAC is shown in Figure 3.6a. It was observed from Figure 3.6a that the adsorption of Cr^{6+} decreased with increase in initial pH from 2.0 to 9.0. The maximum removal (63.57 mg/g) occurred at initial pH 2.0 for BSAC. At lower pH the surface area of the adsorbent was more protonated and competitive negative ions ($HCrO_4^-$ and $Cr_2O_7^{2-}$) adsorption occurred between positive surface and free chromate ion. Adsorption of Cr^{6+} at pH 2.0 shows the bind of the negatively charged chromium species ($HCrO_4^-$) occurred through electrostatic attraction to the positively charged (due to more H^+ ions) surface functional groups of the adsorbent (Uysal and Ar, 2007; Barrera *et al.,* 2006). But in highly acidic medium (pH ≈ 1), H_2CrO_4 (neutral form) is the predominant species of Cr^{6+} as reported by Agrawal *et al.* (2008)

and Hamadi *et al*. (2001). Hence, at pH 1.0 adsorption capacity decreased due to the involvement of less number of $HCrO_4^-$ anions on the positive surface. At higher pH due to more OH^- ions adsorbent surface carrying net negative charges (see zeta values of BSAC in Figure 3.5), which tend to repulse the metal anions (CrO_4^{2-}) (Amarasinghe and Williams, 2007). However, there is also some percentage adsorption at pH > 2.0 but the rate of adsorption is reduced. This might be due to the weakening of electrostatic force of attraction between the oppositely charged adsorbate and adsorbent or physisorption due to weak undirected Van der Waals forces of attraction (Mohanty *et al.,* 2005; Baral *et al.,* 2006). When reaction pH increased after 2.0, Cr^{3+} adsorption also enhanced due to gradual increasing the negative charge on adsorbent. But the adsorption-coupled reduction (explained in adsorption mechanism section) of Cr^{6+} to Cr^{3+} was less after pH 2.0 due to the less adsorption of $HCrO_4^-$. At pH ≈ 8.0 CrO_4^{2-} is the predominant form and it was repulsed by high negative surface (Li *et al.,* 2008). Hence, the solution pH 2.0 was chosen for remaining entire study for Cr^{6+} adsorption.

The pH of the Sr^{2+} solutions (100 mg/l) was varied in the range of 2.0-10.0 keeping all other parameters constant. It was observed from Figure 3.6b that the adsorption of metal increased with increase in initial pH from 2.0 to 6.7. The maximum of Sr^{2+} was observed at pH 6.7 (47.12 mg/g). At low pH, adsorption capacity of Sr^{2+} decreased due to the protonated surface of the BSAC (Dakiky and Khamis, 2002). As the solution pH of Sr^{2+} increased from 2.0 to 6.0, the availability of $-OH^-$ and other negative functional groups increased due to deprotanation for positive metal adsorption. At pH > 7, Sr^{2+} ions precipitate as insoluble hydroxides (Ngah and. Fatinathan, 2010; Kandaha and Meunier, 2007). So, natural or blank pH of Sr^{2+} (between 6.2 ± 0.05) was used as optimum pH throughout the study.

It can be seen from the Figure 3.6c that there is no significant deviation in the adsorption capacity of phenol from pH 2-9 except for a slight decrease at pH 10. The adsorption capacity of phenol was stable from pH 2-9 except for a slight decrease at pH above 9.0 (Figure 3.6c), due to high repulsion of negative phenolate ion $C_6H_5O^-$ with negative cell wall functional groups and $–OH^-$ ions at pH more than 9, which result in decreased adsorption capacity of phenol. Moreover, apart from the electrostatic interaction, phenol having many other interaction with carbon surface

that are discussed in phenol mechanism section (Liu *et al.,* 2010; Girods *et al.,* 2009). Therefore, the blank pH (6.2) of phenol was chosen as optimum pH for the entire study.

The adsorption of *o*-cresol by BSAC was studied at different pH with the initial concentration of 200 mg/l. The effect of pH on the adsorption of *o*-cresol by BSAC has been presented in Figure 3.6d. It is evident from Figure 3.6d that the removal of *o*-cresol by BSAC seemed to show an increased adsorption trend in the pH range of 2 to 6. However, when pH was made to exceed 6, there was a distinct decline in the adsorption of *o*-cresol from solution. At alkaline pH, significant reduction in *o*-cresol adsorption was observed due to the high electrostatic repulsion between the adsorbent and adsorbate (C_7H_8O-) at higher pH. The optimum pH for removal of *o*-cresol by BSAC was found as pH 6.0; hence, all remaining experiments were conducted at blank pH of 6.3.

In case of RB dye adsorption, the maximum adsorption capacity of RB dye was obtained at initial pH 3.5 (199.7 mg/g). There was a sharp increase in adsorption capacity of RB dye (157.2–199.7 mg/g) with increase in pH from 2 to 3.5 (Figure 3.6e) and after pH 3.5, the sorption capacity of RB dye decreased from 199.7 to 113.2 mg/g. At pH ≤ 3.5 RB molecules remain in monomeric form and thus dye molecule can easily enter into the pore structure of the BSAC to enhance the pore diffusion. At pH above 3.5, zwitterionic form of RB in the water might increased the aggregation of RB (bigger molecule) to form the dimer and trimer molecules and thus unable to enter into the micro porous structure of the carbon. Therefore, all further RB dye adsorption studies were carried out at optimum pH 3.5.

Figure 3.6f shows the effect of pH on sorption capacity of MB. It was observed from Figure 3.6f that the sorption of MB increased with increase in initial pH from 2.0 to 7.0. The maximum removal occurred at initial pH 7.0 by BSAC. The amount of dye adsorbed was increased from 94.6 to 193.8 mg/g on the BSAC as the pH was increased from 2 to 7 (Figure 3.6f). At lower pH, positively charged sites of BSAC do not favour for the adsorption of cationic dyes due to the electrostatic repulsion. Adsorption of MB dye at 7.0 pH shows the binding of positively charged MB cations occurred through the electrostatic attraction of the negatively charged (due to more

OH^- ions) functional groups of the adsorbent (Royer *et al.,* 2009). A similar behaviour was observed for MB dye adsorption on different activated carbon reported by El-Qada *et al*. (2008). Also, owing to chemical activation, a number of oxygen-containing functional groups exist in the crystal lattice of the surface, mainly the electron-donors e.g., carbonyl and carboxyl (Anandkumar and Mandal, 2009). It is thus probable that electrostatic interaction occurs between the electron-donor groups of the BSAC and the positive charge of basic dye compound. However, at pH above 8.0, dye removal occurred due to the dissociation of the dye molecules. In this study, the best pH for adsorption of MB on BSAC was observed as 7.0. However, blank pH (6.2) of MB solution was chosen while studying the effect of all other system variables in the adsorption process.

3.3.3 Effect of Other Co-ions in Test Solution

The effect of various co-ions such as K^+, Na^+, NH_4^+, Ca^{2+}, F^-, I^-, Cl^- and NO_2^- on ~~the~~ adsorption capacity of Cr^{6+}, Sr^{2+}, phenol, *o*-cresol, RB and MB dye onto BSAC was studied. The initial concentration of co-ions in the test solution was varied (0.1, 0.5 1, 2 and 5 g/l) by keeping Cr^{6+} (100 mg/l), Sr^{2+} (100 mg/l), phenol (200 mg/l), *o*-cresol (200 mg/l), RB (200 mg/l) and MB dye (200 mg/l) concentration constant in single contaminant system. The presence of NH_4^+, Ca^{2+}, F^-, and I^-, ions in the Cr^{6+} and Sr^{2+} solution significantly reduces the adsorption capacity of Cr^{6+} and Sr^{2+} at higher concentrations (2-5 g/l), but no significant alteration in the adsorption capacity of Cr^{6+} was found when K^+, Na^+, and Cl^- ions were simultaneously present in the metal solution. The adsorption capacity of RB an MB dye was not affected by these co-ions. Whereas in phenol and *o*-cresol adsorption, NH_4^+ and NO_2^- ions considerably enhanced the phenol and *o*-cresol adsorption on BSAC at their higher concentrations and rest of the co-ions had no effect on phenol and *o*-cresol adsorption.

3.3.4 Effect of Binary and Ternary Contaminant System

A study to evaluate the change in Cr^{6+}, phenol and RB dye sorption capacities of BSAC was carried out in various binary and ternary combinations such as (Cr^{6+} + phenol), (phenol + RB dye), (Cr^{6+} + RB dye) and (Cr^{6+} + phenol + RB dye). To study about one component in each combination, only that particular contaminant concentration was changed at a time while others were maintained constant. It was

observed from Figures 3.7a to 3.7c that the individual adsorption capacity of Cr^{6+}, phenol and RB dye in their multi-contaminant system such as [(Cr^{6+} + RB dye) and (Cr^{6+} + phenol + RB dye)], (phenol + Cr^{6+}) and [(RB dye + Cr^{6+}), (RB dye + phenol) and (RB dye + Cr^{6+} + phenol)] decreased while compared to their single system. However, there was a significant enhancement of phenol (Figure 3.7b) adsorption in (phenol + RB dye) and (Phenol + RB dye + Cr^{6+}) combination compared to its single adsorption system. This increasing affinity of phenol on BSAC when RB dye was combined with phenol might be attributed to the modification of overall charge within the system or varying the chemical characteristics of the carbon surface or the reorientation of adsorbed molecules. This impact is known as cooperative adsorption as reported by Aksu *et al.* (2009). Whereas in case of Cr^{6+} adsorption in (Cr^{6+} + phenol) combination, there was no significant change in adsorption capacity. The obtained results from binary and ternary adsorption system indicates that the phenol adsorption in (phenol + RB dye), (phenol + RB dye + Cr^{6+}) system is synergistic behavior (Srivastava *et al.*, 2006; Ngah and Fatinathan, 2010). However, the adsorption behavior of Cr^{6+}, phenol and RB dye in [(Cr^{6+} + RB dye) and (Cr^{6+} + phenol + RB dye)], (phenol + Cr^{6+}) and [(RB dye + Cr^{6+}), (RB dye + phenol) and (RB dye + Cr^{6+} + phenol)] system is antagonistic. Similar observation has been reported for the binary and ternary adsorption of Pb^{2+}, Ni^{2+} and Sr^{2+} in another study (Anandkumar and Mandal, 2012). The BSAC had the highest affinity for phenol and the least affinity for Cr^{6+} in ternary system. The sorption affinity order was found as RB dye > phenol > Cr^{6+} and phenol > RB dye > Cr^{6+} in single and ternary contaminant system, respectively.

Similarly, another set of binary and ternary adsorption system of (Sr^{2+} + *o*-cresol), (*o*-cresol + MB dye), (Sr^{2+} + MB dye) and (Sr^{2+} + *o*-cresol + MB dye) were carried out to check effect of individual adsorption capacities of each elements in the multi contaminant system. The initial concentrations of Sr^{2+} (100 mg/l), *o*-cresol (200 mg/l) and MB dye (200 mg/l) were used to make each single, binary and ternary combinations [for instance (Sr^{2+} + *o*-cresol + MB dye) = (100 mg of Sr^{2+} + 200 mg of *o*-cresol + 200 mg of MB dye) per liter]. Figure 3.7d shows that the adsorption effects of Sr^{2+}, *o*-cresol and MB dye are similar to the results reported for Cr^{6+}, phenol and RB dye adsorption in their binary and ternary contaminant system. The sorption

affinity order was found as MB dye > *o*-cresol > Sr^{2+} and *o*-cresol > MB dye in single and binary (*o*-cresol + MB dye) contaminant system, respectively (Figure 3.6d).

3.3.5 Adsorption Isotherm Studies

In order to optimize the design of adsorption process, the adsorption equilibrium experimental data of Cr^{6+}, Sr^{2+}, phenol, *o*-cresol, RB and MB dye adsorption onto the BSAC were analyzed using Langmuir, Freundlich, Temkin and Halsey isotherms. The theoretical details and mathematical equations of each isotherm model are given in the Appendix-3. The plots of (C_e/q_e versus C_e), ($log\ q_e$ versus $log\ C_e$), (q_e versus $ln\ C_e$) and ($ln\ q_e$ versus $ln\ C_e$) gives the equilibrium data fitting and the linear form of Langmuir (Figure 3.8a to 3.8f), Freundlich (Figure 3.9a-3.9f), Temkin (Figure 3.10a to 3.10f) and Halsey models (Figure 3.11a to 3.11f), respectively in single system. The isotherm constants of single and multi-contaminant system are given in (Tables 3.3a and 3.3b) and (Table 3.4a to 3.4c), respectively. Among the above four models, based on the linear correlation coefficients (refer R^2 values in Tables 3.3a, 3.3b, and 3.4a to 3.4c), Langmuir model is fitted well than other three isotherm models. The sorption capacity of Cr^{6+}, Sr^{2+}, phenol, *o*-cresol, RB and MB dye onto BSAC is competitive in comparison with other recently reported adsorbents in the literature and few are provided in Appendix 4. Moreover, the BSAC simultaneously can remove the toxic Cr^{6+}, Sr^{2+}, phenol, *o*-cresol, RB and MB dye in multi-contaminant system with high efficiency.

3.3.6 Adsorption Kinetics

The sorption kinetics of single contaminant system expressed by the correlation between reaction time and adsorbate (Cr^{6+}, phenol, and RB dye) uptake by BSAC for different initial Cr^{6+} (50-300 mg/l), phenol (100-600 mg/l), and RB dye (100-600 mg/l) concentrations were analyzed with the help of pseudo-first order and pseudo-second-order kinetic models. The theoretical and mathematical details of each kinetic model are given in the Appendix-5. The plots of $log\ (q_e - q_t)$ versus t (Figure 3.12a, 3.13a and 3.14af) and (t/q_t) versus t (Figure 3.12b, 3.13b and 3.14b) for single contaminant system (Cr^{6+}, phenol and RB dye) were used to find out the rate constants of pseudo-first order and pseudo-second-order kinetic models, respectively. The results presented in Table 3.5 shows that pseudo-second-order kinetics could describe the rate-controlling mechanism of single Cr^{6+}, phenol and RB dye system

with extremely high correlation coefficients (R^2) (Reddad *et al.*, 2002). Nevertheless, R^2 value of pseudo-first-order kinetics in Table 3.5 ranging of more than 0.95 for many cases is also acceptable to argue as a best fit, however this model fails to explain the adsorption saturation theoretically (experimental data fit) for all concentrations rather than pseudo second-order kinetics.

3.3.7 Adsorption Thermodynamics

The adsorption capacity of Cr^{6+}, Sr^{2+}, phenol, *o*-cresol, RB and MB dye onto BSAC was studied as a function of temperature from 30ºC to 50ºC in single contaminant system. It has been observed that the sorption capacity of Cr^{6+}, RB and MB dye was increased with increase in temperature. However, for Sr^{2+}, phenol and *o*-cresol adsorption, the adsorption capacity was decreased with increase in temperature. Thermodynamic parameters such as change in free energy ($\Delta G°$), enthalpy ($\Delta H°$) and entropy ($\Delta S°$) associated to the sorption process were obtained using the van't Hoff equation. The theoretical details of adsorption thermodynamics are given in the Appendix-5. The values of $\Delta H°$ and $\Delta S°$ were calculated from the slope and intercept of Van't Hoff plot between $ln\ K_d$ versus $1/T$ (Figures 3.15a to 3.15f) and are listed in Tables 3.6a and 3.6d. The negative values of ΔG^o increased with increase in temperatures indicate the spontaneous nature and the positive ΔH^o values confirmed that the Cr^{6+}, RB and MB dye adsorption process was endothermic. The positive value of ΔS^o showed the increased randomness at the solid–solution interface during adsorption. However, the negative $\Delta H°$ value of Sr^{2+}, *o*-cresol and phenol adsorption indicates the exothermic nature of adsorption and uptake of phenol, Sr^{2+} and *o*-cresol are probably due to the physisorption effect.

3.3.8 Desorption Effect

Desorption experiments of with Cr^{6+}, Sr^{2+}, phenol, *o*-cresol, RB and MB dye loaded BSAC were conducted using various eluents such as 0.1 M HCl, 0.1 M HNO_3, 0.1 M CH_3COOH, 0.01 M EDTA and hot distilled water at equilibrium time. The obtained results are shown in Figure 3.16a, 3.16b and 3.16c. Results depict that highest percentage desorption of (Cr^{6+} and Sr^{2+}), (phenol and *o*-cresol) and (RB and MB dye) with HNO_3 was (85% and 91%), (93% and 94%) and (81% and 74%), respectively. Among all the eluents, water has least desorption efficiency for all adsorbates. The

desorption efficiency of phenol, *o*-cresol, RB and MB dye was high with HNO_3 compared with HCl, CH_3COOH, EDTA and distilled water. Desorption efficiency order of studied eluents with adsorbates were HNO_3 > HCl > CH_3COOH > EDTA and > H_2O.

3.3.9 Adsorption Mechanism

The porosity of activated carbon is not the only factor which contributes to Cr^{6+}, Sr^{2+}, phenol, *o*-cresol, RB and MB dye adsorption. Their chemical characteristics may also have a great influence on the adsorption process. Therefore, it is very important to identify the adsorbate binding mechanism onto BSAC that will ultimately guide for the rational design of the adsorption process.

3.3.9.1 Adsorption Mechanism of Cr^{6+} and Sr^{2+}

The binding mechanism of Cr^{6+} is principally based on ionic equilibrium between Cr^{6+} and Cr^{3+} as well as surface complexation reactions with protonated sites. The main species distribution of Cr^{6+} at pH ≈ 2.0 reported by Barrera *et al.* (2006) and Fahim *et al.* (2006) are $HCrO_4^-$ (≈ 80%) and $Cr_2O_7^{2-}$ (≈ 20%). The reduction of Cr^{6+} to Cr(III) can be suggested by two possible mechanisms and as follows. In first mechanism, Cr^{6+} is directly reduced to Cr^{3+} by BSAC surface electron-donor groups and the reduced Cr^{3+} forms complexes with BSAC or remains in the surrounding test solution. However, Cr^{3+} is not adsorbed by BSAC at pH 2.0 due to the repulsion with protonated surface. But in the second mechanism, the adsorption-coupled reduction of Cr^{6+} to Cr^{3+} occurred with the cell wall functional groups of BSAC (Figure 3.17a). It has three steps; (i) the binding of anions ($HCrO_4^-$ and $Cr_2O_7^{2-}$) to the positively charged groups present on the surface of the BSAC, (ii) the reduction of adsorbed Cr^{6+} to Cr^{3+} takes place by neighbouring electron-donor (C=O and $-OCH_3$) groups of adsorbed sites (Figures 3.17a and 3.17b) and (iii) a fraction of surface reduced Cr^{3+} is released into the aqueous solution due to the electronic repulsion between the positively charged groups of BSAC and the surface bound Cr^{3+}. At pH 2.0, the reduced chromium is in Cr^{3+} form due to adsorption couple reduction of Cr^{6+} and that cannot be adsorbed by positively charged surface of the BSAC (Li *et al.*, 2008; Uysal and Ar, 2007). For this purpose, XPS analysis was employed to verify the oxidation state of the bounded chromium ions on BSAC. XPS spectra collected from the Cr2p orbital core region of BSAC indicated that the sharp peaks observed at 577.15

($Cr2p_{3/2}$) and 586.65 ($Cr2p_{1/2}$) eV were corresponding to the Cr^{3+} oxidation state (Figure 3.17c). This result conforms that the chromium adsorbed on the surface of BSAC was mostly in trivalent form due to adsorption-coupled reduction. Therefore, it can be concluded that the reduction of Cr^{6+} to Cr^{3+} also occurred by adsorption-coupled reduction (indirect reduction) on the BSAC surface by adjacent electron-donor groups (C=O and $–OCH_3$) of Cr^{6+} adsorbed protonated positive sites (Figure 3.17b). Beyond pH 2.0, the adsorption of Cr^{6+} decreases and thus the release of Cr^{3+} decreases steadily. Similar behaviour was reported by Dakiky *et al.* (2002) for both Cr^{6+} and Cr^{3+} removal for seven other plant based adsorbents.

In relation with the change enthalpy of Sr^{2+}, adsorption of Sr^{2+} is mainly contributed by physisorption mechanism. The inter-molecular and intra-molecular binding mechanism can be suggested for Sr^{2+} adsorption with cellulosic and lignin functional groups of BSAC. Similar kind of behaviour is reported in elaborately for Sr^{2+} adsorption using SBS in chapter 4.

3.3.9.2 Adsorption Mechanism of Phenol and *O*-cresol

In relation with the change in enthalpy mentioned earlier, the present work indicates that the phenol and *o*-cresol adsorption on BSAS is largely controlled by physisorption (van der Waals interaction). Ku and Lee (2000) reported that the predominant species of phenol in aqueous solution pH below 4.0 is C_6H_5OH (molecular form) and $C_6H_5O^-$ (ionic form) is negligible, whereas at pH above 9.0 $C_6H_5O^-$ is predominant and C_6H_5OH is negligible. Similarly, at alkaline pH *o*-cresol is in $C_7H_8O^-$ form. The possible interactions between phenol and carbon surface in the wide pH range of 2-10 are proposed in the following steps:

- ***Hydrophobic effect and ion-dipole interaction:*** at acidic pH, the phenol adsorption with carbon surface is highly influenced by the hydrophobic interaction of the aromatic ring (since phenol molecule contains both hydrophilic and hydrophobic groups) with the hydrophobic surface of the BSAC and that retain on the BSAC surface or in the pores (Liu *et al.,* 2010; Castilla, 2004). The ion-dipole binding is due the interaction between non polar group of the phenol with permanent dipole ($\equiv S$) of the BSAC (Anandkumar and Mandal, 2012; Ku and Lee, 2000).

$$\equiv S + C_6H_5OH \rightleftarrows \equiv SC_6H_5OH \qquad (3.2)$$

- ***Electron donor-acceptor interaction and hydrogen bonding:*** the electron donor groups of the BSAC (C=O, $-OCH_3$) and the electron acceptor groups of aromatic phenolic ring (weak acid) may be involved in this surface complex formation (Ku and Lee, 2000). The hydrogen atom of aromatic ring act as a hydrogen donor to make the hydrogen bond with a relatively electronegative atom of oxygen in hydroxyl group and nitrogen in amino group (hydrogen bond acceptors) of BSAC (Figure 3.18a), which removes phenol from solution (Castilla, 2004).
- ***Electrostatic interaction:*** at pH 4-8 the less available $C_6H_5O^-$ species are binded with positively charged cell wall functional groups ($\equiv S$) such as $-OH_2^+$ and amino groups ($-NH_2^+$ and $-NH^+$) through electrostatic interaction.

$$\equiv S + C_6H_5O^- \rightleftarrows \equiv SC_6H_5O^- \qquad (3.3)$$

However, at pH above 9.0 the considerable reduction in phenol adsorption is due to the repulsion of $C_6H_5O^-$ ions with highly deprotonated surface of BSAC.

- **π-π interactions:** the interaction between the π electrons of the phenolic ring and the carbon graphene layers (Figure 3.18b) are making the phenol adsorption which might comprise the charge transfer and the dispersive force. Kawati and Tsutsu (1995) reported that the negative charge of deprotonated phenolate ion is distributed on the aromatic ring in combination with its π electrons, which results in the formation of widely distributed electron cloud and this electron cloud might involve in the charge transfer between the π electrons of aromatic ring and graphene layer of carbon (Figure 3.18b). This mechanism plays a vital role in phenol adsorption, as reported by other studies dealing with adsorption of phenols on other activated carbons.

In case of *o*-cresol adsorption, at alkaline pH the predominant ionic form *o*-cresol is C_7H_8O-. These net negative charged cresol ions are repelled by net negative charged surface functional groups of BSAC mainly hydroxyl and oxygen groups. But, at acidic pH the repulsion between the cationic methyl group of *o*-cresol and protonated surface of BSAC significantly reduces the adsorption capacity. At the neutral pH, positive methyl group of *o*-cresol is easily attached with negative surface of BSAC.

In general, phenol and *o*-cresol adsorption mechanism is complex and the exact binding correlation between the phenol and *o*-cresol with activated carbon cannot be drawn. Therefore, abovementioned possible factors are considered to be important in the adsorption of phenol and *o*-cresol on BSAC.

3.3.9.3 Adsorption Mechanism of RB and MB Dyes

The probable binding mechanism of RB dye on BSAC can be described as follows: at acid pH (2.0-3.0), the highly protonated (excess of H^+ ions) positive sites ($–OH_2^+$) of BSAC do not favour for cationic RB dye adsorption due to its electrostatic repulsion (Chuah *et al.,* 2005). The existence of monomeric form of RB molecules at pH 3.5 enhances both pore diffusion and surface adsorption (Figure 3.19). The diameter of RB molecule is 1.6 nm (monomer) and it can easily enter into the micro pores of BSAC (refer Table 1, micro pore surface area is 337 m^2/g) to increase the pore diffusion (Tsunomori and Ushiki, 1999). Therefore, maximum adsorption capacity was observed at pH 3.5. At pH more than 3.5, the zwitterionic form of RB dye (Figure 3.19) in solution might enhance the aggregation of RB dye molecule to form bigger molecules (dimer and trimer) and thus unable to enter into the micropores of BSAC. The aggregation of zwitterions is due to the electrostatic attraction between the carboxyl and xanthene groups (Figure 3.19) of RB dye. The aggregations of RB in water have been reported by Arbeloa and Ojeda (1982) and Mchedlov-Petrosyan and Kholin (2004). MB dye molecules have a positive net charge but BSAC surface carrying net negative charge at neutral and alkaline pH of the solution due to oxygen and hydroxyl groups. This opposite charge difference between dye molecules and BSAC surface makes the higher adsorption through strong electrostatic interaction. Therefore, at alkaline pH surface diffusion only dominates the higher RB and MB dye adsorption on BSAC.

3.4 SUMMARY

This work presents some important phenomena associated with Cr^{6+}, Sr^{2+}, phenol, *o*-cresol, RB and MB dye removal from aqueous solution using BSAC. The adsorption was found to be strongly dependent on pH and temperature of the solution. The FT-IR spectra revealed that the hydroxyl and amino cell wall functional group was the main binding site for all studied components. The adsorption capacity of phenol was enhanced by RB dye and (NH_4^+ and NO_2^-) in multiple and single contaminant system,

respectively. The adsorption capacity of Cr^{6+} and Sr^{2+} onto BSAC decreased in binary and ternary system. The adsorption behaviour of Cr^{6+}, Sr^{2+}, phenol, *o*-cresol, RB and MB dye onto BSAC matched well with Langmuir isotherm model. The adsorption process was endothermic for Cr^{6+}, RB and MB dye and exothermic for Sr^{2+}, phenol and *o*-cresol. The preference order of single contaminant adsorption on the BSAC was MB dye > RB dye > phenol > *o*-cresol > Cr^{6+} and > Sr^{2+} at 30°C. This work provides new insight for developing Bael shell based novel activated carbons to remove organic and inorganic based multi-contaminants from the aqueous solution including industrial wastewater.

Chapter 3
Figures & Tables

(a)

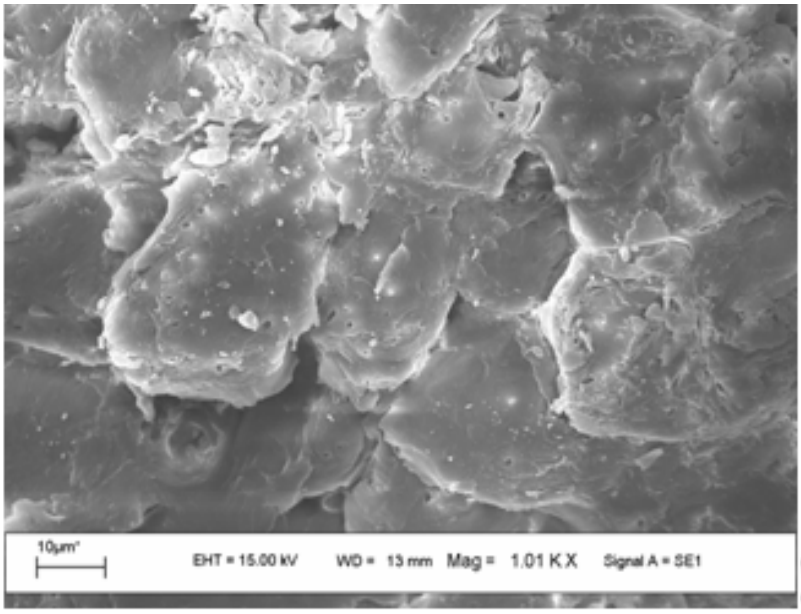

Figure 3.1a SEM image of raw BS (Bael shell)

(b)

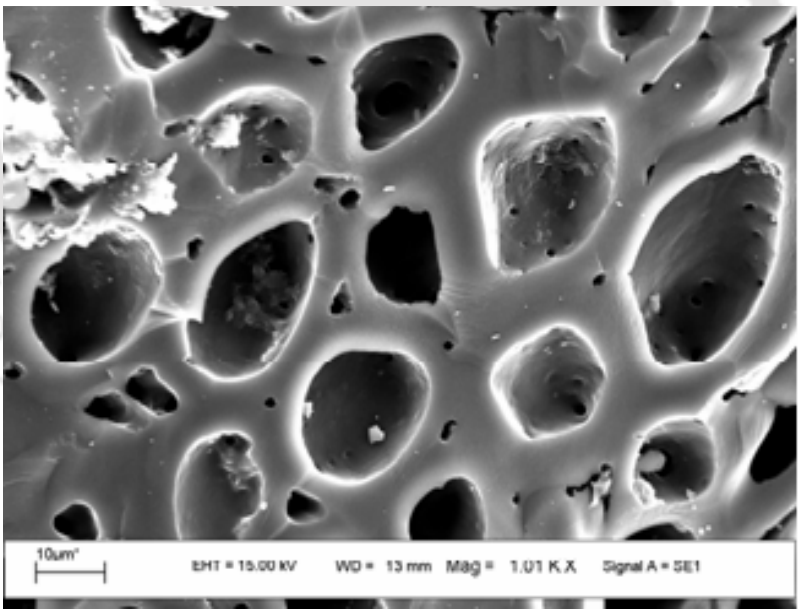

Figure 3.1b SEM image of porous BSAC after activation

(c)

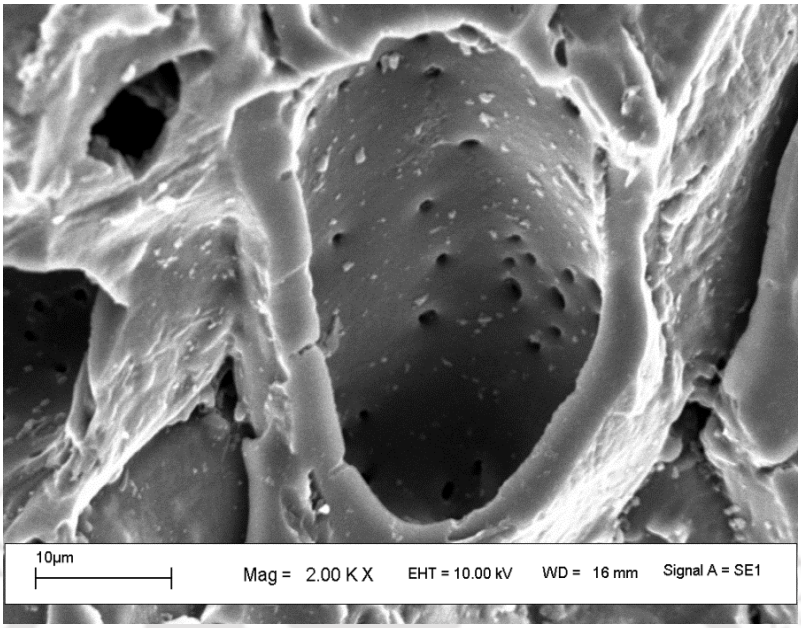

Figure 3.1c SEM image of pore branches of BSAC

(d)

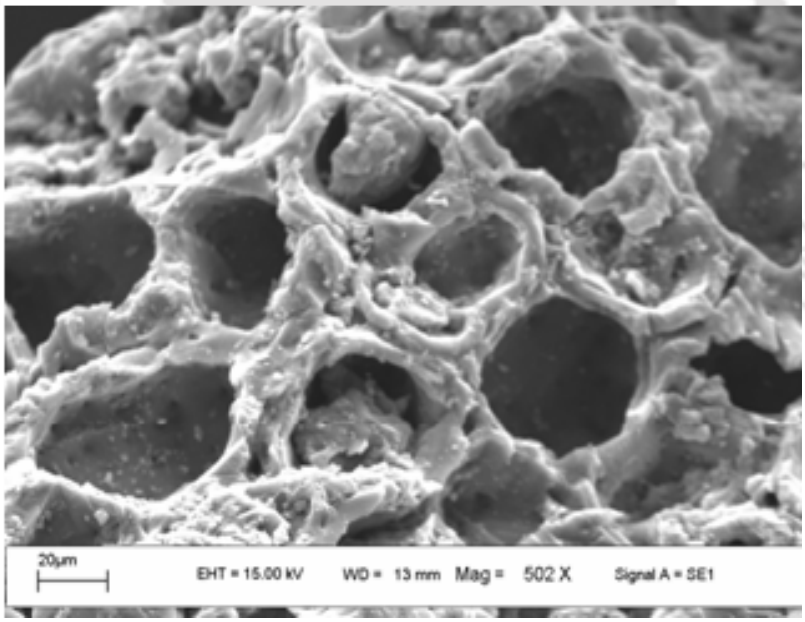

Figure 3.1d SEM image of BSAC after Cr^{6+} adsorption

(e)

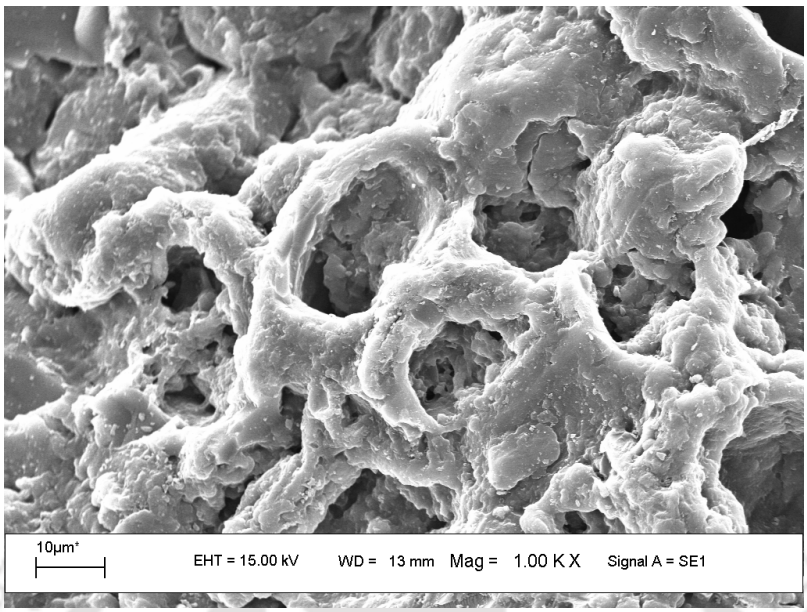

Figure 3.1e SEM image of BSAC after RB dye adsorption

(f)

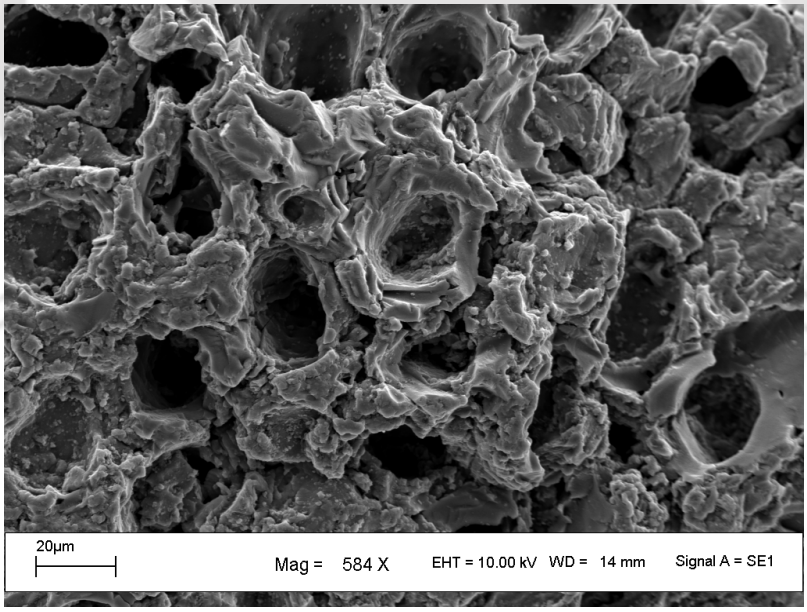

Figure 3.1f SEM image of BSAC after MB dye adsorption

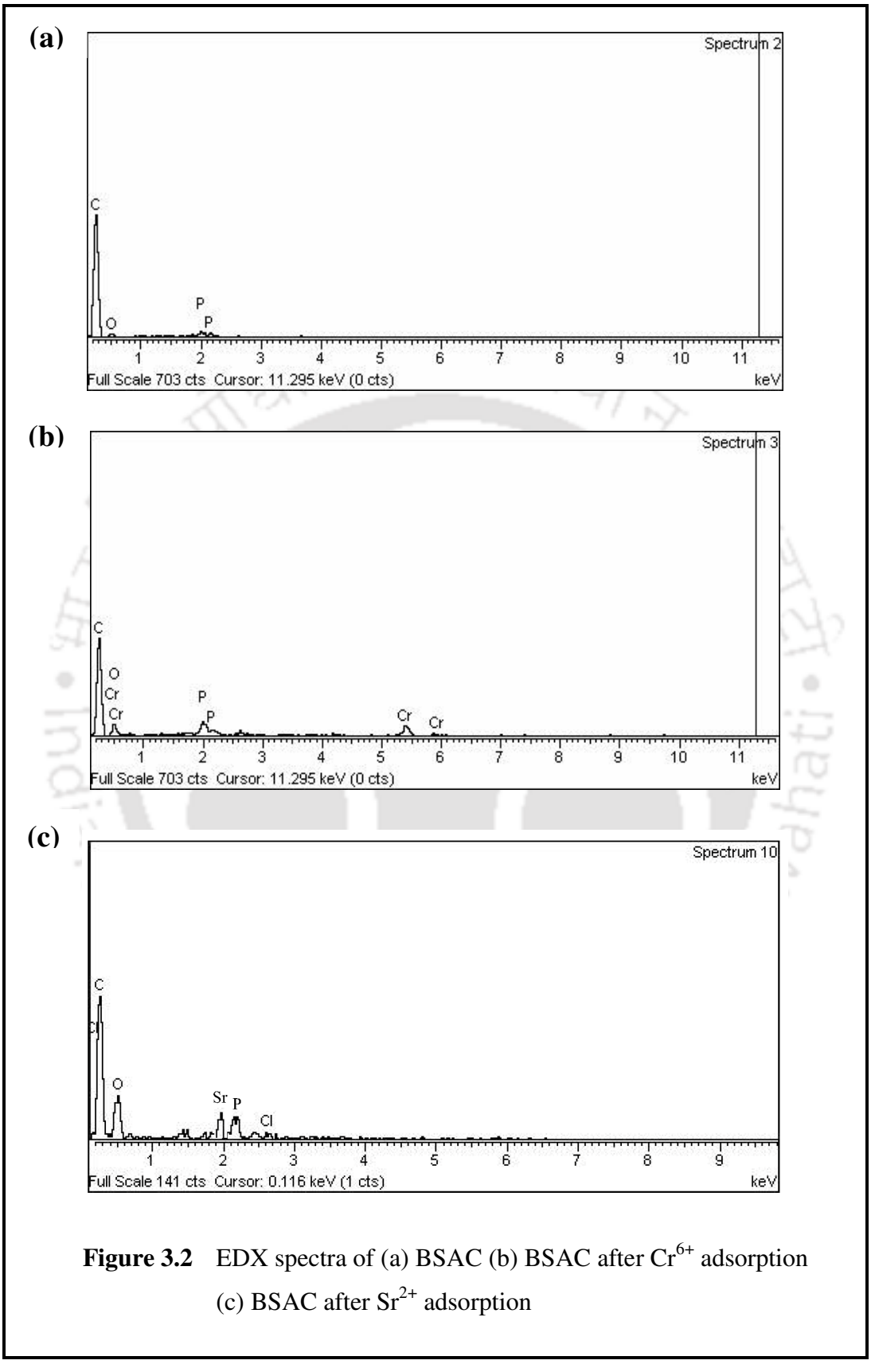

Figure 3.2 EDX spectra of (a) BSAC (b) BSAC after Cr^{6+} adsorption (c) BSAC after Sr^{2+} adsorption

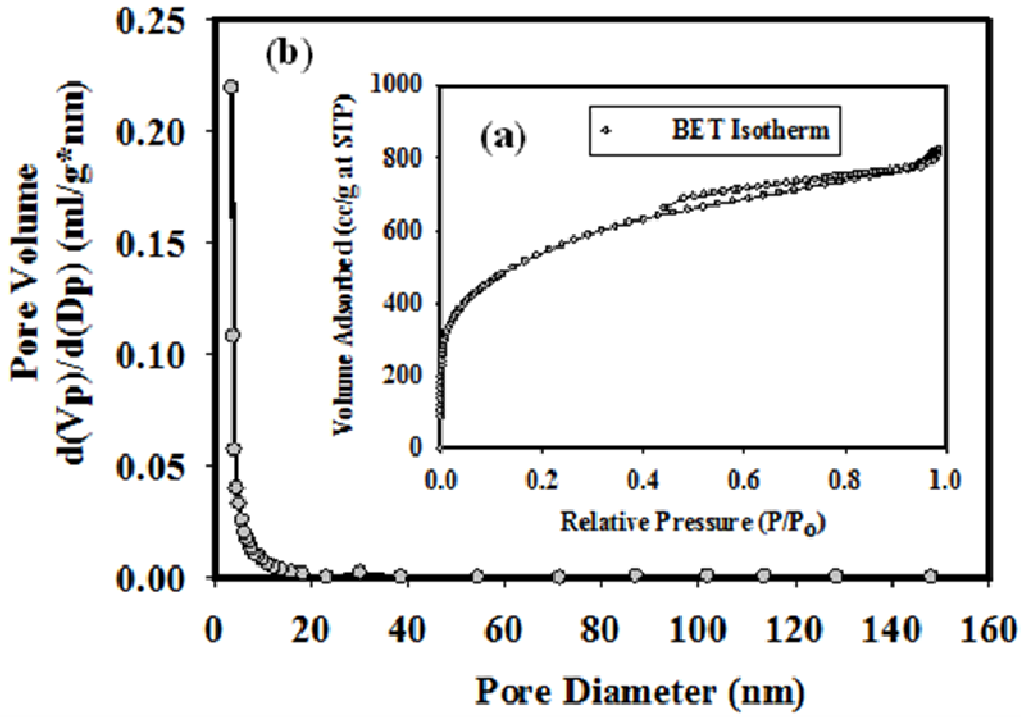

Figure 3.3 BET analysis of BSAC (a) adsorption/desorption isotherm (b) pore size distribution.

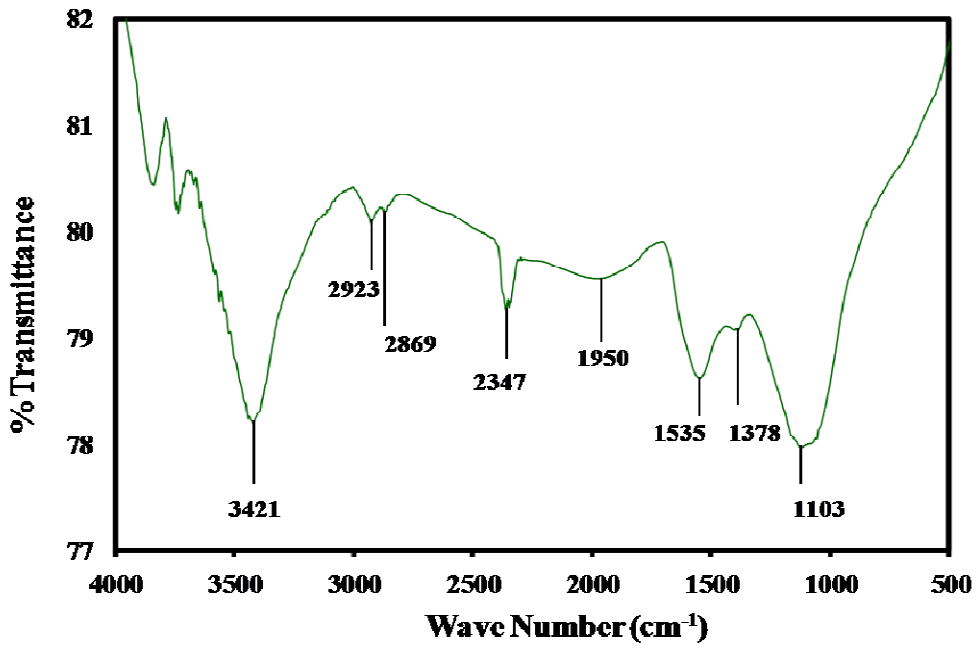

Figure 3.4a FT-IR spectra of BS (raw Bael shell)

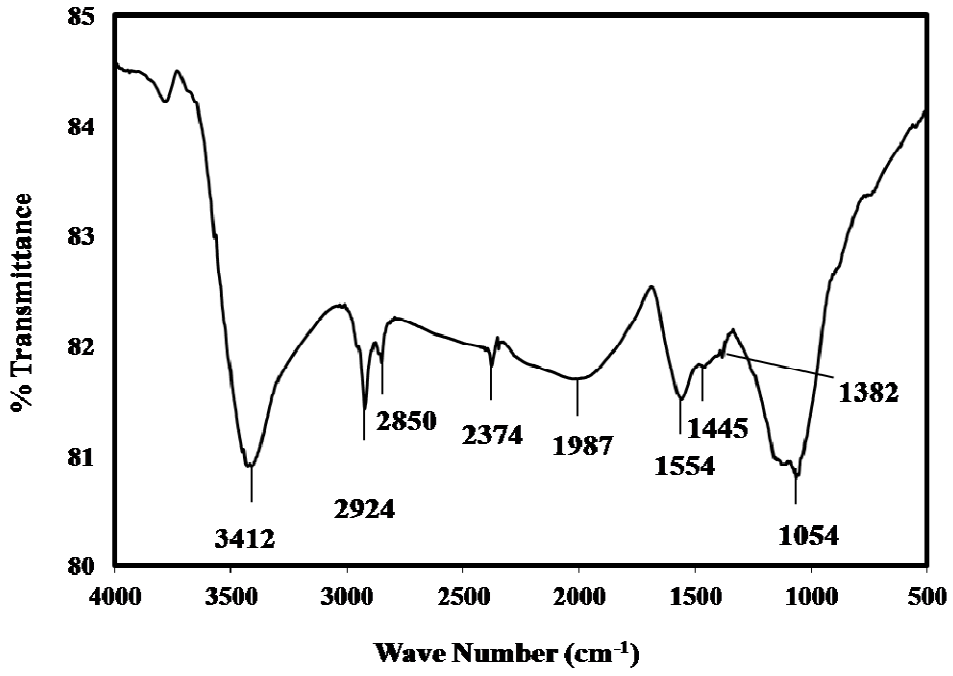

Figure 3.4b FT-IR spectra of BSAC after activation

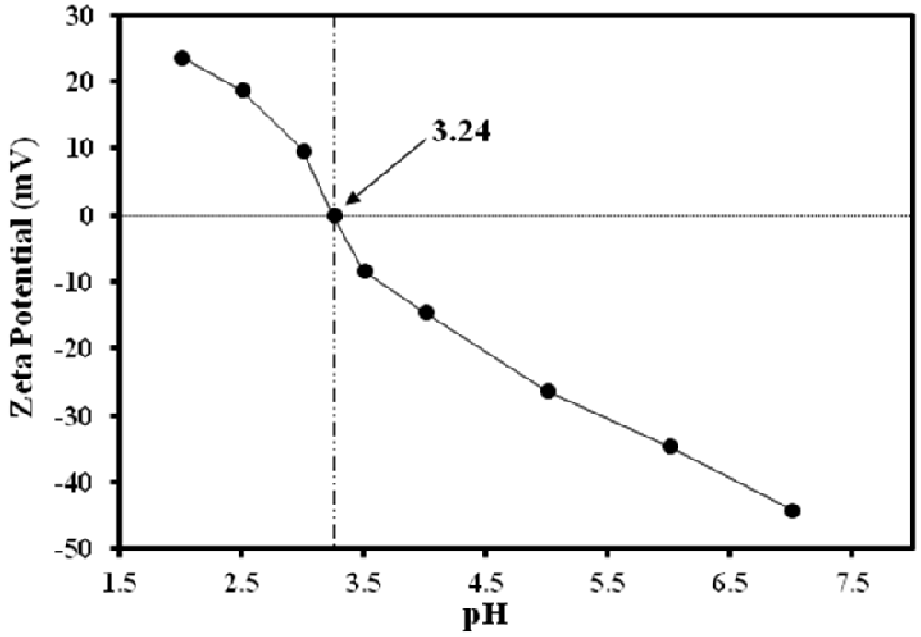

Figure 3.5 Zeta potentials of BSAC as a function of solution pH

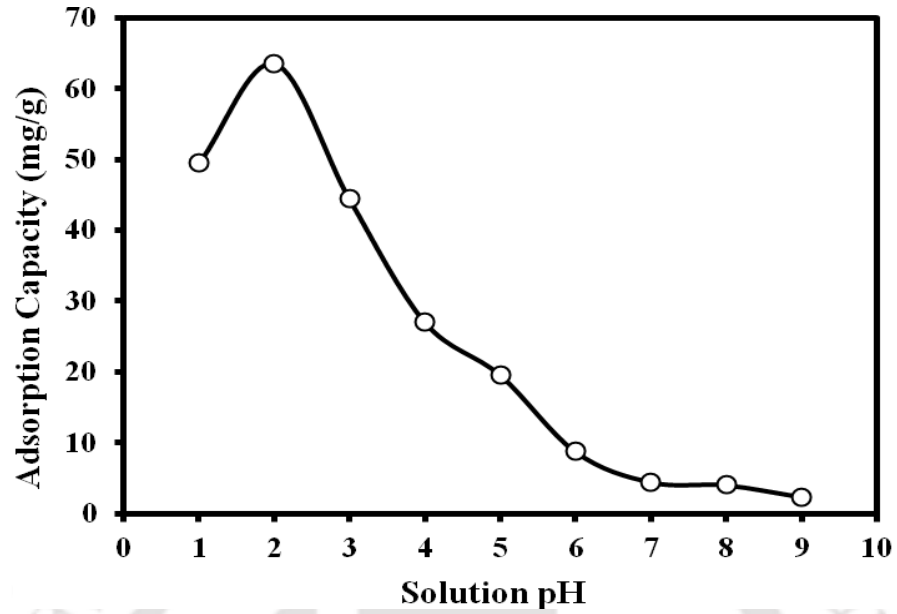

Figure 3.6a Effect of pH on Cr^{6+} adsorption capacity of BSAC (C_o = 100 mg/l, T = 30°C, R = 180 rpm, W = 0.05 g, t = 210 min and V= 50 ml.

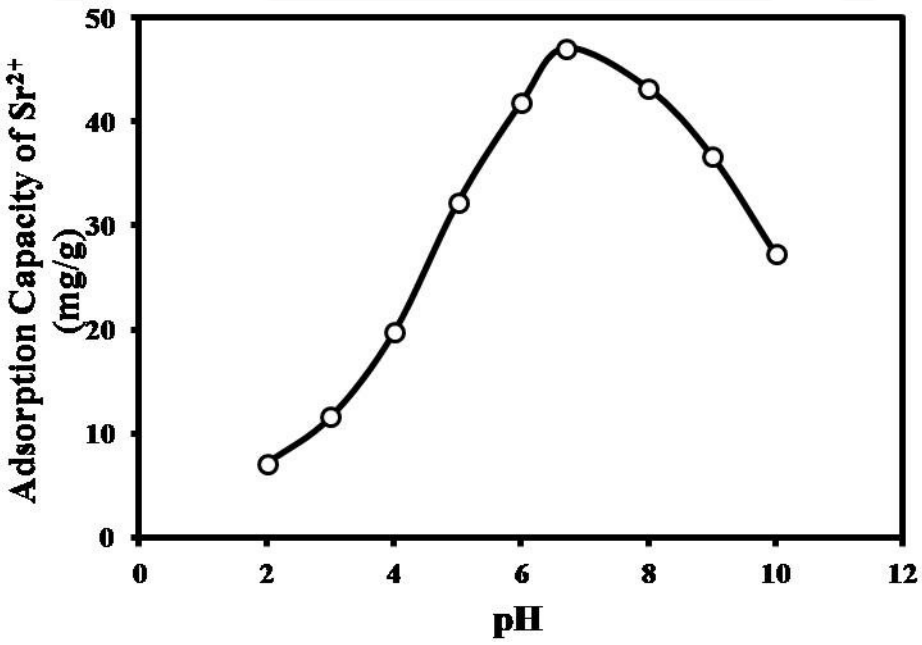

Figure 3.6b Effect of pH on Sr^{2+} adsorption capacity of BSAC (C_o = 100 mg/l, T= 30°C, t = 240 min, R = 180 rpm, V = 50 ml, W = 0.05

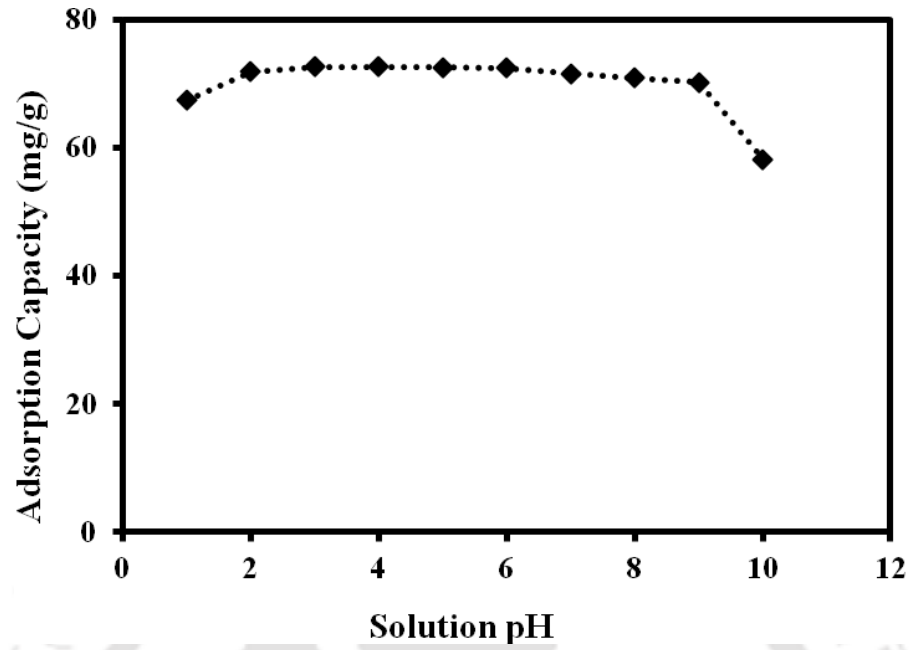

Figure 3.6c Effect of pH on phenol adsorption capacity of BSAC (C_o = 200 mg/l, T = 30°C, R = 180 rpm, W = 0.05 g, t = 180 min and V= 50 ml.

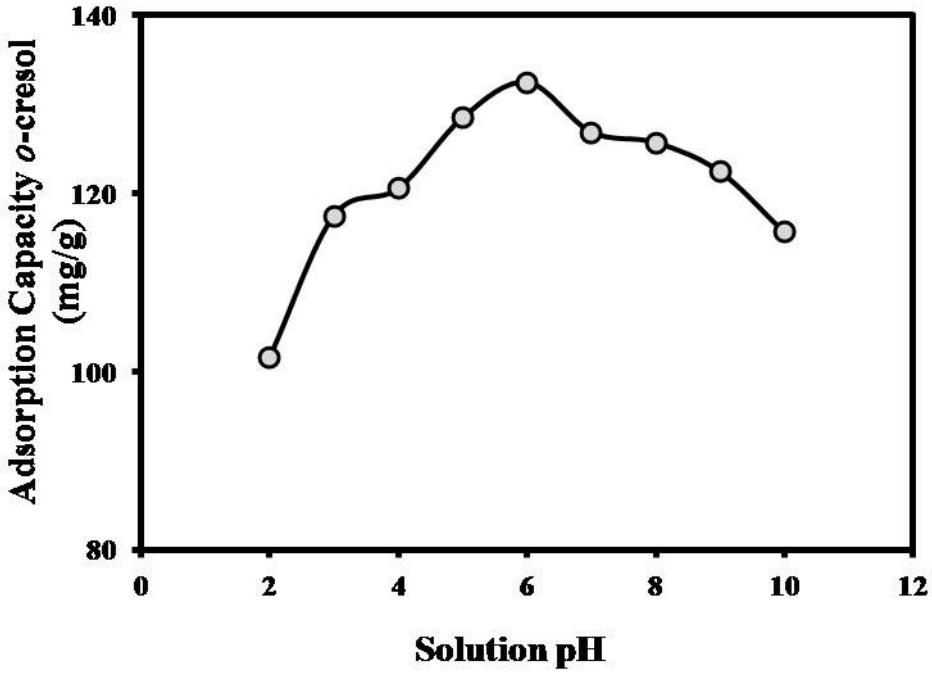

Figure 3.6d Effect of pH on *o*-cresol adsorption capacity of BSAC (C_o = 200 mg/l, T= 30°C, t = 240 min, R = 180 rpm, V = 50 ml, W = 0.05

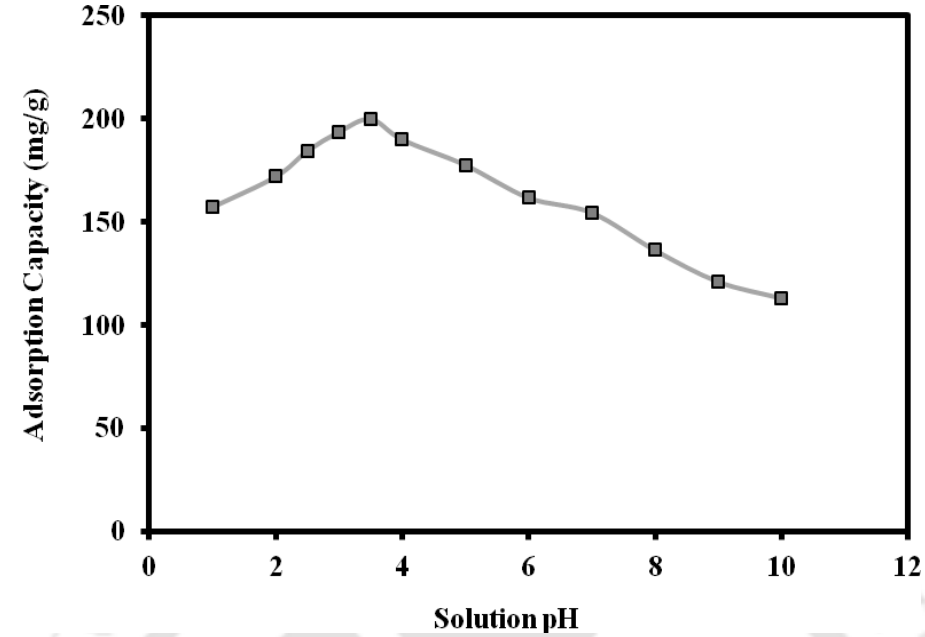

Figure 3.6e Effect of pH on RB dye adsorption capacity of BSAC (C_o = 200 mg/l, T = 30°C, R = 180 rpm, W = 0.05 g, t = 1260 min and V= 50 ml.

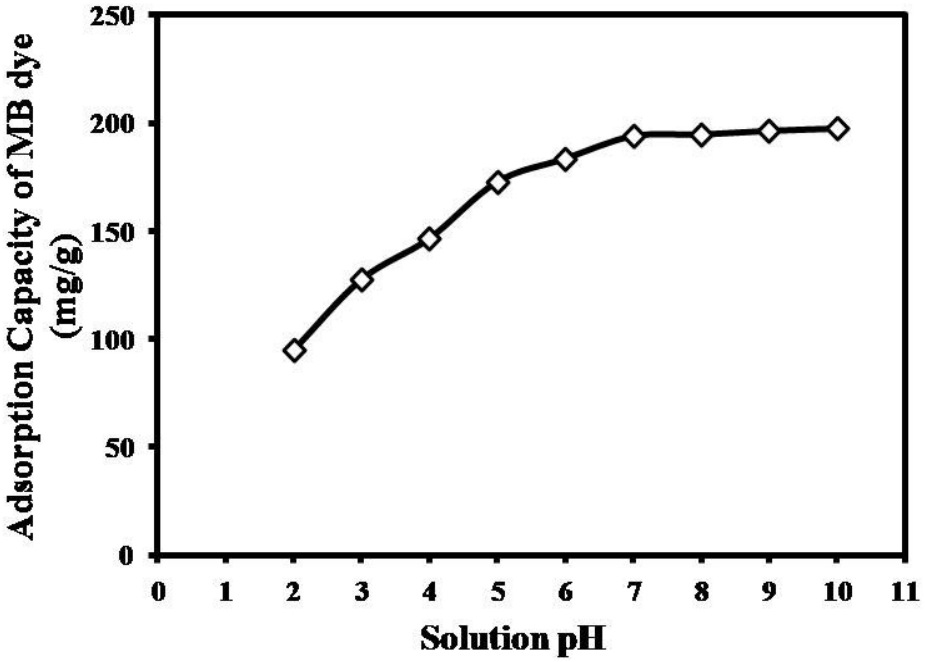

Figure 3.6f Effect of pH on MB dye adsorption capacity of BSAC (C_o = 200 mg/l, T= 30°C, t = 1440 min, R = 180 rpm, V = 50 ml, W = 0.05

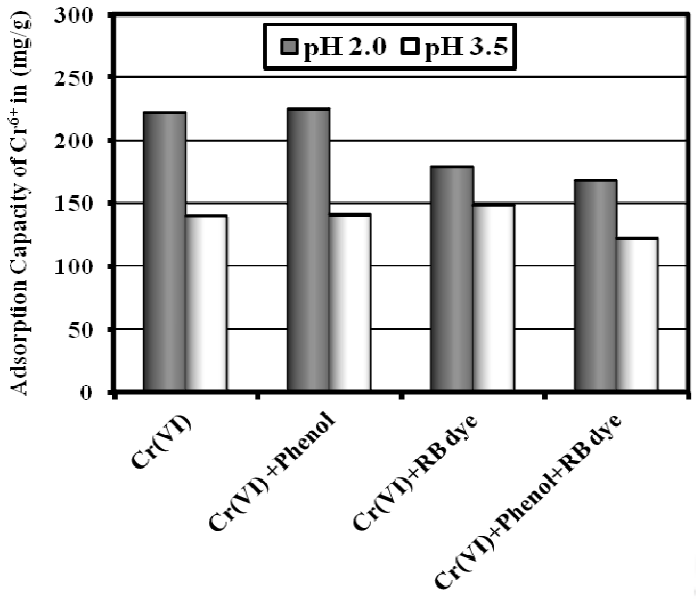

Figure 3.7a Effect of binary and ternary system on Cr^{6+} adsorption (C_o = Cr^{6+} (50-300 mg/l), phenol (200 mg/l), RB (200 mg/l), pH = 2.0 and 3.5, W = 0.05 g, V = 50 ml, and T = 30ºC)

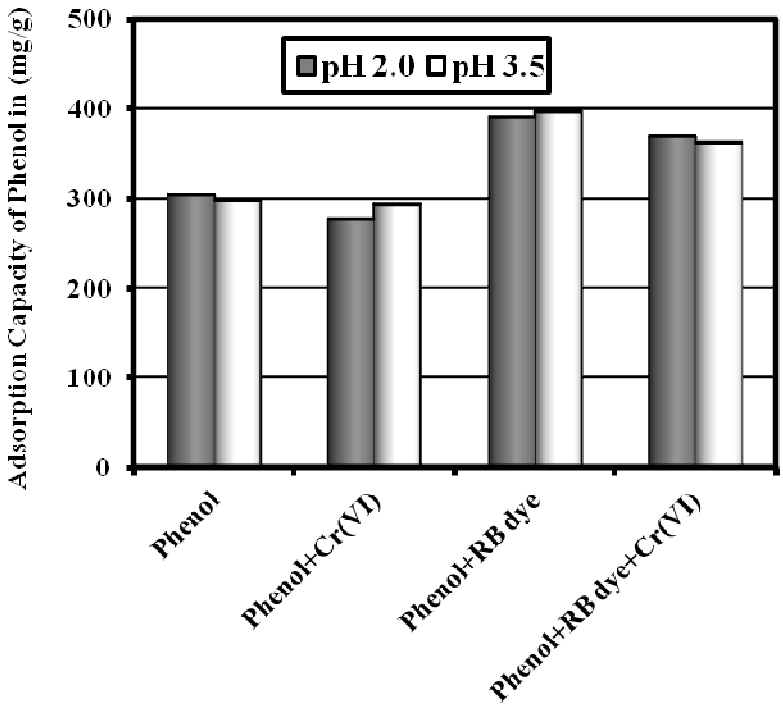

Figure 3.7b Effect of binary and ternary system on phenol adsorption (C_o = phenol (100-600 mg/l), Cr^{6+} (100 mg/l), RB (200 mg/l), pH = 2.0 and 3.5, W = 0.05 g, V = 50 ml, and T = 30ºC)

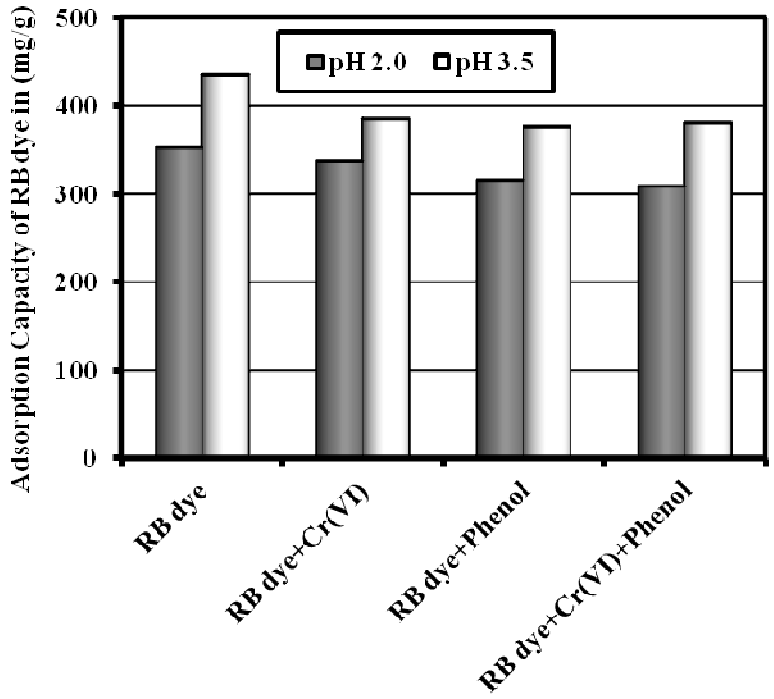

Figure 3.7c Effect of binary and ternary system on RB dye adsorption (C_o = RB dye (100-600 mg/l), Cr^{6+} (100 mg/l), phenol (200 mg/l), pH = 2.0 and 3.5, W = 0.05 g, V = 50 ml, and T = 30ºC)

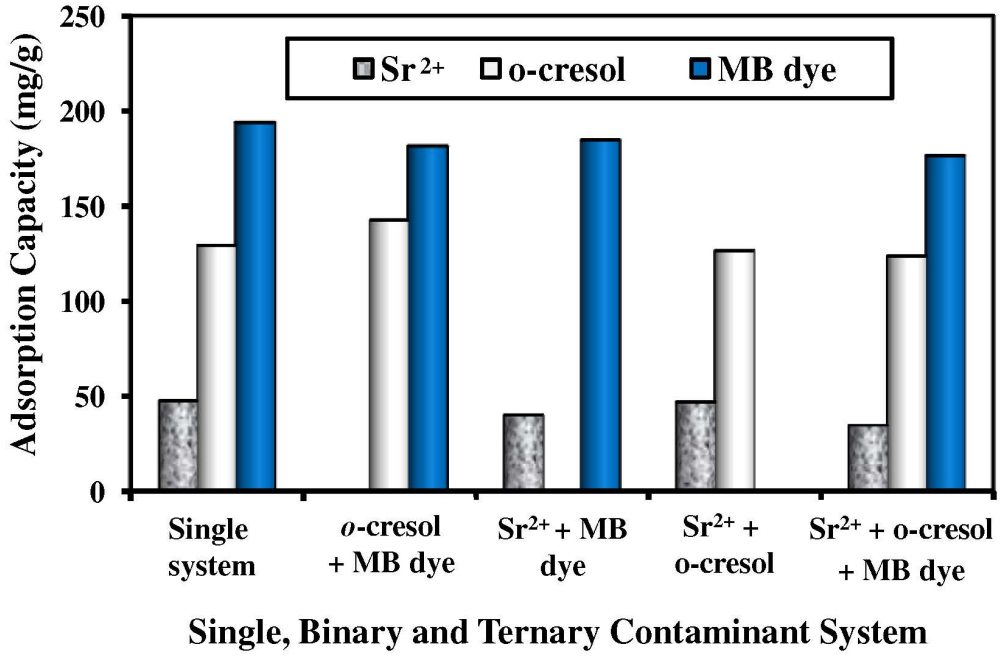

Figure 3.7d Effect of binary and ternary system on Sr^{2+}, *o*-cresol and MB dye adsorption: (C_o = 100 (Sr^{2+}), 200 (*o*-cresol) and 200 (RB dye) mg/l; pH = blank, W = 0.05 g, V = 50 ml, and T = 30ºC)

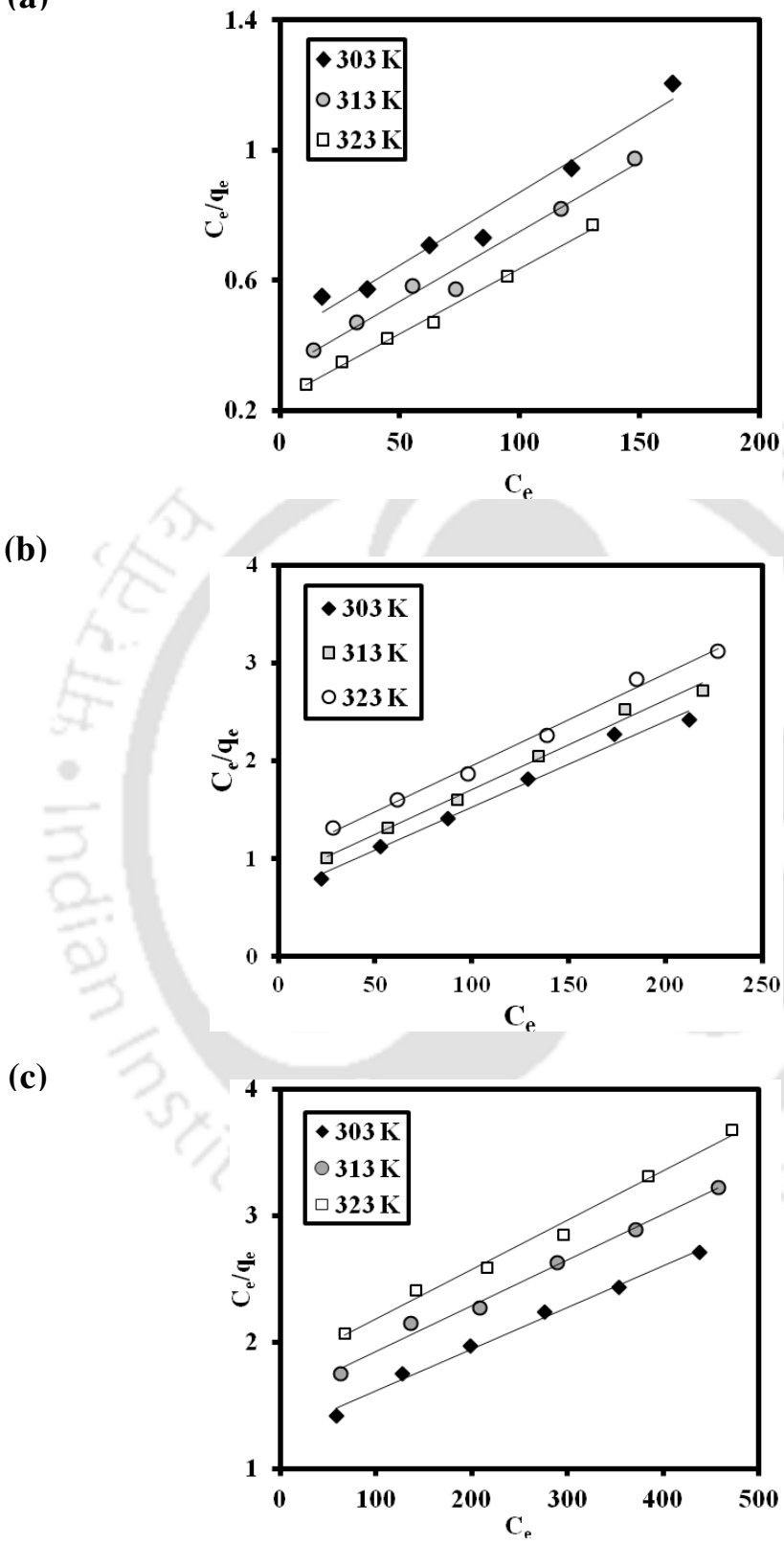

Figure 3.8 Langmuir isotherm plots of (a) Cr^{6+} (b) Sr^{2+} (c) phenol adsorption onto BSAC

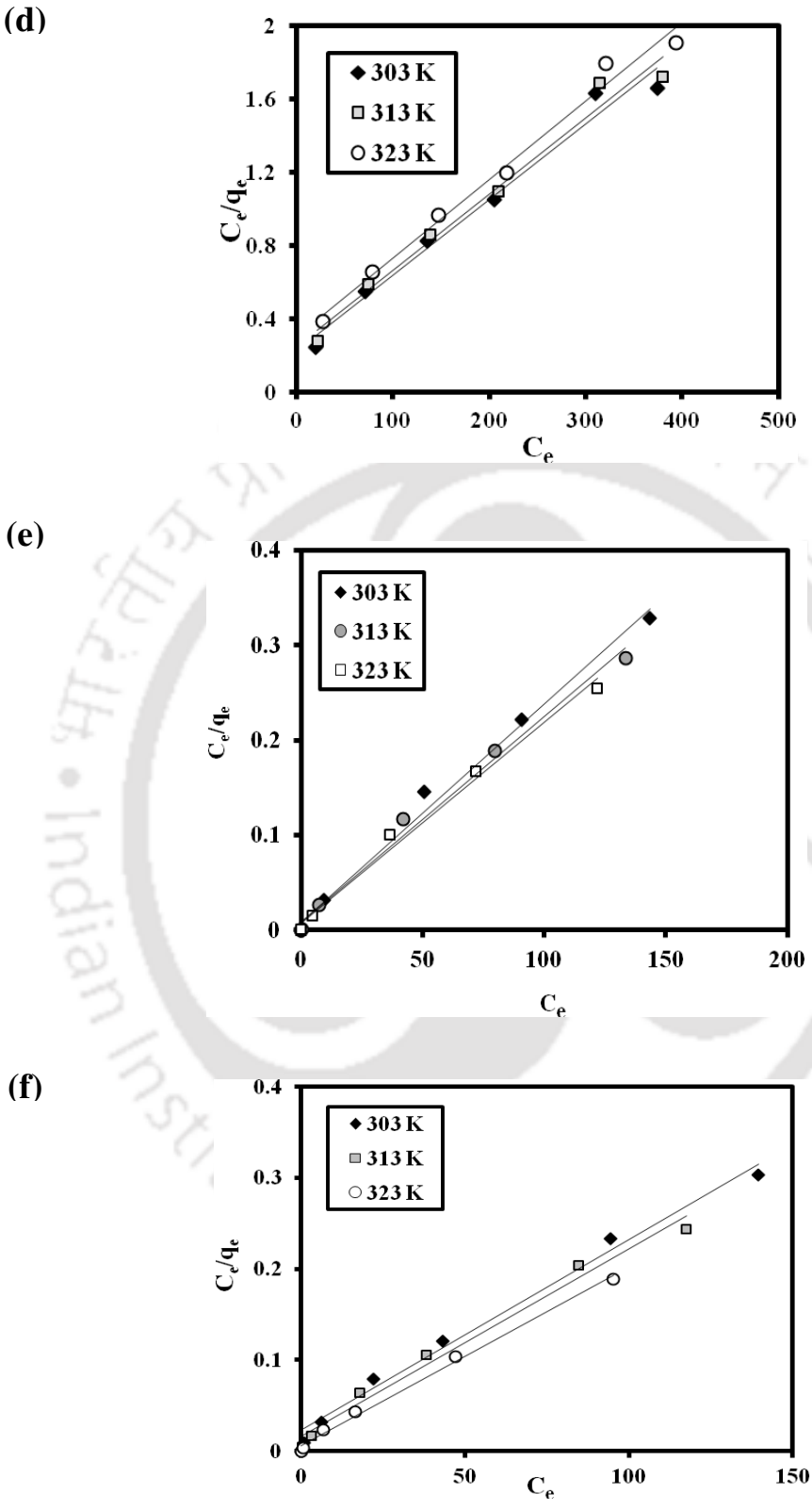

Figure 3.8 Langmuir isotherm plots of (d) *o*-cresol (e) RB dye (f) MB dye adsorption onto BSAC

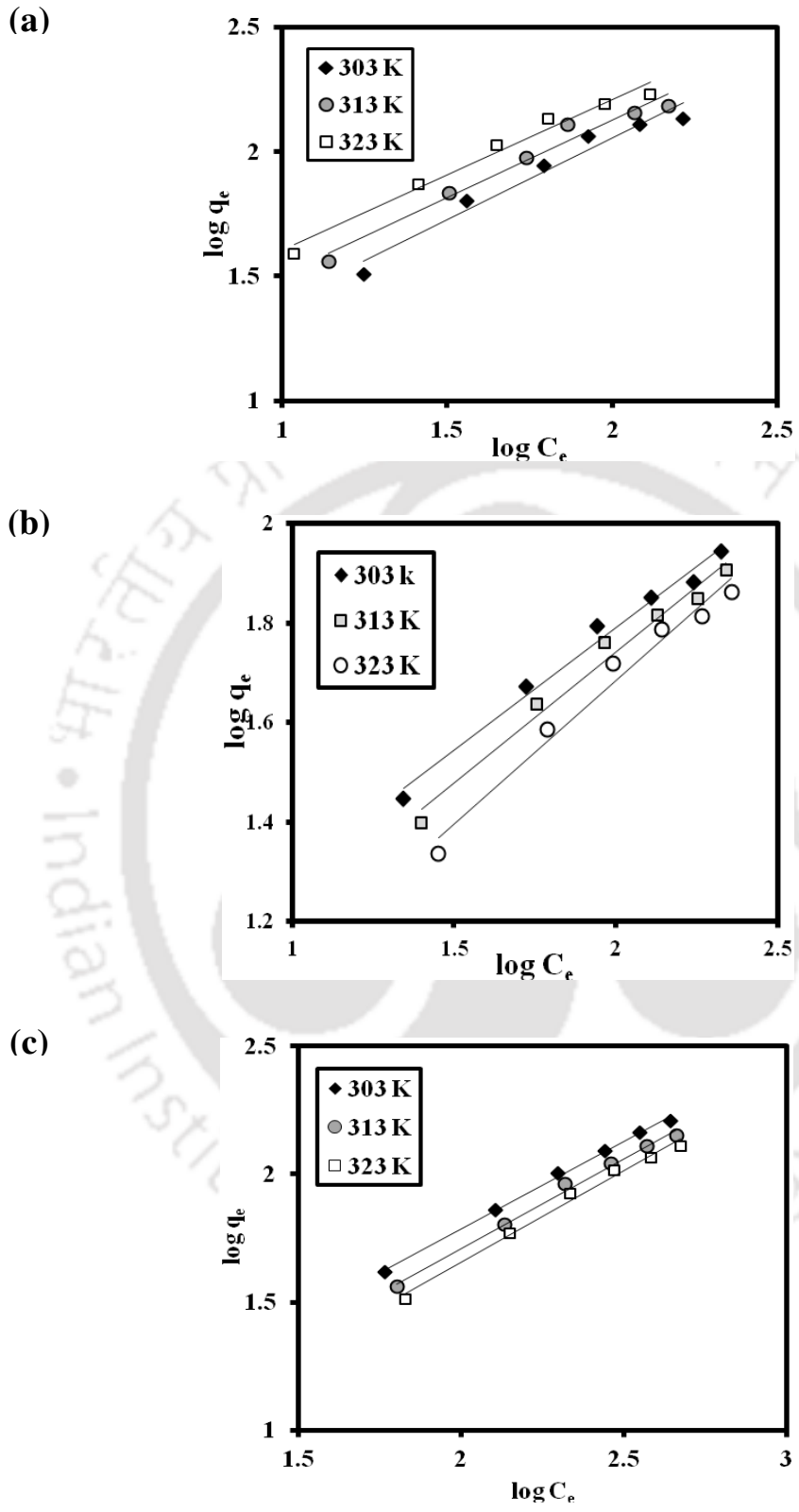

Figure 3.9 Freundlich isotherm plots of (a) Cr^{6+} (b) Sr^{2+} (c) phenol adsorption onto BSAC

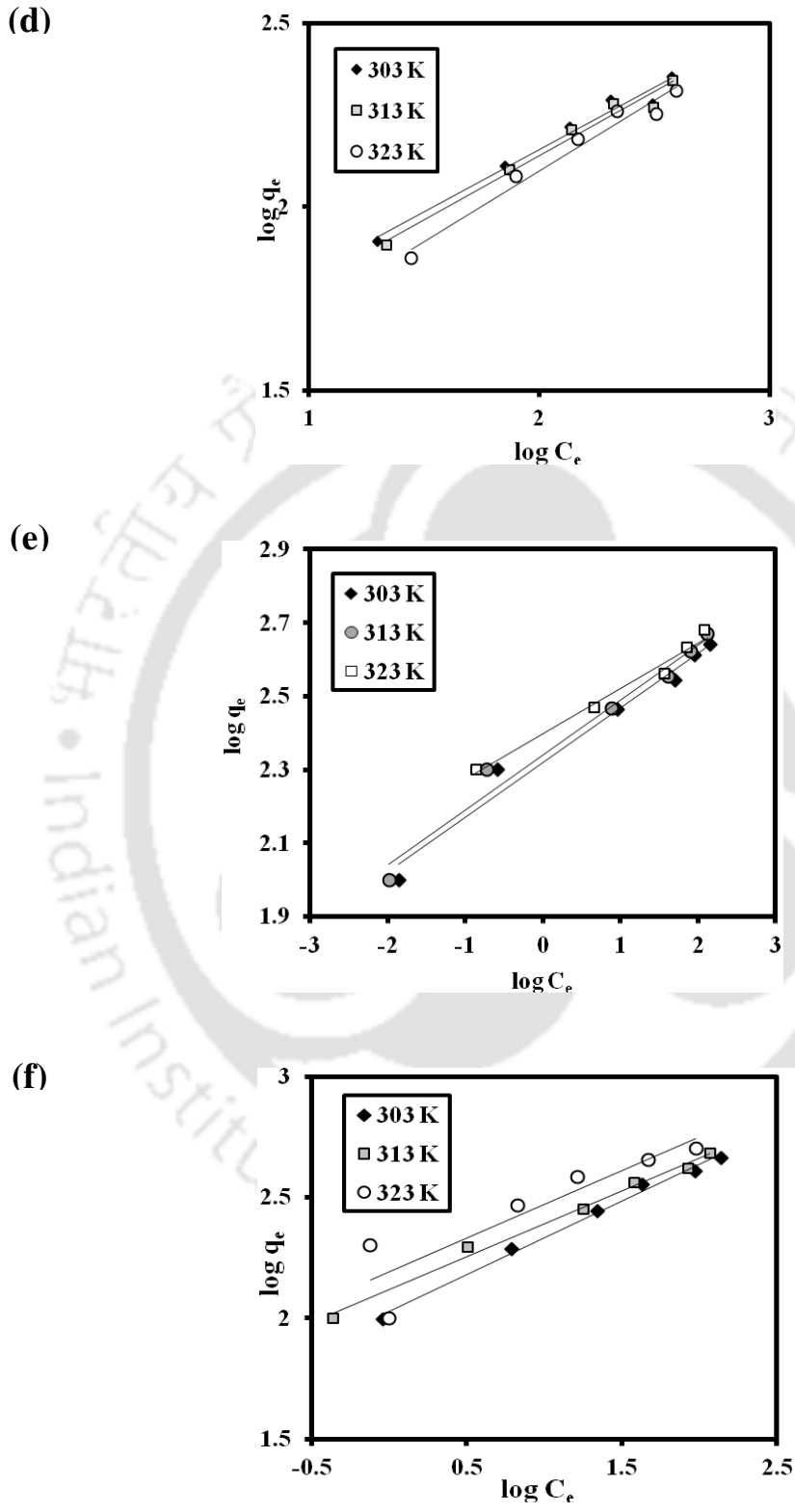

Figure 3.9 Freundlich isotherm plots of (d) *o*-cresol (e) RB dye (f) MB dye adsorption onto BSAC

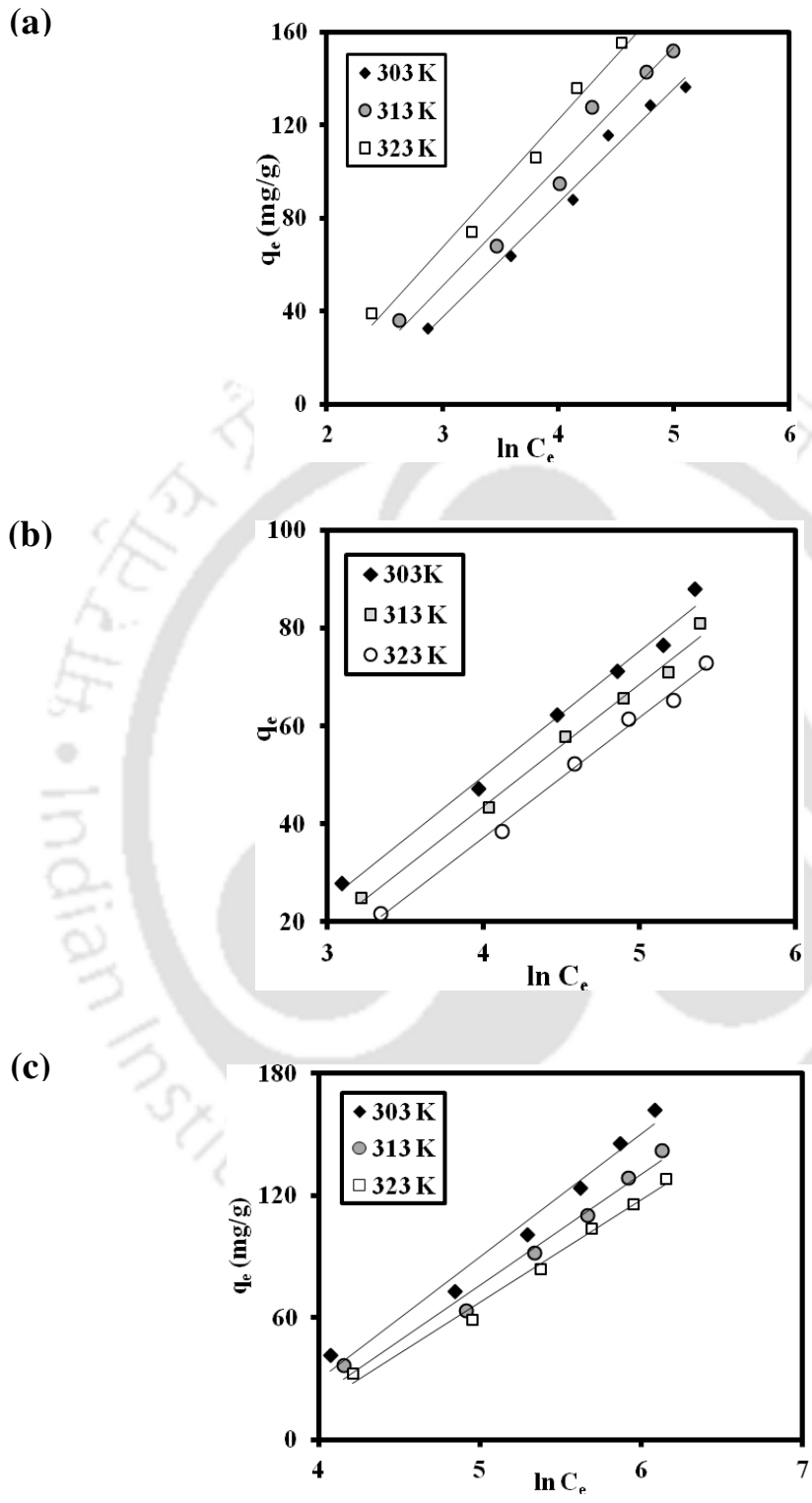

Figure 3.10 Temkin isotherm plots of (a) Cr^{6+} (b) Sr^{2+} and (c) phenol adsorption on to BSAC

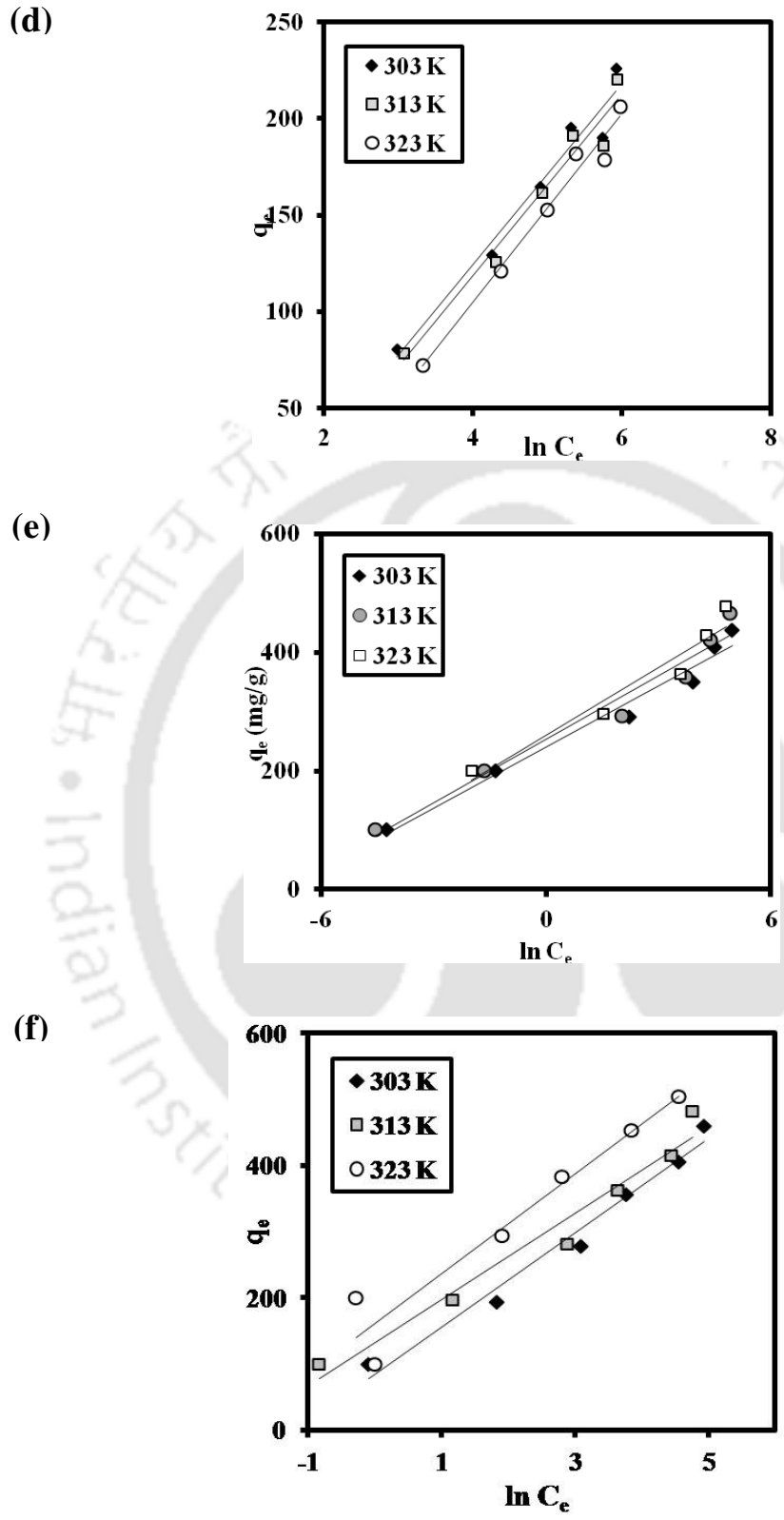

Figure 3.10 Temkin isotherm plots of (d) *o*-cresol (e) RB dye and (f) MB dye adsorption on to BSAC

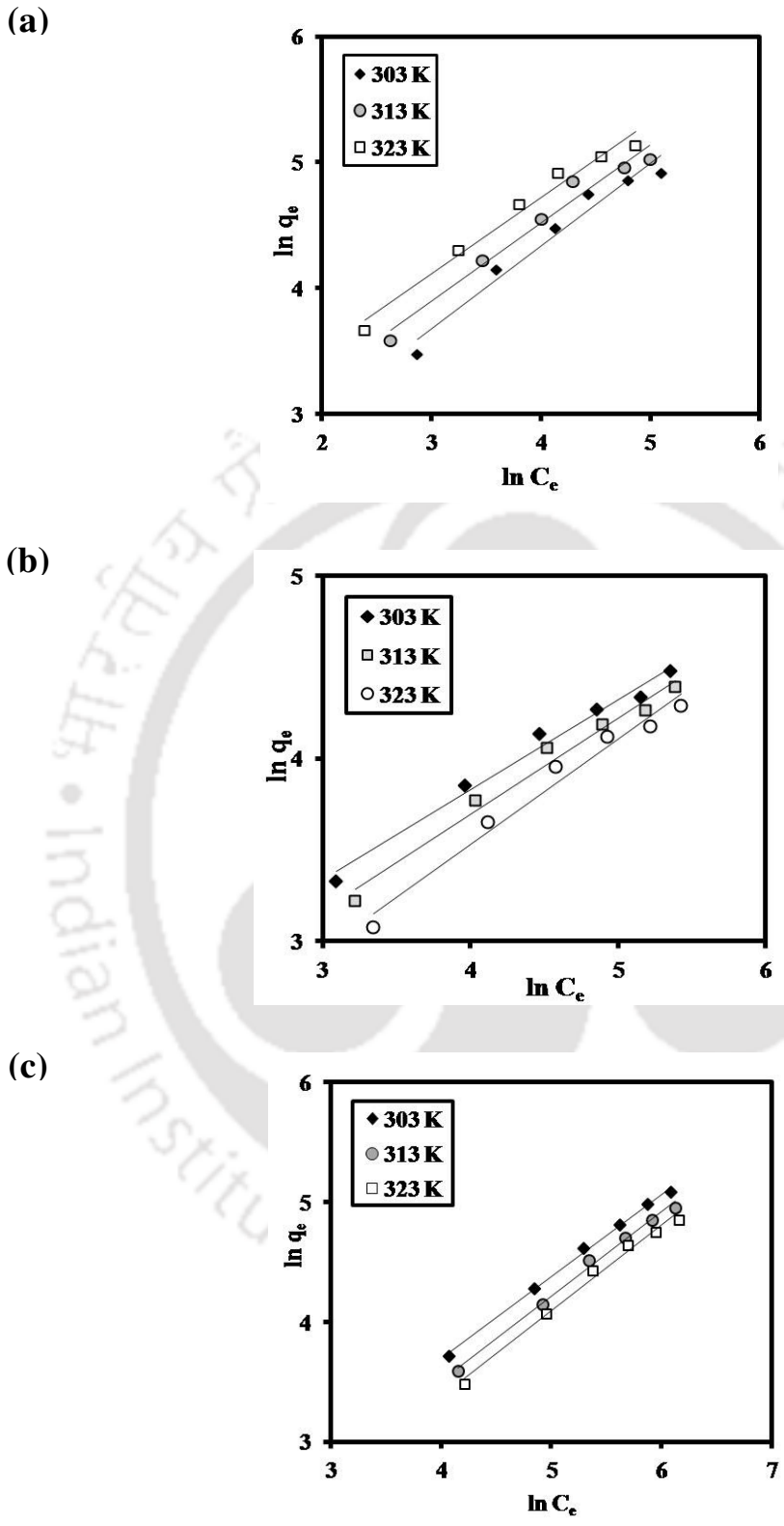

Figure 3.11 Halsey isotherm plots of (a) Cr^{6+} (b) Sr^{2+} and (c) phenol adsorption on to BSAC

(d)

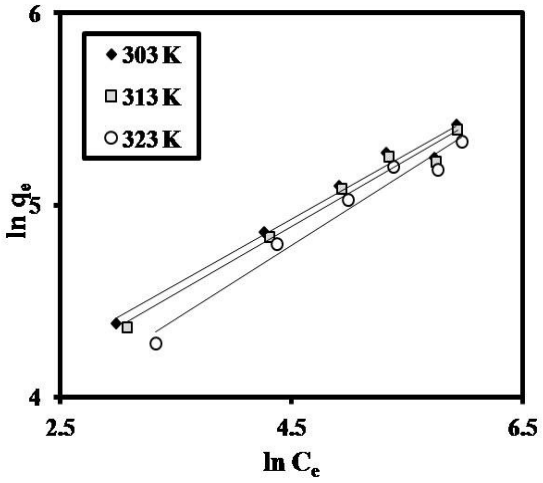

(e)

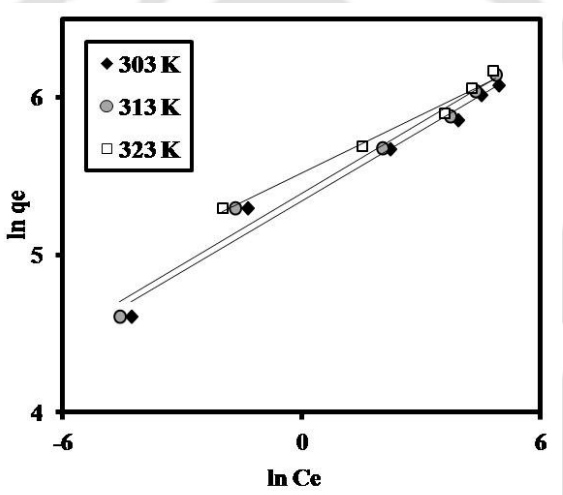

(f)

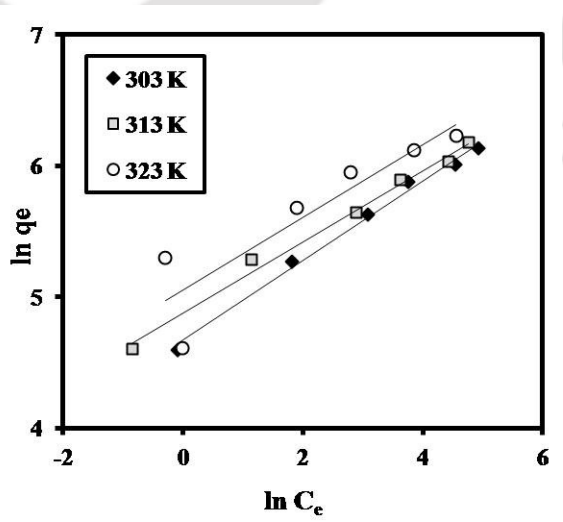

Figure 3.11 Halsey isotherm plots of (d) *o*-cresol (e) RB dye (f) MB dye adsorption on to BSAC

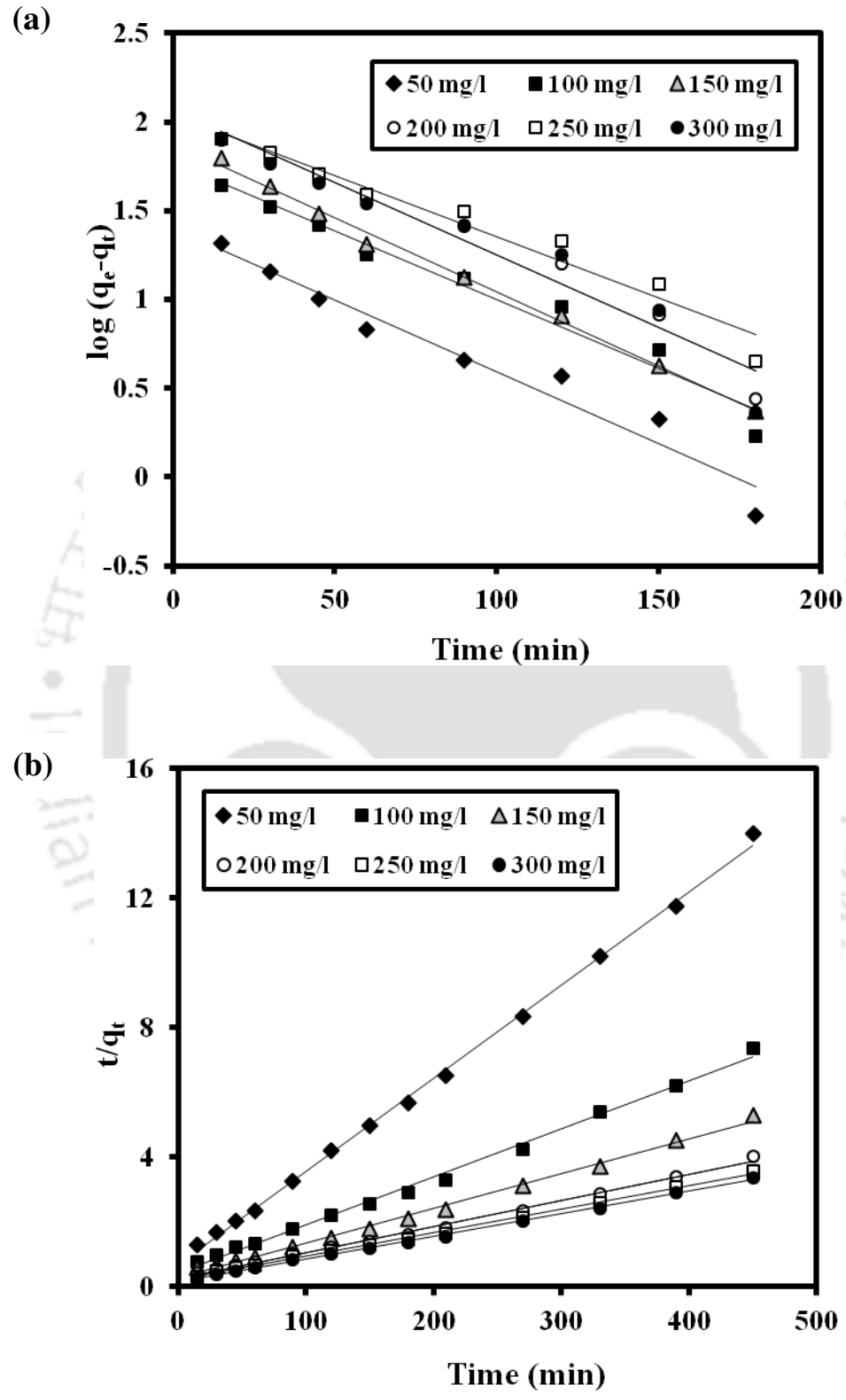

Figure 3.12 Kinetic plots for Cr^{6+} adsorption onto BSAC (a) pseudo-first-order kinetics (a) pseudo-second-order kinetics

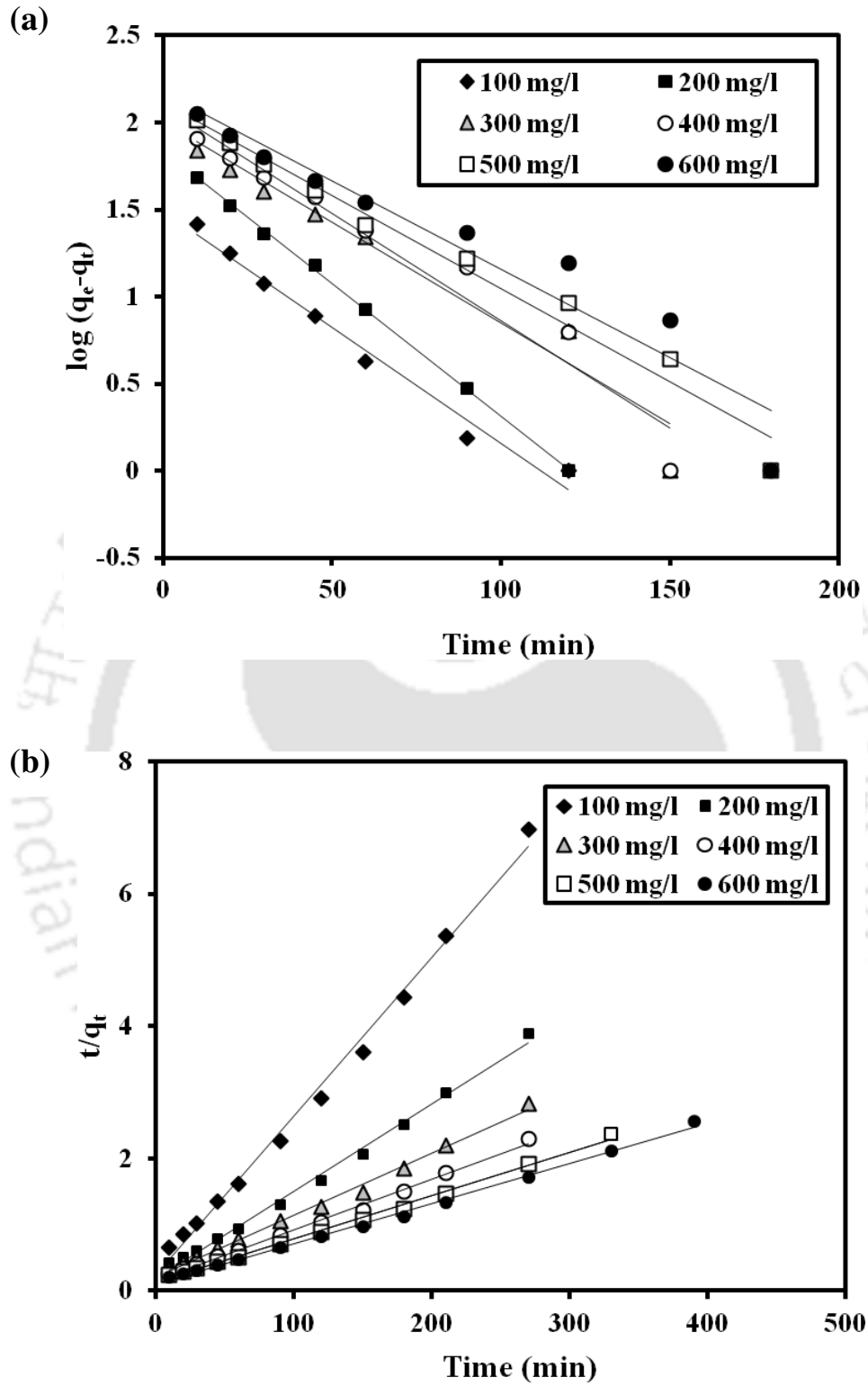

Figure 3.13 Kinetic plots for phenol adsorption onto BSAC (a) pseudo-first-order kinetics (a) pseudo-second-order kinetics

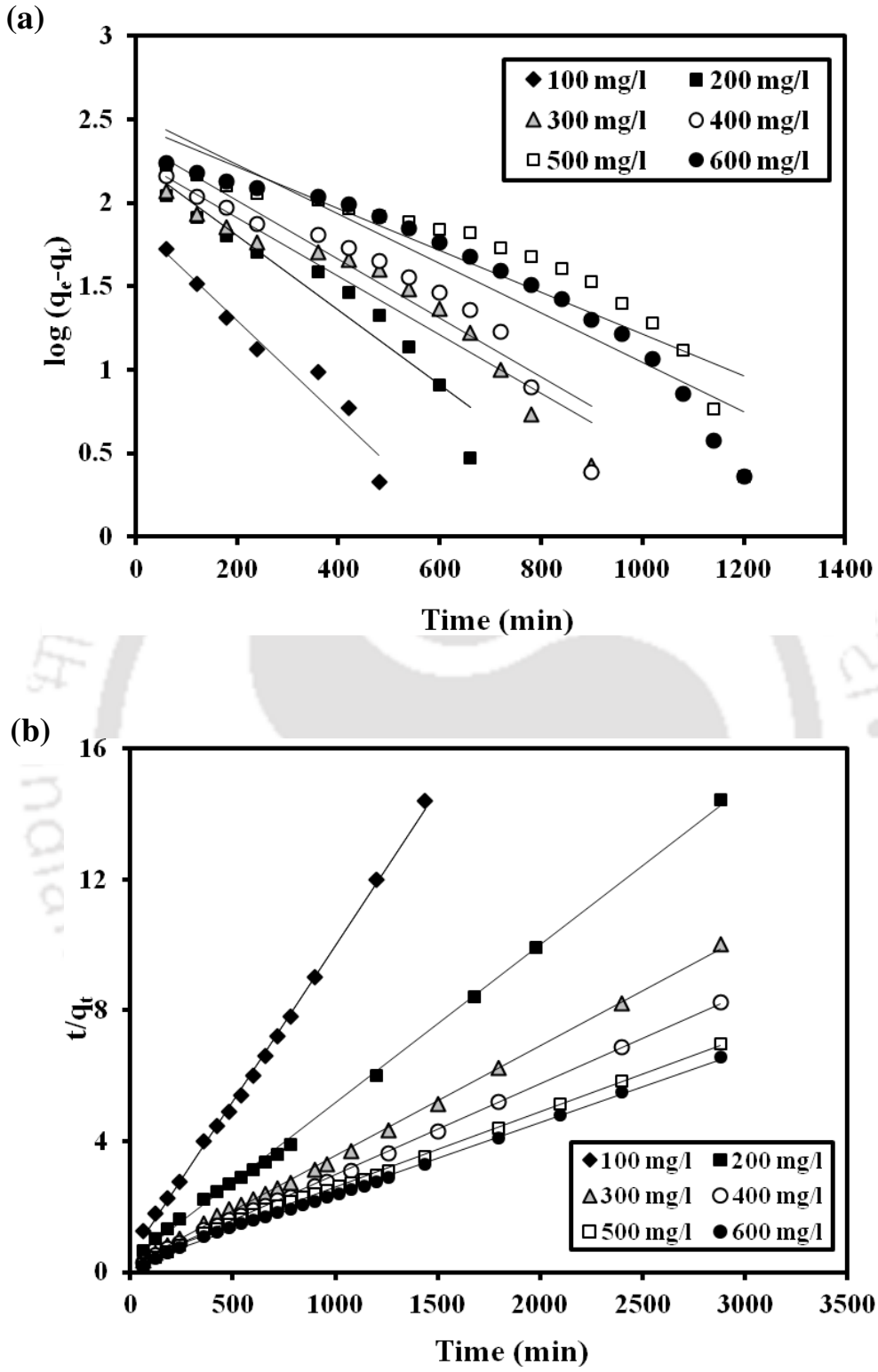

Figure 3.14 Kinetic plots for RB dye adsorption onto BSAC (a) pseudo-first-order kinetics (a) pseudo-second-order kinetics

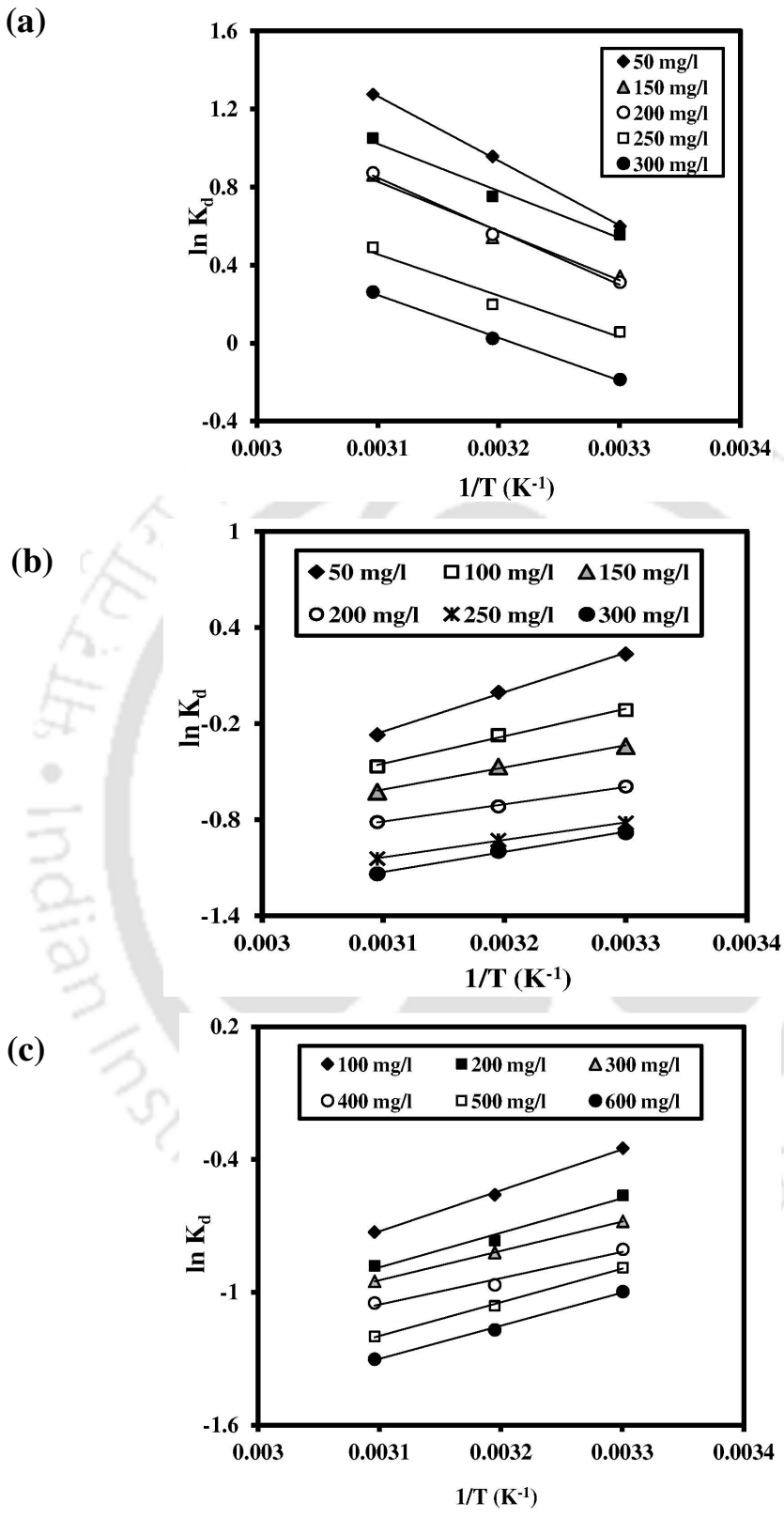

Figure 3.15 Van't Hoff equation plots for (a) Cr^{6+} (b) Sr^{2+} and (c) phenol adsorption onto BSAC

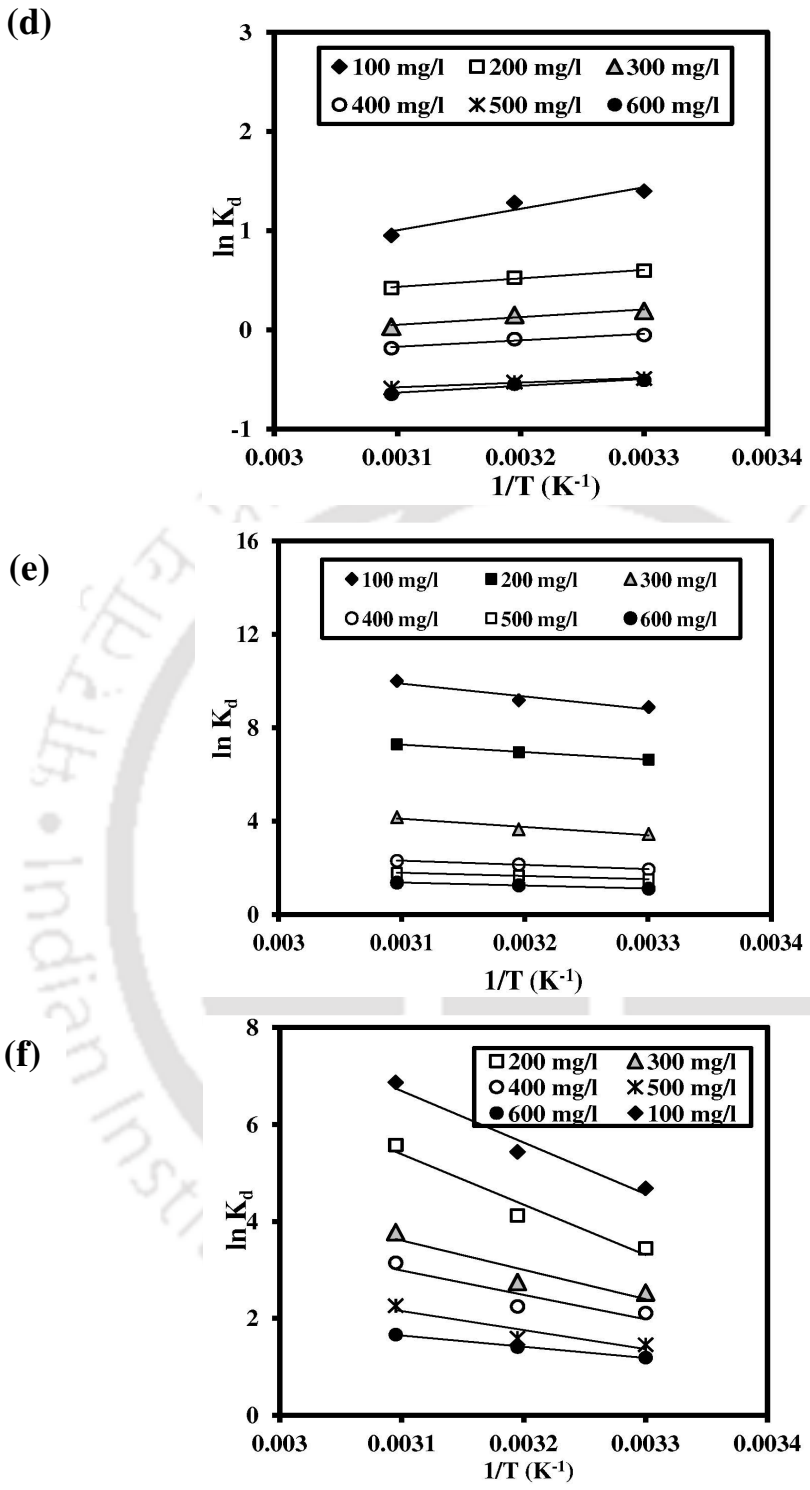

Figure 3.15 Van't Hoff equation plots for (d) *o*-cresol (e) RB dye and (f) MB dye adsorption onto BSAC

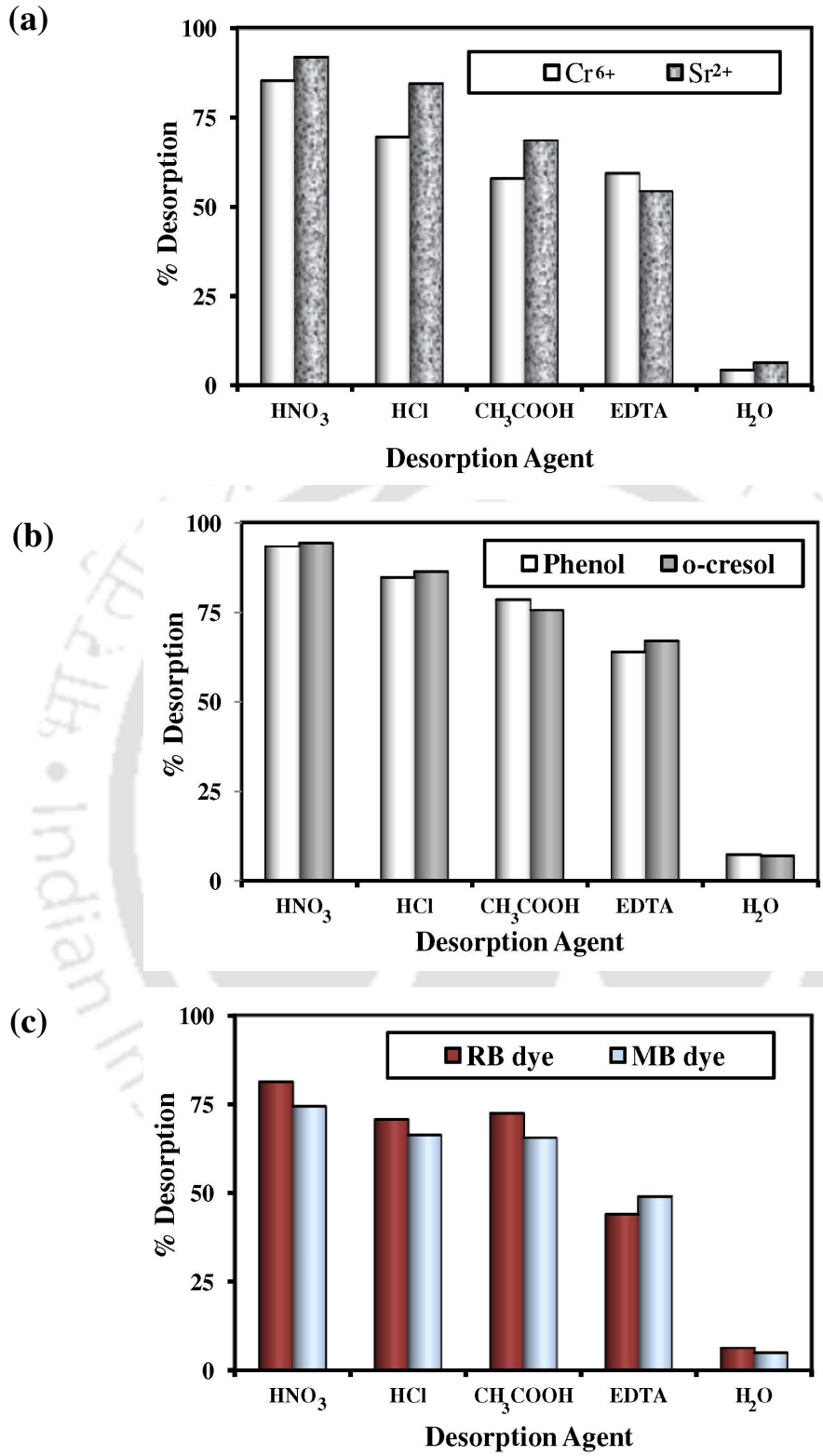

Figure 3.16 Desorption performance of (a) Cr^{6+} & Sr^{2+}; (b) phenol & *o*-cresol and (c) RB & MB dye from BSAC: (W = 0.1 g, V= 50 ml, T = 30°C and t = 300 min (Cr^{6+}, Sr^{2+}, phenol & *o*-cresol) & 1440 min (RB & MB dye)

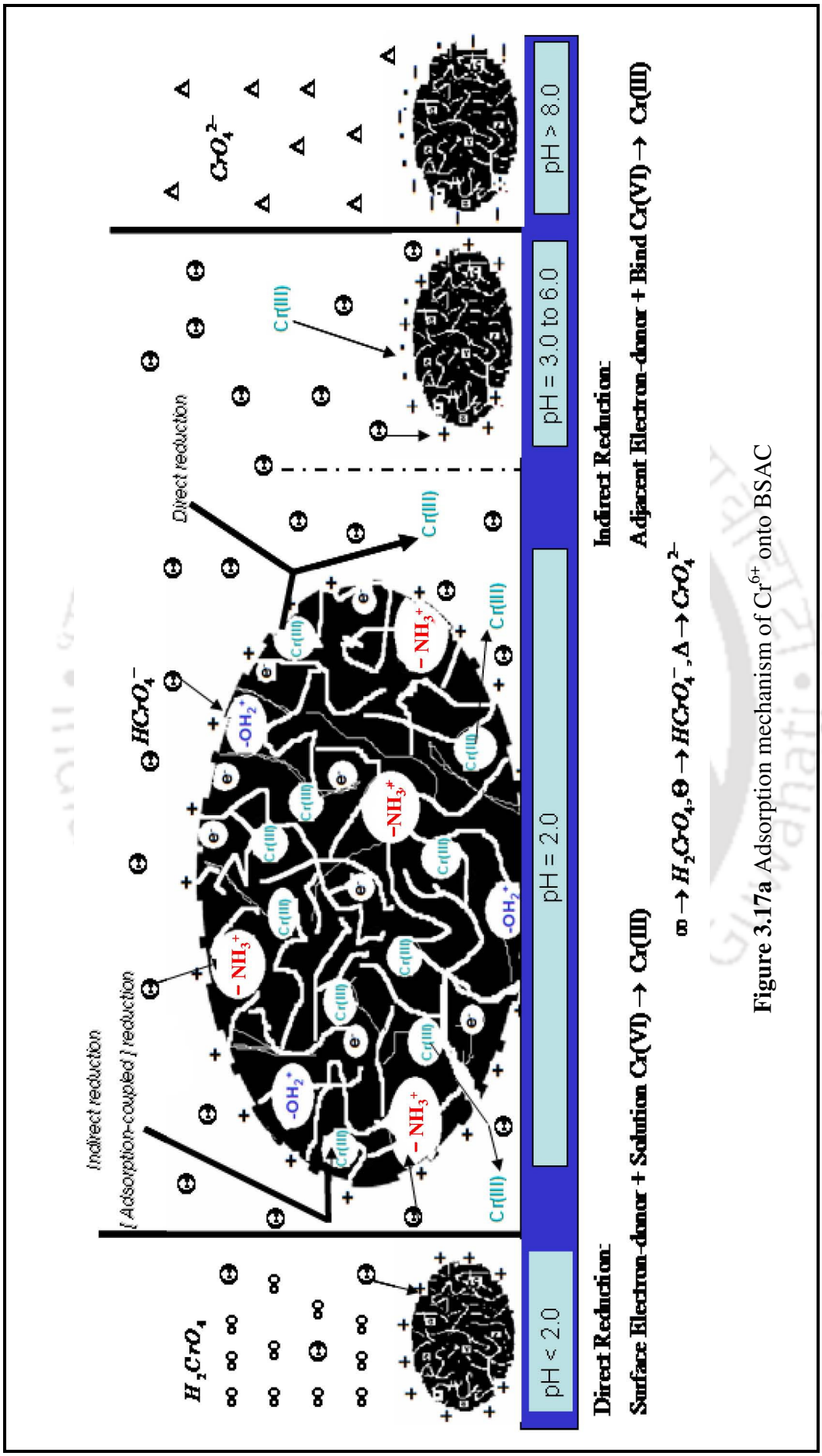

$$\text{e}^- \rightarrow H_2CrO_4, \ominus \rightarrow HCrO_4^-, \Delta \rightarrow CrO_4^{2-}$$

Figure 3.17a Adsorption mechanism of Cr^{6+} onto BSAC

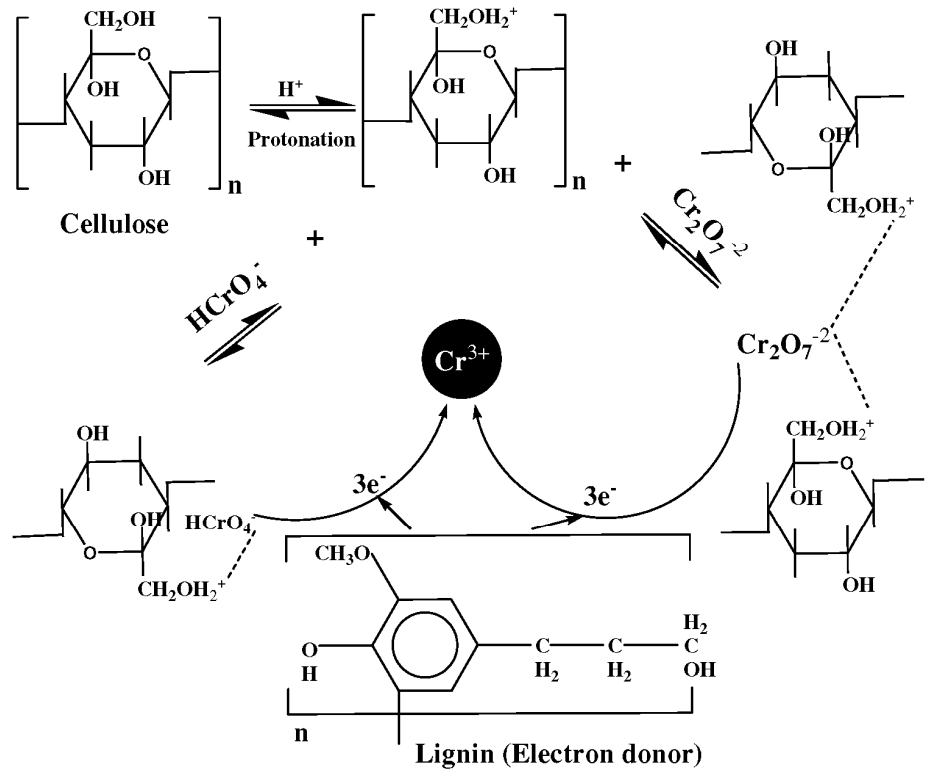

Figure 3.17b Adsorption mechanism of Cr^{6+} onto BSAC

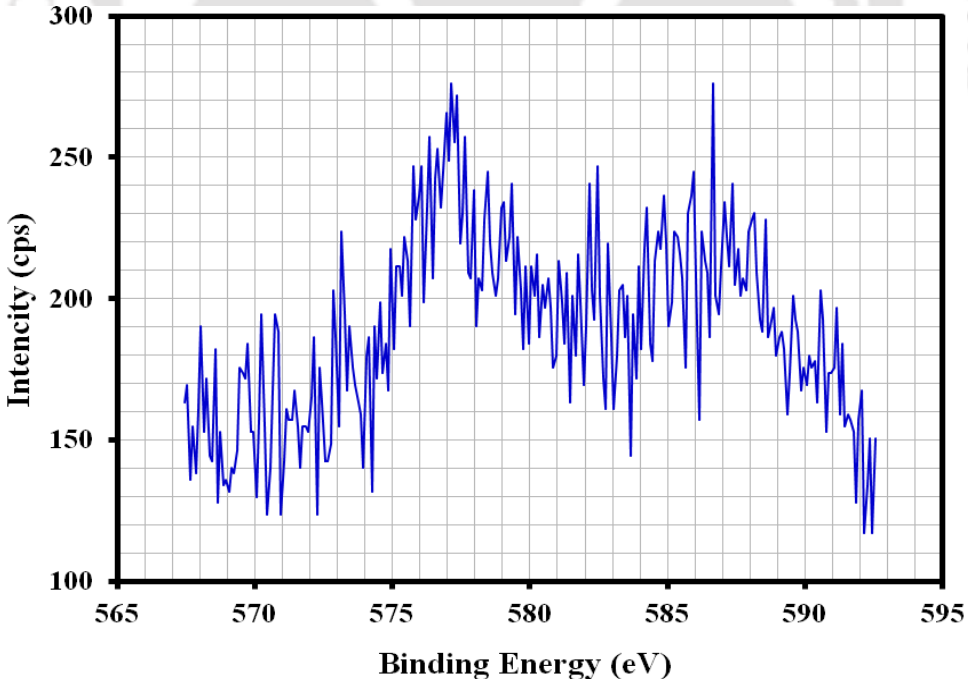

Figure 3.17c XPS spectra of chromium adsorbed BSAC at Cr2p orbital core region

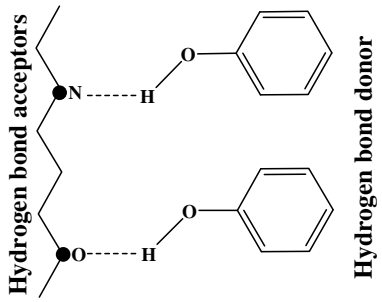

Figure 3.18a Hydrogen bond of phenol on BSAC

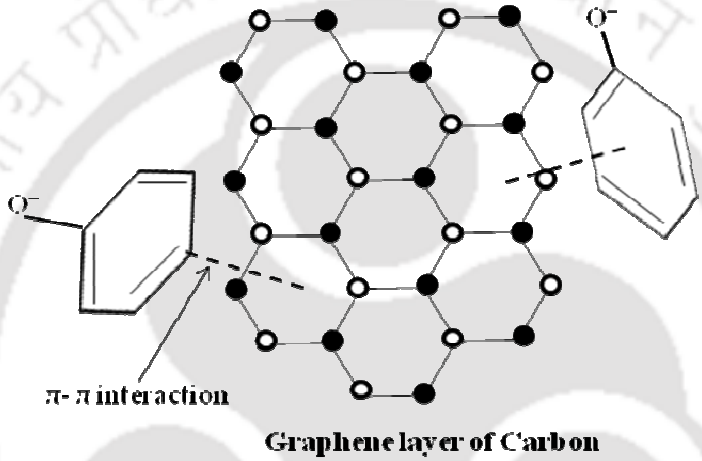

Figure 3.18b π-π interactions of phenol on BSAC

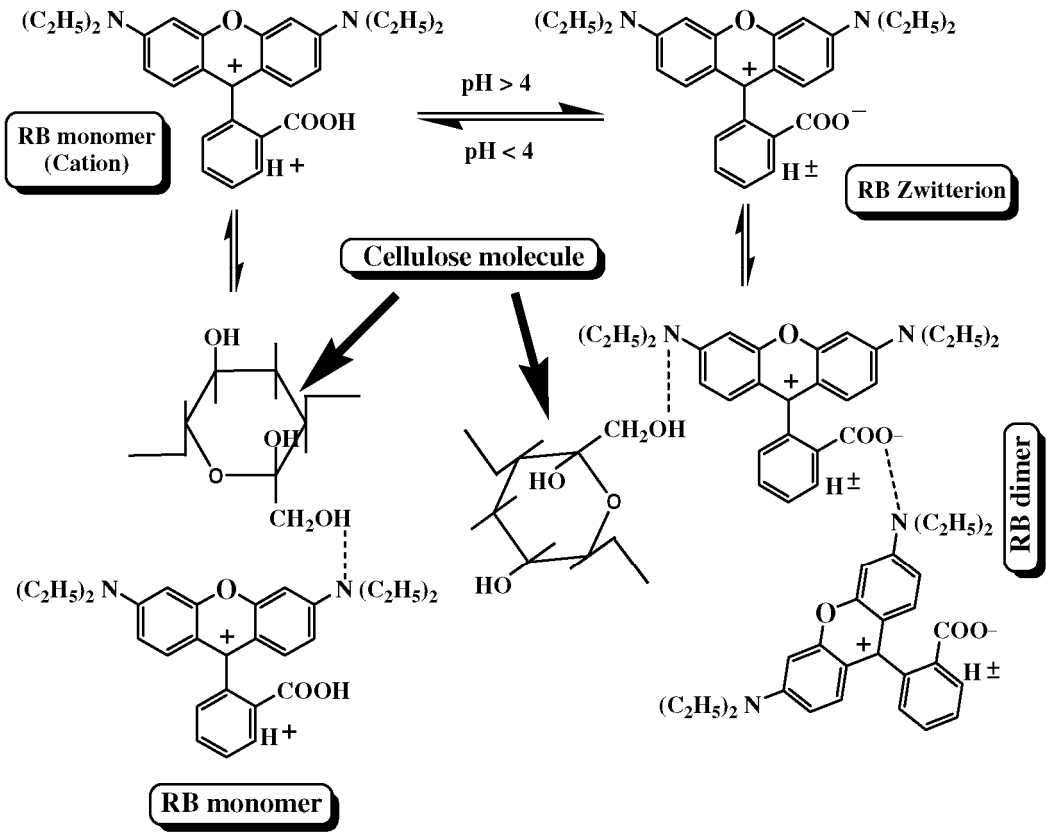

Figure 3.19 Adsorption mechanism of RB dye

Table 3.1

Textural properties of BSAC

Parameters	**Values**
BET surface area (m^2/g)	1953.9
Langmuir surface area (m^2/g)	1853
Monolayer volume (cm^3/g)	448.9
Micropore surface area (by t-plot surface area) (m^2/g)	337.2
Total volume (at Ps/Po = 0.9814, adsorption) (cm^3/g)	1.2658
Micropore volume (by t-plot surface area) (cm^3/g)	0.1189
Meso + macro volume (by t-plot surface area) (cm^3/g)	1.1469

Table 3.2

Some of the fundamental FT-IR frequencies of BS and BSAC

Adsorbent	**Band position (cm^{-1})**					
	O-H	C-H	Amino groups	C=O	C-O	Bending vibrations
BS before activation	3421	2923	2347	1535	1378 & 1103	< 850
BSAC after activation	3412	2924	2374	1554	1382 &1054	545

Table 3.3a

Adsorption isotherm constants of Cr^{6+}, phenol and RB dye onto BSAC at different temperature

Adsorbates at various temperatures		Langmuir constants			Freundlich constants			Temkin constants			Halsey constants		
		Q_o (mg/g)	b (l/mg)	R^2	K_f	1/n	R^2	A (l/g)	B	R^2	K_h	-1/n	R^2
Cr^{6+}	30°C	222.2	0.0107	0.9677	5.469	0.6587	0.9593	0.1057	49.21	0.9852	0.0758	0.6587	0.9593
	40°C	232.6	0.0135	0.9795	7.623	0.6211	0.9703	0.1335	51.45	0.9763	0.0380	0.6211	0.9703
	50°C	249.4	0.0170	0.9952	9.9609	0.6051	0.9777	0.1699	54.87	0.9888	0.0224	0.6051	0.9777
Phenol	30°C	304	2.549×10^{-3}	0.9912	2.597	0.6851	0.9976	0.0297	60.41	0.9772	0.2483	0.6851	0.9976
	40°C	277.8	2.293×10^{-3}	0.9905	2.019	0.7023	0.9941	0.0272	54.56	0.9814	0.3676	0.7023	0.9941
	50°C	256.4	2.176×10^{-3}	0.9894	1.672	0.7158	0.9894	0.0258	50.31	0.9877	0.4877	0.7158	0.9894
RB dye	30°C	434.8	0.2684	0.9928	208.5	0.1484	0.9748	1104	34.31	0.9727	2.361×10^{-16}	0.1484	0.9748
	40°C	463	0.2497	0.9904	218.7	0.1501	0.9761	1206	35.75	0.9616	2.582×10^{-16}	0.1501	0.9761
	50°C	471.7	0.3007	0.9903	50.03	0.1232	0.9812	881.3	38.28	0.9350	3.436×10^{-20}	0.1232	0.9812

Note: C_o = 50-300 (Cr^{6+}), 100-600 (phenol) & 100-600 (RB dye) mg/l, T = 30-50°C, t (equilibrium) = 210 (Cr^{6+}), 180 (phenol) & 1260 (RB dye) min, agitation speed = 180 rpm, V = 50 ml and W = 0.05 g of BSAC.

Table 3.3b

Adsorption isotherm constants of Sr^{2+}, *o*-cresol and MB dye onto BSAC at different temperature

Adsorbates at various temperature		Langmuir constants			Freundlich constants			Temkin constants			Halsey constants		
		Q_o (mg/g)	b (l/mg)	R^2	K_f	1/n	R^2	A (l/g)	B	R^2	K_h	-1/n	R^2
Sr^{2+}	30°C	113.4	0.0138	0.9890	6.4103	0.4923	0.9843	0.1282	25.58	0.9891	0.7672	0.4923	0.9843
	40°C	109.3	0.0116	0.9916	4.8863	0.5267	0.9790	0.1049	24.99	0.9922	0.7175	0.5267	0.9790
	50°C	106.5	0.0093	0.9935	3.4067	0.5261	0.9738	0.0837	24.49	0.9947	0.6510	0.5261	0.9738
o-cresol	30°C	243.3	0.0179	0.9786	29.96	0.3393	0.9764	0.2573	46.89	0.9772	0.9050	0.3393	0.9764
	40°C	239.2	0.0169	0.9794	27.64	0.3488	0.9749	0.2262	47.11	0.9634	0.9002	0.3488	0.9749
	50°C	233.1	0.0142	0.9869	21.44	0.3832	0.9687	0.1570	48.76	0.9770	0.8825	0.3832	0.9687
MB dye	30°C	476.2	0.0935	0.9894	106.5	0.3039	0.9927	3.2293	71.43	0.9763	0.9369	0.3039	0.9927
	40°C	487.8	0.1242	0.9831	131.5	0.2707	0.9915	7.6326	65.05	0.9630	0.9460	0.2707	0.9915
	50°C	510.2	0.3187	0.9951	210.1	0.1971	0.8188	22.99	64.33	0.9370	0.9465	0.1971	0.8188

Note: C_o = 50-300 (Sr^{2+}), 100-600 (*o*-cresol) & 100-600 (MB dye) mg/l, T = 30-50°C, t (equilibrium) = 240 (Sr^{2+}), 210 (*o*-cresol) & 1440 (MB dye) min, agitation speed = 180 rpm, V = 50 ml and W = 0.05 g of BSAC

Table 3.4a

Cr^{6+} adsorption isotherm constants in binary and ternary system by BSAC

Isotherm models	Binary System				Ternary System	
	Cr^{6+} + Phenol		Cr^{6+} + RB dye		Cr^{6+} + Phenol + RB dye	
	pH 2.0	pH 3.5	pH 2.0	pH 3.5	pH 2.0	pH 3.5
Langmuir constants						
Q_o (mg/g)	224.7	141	179.2	148.6	168.1	122.1
b (1×10^{-3}) (l/mg)	10.51	7.188	12.3	7.779	8.006	6.650
R^2	0.9800	0.9847	0.9888	0.9875	0.9926	0.9905
Freundlich constants						
K_f	5.174	2.864	5.378	3.151	3.295	2.319
$1/n$	0.6774	0.6488	0.6326	0.6501	0.6727	0.6528
R^2	0.9846	0.9988	0.9716	0.9925	0.9871	0.9979
Temkin constants						
A (l/g)	0.1126	0.0768	0.1159	0.0813	0.0841	0.0700
B	47.17	29.43	40.32	31.44	35.51	25.63
R^2	0.9832	0.9778	0.9965	0.9849	0.9918	0.9826
Halsey constants						
K_h	0.0883	0.1975	0.1578	0.1711	0.1699	0.2757
$-1/n$	0.6774	0.6488	0.6326	0.6501	0.6727	0.6528
R^2	0.9846	0.9988	0.9716	0.9925	0.9871	0.9979

Note: C_o = 50-250 (Cr^{6+}) mg/l, T = 30°C, t = equilibrium time (min), agitation speed = 180 rpm, V = 50 ml and W = 0.05 g of BSAC.

Table 3.4b

Phenol adsorption isotherm constants in binary and ternary system by BSAC

Isotherm models	Binary System				Ternary System	
	Phenol + Cr^{6+}		Phenol + RB dye		Phenol + Cr^{6+} + RB dye	
	pH 2.0	pH 3.5	pH 2.0	pH 3.5	pH 2.0	pH 3.5
Langmuir constants						
Q_o (mg/g)	277	292.4	390.6	396.8	369	362.3
b (1×10^{-3}) (l/mg)	2.755	2.481	3.585	3.628	3.651	3.416
R^2	0.9223	0.9348	0.9760	0.9839	0.9655	0.9739
Freundlich constants						
K_f	2.284	2.572	3.866	4.141	3.930	3.406
$1/n$	0.7009	0.6810	0.7033	0.6942	0.6907	0.7069
R^2	0.9972	0.9940	0.9829	0.9946	0.9813	0.9856
Temkin constants						
A (l/g)	0.0323	0.0307	0.0409	0.0419	0.0409	0.0383
B	54.53	55.48	78.58	79.22	75.08	73.59
R^2	0.9515	0.9555	0.9892	0.9786	0.9840	0.9850
Halsey constants						
K_h	0.2498	0.3077	0.1462	0.1291	0.1378	0.1767
$-1/n$	0.7009	0.6810	0.7033	0.6942	0.6907	0.7069
R^2	0.9972	0.9940	0.9829	0.9946	0.9813	0.9856

Note: C_o = 100-600 (Phenol) mg/l, T = 30°C, t = equilibrium time (min), agitation speed = 180 rpm, V = 50 ml and W = 0.05 g of BSAC.

Table 3.4c

RB dye adsorption isotherm constants in binary and ternary system by BSAC

Isotherm models	Binary System				Ternary System	
	RB dye + Cr^{6+}		RB dye + Phenol		RB dye + Phenol + Cr^{6+}	
	pH 2.0	pH 3.5	pH 2.0	pH 3.5	pH 2.0	pH 3.5
Langmuir constants						
Q_o (mg/g)	337.8	384.6	315.5	375.9	308.6	380.2
b (1×10^{-3}) (l/mg)	46.1	286.3	21.1	377.8	61.3	230.7
R^2	0.9760	0.9919	0.9936	0.9977	0.9831	0.9916
Freundlich constants						
K_f	69.18	180.2	28.23	182.7	80.30	175.6
$1/n$	0.2857	0.1540	0.4229	0.1531	0.2555	0.1502
R^2	0.9954	0.9946	0.9815	0.9973	0.9966	0.9817
Temkin constants						
A (l/g)	1.643	680.2	0.2241	725.5	3.113	768.9
B	51.42	31.53	67.04	31.51	45.95	30.15
R^2	0.9446	0.9445	0.9812	0.9818	0.9515	0.9137
Halsey constants						
K_h	3.628×10^{-7}	2.248×10^{-15}	3.712×10^{-4}	1.685×10^{-15}	3.510×10^{-8}	1.141×10^{-15}
$-1/n$	0.2857	0.1540	0.4229	0.1531	0.2555	0.1502
R^2	0.9954	0.9946	0.9815	0.9973	0.9966	0.9817

Note: C_o = 100-600 (RB dye) mg/l, T = 30°C, t = equilibrium time (min), agitation speed = 180 rpm, V = 50 ml and W = 0.05 g of BSAC.

Table 3.5

Kinetic constants of Cr^{6+}, phenol and RB dye in single contaminant system

Initial adsorbate concentration (mg/l)		Pseudo-first-order model				Pseudo-second-order model		
		$q_{e,\,exp}$ (mg/g)	k_{ad} (l/min)	$q_{e,\,cal}$ (mg/g)	R^2	k' (1 x 10^{-4}) (g/mg/min)	$q_{e,\,cal}$ (mg/g)	R^2
Cr^{6+}	50	32.28	0.0187	25.46	0.9566	12.19	34.71	0.9985
	100	63.57	0.0178	59.42	0.9666	5.2477	67.29	0.9954
	150	87.77	0.0193	75.33	0.9954	4.4856	92.85	0.9957
	200	115.5	0.0185	116.32	0.9686	2.6729	123.8	0.9954
	250	128.6	0.0159	110.50	0.9591	2.4053	137.7	0.9972
	300	136.1	0.0189	115.26	0.9686	3.1654	143.1	0.9983
Phenol	100	41.36	0.0306	30.97	0.9817	24.65	41.68	0.9939
	200	72.61	0.0350	68.45	0.9993	9.8031	75.70	0.9949
	300	100.9	0.0267	101.39	0.9335	4.5128	106.5	0.9954
	400	123.5	0.0283	125.16	0.9520	3.8926	130.7	0.9957
	500	145.7	0.0246	129.90	0.9767	3.5103	152.7	0.9960
	600	161.7	0.0232	148.35	0.9767	3.5511	165	0.9984
RB dye	100	99.9	0.0067	75.08	0.9507	1.8838	105.3	0.9985
	200	199.7	0.0051	178.66	0.9168	0.6949	207	0.9988
	300	290.8	0.0040	183.03	0.9118	0.6002	297.62	0.9990
	400	349.3	0.0041	233.28	0.8913	0.4183	359.71	0.9992
	500	409.3	0.0029	294.45	0.8272	0.1902	432.9	0.9976
	600	436.6	0.0034	335.78	0.9151	0.2186	458.7	0.9984

Note: C_o = 50-300 (Cr^{6+}), 100-600 (phenol) & 100-600 (RB dye) mg/l, T = 30-50^oC, t (equilibrium) = 210 (Cr^{6+}), 180 (phenol) & 1260 (RB dye) min, agitation speed = 180 rpm, V = 50 ml and W = 0.05 g of BSAC.

Table 3.6a

Thermodynamic parameters of Cr^{6+}, phenol and RB dye adsorption onto BSAC

Initial pollutant concentration (mg/l)		$\Delta H°$ (J/mol)	$\Delta S°$ (J/mol K)	$\Delta G°$ (J/mol)		
				30 ºC	40 ºC	50 ºC
Cr^{6+}	50	27498	95.76	-1510	-2490	-3424
	100	20043	70.61	-1403	-1957	-2821
	150	21013	72.02	-866.3	-1409	-2314
	200	22765	77.61	-786.8	-1452	-2344
	250	17601	58.35	-145.1	-516.9	-1321
	300	18234	58.58	468.7	-64.71	-705.1
Phenol	100	-15416	-53.82	879.4	1457	1954
	200	-12962	-47.56	1416	1996	2363
	300	-11021	-42.03	1712	2137	2552
	400	-9886	-39.43	2031	2515	2815
	500	-12638	-49.13	2239	2762	3220
	600	-12425	-49.34	2511	3043	3496
RB dye	100	45397	222.9	-22365	-23871	-26854
	200	26323	142	-16725	-18090	-19568
	300	28994	123.9	-8696	-9494	-11194
	400	15073	65.85	-4861	-5582	-6175
	500	11361	50.07	-3798	-4332	-4797
	600	10323	43.34	-2804	-3258	-3670

Note: C_o = 50-300 (Cr^{6+}), 100-600 (phenol) & 100-600 (RB dye) mg/l, T = 30-50°C, t (equilibrium) = 210 (Cr^{6+}), 180 (phenol) & 1260 (RB dye) min, agitation speed = 180 rpm, V = 50 ml and W = 0.05 g of BSAC.

Table 3.6b

Thermodynamic parameters of Sr^{2+}, *o*-cresol and MB dye adsorption onto BSAC

Initial pollutant concentration (mg/l)		$\Delta H°$ (J/mol)	$\Delta S°$ (J/mol K)	$\Delta G°$ (J/mol)		
				30 ºC	40 ºC	50 ºC
Sr^{2+}	50	-20423	-65.39	-592.2	10.41	706.2
	100	-14239	-47.88	291.3	706.9	1227
	150	-11517	-40.79	858.9	1219	1643
	200	-8999	-34.65	1492	1864	2138
	250	-9044	-36.64	2063	2412	2738
	300	-10395	-41.58	2218	2594	2987
o-cresol	100	-18004	-47.47	-3526	-3344	-2506
	200	-7050	-18.24	-1506	-1373	-1113
	300	-6427	-19.50	-484.6	-395.6	-87.23
	400	-5393	-18.13	124.9	236.2	480.8
	500	-3916	-16.95	1231	1365	1538
	600	-5644	-22.75	1275	1420	1697
MB dye	100	88353	329.5	-11796	-14142	-18042
	200	86249	312.1	-8676	-10728	-14654
	300	50212	185.6	-6385	-7158	-9930
	400	41719	154.2	-5322	-5854	-8271
	500	32531	118.7	-3672	-4143	-5950
	600	19164	73.10	-3008	-3675	-4380

Note: C_o = 50-300 (Sr^{2+}), 100-600 (*o*-cresol) & 100-600 (MB dye) mg/l, T = 30-50ºC, t (equilibrium) = 240 (Sr^{2+}), 210 (*o*-cresol) & 1440 (MB dye) min, agitation speed = 180 rpm, V = 50 ml and W = 0.05 g of BSAC.

CHAPTER 4

ADSORPTION OF SELECTED CONTAMINANTS ON CHEMICALLY ACTIVATED BAEL SHELL

The detailed adsorption studies of selected heavy metals and dyes which are identified in the preliminary performance evaluation test (PPET) for their higher adsorption capacities with only H_2SO_4 activated bael shell (SBS) are presented in this chapter. In PPET, it was found that Pb^{2+}, Ni^{2+}, Sr^{2+} metal, rhodamine B and methylene blue dye had high adsorption capacities with SBS from the targeted contaminants. Thus, in this chapter the elaborate adsorption studies and its results with the above mentioned heavy metals and dyes are reported and the results also discussed in detail by covering all the aspects for its possible applications in the field of wastewater treatment.

4.1 INTRODUCTION

Heavy metals as well as cationic dyes are extensively used by different kind of industries such as stainless steel, battery recycling plants, lead mining, electronic assembly, wood preservative, textile dyeing, fireworks, tanneries and metal plating industries. Among all the heavy metals and dyes, special attention has been given to Pb^{2+}, Ni^{2+}, Sr^{2+} ions and cationic dyes such as rhodamine B (RB) and methylene blue (MB) because of their common and extensive use in industries. Ingestion of Pb^{2+} and Ni^{2+} higher than its permissible level causes brain damage and dysfunction of the kidneys, liver and the central nervous system (Lalhruaitluanga and Jayaram, 2010; Ngah and Fatinathan, 2010; Srivastava *et al.,* 2006). On the contrary, Sr^{2+} has fatal effect if induced at high dosage as a result of its high solubility, long life and bio-toxicity (Ahmadpoura *et al.,* 2010). Dyes create aesthetical and toxicological problems in the aqueous system. Therefore, the removal of these contaminants from wastewater is very important before its discharge. In this chapter, batch adsorption experiment results of single and multi component systems of selected metals and dyes are presented and discussed in detail using H_2SO_4 treated Bael shell adsorbent (SBS). In preliminary performance evaluation test, SBS was found as an effective adsorbent for the removal of Pb^{2+}, Ni^{2+}, Sr^{2+} metal as well as cationic dyes (rhodamine B and methylene blue) from the targeted contaminants of this research work. The operating parameters that affect the adsorption process such as effect of pH, influence of other ions, multi component systems and solution temperature were monitored in this study to optimize the sorption process for its possible use as a low-cost adsorbent in the field of wastewater treatment to remove the single and multi contaminants from aqueous solution.

4.2 EXPERIMENTAL METHODS

4.2.1 Preparation of Synthetic Wastewater

Stock solutions of Pb^{2+}, Ni^{2+}, Sr^{2+}, rhodamine B (RB) and methylene blue (MB) dye (1000 mg per litre of each metal solution separately) were prepared by dissolving appropriate quantity of $Pb(NO_3)_2$, $NiCl_2.6H_2O$, $SrCl_2.6H_2O$ (Merck, India), RB and MB dye (C.I. 45170 and 52015, LOBA Chemie, India) in Millipore water, respectively. The chemical structure of RB and MB is illustrated in Appendix 1. Equal mass of binary {(1000 mg of Pb^{2+} + 1000 mg of Ni^{2+}) per litre, (1000 mg of

metal Pb^{2+} + 1000 mg of Sr^{2+}) per litre and (1000 mg of Ni^{2+} + 1000 mg of Sr^{2+}) per litre} and equal mass of ternary {(1000 mg of metal Pb^{2+} + 1000 mg of Ni^{2+} + 1000 mg of Sr^{2+}) per litre} metal solutions were prepared for binary and ternary metal adsorption. Similarly, equal mass of each dye and each metal combination (150 mg of dye + 150 mg of metal) were prepared for another set of binary system. All stock solutions were shaken for 10 min at 180 rpm to obtain complete dissolution and then suitably diluted with Millipore water to get the required initial concentrations (100 to 300 mg/l for metals). Before mixing the adsorbent, the pH of the solution was adjusted using 0.1 N HCl or 0.1N NaOH. The pH of the solution was measured by pH meter (Eutech, model: 510).

4.2.2 Experimental Protocol

4.2.2.1 Adsorption Experiment

Adsorption experiments were carried out under batch mode at 30°C, 40°C and 50°C. Initially, the effect of acid treatment, solution pH, other ions and solution temperatures on sorption capacity of adsorbate (Pb^{2+}, Ni^{2+}, Sr^{2+}, RB and MB dye) onto SBS were carried out only in single metal and dye system using fixed doses of adsorbents in 50 ml solution at 180 rpm. The pH of each solution was adjusted using required quantity of 1N HCl (or) 1N NaOH before mixing the adsorbent. Subsequently, the effect of equal concentrations of binary and ternary system was conducted at natural pH using desired amount of adsorbent per 50 ml of multi-metal and (metal + dye) solutions. In a set of 250 ml Borosil conical flasks containing adsorbate solution (50 ml) of particular initial concentration was placed. Fixed doses of adsorbent were then added to the adsorbate solutions. The pH of the each solution was maintained at natural condition. Each sample was agitated in an incubating shaker (LabTech, Model LSI-1005R) at a particular temperature. Samples at different time intervals were withdrawn and the supernatant of metal and dye solution was separated by filtration using Whatman filter paper no. 42 and centrifuging dye at 5000 rpm, respectively. Final residual metal concentration was directly measured by flame atomic absorption spectrophotometer (AAS) (Varian spectra, AA240) with an air–acetylene flame. The supernatant of RB and MB dye solutions were analyzed for the residual dye concentrations using UV–visible spectrophotometer (Perkin-Elmer, model: Lambdas 45) at the maximum wavelength (λ_{max} = 555 nm for RB and 667 nm

for MB) of the dyes. Calculation methods of adsorption capacity of adsorbent are given in Appendix 2.

4.2.2.2 Desorption Experiment

After adsorption, the elution of metals and dyes could be interesting for the reutilization of exhausted adsorbent and the recovery of the adsorbed metals and dyes. The SBS utilized for the adsorption of initial Pb^{2+}, Ni^{2+}, Sr^{2+}, RB and MB dye concentrations of 100 mg/l using 0.1 g of SBS in 50 ml at 30°C were separated from solution by filtration. Then, metal and dye loaded adsorbents was mixed with 50 ml of different eluent solvents such as (0.1 M of HCl, HNO_3, CH_3COOH, NaOH; 0.01 M of EDTA; and hot distilled water) and agitated in incubating shaker (LabTech, Model LSI-1005R) at 30°C temperature for 24 hr. After desorption, the supernatant of desorbed metal and dye eluent solutions were collected for the desorbed metal and dye analysis. The detailed procedure to calculate the amount of desorbed metal and dye is presented in the Appendix-2.

4.2.3 Adsorbent Characterization

(i) Scanning electron microscopy (SEM) (Leo, 1430 vp, Carl Zeiss, German) characterisation was carried out to observe the surface texture and porosity for two states of BS such as BS without activation and BS with H_2SO_4 activation (SBS). (ii) Due to the lower surface area of SBS adsorbent, to find out the BET surface area and monolayer volume of SBS, the single point surface area analyser (ChemiSorb 2720/2750) was used to analyze the nitrogen adsorption isotherm at -196°C. Before measurement, the samples were degassed using Helium at 150°C for 30 min. (iii) To resolve the functional groups and its wave numbers, spectra analysis was done for BS before and after adsorption using Fourier transform infrared spectrometer (FT-IR) (Perkin Elmer, PE-RXI) in the range of 500–4000 cm^{-1}. (iv) Zeta potential of SBS was measured using Beckman Coulter zeta potential analyzer (Delsa™ Nano C) at various pH based on the laser Doppler electrophoresis technique. (v) Energy dispersive X-ray spectroscopy (EDX) analysis was employed for further confirmation of metal adsorption over the surface of the SBS.

4.3 RESULTS AND DISCUSSION

4.3.1 Effect of Acid Activation

The effect of various percentage concentrations of H_2SO_4 activation on adsorption capacity of single metal and dye system was studied (Figure 4.1). The sorption capacity of Pb^{2+}, Ni^{2+}, Sr^{2+}, RB and MB dye increased from 21.48 mg/g to 81.6 mg/g, 6.37 to 52.89 mg/g, 19.57 to 69.95, 81.22 to 131.25 and 99.17 to 138.5 mg/g, respectively, as the H_2SO_4 concentration increased from 24.5 % to 98 %. The increase in chemical concentration in BS activation increased the porous structure and BET surface area. During activation, H_2SO_4 reacts with the cellulosic, lignin and other surface functional groups of BS. Besides, reaction produces enormous amount of heat that helps to produce active sites and pores on BS, that enhanced the sorption capacity of metals (Anandkumar and Mandal, 2009; Giris *et al.,* 2002; Serrano *et al.,* 2004). Therefore, the sorbent which was prepared by only absolute H_2SO_4 was utilized for the entire study.

4.3.2 Surface Characterization of Adsorbent

4.3.2.1 SEM Analysis

The SEM image of BS before and after H_2SO_4 activation is shown in Figure 4.2b and 2c. It could be observed from Figure 4.2a that prior to H_2SO_4 activation BS had regular plain surface with no pores on it, whereas Figure 4.2b. (i.e., BS after activation) reveals the progressive changes and well developed pores on the surface of the BS. The pore formation of activated BS is mainly attributed to the addition of H_2SO_4 that causes the BS to swell and it opens the surface structure. During the activation, H_2SO_4 reacts with the cellulosic structure of the material with enormous amount of heat formation and thus forms the porous structure with active sites on the surface of adsorbent (Anandkumar and Mandal, 2009).

4.3.2.2 ChemiSorb Surface Area Analysis

The BET surface area of synthesized adsorbents using various acid concentrations is presented in Table 4.1. As given in Table 4.1, the surface area (17.61 to 34.28 m^2/g) and total pore volume (0.0089 to 0.0173 ml/g) increased with increase in concentration of H_2SO_4 from 24.5 to 98 %. The improvement in surface texture and pore formation might be due to the high reaction between acid and BS surface

functional groups on the adsorbent in formation of porous surface. Similar observation has been reported in Chapter 3 for Bael shell adsorbent with (H_3PO_4 + thermal) treatment.

4.3.2.3 Fourier Transform-Infrared (FT-IR) Spectra Analysis

The FT-IR spectra of SBS before and after Pb^{2+}, Ni^{2+}, Sr^{2+}, RB and MB dye adsorption (Figure 4.3a and 4.3b) were recorded to acquire the information regarding wave number changes (peak shifting) on the functional groups in the range of 500 to 4000 cm^{-1}. The bands of SBS at 3422, 2928, 1611, 1100, and 1023 cm^{-1} are the stretching vibrations of the surface hydroxyl group (O–H), symmetric vibrations of C–H predominantly for aliphatic acids, COO and C=C groups, C–O stretch and stretching vibrations of C–O–C and $–OCH_3$ (indicative of lignin structure), respectively. The other bending vibrations less than 666 cm^{-1} are the finger print zone that indicates the phosphate functional groups (Mohan and Sreelakshmi, 2008). In case of SBS spectrum after metal adsorption, the major shift (Figure 4.3a and 4.3b) of –OH stretching mode from 3422 cm^{-1} to 3392, 3383, 3402, 3389 and 3407 cm^{-1} in Pb^{2+}, Ni^{2+}, Sr^{2+}, RB and MB dye adsorbed SBS indicates the –OH group involvement in the metal and dye binding through electrostatic interaction. In addition to this, small peak shifting of other functional groups in metal adsorbed SBS and major shifts below 1700 cm^{-1} in dye adsorbed SBS are confirmed the Pb^{2+}, Ni^{2+}, Sr^{2+}, RB and MB dye binding with SBS surface functional groups.

4.3.2.4 Point of Zero Charge (pH_{pzc}) Analysis

The protonation and deprotanation of surface functional groups due to the solution pH also create an electrical charge on the surface of the adsorbent. Hence, a charge potential due to pH alterations on the surfaces of SBS plays a vital role in adsorption process. Figure 4.2a shows the measured zeta potential as a function of solution pH for SBS. The zeta potential of SBS was measured based on the electrophoretic light scattering (ELS), which determines electrophoretic movement of charged particles under an applied electric field from the Doppler shift of scattered light. Figure 4.4b show the electrophoretic mobility distribution of the SBS partical at solution pH 7.0. The zeta potential of SBS decreased from the positive value to negative with increasing pH. The pH at which the zeta potential is zero is measured as point of zero charge (pH_{pzc}) and hence the net charge on the surface at (pH_{pzc}) is zero. The pH_{pzc} of

SBS was 3.13. The above pH_{pzc}, surface of SBS will becomes negative and favoured for adsorbing Pb^{2+}, Ni^{2+}, Sr^{2+}, RB and MB cations.

4.3.2.5 Energy Dispersive X-ray Spectroscopy (EDX) Analysis

An energy dispersive X-ray spectrum of SBS before and after metal (Pb^{2+}, Ni^{2+} and Sr^{2+}) adsorption is shown in Figure 4.5a, 4.5b, 4.5c and 4.5d. It has been found from Figure 4.5a that SBS having the carbon, oxygen and sulfur elements on its surface before interaction with Pb^{2+}, Ni^{2+} and Sr^{2+} ions, whereas in Figure 4.5b, 4.5c and 4.5d new lead, nickel and strontium peaks were observed with the surface bearing groups of carbon and oxygen, which confirmed the lead, nickel and strontium adsorption on SBS. Sulfur peak on SBS is due to the treatment of H_2SO_4 with BS.

4.3.3 Effect of pH

Solution pH is of prime importance for efficient removal of trace elements on the adsorbent (Lalhruaitluanga and Jayaram, 2010). The pH of the metal (each metal, 100 mg/l) and dye (each metal, 200 mg/l) solutions were varied in the range of 2.0-8.0 and 2-12, respectively keeping all other parameters constant. It was observed from Figure 4.6a that the adsorption of metals increased with increase in initial pH from 2.0 to 6.0. Based on Figure 4.5a, it was found that the maximum adsorption capacities of Pb^{2+}, Ni^{2+} and Sr^{2+} ions were observed at pH 5.2 (82.9 mg/g), 6.0 (54.89 mg/g) and 6.8 (72.95 mg/g), respectively. Similarly, adsorption capacity of dyes increased with increase in pH up to pH 3.5 for RB dye and pH 7.2 for MB dye (Figure 4.6b). The maximum adsorption capacity of RB and MB was found at pH 3.5 (167.8 mg/g) and 7.0 (168.2 mg/g).

At low pH, the surface of the sorbent was more protonated (due to more H^+ ions), which tend to repel the positively charged metal and dye ions, and thus decreased adsorption of all metal cations and dyes in acidic pH (Dakiky and Khamis, 2002). As the solution pH of Pb^{2+} and Ni^{2+} increased from 2.0 to 6.0, the availability of $-OH^-$ and other negative functional groups are increased due to deprotanation and that enhances metal and dye adsorption. At pH > 6, both Pb^{2+} and Ni^{2+} ions precipitate as insoluble hydroxides (Ngah and. Fatinathan, 2010; Kandaha and Meunier, 2007). Similarly, for Sr^{2+} the pH > 7 leads to decrease in adsorption capacity was due to the formation of soluble hydroxylated complexes of Sr^{2+} ions (Li et al., 2010). Maximum

RB dye adsorption observed at pH 3.5 (Figure 4.6b) due the monomeric form of RB dye and that reduces in the alkaline pH owing to the formation dimmers and trimmers, which might reduce the pore diffusion. MB dye adsorption capacity also gradually increases with increase in pH up to pH 7.2. Thereafter, MB dye removal from solution was due to the dissociation of dye structure. Hence, natural pH of all metals (between 5.0-6.0 ± 0.05) and dyes (3.63, RB and 6.76, MB) was used as optimum pH throughout the study.

4.3.4 Effect of Other Ions in Test Solution

The effect of different co-ions such as K^+, Na^+, NH_4^+ and Ca^{2+}, which are commonly present in water and wastewater, on the adsorption capacity of Pb^{2+}, Ni^{2+}, Sr^{2+}, RB and MB dye onto SBS was studied. The initial concentration of co-ions in the metal solutions was varied from 0.5 to 20 g/l by keeping all metal (100 mg/l) and dye (150 mg/l) concentration constant in single component system. The effect of other ions on the adsorption capacity of Pb^{2+}, Ni^{2+}, Sr^{2+}, RB and MB dye sorption on SBS is shown in the Figure 4.7a, 4.7b, 4.7c, 4.7d and 4.7e, respectively. Figures clearly depicts that the adsorption capacity of metals decreased when other cations were simultaneously present in the metal solution. However, there was no significant reduction in the adsorption both RB and MB dye. Results revels that the Pb^{2+}, Ni^{2+}, Sr^{2+}, RB and MB dye adsorption is about 81.6, 52.89, 69.95, 131.2 and 138.5 mg/g in the absence of other ions. However, the sorption capacity of Pb^{2+}, Ni^{2+} and Sr^{2+} decreased with increase in the concentration of other ions such as K^+, Na^+, NH_4^+ and Ca^{2+}. Similar observation has been reported for Ni^{2+} adsorption using bagasse fly ash (Gupta *et al.*, 2003). It has been proposed that for activated adsorbent, other cations may partially neutralize the negative charge of the adsorbent surface, thus reduces the attractive forces between the adsorbent and adsorbate. Moreover, some of the binded K^+, Na^+, NH_4^+ and Ca^{2+} cations on the surface of adsorbent may create the repulsive force towards the positive heavy metal ions near the adsorbent surface. Figure 4.7c depicts that the addition of low concentration of Ca^{2+} with Sr^{2+} decreases the adsorption capacity but slowly increases at higher concentrations of Ca^{2+}. The Ca^{2+} might be acted as a cement matrix to bind the Sr^{2+} ions from the test solution (Wieland *et al.*, 2008). Nevertheless, SBS efficiently adsorbed Ni^{2+} and Sr^{2+} ions in presence of low

concentrations of Na^+ and K^+ ions. Dyes are not affected in presence of other co-ions this fact might be due to the high interaction of dyes with adsorbent surface.

4.3.5 Effect of Binary and Ternary System

A study to assess the change in metal and dye sorption capacities of SBS was conducted for various binary metal and binary (metal + dye) combinations. An equal concentrations of three binary metal system such as (Pb^{2+} + Ni^{2+}), (Pb^{2+} +Sr^{2+}) and (Ni^{2+} + Sr^{2+}) of each metal combination ranging from (100+100) to (300+300) mg/l was used in this study. Subsequently, six equal concentrations of metal mixed dye (150 mg/l of metal + 150 mg/l of dye) combinations such as (Pb^{2+} + RB), (Pb^{2+} + MB), (Ni^{2+} + RB), (Ni^{2+} + MB), (Sr^{2+} + RB) and (Sr^{2+} + MB) were tested for the effect of binary adsorption capacity on SBS. It was observed from Figures 4.8b, 4.8c, 4.8d, 4.8f and 4.8g that the individual adsorption capacity of Pb^{2+}, Ni^{2+} and Sr^{2+} (Figure 4.8a) decreased in their binary metal and dye mixed metal system while compared with their single metal adsorption. However, there is no significant reduction in the adsorption capacity of dyes with metal combinations. This might be due to the higher interaction of dyes with SBS surface rather than metals.

In general, multi-component system may follow three types of adsorption behaviour: (i) synergism (the effect of the mixture is greater than that of each of the individual adsorbates in the mixture), (ii) antagonism (the effect of the mixture is less than that of each of the individual adsorbates in the mixture) and (iii) non interaction (the mixture has no effect on the adsorption of each of the adsorbates in the mixture). The combined effect of the two components seems to be antagonistic (Srivastava *et al.*, 2006; Mahamadi and Nharingo, 2010). To examine the antagonistic adsorption interaction of the two metal ions, the adsorption yields of the single and binary component systems were also compared. For instance, in Figure 4.8a and Figure 4.8c, it was expected that the total adsorption capacity must be equal to 179.43 mg/g for the total metal concentration of 600 mg/l containing equal (300 mg/l) concentration of Pb^{2+} and Sr^{2+} in the binary mixture [Ad_{Tot} = (single Pb^{2+} sorption capacity + single Sr^{2+} sorption capacity) = (104.34 mg/g Pb^{2+} + 75.09 mg/g Sr^{2+} ion) = 179.43 mg/g]. However, the total experimental adsorption capacity was 122.74 mg/g for total metal ions concentration of 600 mg/l consisting of 300 mg/l each of Pb^{2+} and Sr^{2+} ions [Ad_{Tot} = (single Pb^{2+} sorption capacity + single Sr^{2+} sorption capacity) = (77.91 mg/g

Pb^{2+} + 44.83 mg/g Sr^{2+} ion) = 122.74 mg/g]. This shows that the binary system exhibited inhibitory (antagonistic) adsorption for each metal, thereby resulting in a lower sorption yield. However, the overall unit adsorption capacity of adsorbent (combined sorption capacity of two metals in binary system) increased as compared to the individual sorption capacity of only single metal (Anandkumar and Mandal, 2009). In the other hand, dyes had no interaction with metals while adsorbing with SBS.

The ternary metal adsorption of Pb^{2+}, Ni^{2+} and Sr^{2+} ions by SBS was investigated to establish the effect of the presence of three metal ions on the adsorption of each one of them in equal concentrations. The SBS had the highest affinity for Pb^{2+} ions and the least affinity for Ni^{2+} ions in ternary metal system. The sorption affinity order in ternary metal system was found to be: $Pb^{2+} > Sr^{2+} > Ni^{2+}$. As expected, it can be observed from Figure 4.8e that there was no adsorption of Ni^{2+} at higher concentration range in ternary metal system compared with binary metal system. This effect might be due to the (combined effect of other two metal ions on Ni^{2+} adsorption at higher concentration range) less affinity of Ni^{2+} ions when other metals were present in the Ni^{2+} solution. These results depict that the presence of both Pb^{2+} and Sr^{2+} with Ni^{2+} had an adverse effect on Ni^{2+} adsorption. The combined effect of the ternary system also seems to be antagonistic behaviour as observed in binary metal system.

4.3.6 Isotherm Studies

To examine the relationship between SBS and Pb^{2+}, Ni^{2+}, Sr^{2+} metal, RB and MB dye at equilibrium and the maximum adsorption capacity of SBS, four adsorption isotherm models namely the Langmuir, Freundlich, Temkin and Halsey isotherms were analyzed to find the most suitable one. The theoretical details and mathematical equations of each isotherm model are given in the Appendix-3.

The liner equation plots of (C_e/q_e versus C_e), ($log\ q_e$ versus $log\ C_e$), (q_e versus $ln\ C_e$) and ($ln\ q_e$ versus $ln\ C_e$) gives the equilibrium data fitting of Langmuir (Figures 4.9a to 4.9h), Freundlich (Figures 4.10a to 4.10h), Temkin (Figures 4.11a to 4.11h) and Halsey adsorption models (Figures 4.12a to 4.12h), respectively for Pb^{2+}, Ni^{2+}, Sr^{2+} metal, RB and MB dye in single as well as multi-metal system. The isotherm

constants of single and multi-component system are given in (Tables 4.2a and 4.2b) and (Table 4.3), respectively. Among the aforementioned four models, based on the liner correlation coefficients (R^2), Langmuir model is fitted well that other three models for all the cases of both single and multi component system. As observed, the adsorption capacity of Pb^{2+}, Ni^{2+}, Sr^{2+} metal, RB and MB dye onto SBS is competitive in comparison with many literature reported adsorbents and few are given in Appendix 4. In addition, the SBS can remove the toxic Pb^{2+}, Ni^{2+} and Sr^{2+} in single, various binary and ternary metal systems with high efficiency, and this is the main advantage that other adsorbents do not possess.

4.3.7 Sorption Kinetics

The adsorption kinetics of single metal and dye component system described by the relationship between the reaction time and adsorbate uptake by SBS for various initial Pb^{2+}, Ni^{2+}, Sr^{2+}, RB and MB dye concentrations are discussed below with the help of two models such as pseudo-first order and pseudo-second-order models. The theoretical and mathematical details of adsorption kinetics are given in the Appendix 5. The pseudo-first-order and pseudo-second-order plots of $log\ (q_e - q_t)$ versus t and (t/q_t) versus t were used to determine the rate constants of K_{ad} and k', respectively (figure not given). Among the two models, pseudo second-order rate equation could describe the Pb^{2+}, Ni^{2+}, Sr^{2+} and MB dye system with extremely high correlation coefficients (R^2) highlighting the rate-controlling mechanism, (Reddad *et al.,* 2002) and the parameters are tabulated in Tables 4.4a to 4.4c. However, R^2 value of pseudo first-order kinetics in Tables 4.4a to 4.4c ranging of more than 0.94 is also acceptable to argue as a best fit, but this model fails to explain the sorption saturation theoretically (experimental data fit) rather than pseudo second-order kinetics. On the other hand for RB dye, pseudo first-order model is fitted well rather than second-order model (Table 4.4b).

4.3.8 Sorption Thermodynamics

Adsorption experiments of Pb^{2+}, Ni^{2+}, Sr^{2+}, RB and MB dye onto SBS were performed at different temperatures varying from 30 to 50°C. The adsorption capacity of Pb^{2+} and Sr^{2+} decreased from 122.7 to 117.5 and 86.7 to 78.4 mg/g, respectively when the temperature increased from 30 to 50°C (Table 4.2a and Figures 4.18a to

4.18c). However, the adsorption capacity of Ni^{2+}, RB and MB dye increased from 70.2 to 72.3, 221.2 to 255.8 and 330 to 427.4 mg/g, respectively while solution temperature increased from 30 to 50°C (Tables 4.2a and 4.2b and, Figures 4.18b, 4.18d and 4.18e). The decrease in adsorption capacity of Pb^{2+} and Sr^{2+} with increase in temperature might be due to desorption caused by an increase in the thermal energy. Increasing the temperature induces higher mobility of the adsorbate causing desorption (Baral *et al.,* 2006). An interesting point which can be observed from Ni^{2+} metal as well as dyes adsorption that there was an increase in adsorption capacity when temperature was changed from 30 to 50 ºC.

Thermodynamic parameters such as Gibbs free energy (ΔG^o), enthalpy (ΔH^o) and entropy (ΔS^o) of Pb^{2+}, Ni^{2+}, Sr^{2+}, RB and MB dye adsorption were calculated using the equation A5.1 and A5.2 (Appendix 5), and results are presented in Table 4.5a, 4.5b and 4.5c. ΔH^o and ΔS^o were obtained from the slope and intercept of linear Van't Hoff plots of ln K_d versus 1/T. The negative values of free energy at various temperatures indicate the spontaneous nature of adsorption process. The increasing and decreasing value of ΔG^o with increasing temperature shows that the adsorption is more favourable for dyes and less favourable for metals at high temperature. The positive ΔS^o value of dyes (RB = 0.0674 to 0.1807 KJ/mol K and MB = 0.1568 to 0.2808 KJ/mol K) indicate that there is an increase in entropy (randomness) in the system solid/solution interface during the adsorption process (Argun and Dursun *et al.,* 2008). Hence, the overall adsorption process for RB and MB seems to be endothermic (Gerçel *et al.,* 2007). The small negative value of the standard enthalpy change for Pb^{2+} (-3.505 to -19.690 KJ/mol) and Sr^{2+} (-6.063 to -19.102 KJ/mol) indicate that the adsorption is physical in nature involving weak forces of attraction and is also exothermic. However, the positive value of $\Delta H°$ for Ni^{2+} (+4.175 to +4.930 KJ/mol), RB (+19.28 to +46.14 KJ/mol) and MB (+34.78 to +82.68 KJ/mol) dye adsorption indicates that the adsorption process follows a chemisorption mechanism in nature involving strong forces of attraction (Gerçel *et al.,* 2007). The decrease in adsorption capacity of (Pb^{2+} and Sr^{2+}) and the increase in adsorption capacity of (Ni^{2+} and dyes) confirmed the exothermic and endothermic nature of the process.

4.3.9 Desorption Studies

Regeneration of adsorbents through desorption of adsorbates from the adsorbent is very much essential for practical applications in industrial. The influence of six desorption agents such as HCl (0.1 M), HNO_3 (0.1 M), CH_3COOH (0.1 M), EDTA (0.01 M), NaOH (0.1 M) and hot distilled water (H_2O) were tested with Pb^{2+}, Ni^{2+}, Sr^{2+}, RB and MB dye adsorbed adsorbents. Figure 4.19 shows the elution efficiency of each metal and dye adsorbed adsorbent. HNO_3 had high desorption efficiency with Pb^{2+} (98 %), Sr^{2+} (91 %), RB (53 %) and MB dye (67%) compared to other eluents. However, high Ni^{2+} (87%) desorption was achieved with HCl rather than HNO_3 (78 %). From the results presented in Figure 4.19, it can be seen that H_2O and NaOH had the least value of percentage desorption as compared with other solvents. Water can desorbs only physically attached metals and dyes with SBS. The strong inorganic acids (HNO_3 and HCl) were found to desorb a high percentage of metals and dyes little higher than weak acids (CH_3COOH and EDTA) from the SBS. Therefore, strong acids could be applicable for the successful regeneration of metal and dye adsorbed SBS for reuse.

4.3.10 Adsorption Mechanism

It is very important to identify the mechanism of metal and dye uptake by SBS adsorbent which will ultimately guide for the rational design of the adsorption process.

4.3.10.1 Adsorption Mechanism of Metals

In relation with the change in enthalpy mentioned earlier, metal adsorption shows that Pb^{2+}, Ni^{2+} and Sr^{2+} ions adsorption on SBS is largely controlled by physisorption. In this case, van der Waals interaction plays vital role to make the metal binding. As discussed earlier (see FT-IR result), SBS has three main components such as cellulose, hemicelluloses and lignin, besides other minor functional groups. Both cellulose and hemicelluloses contain majority of oxygen functional groups that are present in the lingo cellulosic materials. But lignin is a highly aromatic, complex and systematically polymerized substance and act as a cementing matrix (El-Hendawy, 2006).

Two possible metal binding mechanisms such as intermolecular binding (ion–dipole) of Pb^{2+} and Sr^{2+} and intermolecular binding coupled with intramolecular binding of Ni^{2+} can be suggested with cellulosic and lignin molecules. In the first mechanism (intermolecular binding by ion–dipole interaction), Pb^{2+} and Sr^{2+} ions attracted and attached through electrostatic interaction with –OH (dipole) in the lignin and cellulosic structure (Figures 4.20a and 4.20b). But in the second mechanism (Figures 4.20c, 4.20d and 4.20e), the intermolecular binding coupled with intramolecular binding of Ni2+ ion occurred in the cellulosic and lignin groups. It contains two steps: (i) Ni^{2+} ion attracted and attached with the –OH (dipole) in the lignin and cellulosic structure and (ii) later at higher temperature, consumption of heat energy (endothermic) creates the small induced dipole in the neighborhood oxygen atom, which may attract one more Ni^{2+} metal ion because of its high charge density (small ionic size) compared with Pb^{2+} and Sr^{2+} with cellulose and lignin molecules. These possibilities might not happen in Pb^{2+} and Sr^{2+} adsorption because of their ionic size, ionic charge, electrode potential and van der Waals radii (Al-Ghouti *et al.,* 2010).

In addition to this, an interesting point that can be observed from the Pb^{2+}, Ni^{2+} and Sr^{2+} adsorption is that if the temperature increased from 30°C to 50°C, the adsorption capacity of Pb^{2+} and Sr^{2+} ions decreased, whereas adsorption capacity of Ni^{2+} increased. Increase in temperature causes increase in the mobility (kinetics) of physically attached ions on the surface of the adsorbent that leads to desorbs (release) the ions from the surface to solution at higher temperature (Baral *et al.,* 2006). Moreover, at higher temperature, the kinetic energies of metal ions become higher than the potential attractive forces between active sites and ions (Daneshvar *et al.,* 2002; Uysal and Ar, 2007). In Table 4.2a, the monolayer adsorption capacity of Pb^{2+} slightly decreased while solution temperature was increased from 30°C to 50°C compared with Sr^{2+} (considerable reduction) ion. Desorption of Pb^{2+} and Sr^{2+} ions at higher temperature might be attributed to the size of the adsorbed metal atom (Saygideger *et al.,* 2005). Here, the atomic radius of Pb^{2+} (175 pm) is lesser than Sr^{2+} (249 pm). The bigger Sr^{2+} molecules are easily desorbed at higher temperature rather than smaller Pb^{2+} molecules. However, Ni^{2+} adsorption is higher than Pb^{2+} and Sr^{2+} because of its smaller atomic (124 pm) size, higher charge density and strong

attraction toward the small induced dipoles of adsorbent at higher solution temperature.

4.3.10.2 Adsorption Mechanism of Dyes

FT-IR spectrum of the SBS after RB and MB dye adsorption had significant peak shifting at 668, 1104 and 1374 and 1610 cm^{-1}, which was due to the RB and MB dye molecule attachments on the SBS surface (Figure 4.3b). Moreover, it could be seen Figure 4.3b that the peak of C-O stretches and stretching vibrations of C-O-C around 1610 cm^{-1} and hydroxyl functional groups (O–H) were also shifted significantly after dye adsorption. These changes demonstrated that carboxyl and hydroxyl groups were involved in the adsorption of RB and MB dye. The adsorption of RB and MB dye on the SBS adsorbent might be attributed to (i) electrostatic interaction between the dye molecules and carboxylate ions on the biomass surface, (ii) weak physical forces such as hydrogen bonding between nitrogen atom of RB and MB with hydroxyl groups on the SBS surface, and (3) van der Waals interactions between the hydrophobic parts of the dye molecules (e.g., the aromatic rings) and the polysaccharides of the SBS. A schematic diagram of RB and MB dye molecule absorbed on the SBS surface is presented in Figures 4.21a and 4.21b, respectively.

4.4 SUMMARY

In this chapter, batch adsorption studies of Pb^{2+}, Ni^{2+}, Sr^{2+}, RB and MB dye using H_2SO_4 activated BS at 30°C to 50°C solution temperature was discussed. The results demonstrated that the adsorption capacity and BET surface area of the adsorbent increased significantly with increase in the concentration of H_2SO_4 for BS activation. The pH of the metal and dye solution significantly influences the adsorption capacity of metals and dyes onto SBS. The pH 5.2, 5.8, 6.8, 3.5 and 7.0 for Pb^{2+}, Ni^{2+}, Sr^{2+}, RB and MB dye was found to be the most favourable. The adsorption capacity of single metals onto SBS was decreased in binary and ternary system, but no significant alterations in the adsorption capacity in its metal-dye binary system. Presence of other cations at high concentration level decreases the adsorption capacity of three metals onto SBS, but no impact on dye adsorption capacities. The adsorption behaviour of heavy metal ions and cationic dyes onto SBS matched well with Langmuir isotherm model. The sorption kinetics of Pb^{2+}, Ni^{2+}, Sr^{2+} and MB dye was found to pseudo-second-order kinetics model. The adsorption process was exothermic for Pb^{2+} and

Sr^{2+} and endothermic for Ni^{2+}, RB and MB dye. This work provides new insight for developing low-cost adsorbents from BS to remove the multimetal contaminants and cationic dyes from the aqueous solution including industrial wastewater.

.

Chapter 4
Figures & Tables

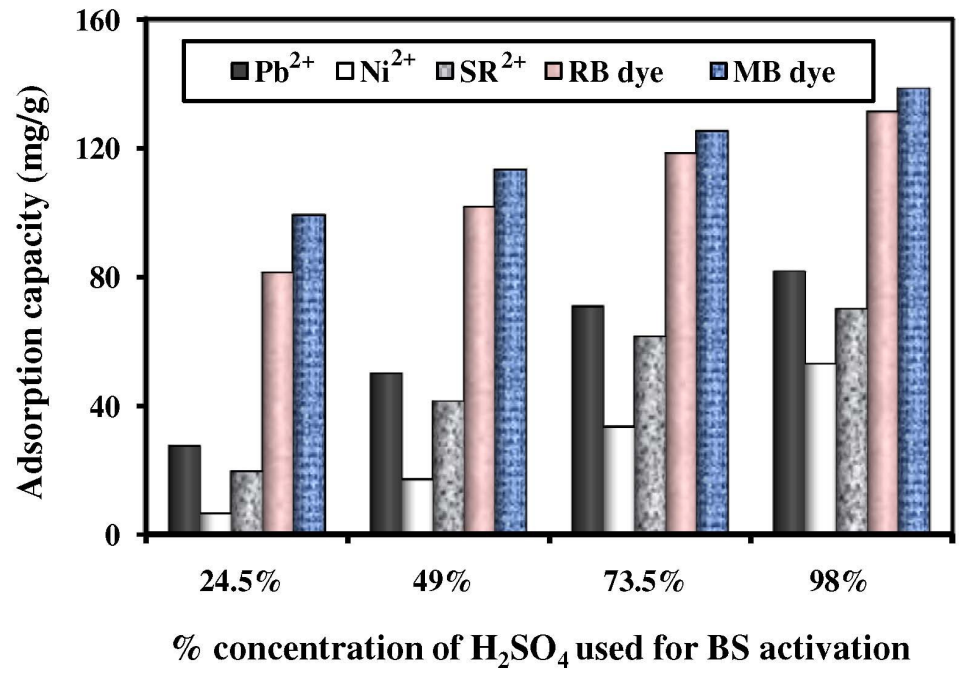

Figure 4.1 Effect of acid concentration on adsorption capacity; (C_o = 100 (metals), 150 (dyes) mg/l, W = 0.06 g, V = 50 ml, T = 30°C, t = 24 hr and R = 180 rpm)

(a)

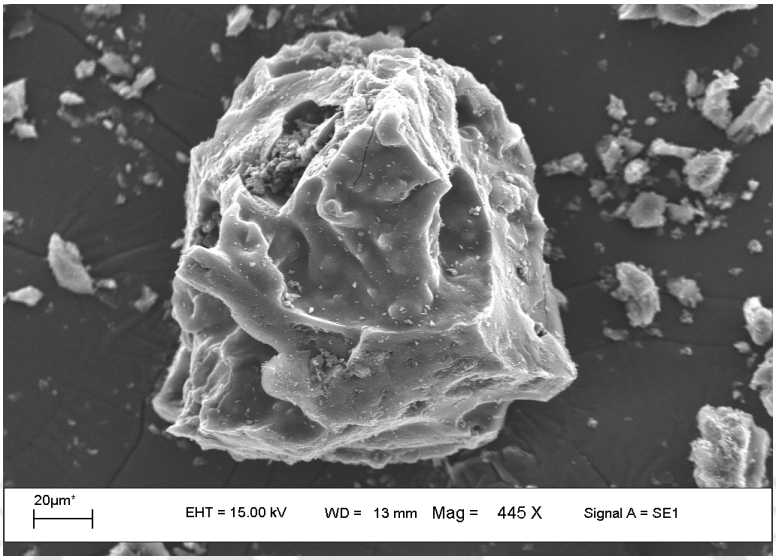

(b)

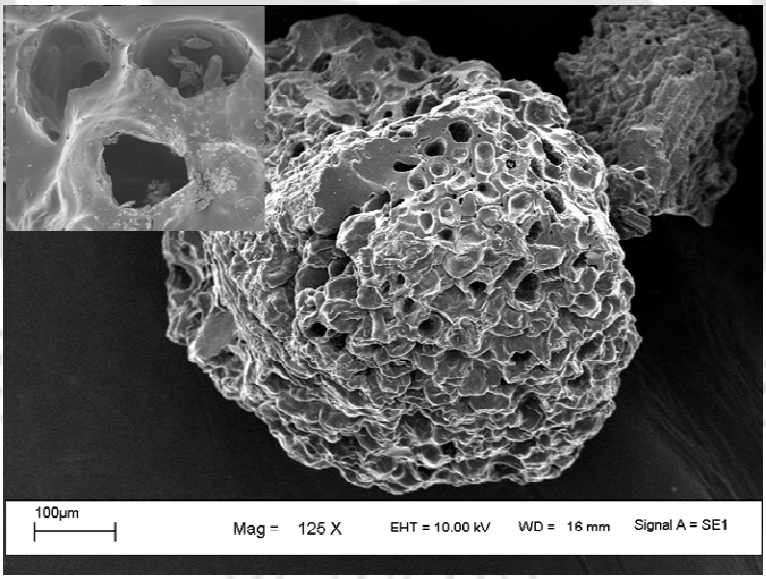

Figure 4.2 SEM picture of (a) BS before H_2SO_4 treatment (b) BS after H_2SO_4 treatment

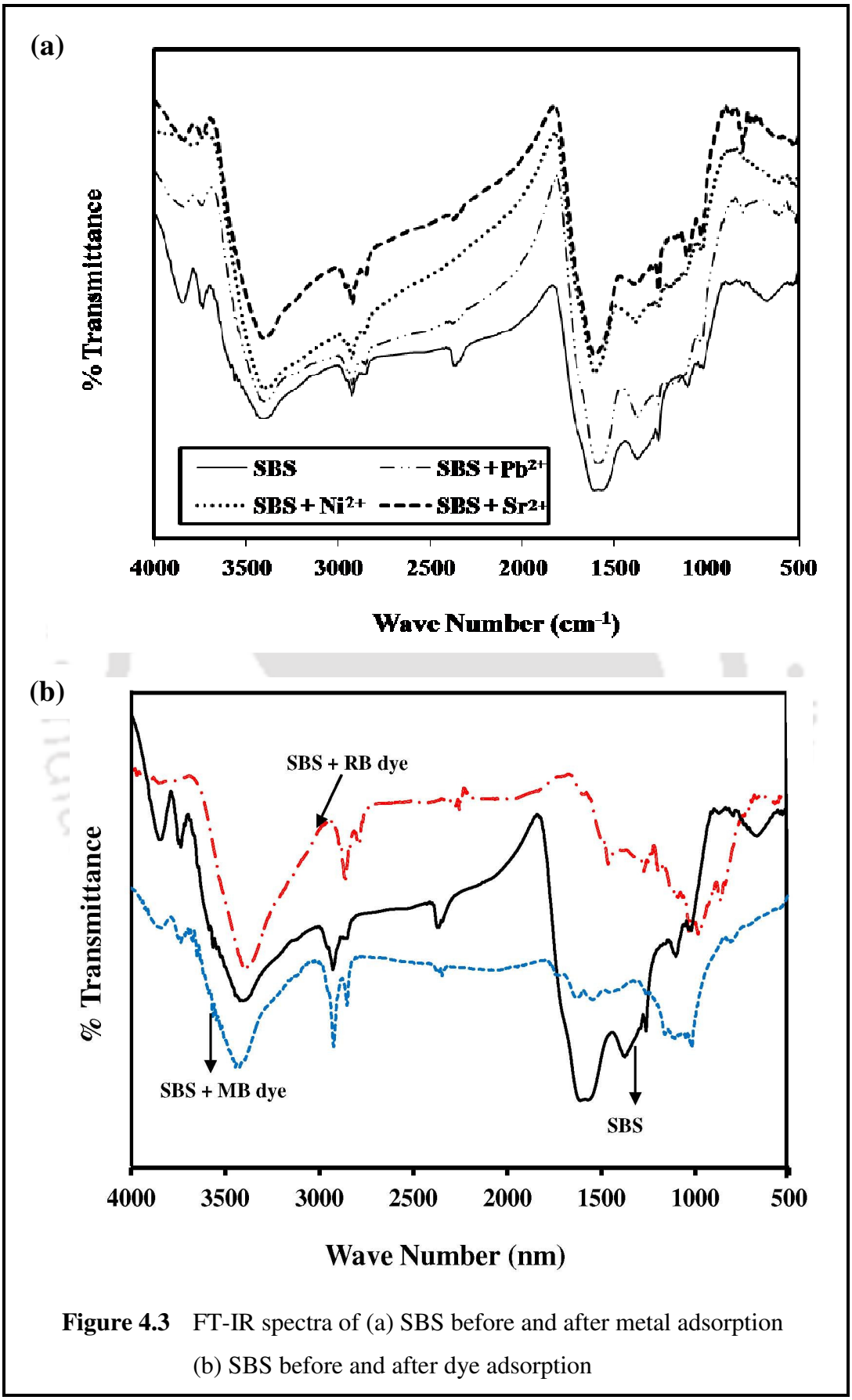

Figure 4.3 FT-IR spectra of (a) SBS before and after metal adsorption (b) SBS before and after dye adsorption

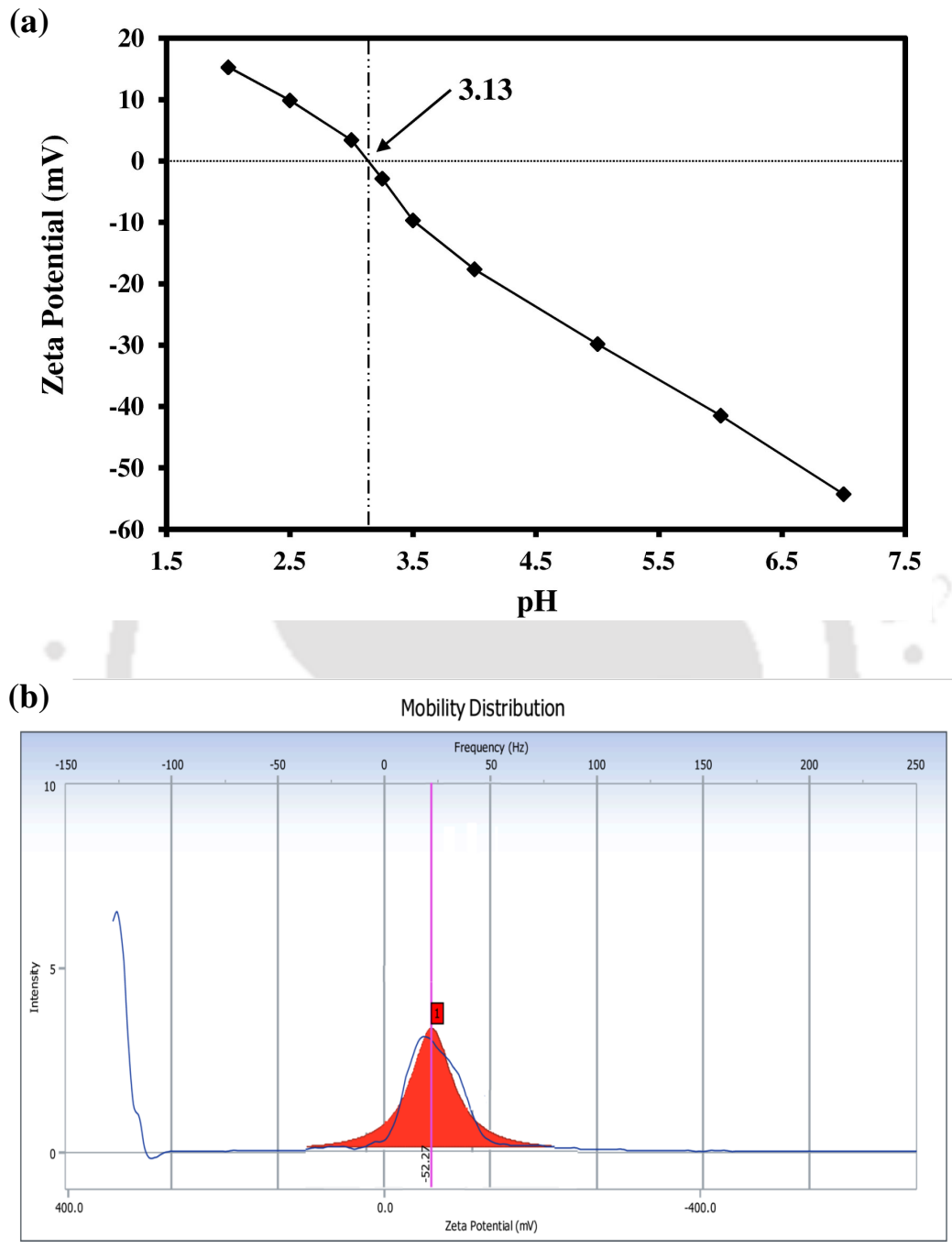

Figure 4.4 (a) Zeta potentials of SBS as a function of solution pH and (b) Electrophoretic mobility distribution of the SBS at pH 7.0

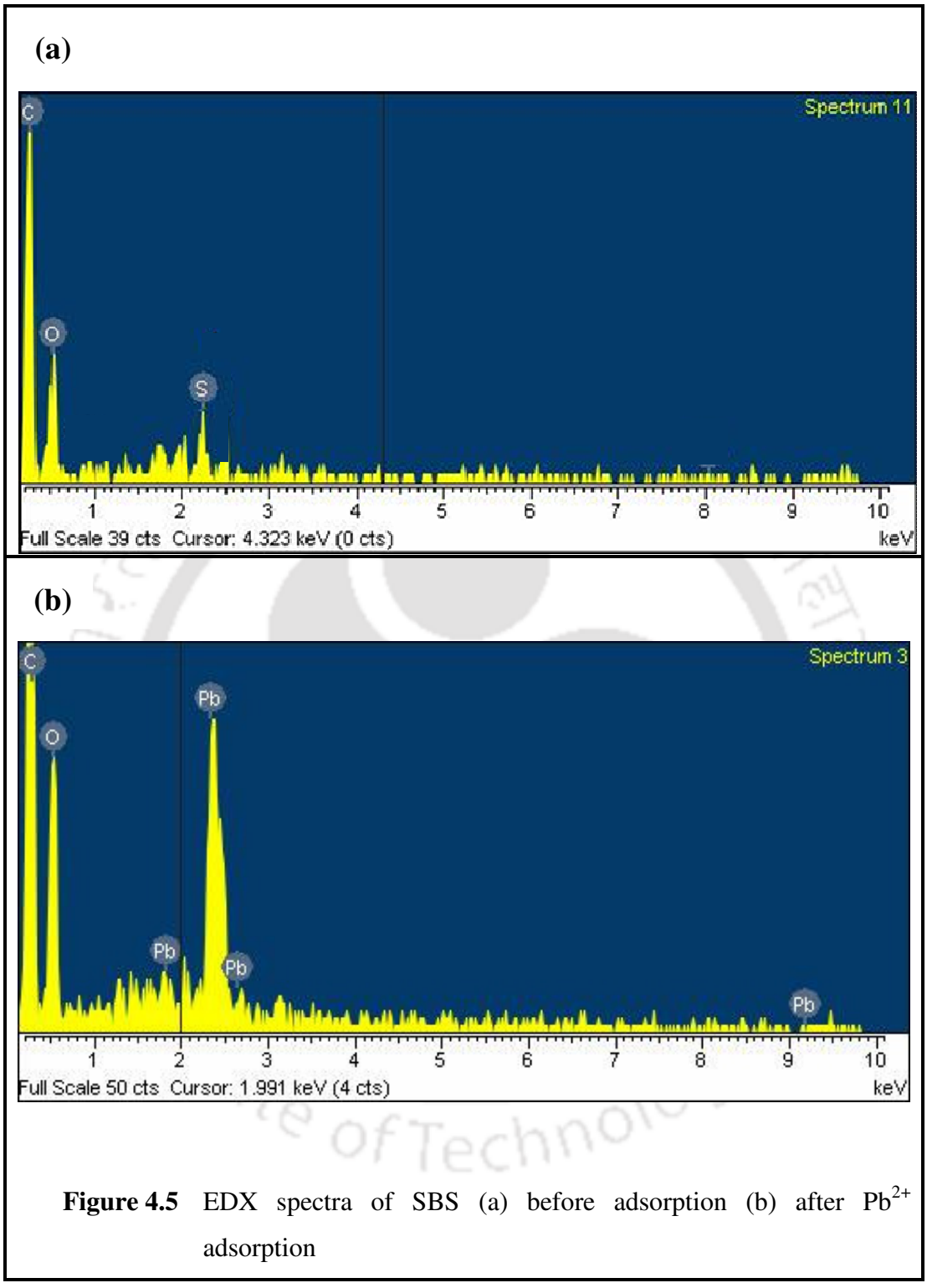

Figure 4.5 EDX spectra of SBS (a) before adsorption (b) after Pb^{2+} adsorption

(c)

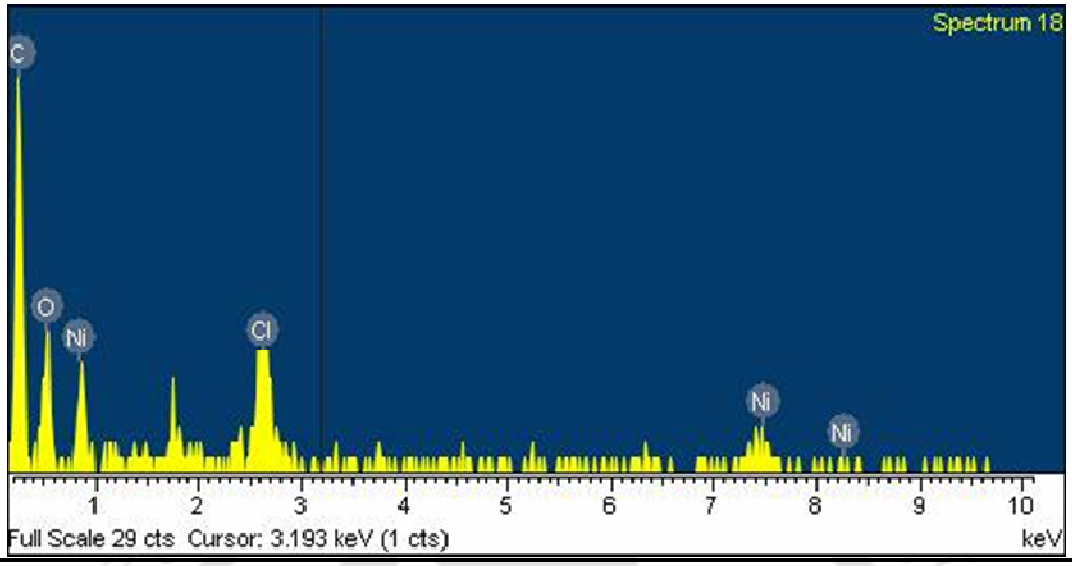

(d)

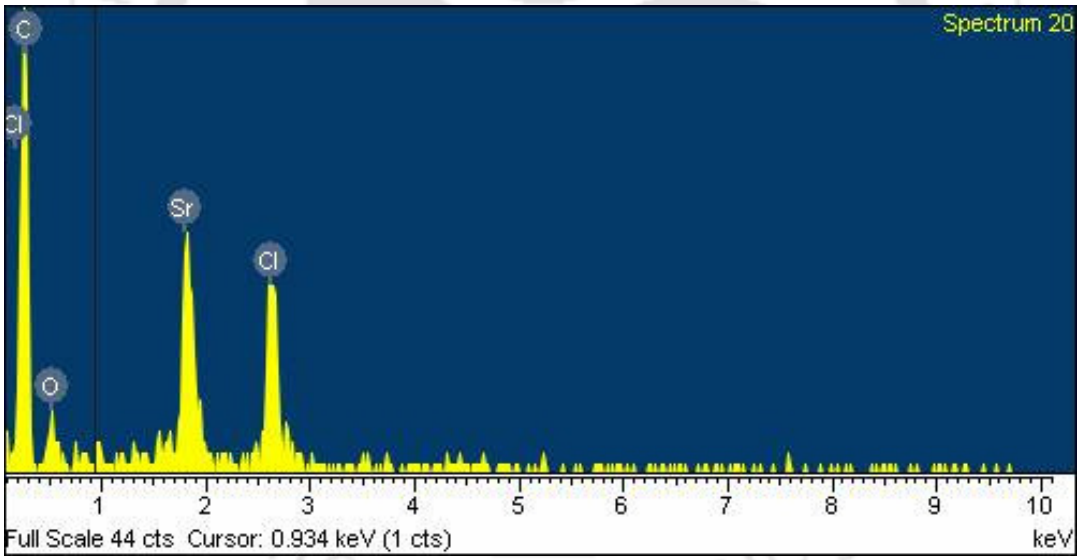

Figure 4.5 EDX spectra of SBS (c) after Ni^{2+} adsorption (d) after Sr^{2+} adsorption

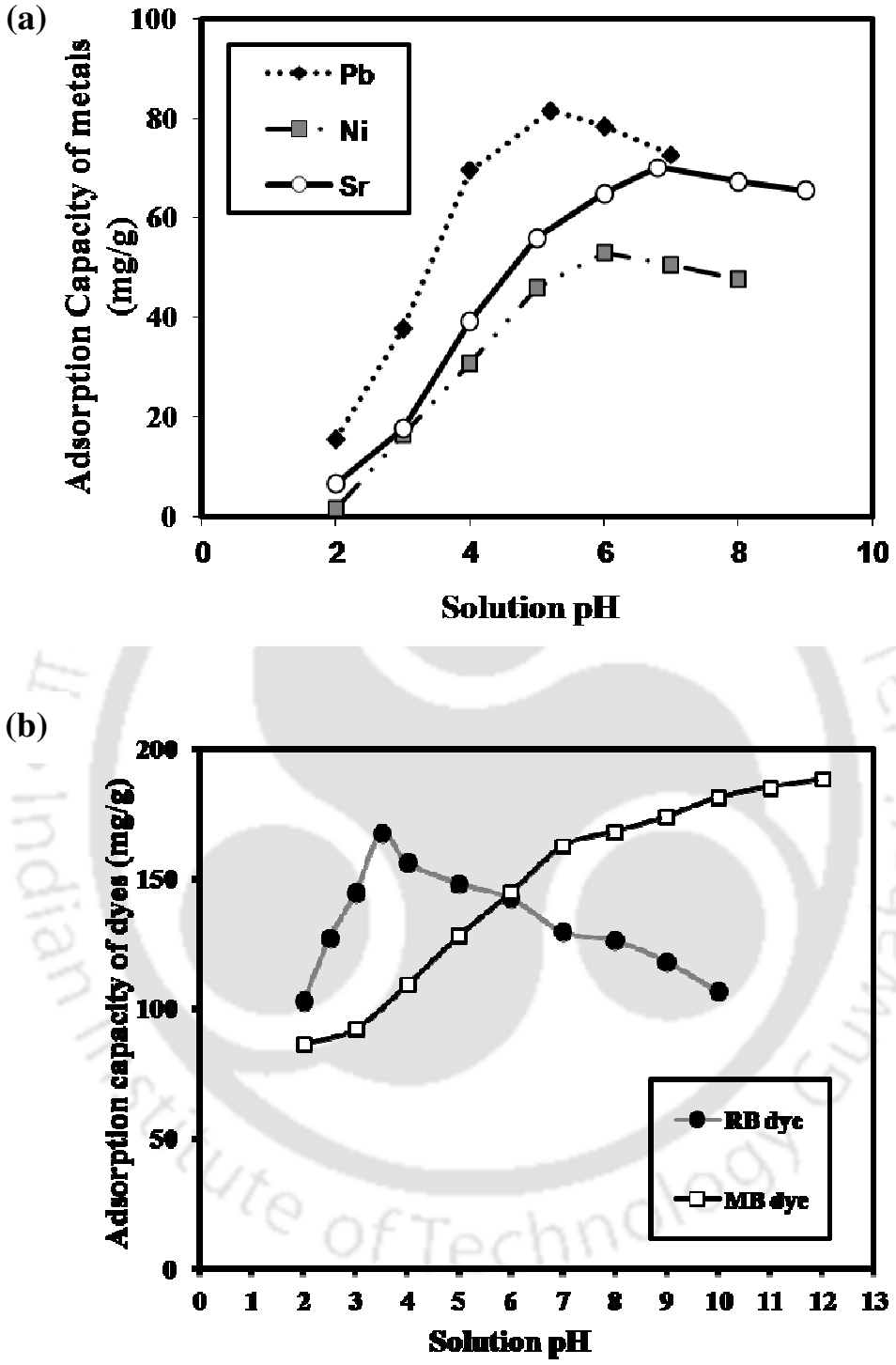

Figure 4.6 Effect of pH on adsorption of (a) Pb^{2+}, Ni^{2+} and Sr^{2+} metal (b) RB and MB dye [C_o = 100 (Pb^{2+}, Ni^{2+} and Sr^{2+}) and 200 (RB & MB dye) mg/l; pH = blank; W = 0.06 (Pb^{2+}, Ni^{2+}, Sr^{2+} and MB) and 0.05 (RB) g; V = 50 ml; t = equilibrium time (min); and T = 30°C]

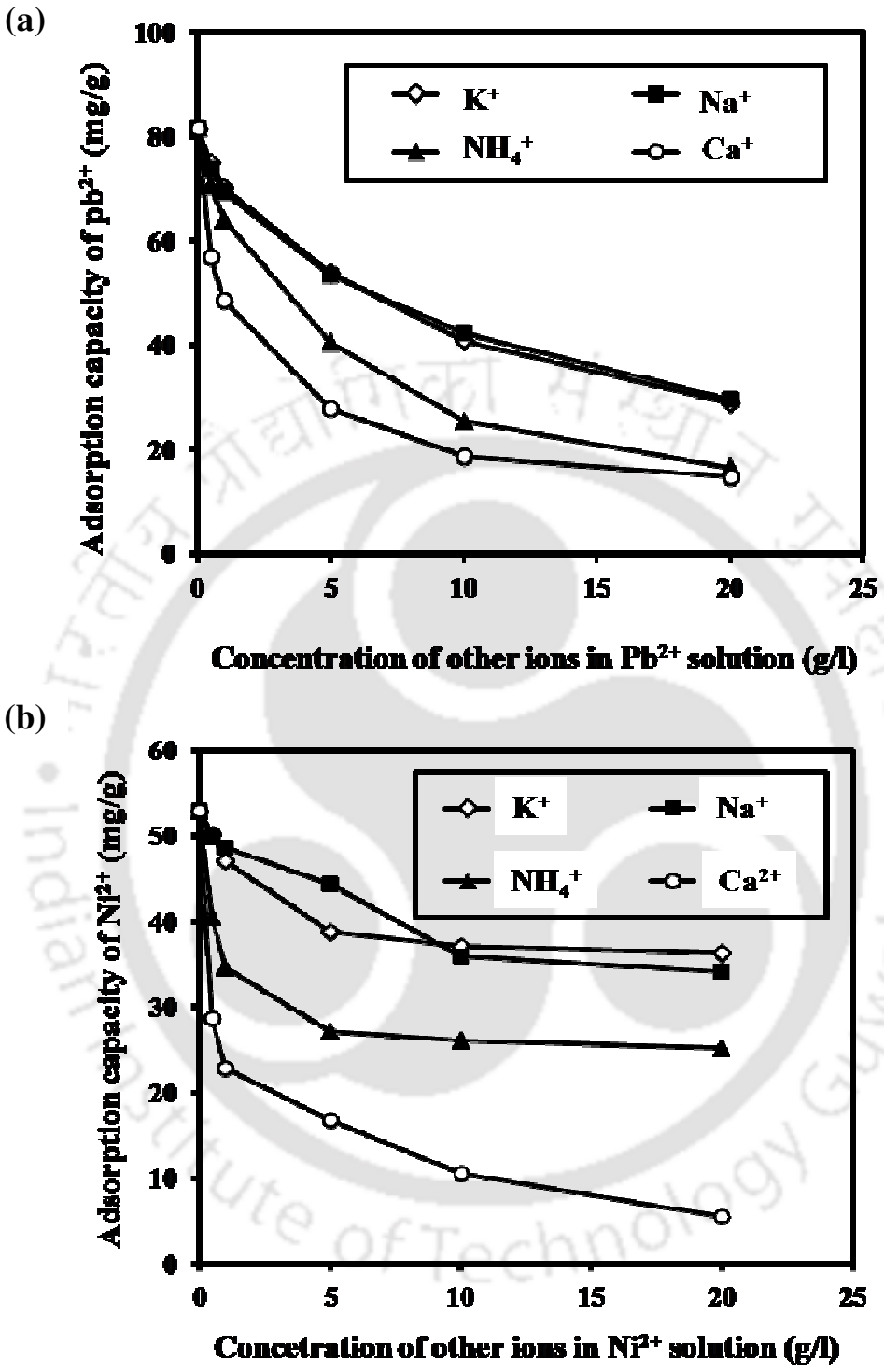

Figure 4.7 Effect of pH other ions on metal adsorption of (a) Pb^{2+} and (b) Ni^{2+} onto SBS: [C_o = 100 mg/l (Pb^{2+} and Ni^{2+}); pH = blank; W = 0.06 g; V = 50 ml; t (equilibrium) = 90 (Pb^{2+}) and 180 (Ni^{2+}) min; and T = 30°C]

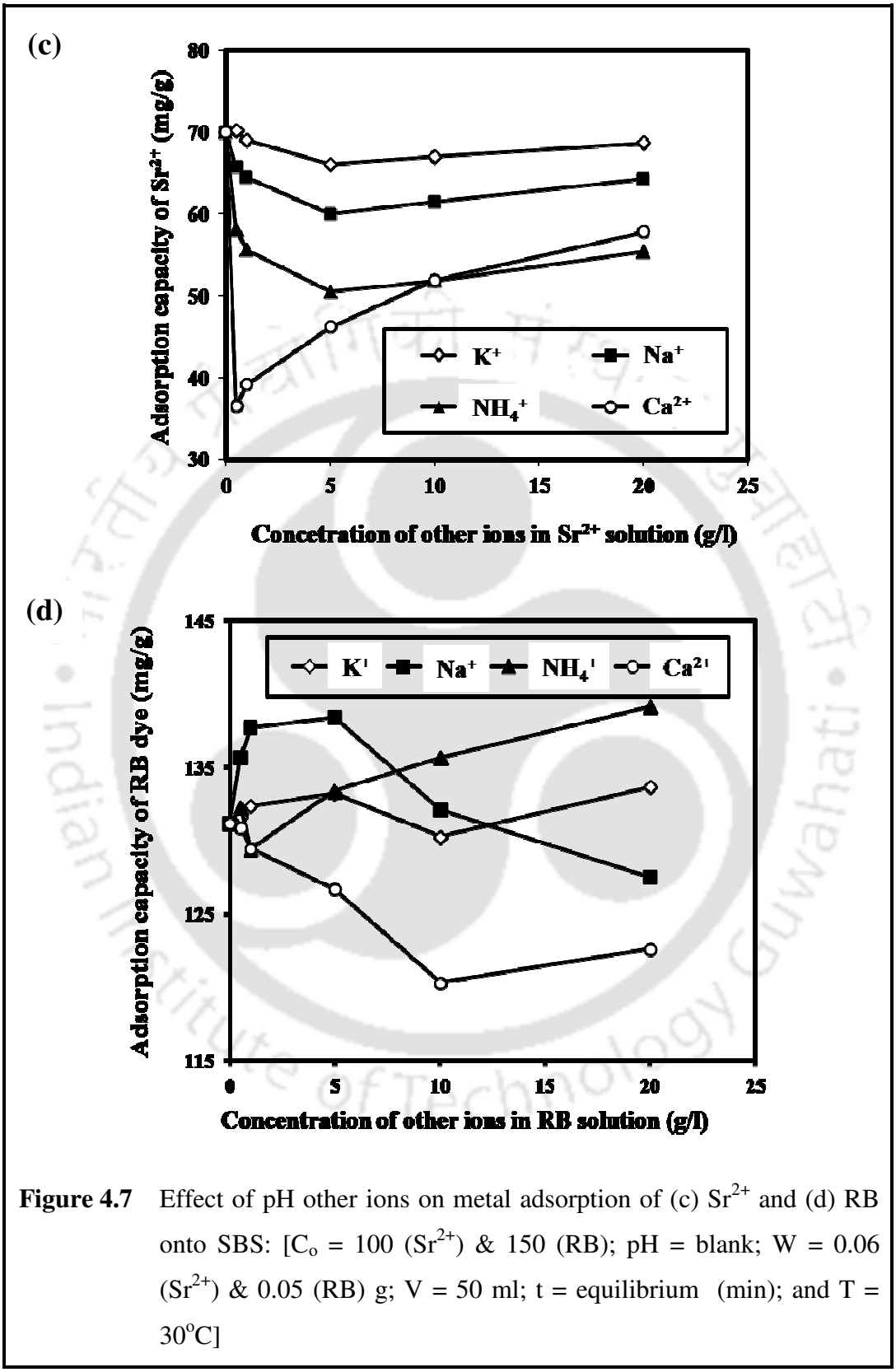

Figure 4.7 Effect of pH other ions on metal adsorption of (c) Sr^{2+} and (d) RB onto SBS: [C_o = 100 (Sr^{2+}) & 150 (RB); pH = blank; W = 0.06 (Sr^{2+}) & 0.05 (RB) g; V = 50 ml; t = equilibrium (min); and T = 30^oC]

(e)

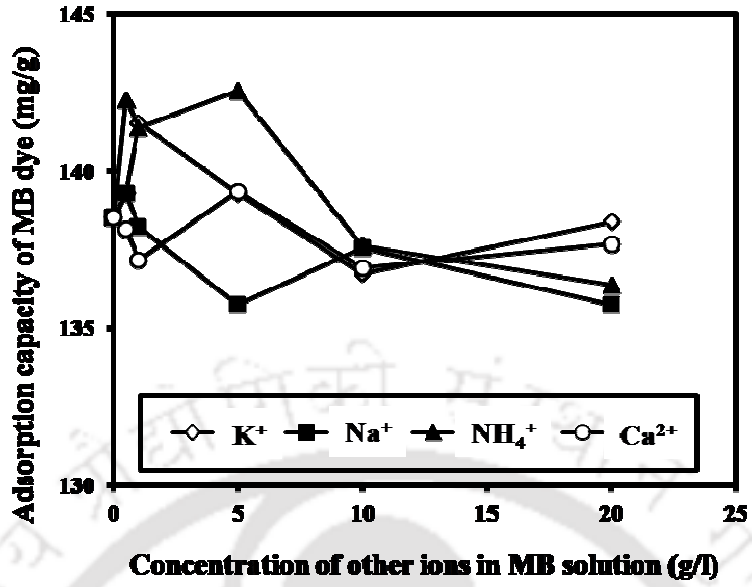

Figure 4.7e Effect of other ions on MB dye adsorption onto SBS: [C_o = 150 mg/l; pH = blank; W = 0.06 MB g; V = 50 ml; t = equilibrium (min); and T = 30°C]

(a)

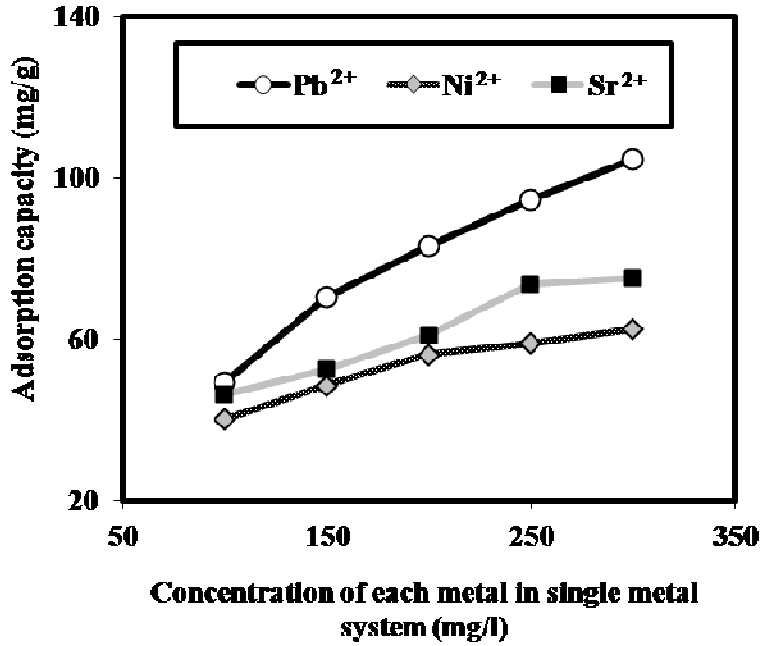

Figure 4.8 Effect of (a) single metal adsorption at various metal concentrations onto SBS: (pH = blank, W = 0.1 g, V = 50 ml, t (equilibrium) = 90 (Pb^{2+}), 180 (Ni^{2+}) & 180 (Sr^{2+}) min and T = 30ºC).

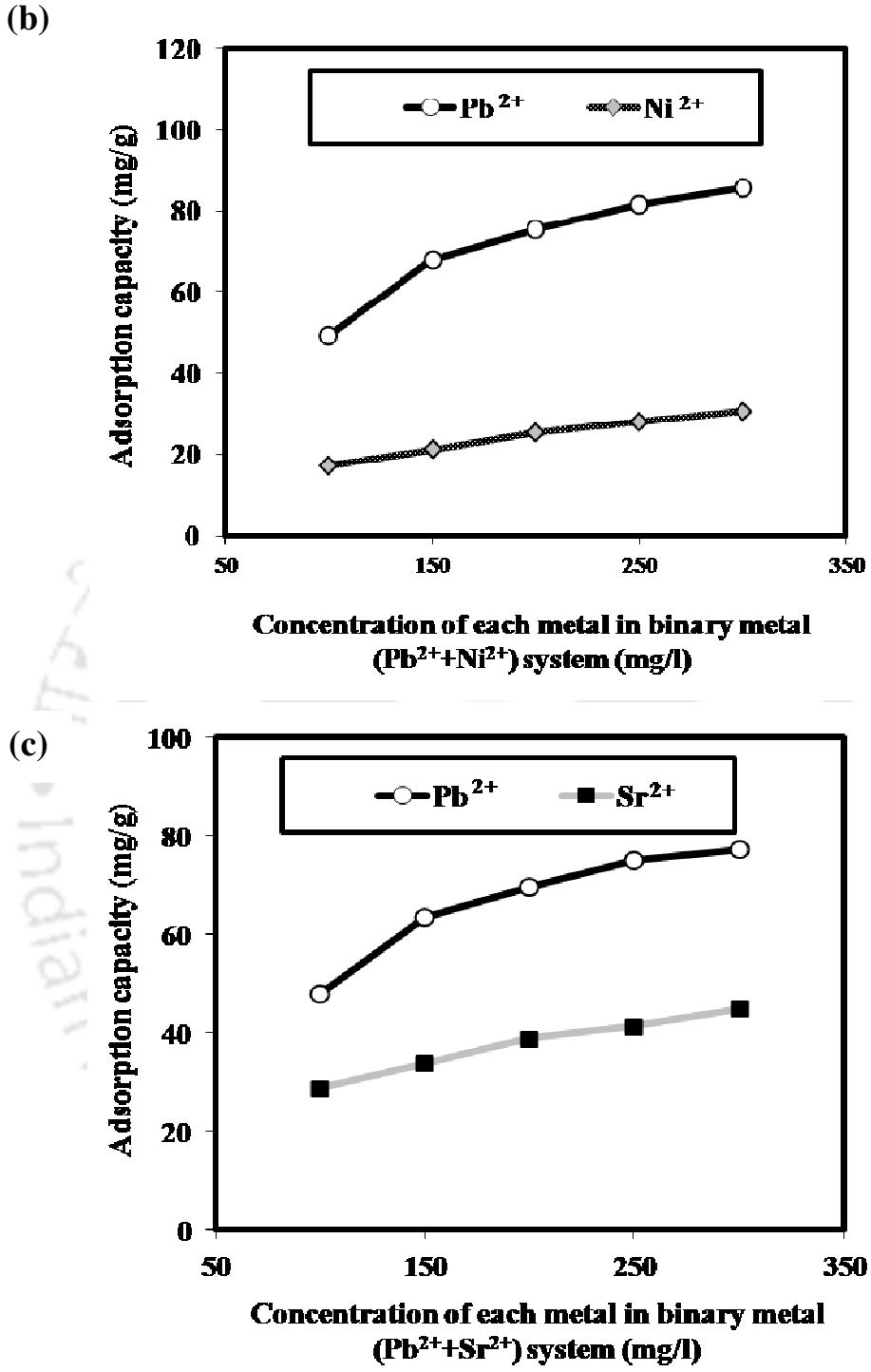

Figure 4.8 Effect of binary (b) (Pb^{2+}+ Ni^{2+}) and (c) (Pb^{2+}+ Sr^{2+}) metal adsorption at various metal concentrations onto SBS: (pH = blank, W = 0.1 g, V = 50 ml, t (equilibrium) = 90 (Pb^{2+}), 180 (Ni^{2+}) & 180 (Sr^{2+}) min and T = 30ºC).

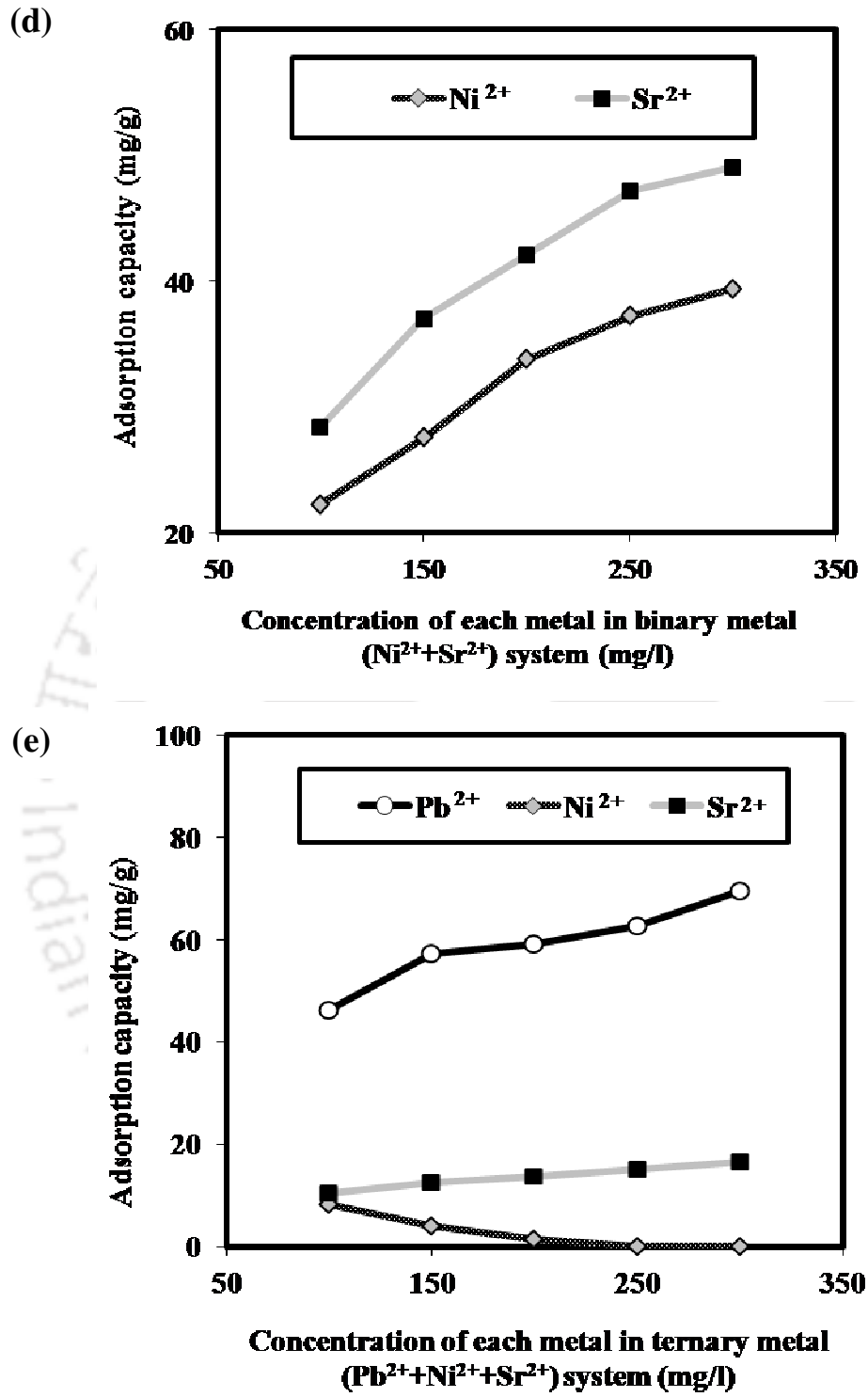

Figure 4.8 Effect of binary (d) (Ni^{2+} + Sr^{2+}) and (e) ternary metal (Pb^{2+} + Ni^{2+} + Sr^{2+}) adsorption system at various metal concentrations onto SBS: (pH = blank, W = 0.1 g, V = 50 ml, t (equilibrium) = 90 (Pb^{2+}), 180 (Ni^{2+}) & 180 (Sr^{2+}) min and T = 30ºC).

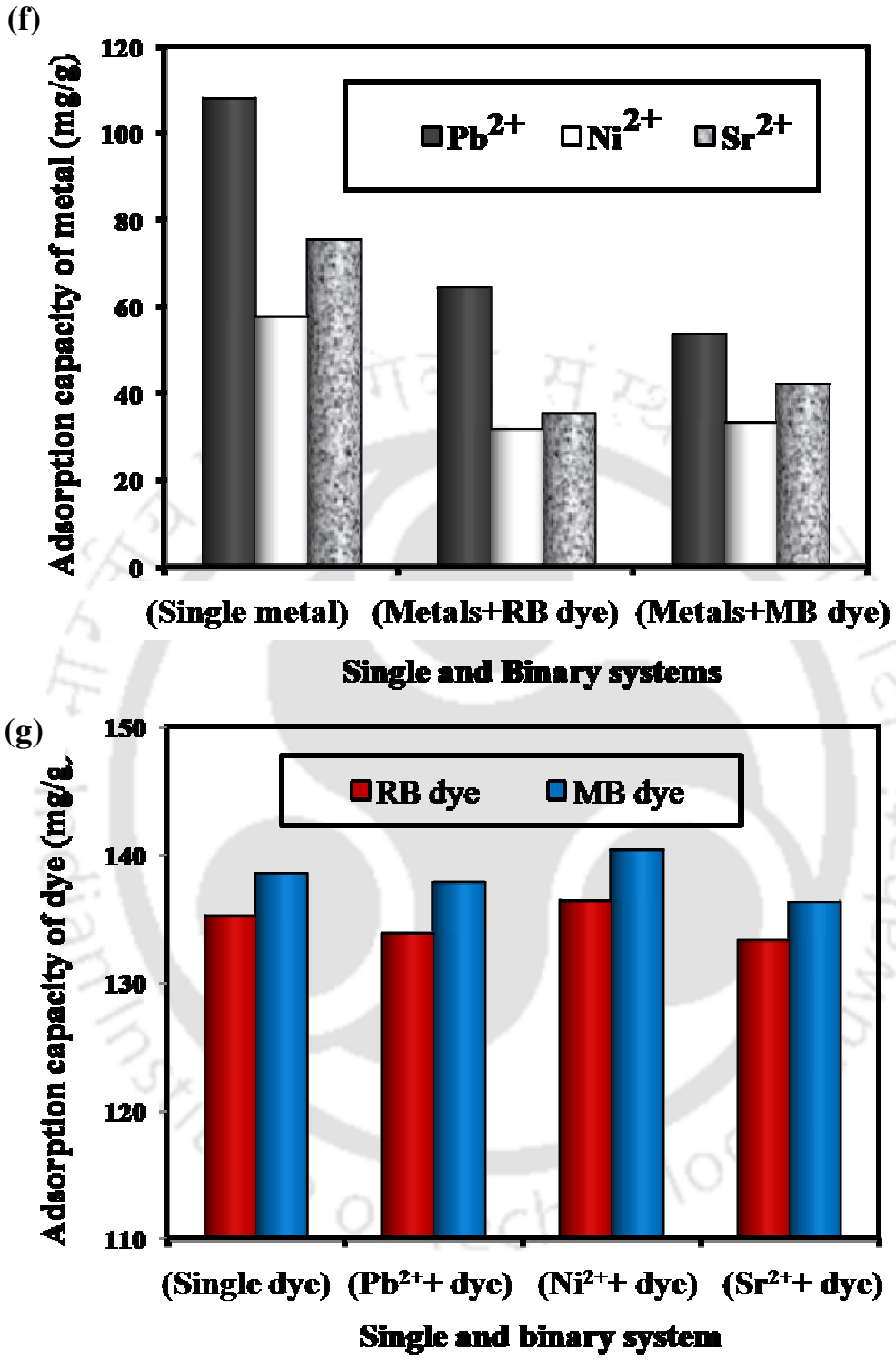

Figure 4.8 Effect of binary adsorption system of (f) equal mass of each (metal + dye) and (g) equal mass of each (dye + metal) onto SBS: (C_o = 150 mg/l of each metal and each dye; pH = blank; W = 0.06 g; V = 50 ml; t (equilibrium) = 1440 min; and T = 30ºC).

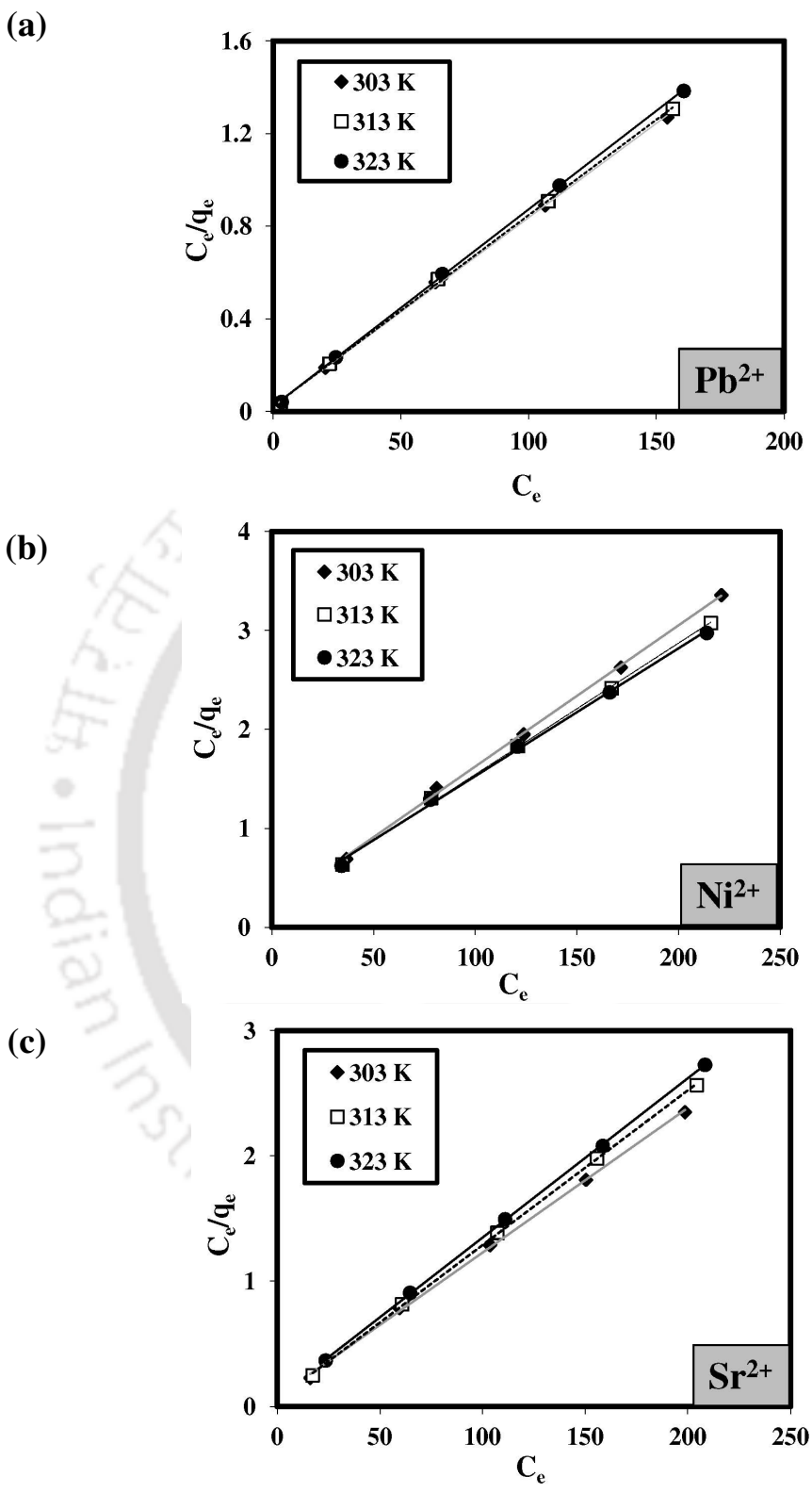

Figure 4.9 Langmuir isotherm plots of (a) Pb^{2+} (b) Ni^{2+} and (c) Sr^{2+} adsorption onto SBS: (pH = blank; W = 0.06 g; V = 50 ml; t = equilibrium (min); and T = 30°C)

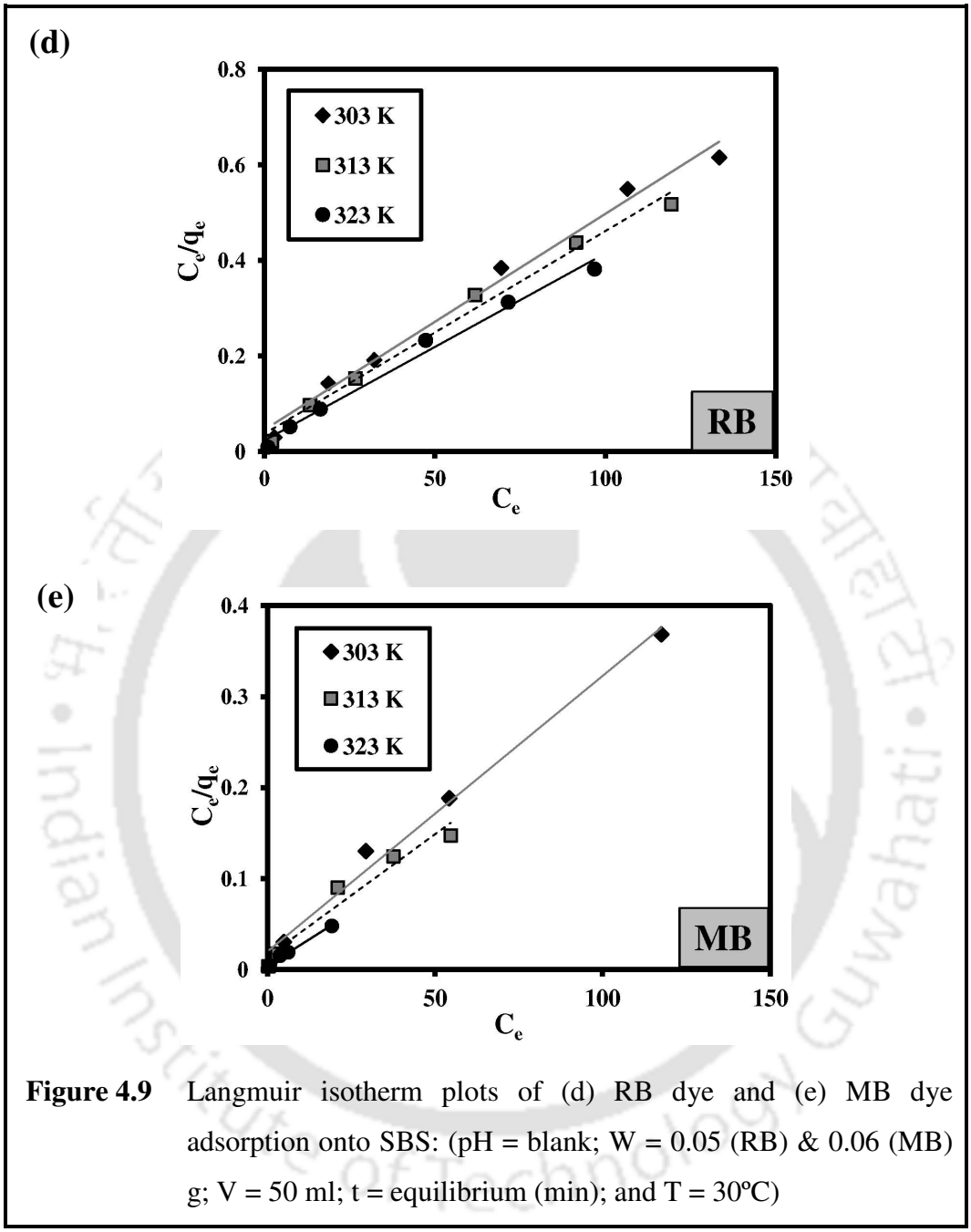

Figure 4.9 Langmuir isotherm plots of (d) RB dye and (e) MB dye adsorption onto SBS: (pH = blank; W = 0.05 (RB) & 0.06 (MB) g; V = 50 ml; t = equilibrium (min); and T = 30ºC)

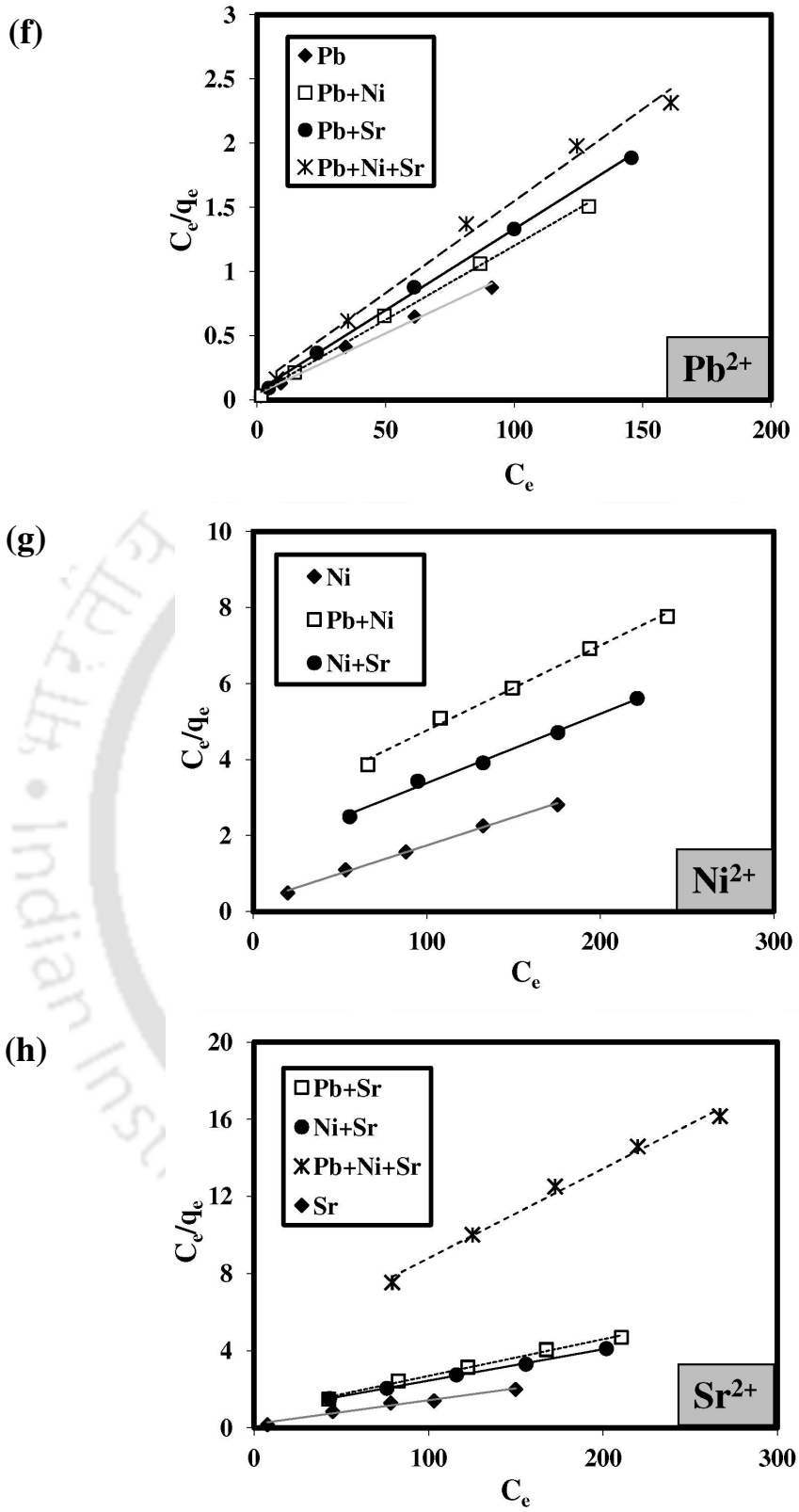

Figure 4.9 Langmuir isotherm plots of (f) Pb^{2+} (g) Ni^{2+} and (h) Sr^{2+} adsorption onto SBS in binary and ternary system: (pH = blank; W = 0.1 g; V = 50 ml; t = equilibrium (min); and T = 30ºC)

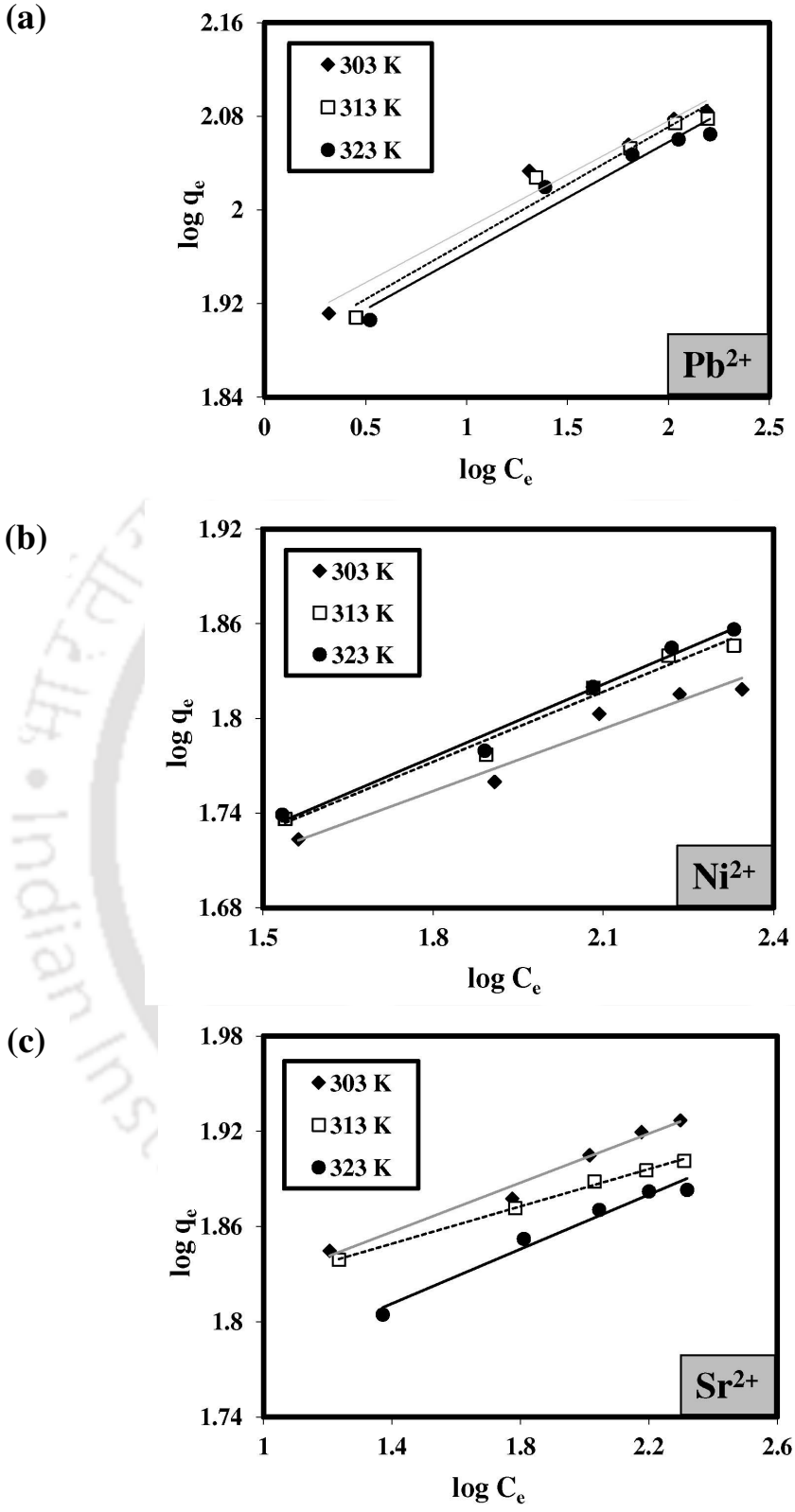

Figure 4.10 Freundlich isotherm plots of (a) Pb^{2+} (b) Ni^{2+} and (c) Sr^{2+} adsorption onto SBS: (pH = blank; W = 0.1 g; V = 50 ml; t = equilibrium (min); and T = 30ºC)

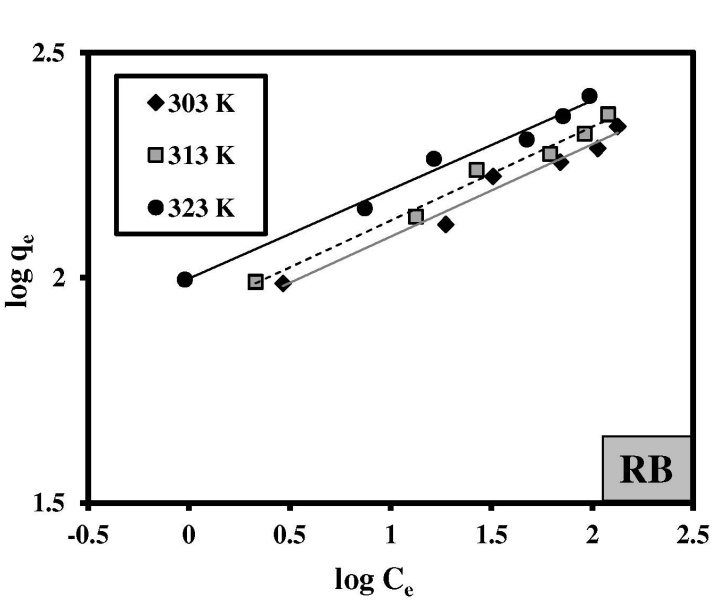

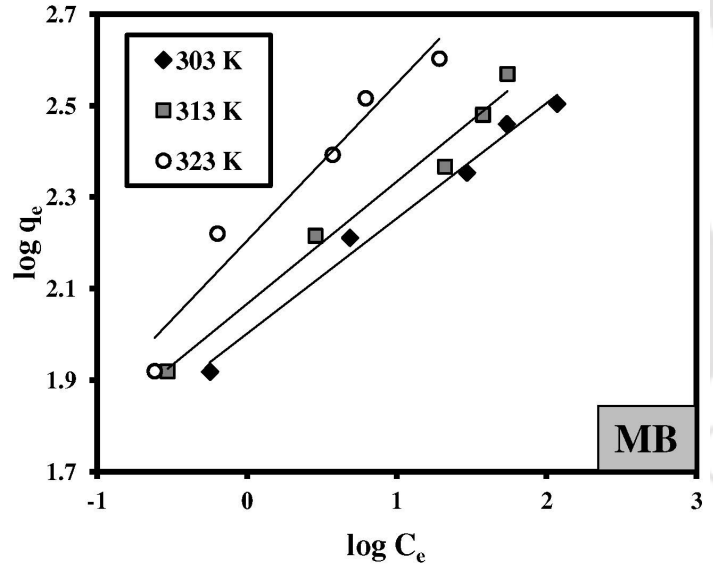

Figure 4.10 Freundlich isotherm plots of (d) RB dye and (e) MB dye adsorption onto SBS: (pH = blank; W = 0.1 g; V = 50 ml; t = equilibrium (min); and T = 30ºC)

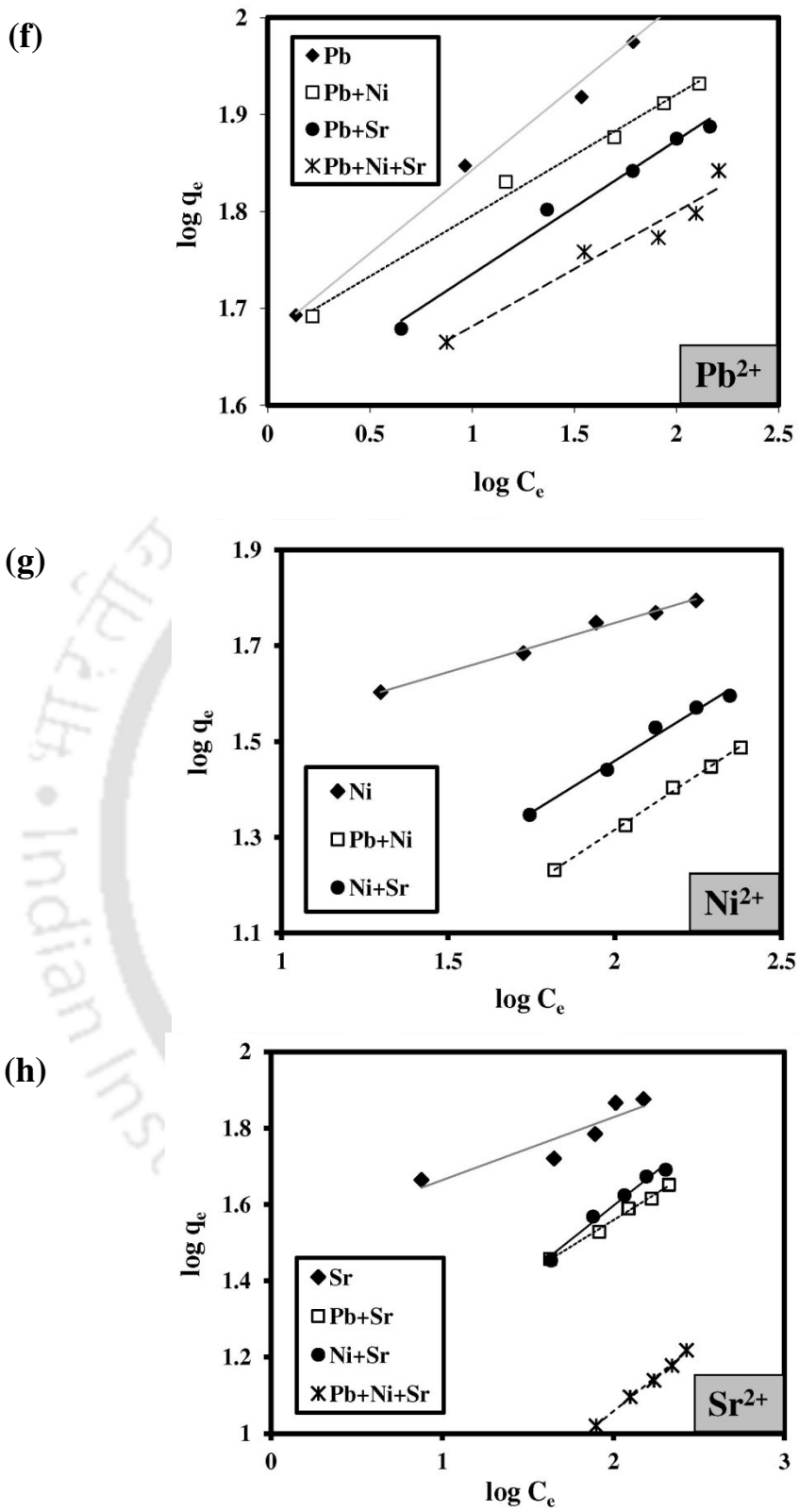

Figure 4.10 Freundlich isotherm plots of (f) Pb^{2+} (g) Ni^{2+} and (h) Sr^{2+} adsorption onto SBS in binary and ternary system: (pH = blank; W = 0.1 g; V = 50 ml; t = equilibrium (min); and T = 30ºC)

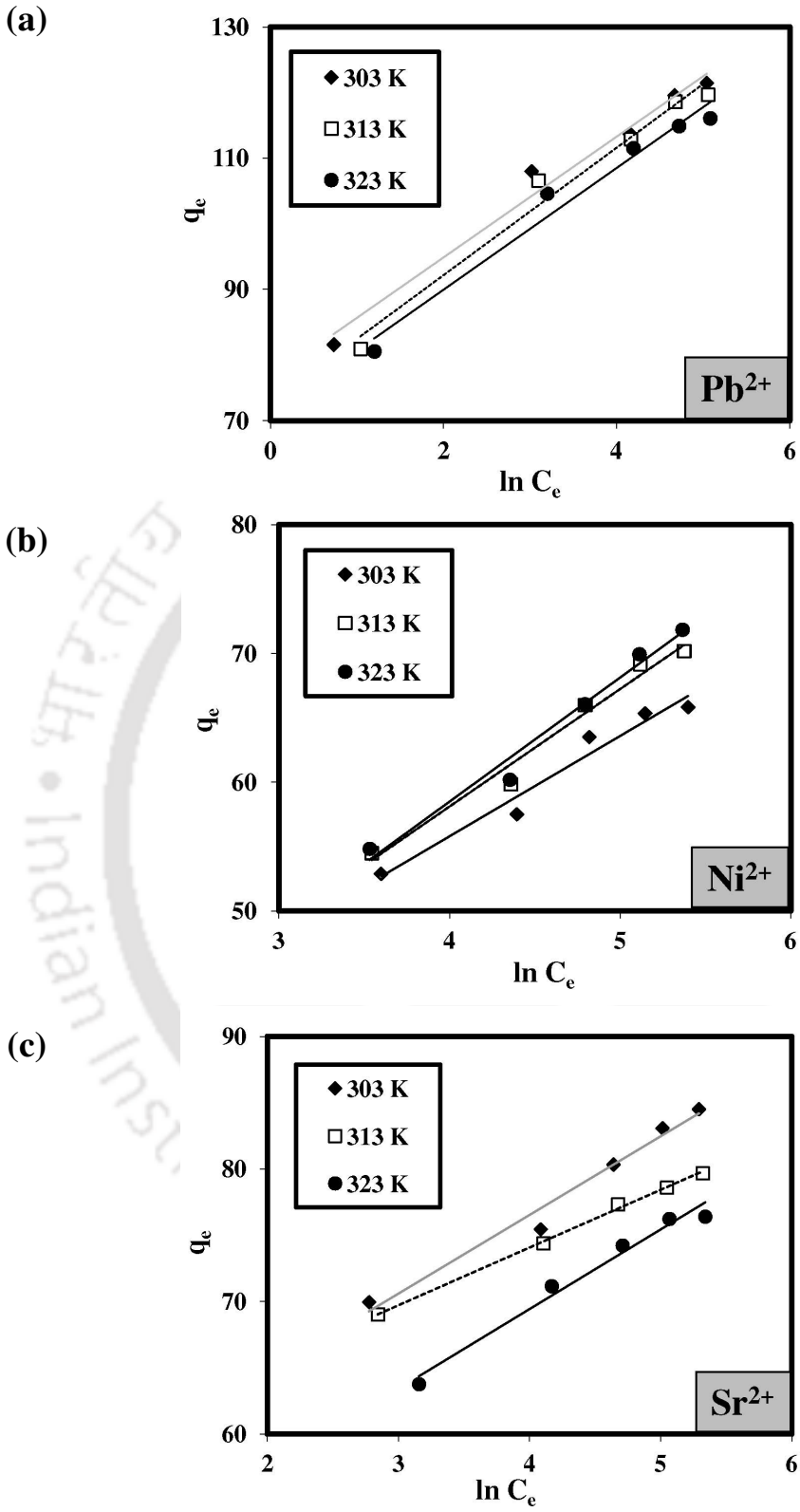

Figure 4.11 Temkin isotherm plots of (a) Pb^{2+} (b) Ni^{2+} and (c) Sr^{2+} adsorption onto SBS: (pH = blank; W = 0.1 g; V = 50 ml; t = equilibrium (min); and T = 30ºC)

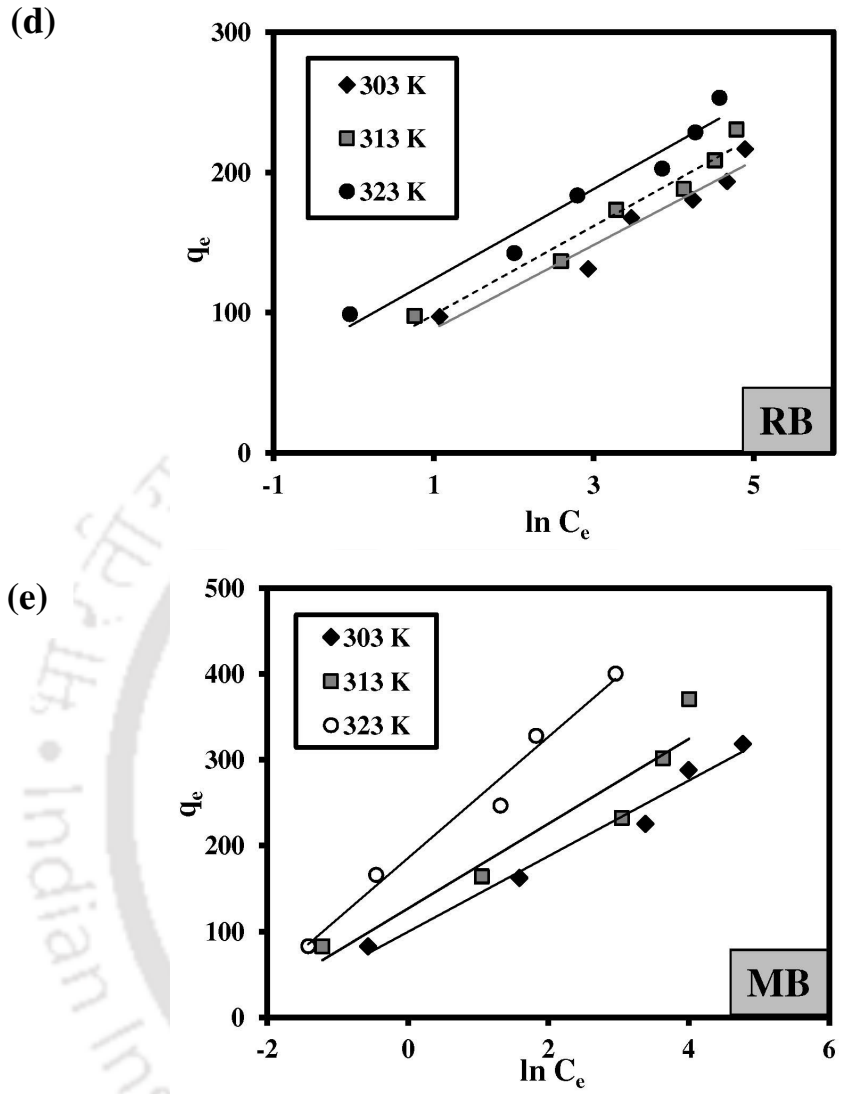

Figure 4.11 Temkin isotherm plots of (d) RB dye and (e) MB dye adsorption onto SBS: (pH = blank; W = 0.1 g; V = 50 ml; t = equilibrium (min); and T = 30ºC)

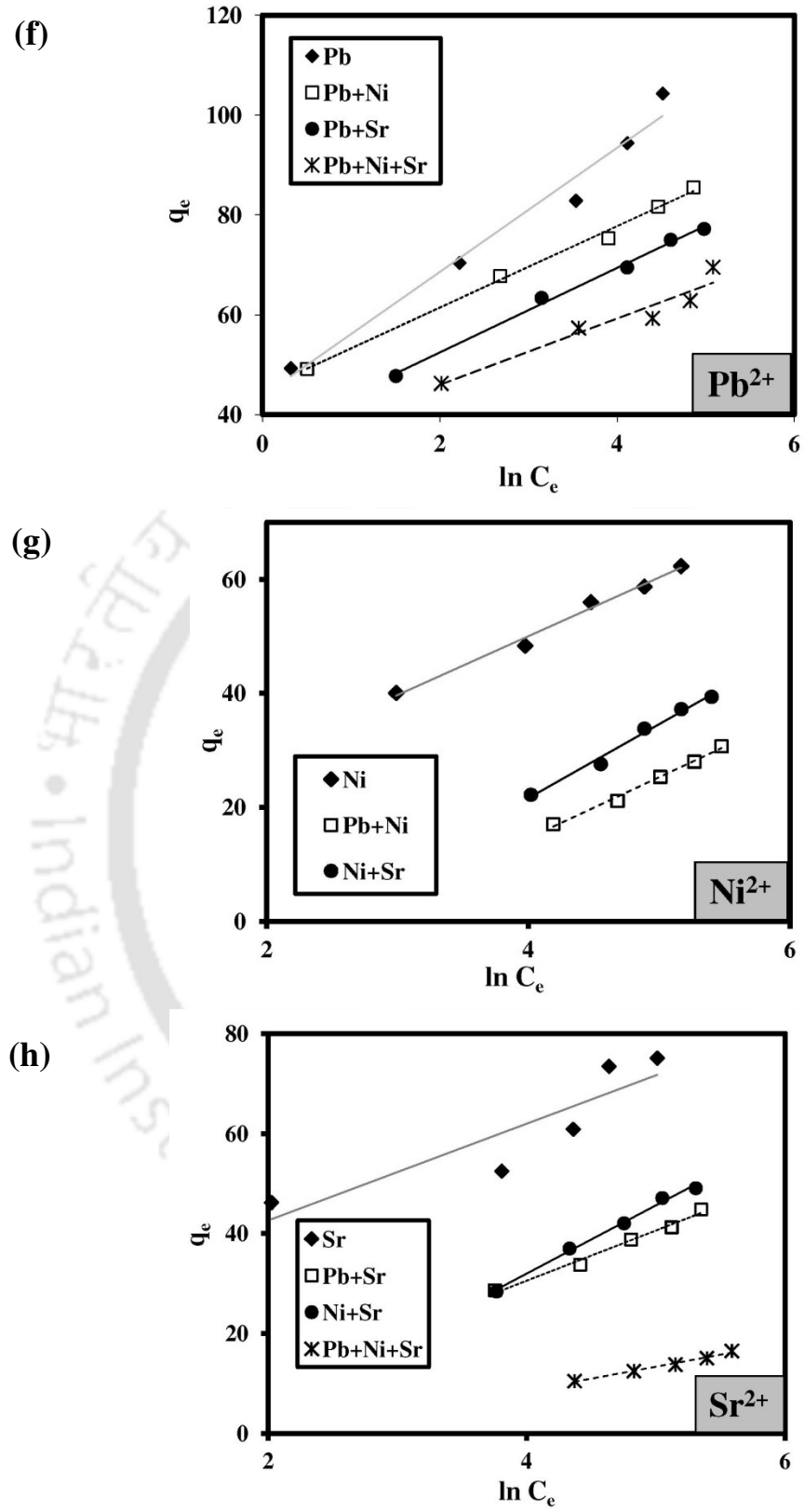

Figure 4.11 Temkin isotherm plots of (f) Pb^{2+} (g) Ni^{2+} and (h) Sr^{2+} adsorption onto SBS in binary and ternary system: (pH = blank; W = 0.1 g; V = 50 ml; t = equilibrium (min); and T = 30ºC)

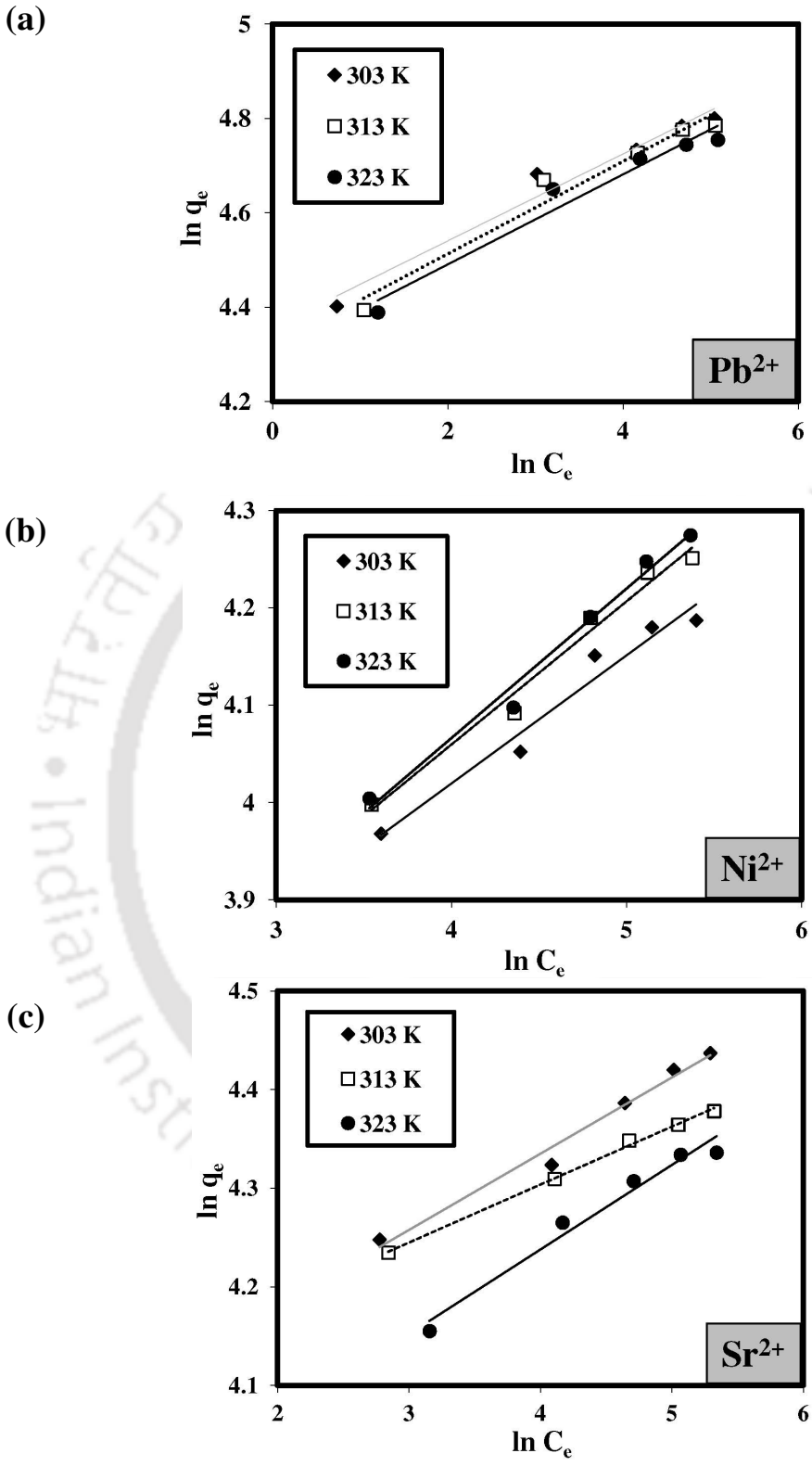

Figure 4.12 Halsey isotherm plots of (a) Pb^{2+} (b) Ni^{2+} and (c) Sr^{2+} adsorption onto SBS: (pH = blank; W = 0.1 g; V = 50 ml; t = equilibrium (min); and T = 30ºC)

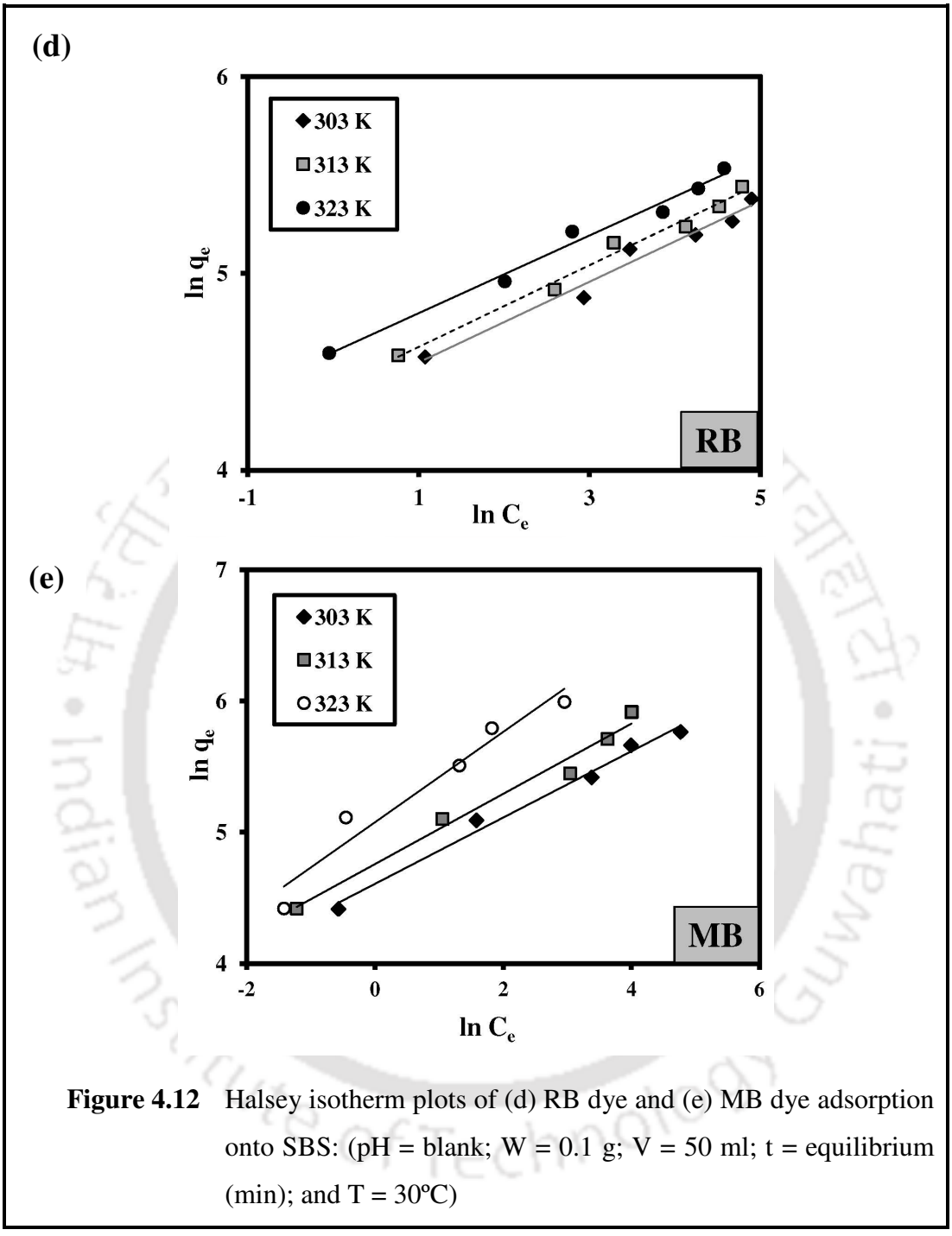

Figure 4.12 Halsey isotherm plots of (d) RB dye and (e) MB dye adsorption onto SBS: (pH = blank; W = 0.1 g; V = 50 ml; t = equilibrium (min); and T = 30ºC)

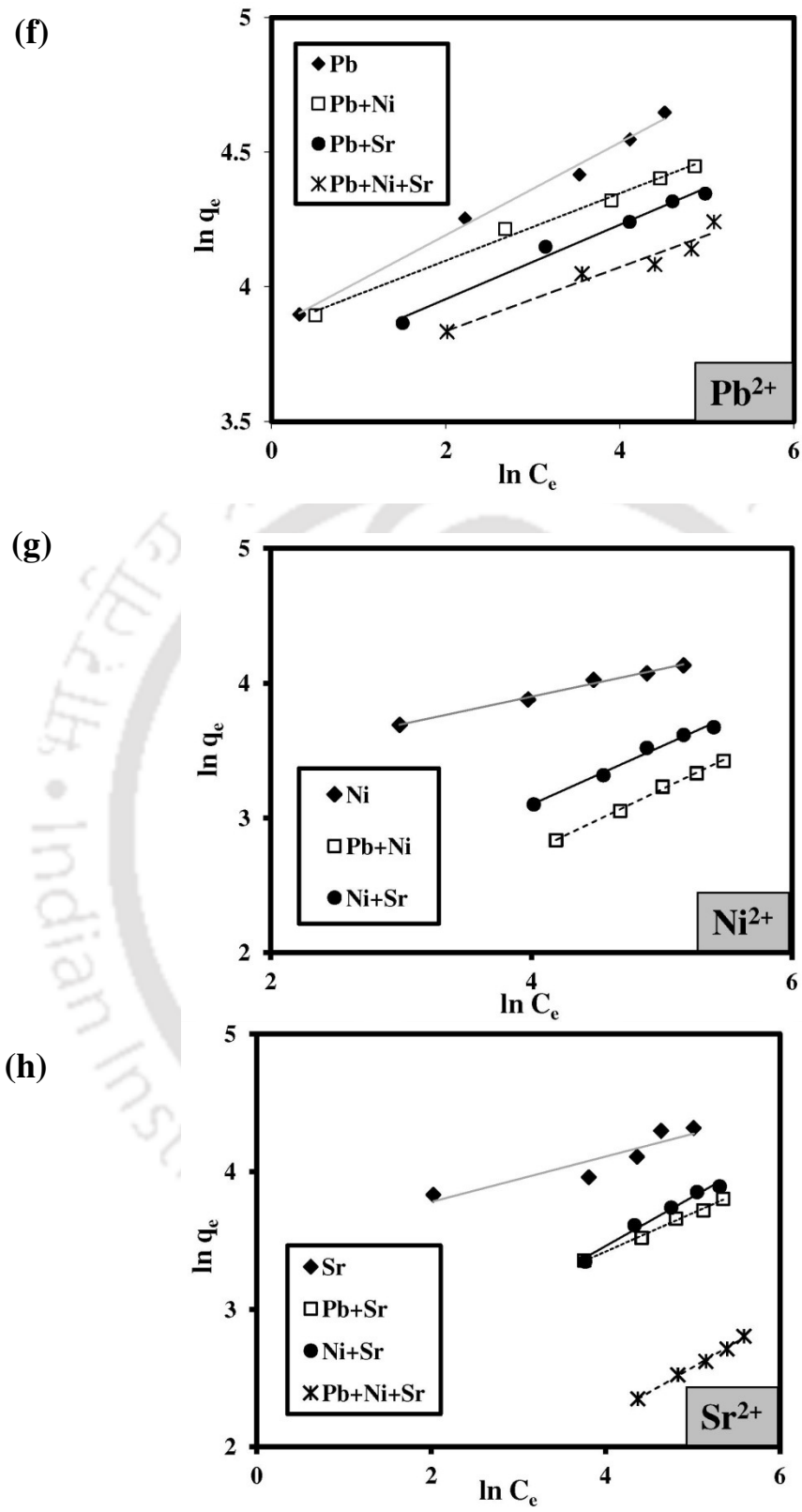

Figure 4.12 Halsey isotherm plots of (f) Pb^{2+} (g) Ni^{2+} and (h) Sr^{2+} adsorption onto SBS in binary and ternary system: (pH = blank; W = 0.1 g; V = 50 ml; t = equilibrium (min); and T = 30ºC)

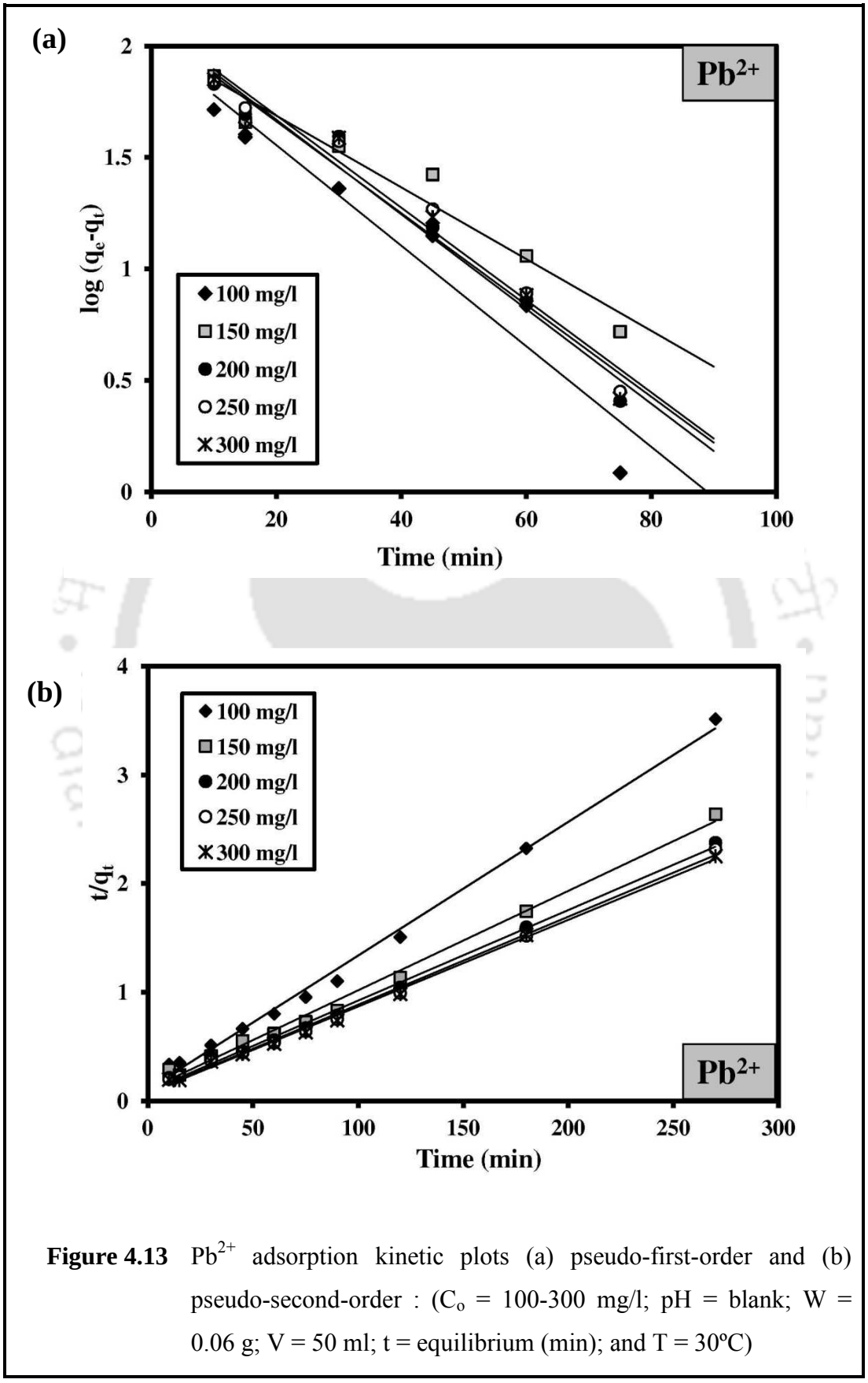

Figure 4.13 Pb^{2+} adsorption kinetic plots (a) pseudo-first-order and (b) pseudo-second-order : (C_o = 100-300 mg/l; pH = blank; W = 0.06 g; V = 50 ml; t = equilibrium (min); and T = 30ºC)

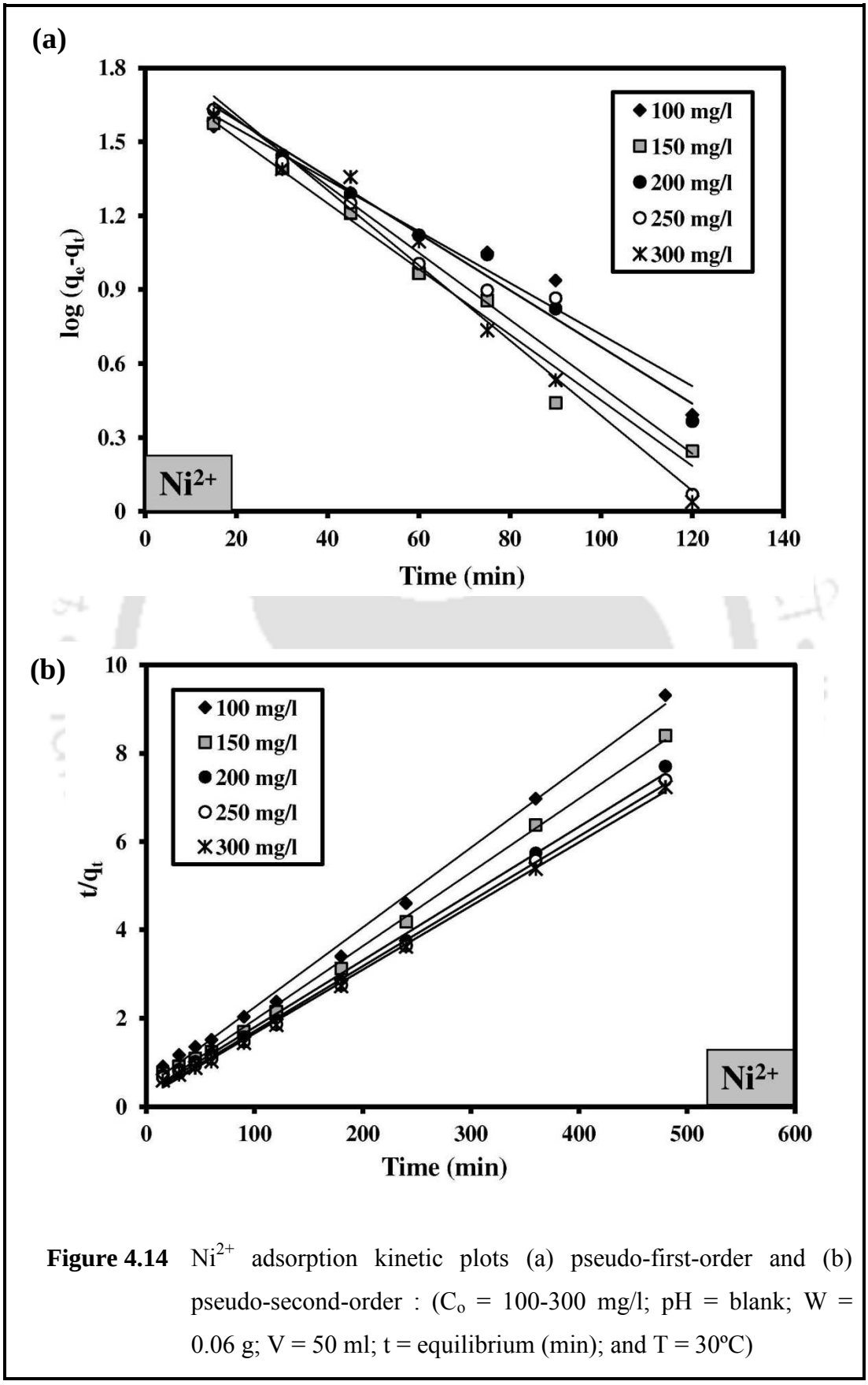

Figure 4.14 Ni^{2+} adsorption kinetic plots (a) pseudo-first-order and (b) pseudo-second-order : (C_o = 100-300 mg/l; pH = blank; W = 0.06 g; V = 50 ml; t = equilibrium (min); and T = 30ºC)

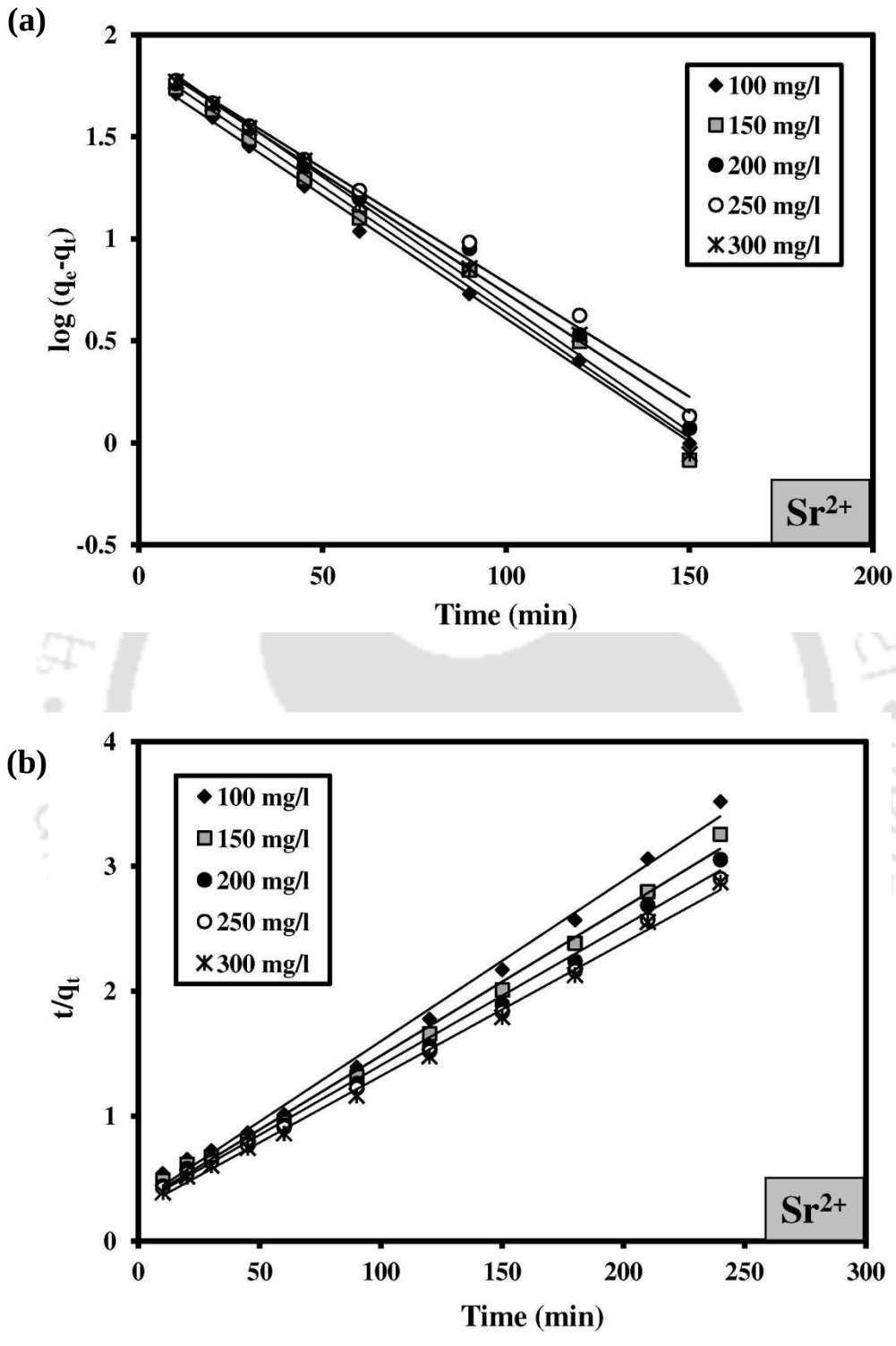

Figure 4.15 Sr^{2+} adsorption kinetic plots (a) pseudo-first-order and (b) pseudo-second-order : (C_o = 100-300 mg/l; pH = blank; W = 0.06 g; V = 50 ml; t = equilibrium (min); and T = 30ºC)

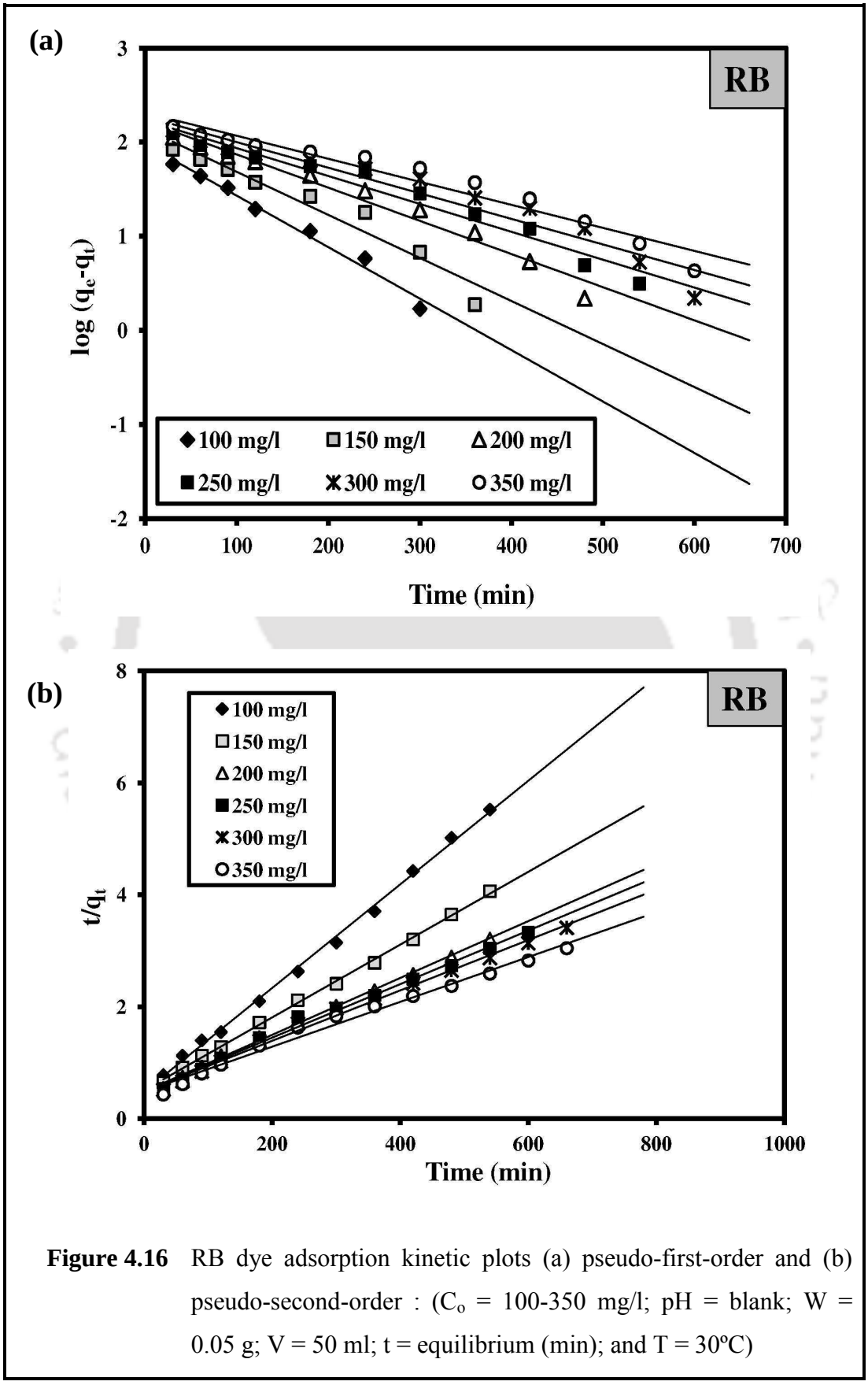

Figure 4.16 RB dye adsorption kinetic plots (a) pseudo-first-order and (b) pseudo-second-order : (C_o = 100-350 mg/l; pH = blank; W = 0.05 g; V = 50 ml; t = equilibrium (min); and T = 30ºC)

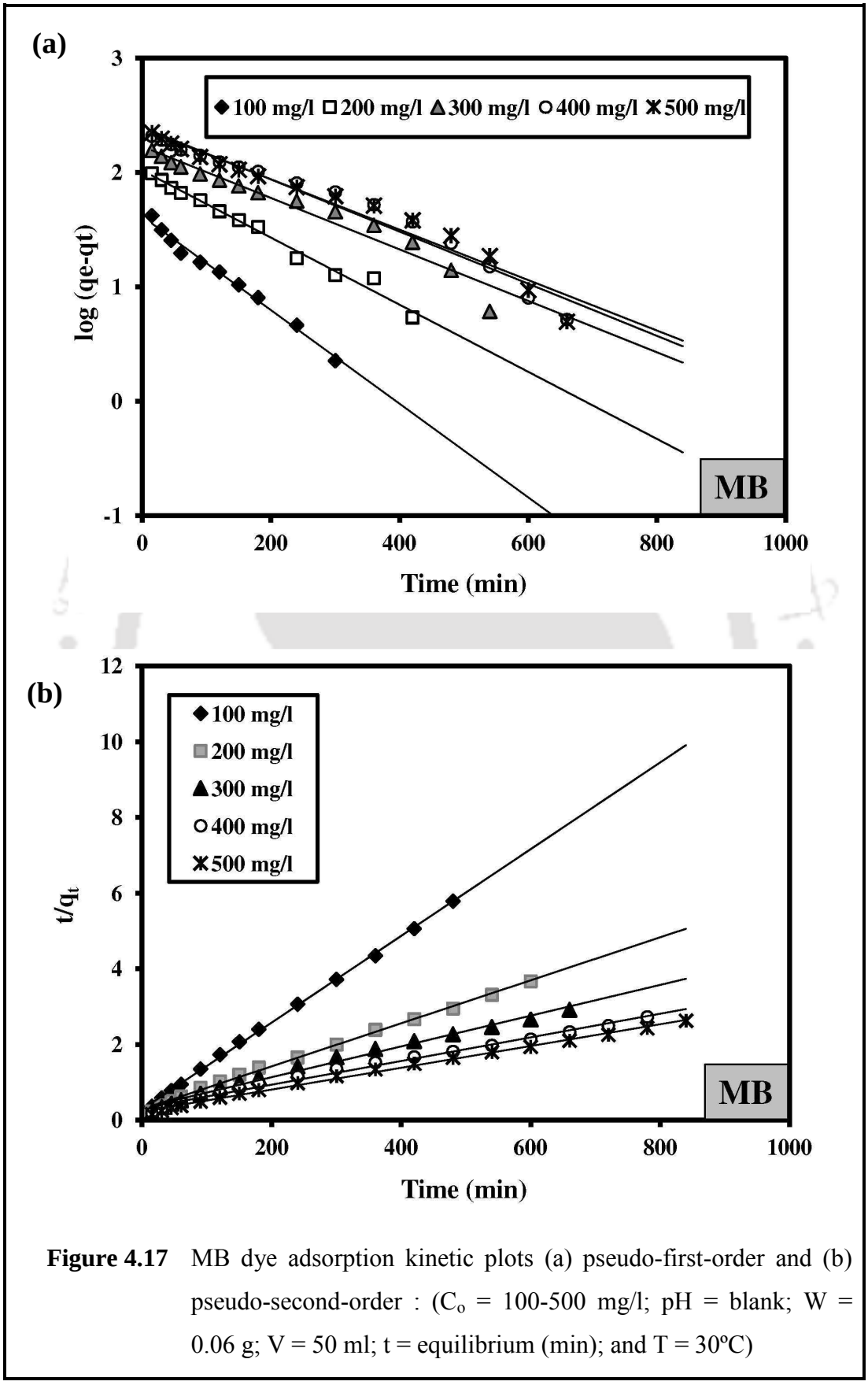

Figure 4.17 MB dye adsorption kinetic plots (a) pseudo-first-order and (b) pseudo-second-order : (C_o = 100-500 mg/l; pH = blank; W = 0.06 g; V = 50 ml; t = equilibrium (min); and T = 30ºC)

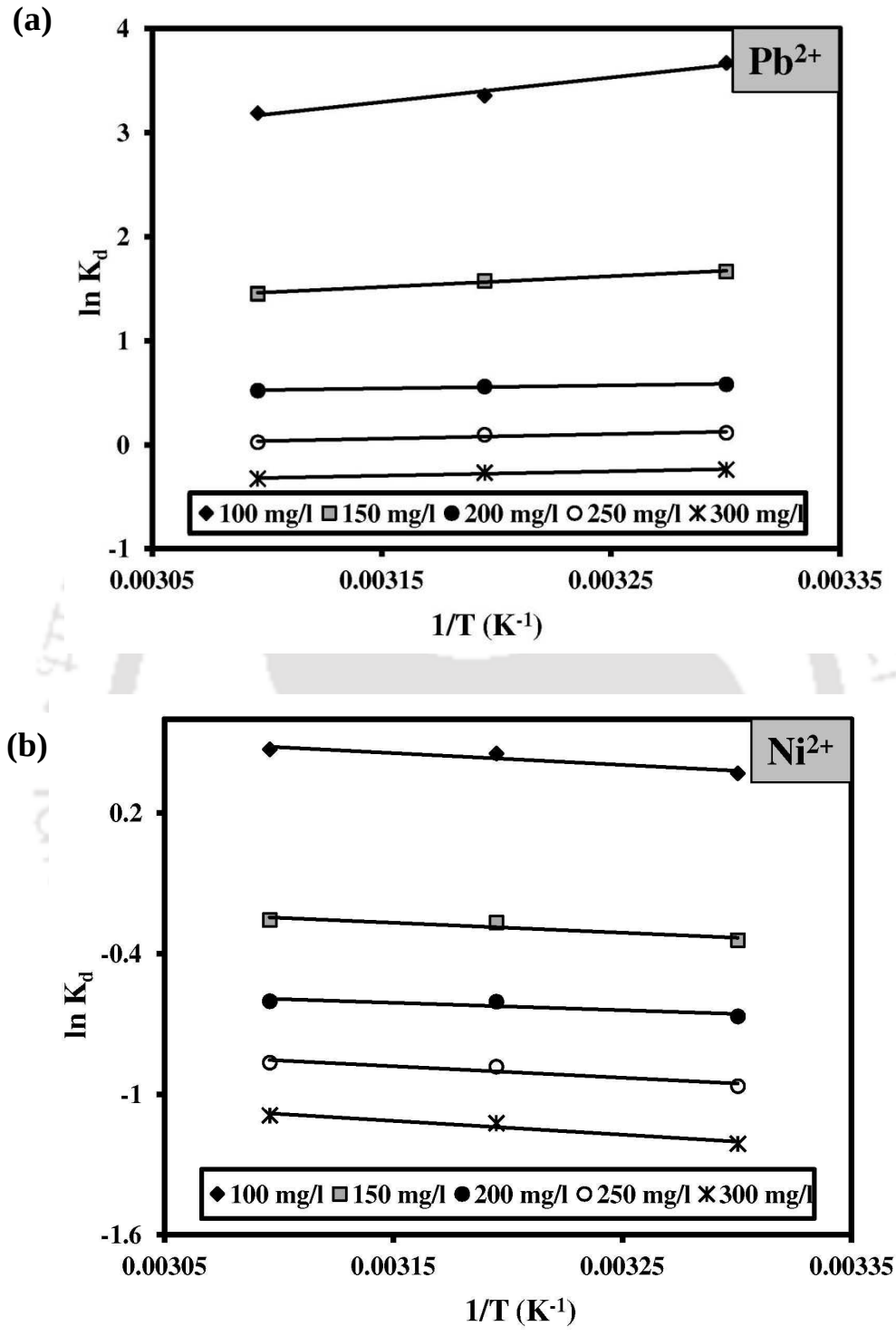

Figure 4.18 Van't Hoff equation plots for (a) Pb^{2+} and (b) Ni^{2+} adsorption : (pH = blank; W = 0.06 g; V = 50 ml; t = equilibrium (min); and T = 30-50ºC)

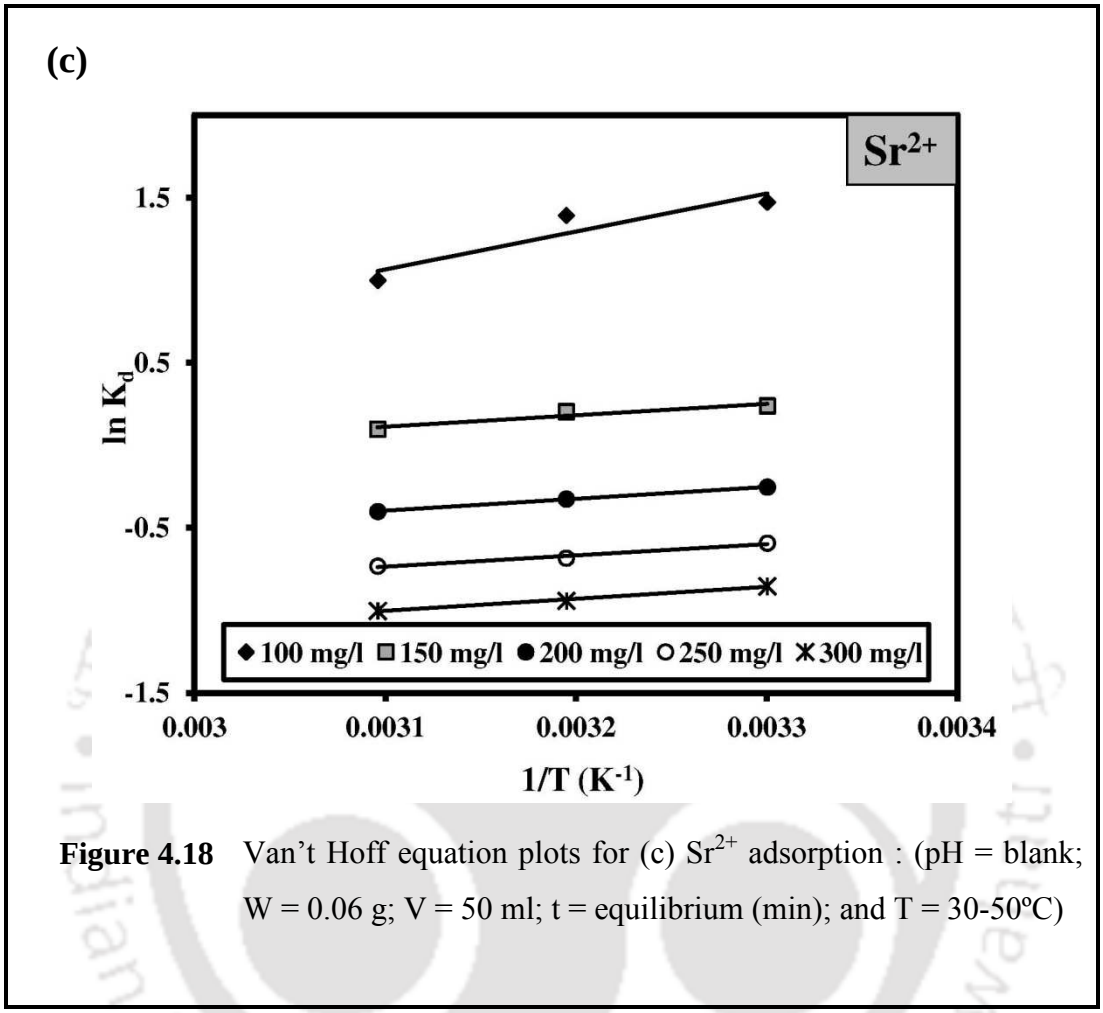

Figure 4.18 Van't Hoff equation plots for (c) Sr^{2+} adsorption : (pH = blank; W = 0.06 g; V = 50 ml; t = equilibrium (min); and T = 30-50ºC)

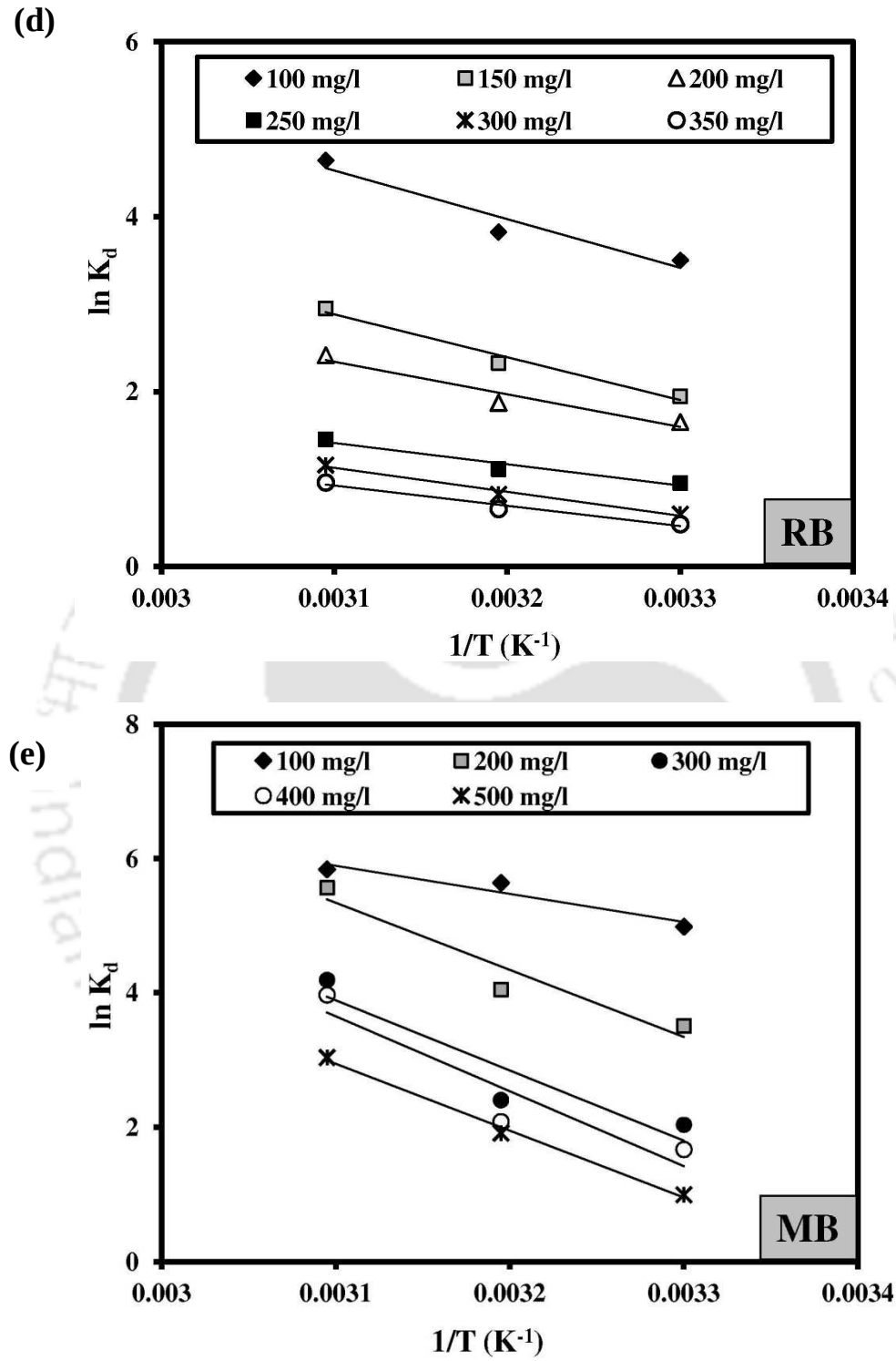

Figure 4.18 Van't Hoff equation plots for (d) RB dye and (e) MB dye adsorption : (pH = blank; W = 0.05 (RB) & 0.06 (MB) g; V = 50 ml; t = equilibrium (min); and T = 30-50ºC)

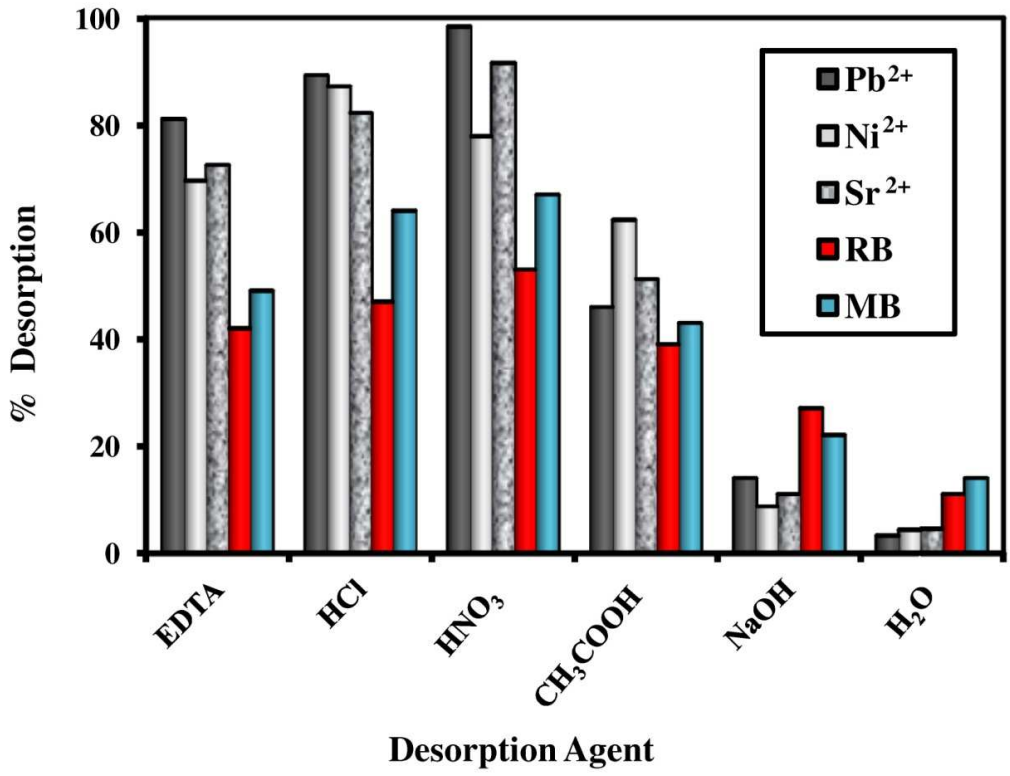

Figure 4.19 Desorption efficiency of metals and dyes: (Eluent volume (V) = 50 ml; T = 30°C; speed = 180 rpm; and time = 1440 min.

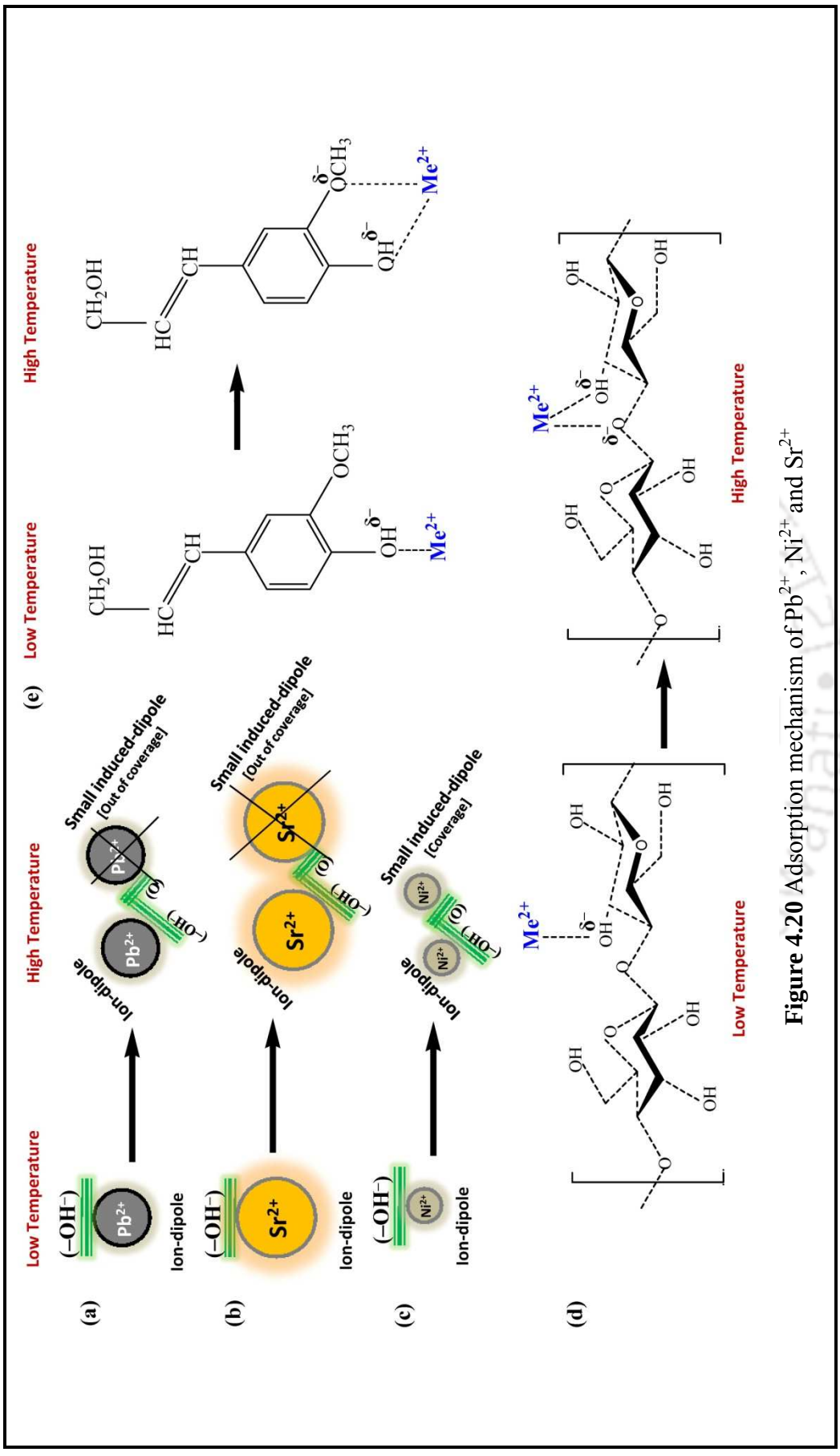

Figure 4.20 Adsorption mechanism of Pb^{2+}, Ni^{2+} and Sr^{2+}

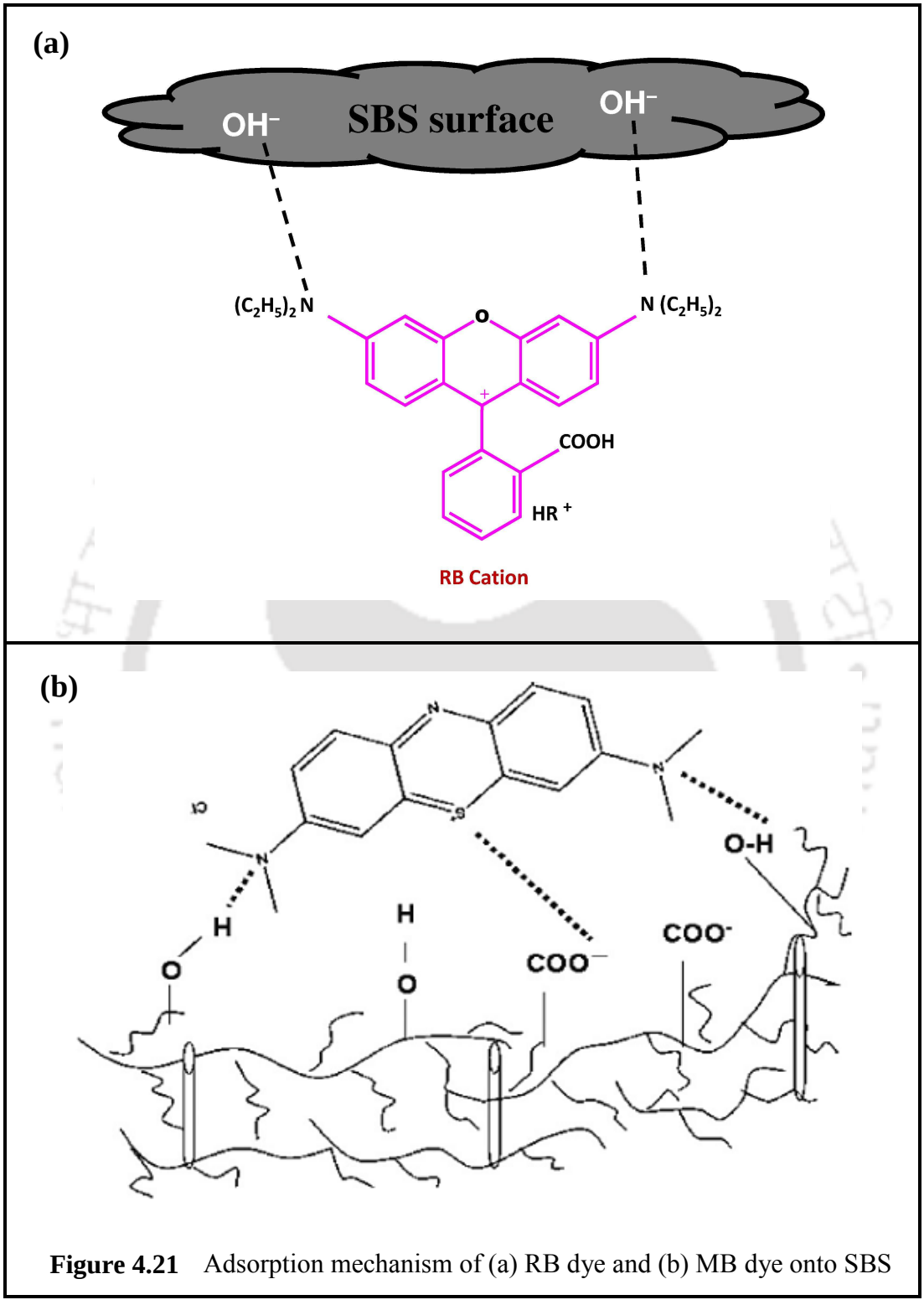

Figure 4.21 Adsorption mechanism of (a) RB dye and (b) MB dye onto SBS

Table 4.1 Physical properties of SBS

Properties	**Percentage of H_2SO_4 treated with SBS**			
	24.5%	**49%**	**73.5%**	**98%**
BET surface area (m^2/g)	17.61	21.39	28.45	34.28
BET mono layer volume (cc/g)	4.046	4.914	6.534	7.875
Total pore volume (ml/g)	0.0089	0.0108	0.0143	0.0173

Table 4.2a Adsorption isotherm constants of Pb^{2+}, $Ni^{2+}$and Sr^{2+} in single metal system onto SBS at different temperature

Metals at various temperature		Langmuir constants			Freundlich constants			Temkin constants			Halsey constants		
		Q_o (mg/g)	b (l/mg)	R^2	K_f (mg/g)	1/n	R^2	A (l/g)	B	R^2	K_h	1/n	R^2
Pb^{2+}	30°C	122.7	0.3791	0.9997	77.96	0.0921	0.9846	4040	9.207	0.9906	2.817×10^{-21}	0.0921	0.9846
	40°C	121.4	0.3624	0.9998	74.95	0.0979	0.9816	1783	9.715	0.9885	7.376×10^{-20}	0.0979	0.9817
	50°C	117.5	0.3904	0.9999	73.67	0.0954	0.9789	2174	9.289	0.9859	2.659×10^{-20}	0.0954	0.9789
Ni^{2+}	30°C	70.18	0.0717	0.9995	32.9	0.1315	0.9816	23.49	7.796	0.9809	2.906×10^{-12}	0.1315	0.9816
	40°C	78.43	0.0514	0.9983	30.04	0.1646	0.9828	5.056	10.36	0.9780	1.056×10^{-9}	0.1646	0.9828
	50°C	72.25	0.0715	0.9992	33.87	0.1314	0.9745	23.89	8.008	0.9727	2.289×10^{-12}	0.1314	0.9745
Sr^{2+}	30°C	86.73	0.1534	0.9996	56.02	0.0773	0.9909	7233	5.939	0.9881	2.444×10^{-23}	0.0773	0.9909
	40°C	80.97	0.2319	0.9999	58.48	0.0587	0.9986	4595	4.353	0.9989	8.096×10^{-31}	0.0587	0.9986
	50°C	78.74	0.1625	0.9999	49.13	0.0858	0.9858	1899	6.011	0.9887	1.928×10^{-20}	0.0858	0.9858

Note: C_o = 100-300 (Pb^{2+}), 100-300 (Ni^{2+}) & 100-300 (Sr^{2+}) mg/l, T = 30-50°C, t (equilibrium) = 90 (Pb^{2+}), 180 (Ni^{2+}) & 120 (Sr^{2+}) min, agitation speed = 180 rpm, V = 50 ml and W = 0.06 g of SBS.

Table 4.2b Adsorption isotherm constants of dyes in single component system onto SBS at different temperature

Dye solution at various temperature		Langmuir constants			Freundlich constants			Temkin constants			Halsey constants		
		Q_o (mg/g)	b (l/mg)	R^2	K_f	$1/n$	R^2	A (l/g)	B	R^2	K_h	$-1/n$	R^2
RB dye	**30°C**	221.2	0.0992	0.9883	76.90	0.2049	0.9729	7.012	29.94	0.9497	6.274×10^{-10}	0.2049	0.9729
	40°C	235.9	0.1151	0.9883	82.94	0.2078	0.9857	8.197	31.69	0.9626	5.863×10^{-10}	0.2078	0.9857
	50°C	255.8	0.1693	0.9877	99.47	0.1975	0.9856	17.79	31.96	0.9597	7.692×10^{-11}	0.1975	0.9856
MB dye	**30°C**	330	0.1551	0.9909	100.2	0.2522	0.9869	9.609	44.06	0.9757	1.166×10^{-8}	0.2522	0.9869
	40°C	371.8	0.1928	0.9503	116.5	0.2675	0.9803	12.97	49.45	0.9087	1.879×10^{-8}	0.2675	0.9803
	50°C	427.4	0.6341	0.9911	160.1	0.3439	0.9462	13.77	70.69	0.9781	3.883×10^{-7}	0.3439	0.9462

Note: C_o = 100-300 (RB) and 100-500 (MB) mg/l, pH = blank, t = equilibrium time (min), agitation speed = 180 rpm, V = 50 ml and W = 0.05 (RB) and 0.06 (MB) g of SBS.

Table 4.3 Adsorption isotherm constants of binary and ternary metal adsorption onto SBS

Metal solution at various combination		Langmuir constants			Freundlich constants			Temkin constants			Halsey constants		
		Q_o (mg/g)	b (l/mg)	R^2	K_f	1/n	R^2	A (l/g)	B	R^2	K_h	-1/n	R^2
Pb^{2+}	Pb	106.3	0.1976	0.9907	46.88	0.1718	0.9921	33.68	12.43	0.9743	1.866×10^{-10}	0.1718	0.9921
	Pb+Ni	86.66	0.2515	0.9976	46.84	0.1249	0.9921	252.8	8.155	0.9953	4.274×10^{-14}	0.1249	0.9921
	Pb+Sr	79.24	0.1866	0.9986	39.56	0.1379	0.9857	67.16	8.453	0.9947	2.653×10^{-12}	0.1379	0.9857
	Pb+Ni+Sr	69.88	0.1228	0.9908	36.56	0.1184	0.9481	137.7	6.634	0.9286	6.261×10^{-14}	0.1184	0.9481
Ni^{2+}	Ni	67.57	0.0573	0.9973	21.69	0.2056	0.9910	2.345	10.31	0.9889	3.157×10^{-7}	0.2056	0.9910
	Pb+Ni	44.80	0.0088	0.9941	2.464	0.4619	0.9976	0.0719	10.68	0.9930	0.1419	0.4619	0.9976
	Ni+Sr	54.85	0.0117	0.9943	3.946	0.4317	0.9865	0.0969	12.98	0.9882	0.0416	0.4317	0.9865
	Pb+Ni+Sr	0.9853	-0.0118	0.8866	38834	-1.889	0.9459	240.0	-7.920	-1.000	268.4	1.889	-0.9459
Sr^{2+}	Sr	80.91	0.0643	0.9738	31.54	0.1645	0.9169	11.17	9.661	0.7988	7.732×10^{-10}	0.1645	0.9169
	Pb+Sr	52.44	0.0244	0.9942	10.00	0.2791	0.9973	0.3875	10.02	0.9871	2.612×10^{-4}	0.2791	0.9946
	Ni+Sr	61.65	0.0196	0.9989	7.592	0.3581	0.9820	0.1918	13.63	0.9940	3.479×10^{-3}	0.3581	0.9820
	Pb+Ni+Sr	21.58	0.0111	0.9913	2.133	0.3643	0.9967	0.1084	4.8060	0.9877	0.1249	0.3643	0.9967

Note: C_o = 100-300 (Pb^{2+}), 100-300 (Ni^{2+}) & 100-300 (Sr^{2+}) mg/l, T = 30°C, t = equilibrium time (min), agitation speed = 180 rpm, V = 50 ml and W = 0.1 g of SBS.

Table 4.4a Kinetic constants of single metal adsorption onto SBS

Initial adsorbate concentration (mg/l)		Pseudo-first-order model				Pseudo-second-order model		
		$q_{e,exp}$ (mg/g)	k_{ad} (l/min)	$q_{e,cal}$ (mg/g)	R^2	k′ (g/mg/min) (1×10^{-3})	$q_{e,cal}$ (mg/g)	R^2
100	**Pb^{2+}**	81.60	0.0382	38.56	0.9643	4.364	81.17	0.9996
	Ni^{2+}	52.89	0.0226	52.74	0.9820	0.7398	55.37	0.9979
	Sr^{2+}	69.95	0.0256	49.35	0.9965	1.272	72.05	0.9988
150	**Pb^{2+}**	108	0.0355	74.27	0.8321	1.261	108.70	0.9989
	Ni^{2+}	57.52	0.0230	43.46	0.9599	0.9549	59.92	0.9988
	Sr^{2+}	75.45	0.0292	50.51	0.9963	1.663	76.75	0.9989
200	**Pb^{2+}**	113.7	0.0491	96.41	0.9874	1.308	117.37	0.9996
	Ni^{2+}	63.51	0.0235	54.94	0.9841	0.7967	66.14	0.9984
	Sr^{2+}	80.35	0.0263	51.42	0.9935	1.682	80.32	0.9989
250	**Pb^{2+}**	119.6	0.0468	82.45	0.9782	1.435	122.70	0.9998
	Ni^{2+}	65.36	0.0246	48.69	0.9225	0.9064	68.07	0.9987
	Sr^{2+}	83.09	0.0316	57.15	0.9984	1.566	84.67	0.9992
300	**Pb^{2+}**	121.5	0.0629	106.8	0.9497	1.918	124.38	0.9999
	Ni^{2+}	65.84	0.0242	40.83	0.9022	0.9666	69.35	0.9992
	Sr^{2+}	84.52	0.0364	58.13	0.9937	1.299	87.72	0.9996

Note: C_o = 100-300 (Pb^{2+}), 100-300 (Ni^{2+}) & 100-300 (Sr^{2+}) mg/l, T = 30-50°C, t (equilibrium) = 90 (Pb^{2+}), 180 (Ni^{2+}) & 120 (Sr^{2+}) min, mixing = 180 rpm, V = 50 ml and W = 0.06 g of SBS

Table 4.4b Kinetic constants for RB dye adsorption onto SBS

Initial RB concentration (mg/l)		Pseudo-first-order model			Pseudo-second-order model		
Co	**$q_{e,\ exp}$ (mg/g)**	**K_{ad} (l/min)**	**$q_{e,\ cal}$ (mg/g)**	**R^2**	**k' (g/mg/min) ($1x10^{-5}$)**	**$q_{e,\ cal}$ (mg/g)**	**R^2**
100	97.07	0.0127	94.78	0.9838	17.99	107.5	0.9977
150	131.3	0.0106	138.17	0.9458	8.369	153.8	0.9985
200	167.8	0.0081	166.38	0.9707	5.455	196.1	0.9977
250	180.6	0.0069	170.65	0.9633	4.725	208.3	0.9929
300	193.6	0.0062	186.81	0.9375	4.164	222.2	0.9935
350	216.7	0.0055	204.83	0.9482	4.266	250	0.9855

Table 4.4c Kinetic constants for MB dye adsorption onto SBS

Initial MB concentration (mg/l)		Pseudo-first-order model			Pseudo-second-order model		
Co	**$q_{e,\ exp}$ (mg/g)**	**K_{ad} (l/min) ($1x10^{-3}$)**	**$q_{e,\ cal}$ (mg/g)**	**R^2**	**k' (g/mg/min) ($1x10^{-5}$)**	**$q_{e,\ cal}$ (mg/g)**	**R^2**
100	82.86	9.442	41.28	0.9887	46.27	86.96	0.9992
200	162.6	6.679	104.1	0.9866	11.34	175.4	0.997
300	225.5	5.067	169.2	0.9539	5.195	243.9	0.9896
400	288.2	5.297	248.9	0.968	3.053	302.6	0.9911
500	318.8	5.067	241.2	0.9642	3.605	344.8	0.9956

Table 4.5a Thermodynamic parameters for adsorption of Pb^{2+}, Ni^{2+} and Sr^{2+} onto SBS

Initial metal concentration (mg/l)		$\Delta H°$ (KJ/mol)	$\Delta S°$ (KJ/mol K)	$\Delta G°$ (KJ/mol)		
				30°C	40°C	50°C
100	Pb^{2+}	-19.69	-0.0346	-9.248	-8.730	-8.377
	Ni^{2+}	4.175	0.0169	-0.9325	-1.181	-1.240
	Sr^{2+}	-19.10	-0.0504	-3.708	-3.621	-2.624
150	Pb^{2+}	-8.647	-0.0146	-4196.82	-4.099	-3.817
	Ni^{2+}	3.523	0.0089	0.8616	0.6957	0.6727
	Sr^{2+}	-5.724	-0.0168	-600.33	-0.5284	-0.2544
200	Pb^{2+}	-2.449	-0.0032	-1.466	-1.458	-1.370
	Ni^{2+}	2.656	0.0033	1.681	1.574	1.584
	Sr^{2+}	-6.012	-0.0219	0.6397	0.8493	1.056
250	Pb^{2+}	-3.684	-0.0111	-292.05	-0.2525	-0.0651
	Ni^{2+}	4.113	0.0056	2.431	2.295	2.272
	Sr^{2+}	-5.683	-0.0237	1492.9	1.779	1.923
300	Pb^{2+}	-3.505	-0.0135	601.29	0.6966	0.8543
	Ni^{2+}	4.930	0.0063	3.051	2.922	2.865
	Sr^{2+}	-6.063	-0.0271	2151.77	2.451	2.635

Note: C_o = 100-300 (Pb^{2+}), 100-300 (Ni^{2+}) & 100-300 (Sr^{2+}) mg/l, T = 30-50°C, t (equilibrium) = 90 (Pb^{2+}), 180 (Ni^{2+}) & 120 (Sr^{2+}) min, agitation speed = 180 rpm, V = 50 ml and W = 0.06 g of SBS.

Table 4.5b Thermodynamic parameters for adsorption of RB onto SBS

Initial RB concentration (mg/l)	ΔS° (KJ/mol K)	ΔH° (KJ/mol)	-ΔG° (J/mol)		
			303 K	313 K	323 K
100	0.1807	46.14	8822	9952	12201
150	0.1503	40.77	4902	6058	7759
200	0.1153	30.92	4162	4875	6351
250	0.0745	20.24	2408	2902	3827
300	0.0802	22.84	1507	2149	3054
350	0.0674	19.28	1223	1714	2528

Table 4.5c

Thermodynamic parameters for adsorption of MB onto SBS

Initial MB concentration (mg/l)	ΔS° (KJ/mol K)	ΔH° (KJ/mol)	-ΔG° (J/mol)		
			303 K	313 K	323 K
100	0.1568	34.78	12560	14674.2	15344
200	0.3022	83.15	8838	10543.6	14626
300	0.3017	86.89	5136	6260.78	11019
400	0.3179	92.78	4208	5426.24	10433
500	0.2808	82.68	2514	4983	7984

CHAPTER 5

ADSORPTION OF SELECTED CONTAMINANTS ON CHEMICALLY ACTIVATED TANNERY RESIDUAL BIOMASS

The detailed adsorption studies of Cr^{6+}, rhodamine B metals and methylene dye are presented in this chapter. These three components were identified as high removal capacity adsorbates with HCl treated tannery residual biomass adsorbent (HTB) in the preliminary performance evaluation test among the targeted heavy metals, phenols and cationic dyes of this research work. Thus, in this chapter the elaborate adsorption studies and the results of Cr^{6+}, rhodamine B and methylene dye using HTB are reported and discussed in detail by covering all the aspects for its applications in the field of water and wastewater treatment.

5.1 INTRODUCTION

In India, tannery industrial wastes are major sources of environmental pollution and water contamination. A large amount of waste produced by these tanneries is discharged in natural water bodies directly or indirectly through open drains without any treatment (Nalawade *et al.,* 2009). Tannery wastewater contains large of amount chromium, cadmium, various dyes and phenolic compounds due their various application in leather processing. The water in the low lying areas in developing countries, like India and Bangladesh, is polluted in such a degree that it has become unsuitable for public uses. Simultaneously, solid waste generation from all stages of leather making process also creates a huge problem in solid waste disposal. In particular, vegetable tanning process section generates huge amount of plant based solid wastes after extraction of tannin content in tanneries. These solid wastes are simply thrown out by the tanneries in the surrounding areas without any proper disposal. When the rate of decomposition of this solid waste is higher, serious air pollution is caused in surrounding residential areas by producing intolerable obnoxious odours (Nalawade *et al.,* 2009). Hence, in this research work we have chosen the tannery residual biomass from the vegetable tanning process to convert as useful product through recycling process for the treatment of tannery wastewater pollutants such as Cr^{6+} and cationic dyes.

In this work, an investigation has been carried out to check the reusability of tannery residual biomass by proper activation with HCl as a locally available adsorbent to remove the Cr^{6+}, rhodamine B and methylene blue from synthetic wastewater. The influence of principal operational parameters of adsorption process such as the effect of pH, influence of other co-ions, binary system and temperature was monitored to optimize the sorption process for its possible use as a low-cost adsorbent in the field of wastewater treatment and waste recycling management to solve the local wastewater issues. This study may help to reduce the cost of waste disposal (recycling) in tanneries and provides an alternative adsorbent to the existing commercial adsorbents to remove toxic heavy metals and dyes especially from tannery wastewater since they produces heavy metals, phenols and dyes.

5.2 EXPERIMENTAL METHODS

5.2.1 Preparation of Synthetic Solution

A stock solution of Cr^{6+}, RB and MB (1000 mg/l) was prepared by dissolving appropriate quantity of $K_2Cr_2O_7$ (Merck, India), rhodamine B and methylene blue (C.I. 45170 and 52015, LOBA Chemie, India) in Millipore water. The chemical structure of RB and MB is illustrated in Appendix 1. The stock solution was shaken for 10 min at 180 rpm to obtain complete dissolution and then suitably diluted with water to get the required initial concentrations of Cr^{6+} (100 to 350 mg/l), RB dye (100 to 350 mg/l) and MB dye (100 to 600 mg/l). Before mixing the adsorbent, the pH of the solution was adjusted using 0.1N HCl or 0.1N NaOH. The pH of the solution was measured by pH meter (Eutech, model: 510).

5.2.2 Experimental Protocol

Adsorption experiments were carried out under batch mode at 30°C, 40°C and 50°C. Initially, the effect of pH on sorption capacity of adsorbate (Cr^{6+}, RB and MB dye) onto HTB was carried out and then the effect of other ions, binary system, temperature and initial concentration of the adsorbates were carried at optimum pH. The pH of each solution was adjusted using required quantity of 1N HCl (or) 1N NaOH before mixing the adsorbent. In a set of 250 ml Borosil conical flasks containing adsorbate solution (50 ml) of particular initial concentration was placed. Fixed doses (0.05 g/50 ml) of adsorbent were added to the adsorbate solutions. The pH of the each solution was maintained at optimum condition. Each sample was agitated in an incubating shaker (LabTech, Model LSI-1005R) at a particular temperature. Samples at different time intervals were withdrawn and the supernatant of two dye solutions was separated by centrifuge (5000 rpm) and the filtrate was analyzed for the residual RB an MB dye concentration using UV–visible spectrophotometer (Perkin-Elmer, model: Lambdas 45) at the maximum wavelength (λ_{max} = 555 nm for RB and 667 nm for MB) of the dye. Similarly, after completion of every set of experiments the supernatant of Cr^{6+} solution was separated by filtration using Whatman filter paper no. 42 and sample was stored for residual chromium analysis. Final residual metal concentration was directly measured by flame atomic absorption spectrophotometer (AAS) (Varian spectra, AA240) with an air–acetylene flame.

5.2.3 Adsorbent Characterization

Scanning electron microscopy (SEM) (Leo, 1430 vp, Carl Zeiss, German) characterization was carried out to observe the surface texture and porosity for two states of TB such as TB without activation and TRB with HCl activation (HTB) (1:3, w/v, ratio). Energy dispersive X-ray spectroscopy (EDX) analysis was employed for further confirmation of chromium adsorption over the surface of the HTB. To resolve the functional groups and its wave numbers, spectra analysis was done for TRB before and after treatment using Fourier transform infrared spectrometer (FT-IR) (Perkin-Elmer, PE-RXI) in the range of 500 to 4000 cm^{-1}. In this analysis, finely grounded sorbent was encapsulated with KBr in the ratio 1:20 in order to prepare the translucent sample disks. The BET surface areas and monolayer volumes of the different impregnation ratio of HCl treated TBs were measured in single point surface area analyser (ChemiSorb 2720/2750) using nitrogen adsorption isotherm at −196^{o}C. Before measurement, the samples were degassed using Helium at 150^{o}C for 0.5 h. X-ray photoelectron spectroscopy (XPS) (Zetasizer Nano, Malvern Instruments Ltd UK) analysis was done to analyze the oxidation states of chromium at Cr2P orbital.

5.3 RESULTS AND DISCUSSION

5.3.1 Effect of Impregnation Ratio

The effect of impregnation ratio on adsorption capacity of Cr^{6+}, RB and MB dye is shown in Figure 5.1. It can be seen from the figure that the sorption capacity of Cr^{6+}, RB and MB increased from 72 to 136 mg/g, 96 to 146 mg/g and 112 to 196 mg/g as the impregnation ratio (TB/HCl, w/v) increased from 1:1 to 1:3, respectively. The increase in chemical ratio in TB activation increased the pore development, surface area (see BET analysis) and thus, enhanced the sorption capacity of Cr^{6+} metal, RB and MB dye. However, beyond 1:3 ratios the sorption capacity remains constant. It may be due to the fact that the number of active binding sites remains unchanged. Therefore, the sorbent which was prepared by only the HCl activation at 1:3 (TB: HCl) ratio was utilized for the entire study.

5.3.2 Surface Characterization of Adsorbent

5.3.2.1 SEM Analysis

The SEM image of TRB prior to HCl activation is shown in Figure 5.2a. A regular plain surface with no pores on TRB was observed from this figure. The SEM image of TRB after the HCl treatment is shown in Figure 5.2b. The progressive change and well developed honeycomb structured pores on the surface of the HTB were observed from this figure. The pore formation of activated TB is mainly attributed to the addition of hydrochloric acid which reacts with TB to swell and it opens the surface structure to create active sites.

5.3.2.2 BET Surface Area Analysis

The effect of impregnation ratio (TB (g)/HCl (ml)) on single point BET surface area is presented in Table 5.1. As given in Table 5.1, the surface area (3.844 to 10.42 m^2/g) and total pore volume (0.0289 to 0.0508 ml/g) increases with increase in chemical ratio. This is due to the improvement in surface texture and the pore formation. However, beyond 1:3 impregnations ratio the surface area was slightly decreased. This is might be due to the formation of multi-layer of activating agent at higher chemical ratio. Similar observation has been reported by Mohanty *et al.*, 2005.

5.3.2.3 FT-IR Spectra Analysis

The FT-IR spectra of native TB are shown in Figure 5.3a. The bands of raw TB at 3414, 2927, 1640, 1108, and 1019 cm^{-1} are the stretching vibrations of the surface hydroxyl group (O–H), symmetric vibrations of C–H predominantly for aliphatic acids, COO and C=C groups, C–O stretch and stretching vibrations of C–O–C and –OCH_3 (indicative of lignin structure), respectively. The other bending vibrations less than 823 cm^{-1} are the finger print zone that indicates the phosphate functional groups (Mohan and Sreelakshmi, 2008). But, fundamental peaks of the above functional groups on TB were shifted from its position after HCl treatment (Figure 5.3b). It might be due to the formation of active sites on the surface of HTB by HCl. Similarly, the significant peak shaftings were observed on the HTB surface after metal and dye adsorption (Figures 5.3c and 5.3d). The surface hydroxyl, carboxyl, lignin and phosphate functional groups present on the HCl treated TB were responsible for the metal and cationic dye molecule adsorption due to the electrostatic attraction

(discussed in adsorption mechanism section) between the oppositely charged functional groups of HTB (Ju *et al.,* 2009; Das *et al.,* 2006).

5.3.2.4 EDX Spectra Analysis

EDX analysis was employed to analyze the surface elements before (Figures 5.4a) and after chromium adsorption (Figure 5.4b) on HTB. Before interaction with chromium ion, only carbon, oxygen and chlorine atoms were observed on HTB, whereas chromium peak was present after adsorption. Chlorine peak was present due to the treatment of hydrochloric acid with TB during the activation.

5.3.3 Effect of pH

5.3.3.1 Effect of pH on Cr^{6+} adsorption

One of the most important process parameter for the adsorption of metal and dye on HTB is the pH of the solution. The pH of the solution was varied in the range of 1-11 keeping all other parameters constant. The maximum removal of Cr^{6+} was occurred at initial pH 2.0 for HTB (Figure 5.5). At lower pH the surface area of the adsorbent was more protonated and competitive negative ions adsorption occurred between positive surface ($-OH^+$) and free chromate ion. Adsorption of Cr^{6+} at pH 2.0 shows the bind of the negatively charged chromium species ($HCrO_4^-$) occurred through electrostatic attraction to the positively charged (due to more H^+ ions) surface functional groups of the adsorbent (discussed in mechanism section). But in highly acidic medium (pH ≈1) H_2CrO_4 (neutral form) is the predominant species of Cr^{6+} as reported by Agrawal *et al*. (2008). Hence, at pH 1.0 percentage adsorption decreased due to the involvement of less number of $HCrO_4^-$ anions on the positive surface. At higher pH due to more OH^- ions adsorbent surface carrying net negative charges, which tend to repulse the metal anions (CrO_4^{2-}) (Amarasinghe and Williams, 2007). However, there is also some percentage adsorption at pH > 2.0 but the rate of adsorption is reduced. This might be due to the weakening of electrostatic force of attraction between the oppositely charged adsorbate and adsorbent or physisorption due to weak undirected Van der Waals forces of attraction (Mohamed, 2006 and Baral *et al*., 2004). When solution pH increased above 2.0, Cr^{3+} adsorption also enhanced due to gradual increase in the negative charge on adsorbent. But the adsorption-coupled reduction of Cr^{6+} to Cr^{3+} was less above pH 2.0 due to the less adsorption of $HCrO_4^-$ (discussed in

section 3.9). At pH ≈ 8.0, CrO_4^{2-} is the predominant form and repulsion take place by high negative surface (Amarasinghe and Williams, 2007).

5.3.3.2 Effect of pH on RB Dye Adsorption

There was a sharp increase in sorption capacity (34.39 to 146.80 mg/g) with increase in pH of the RB solution from 2 to 3.5 as shown in Figure 5.5. At very low pH (2.0), the surface of the sorbent was more protonated (due to more H^+ ions). As the pH increased from 2.0 to 3.5, the availability of $-OH^-$ group increased. Also, below pH 3.5 RB molecules remain in monomeric form and dye molecule can easily enter into the pore structure of the adsorbent (Guo *et al.*, 2005). Hence, sorption capacity increases with increase in solution pH up to 3.5. However, above pH 3.5 the sorption capacity of RB decreased from 146.80 to 111.48 mg/g. The pH higher than 3.5, zwitterionic form of RB in the water might increased the aggregation of RB (bigger molecules) and thus unable to enter into the pore structure on the surface. The maximum sorption capacity of RB was 146.80 mg/g at pH 3.5. Thus, all further RB studies were carried out at pH 3.5.

5.3.3.3 Effect of pH on MB Dye Adsorption

Effect of pH on adsorption capacity of methylene blue is shown in Figure 5.5. When MB solution pH increased from 1.0 to 7.0, the adsorption capacity of MB increased from 104.2 to 196.6 mg/g. Thereafter, the removal of dye at above pH 8.0 was due to the dissociation of MB dye at higher alkaline pH. As the pH of the MB solution becomes higher (from 2 to 7), the association of dye cations with negatively charged HTB surface could be more easily takes place as follows.

$$S\text{-}OH + OH^- = SO^- + H_2O \quad (5.1)$$

$$SO^- + MB^+ = S^-O^-MB \quad (5.2)$$

Lower adsorption of MB at acidic pH was due to the presence of excess H^+ ions competing with the dye cation for the adsorption sites. At acidic pH, the adsorbent surface and dye molecules both are highly in protonated form hence, there is electrostatic repulsion between cationic dye and protonated adsorbent surface which leads to lower removal of dye. Similar results have been reported by Kadirvelu *et al.*

(2005). Therefore, the blank pH (6.3 ± 0.05) which is near to optimum pH 7.0 was chosen for remaining entire study.

5.3.4 Effect of Other Ions in Test Solution

The influence of other co-ions such as Na^+, Ca^{2+}, and NH_4^+, which are commonly present in water and wastewater, on the percentage adsorption of both Cr^{6+}, RB and MB dye by HTB was investigated separately with varying initial concentrations of these ions *viz*., 0, 0.5, 1.0, 5.0, 10 and 20 mg/l by keeping Cr^{6+}, RB and MB dye concentration constant (200 mg/l). The effect of other ions on percentage adsorption of Cr^{6+}, RB and MB dye sorption on HTB is shown in the Figures 5.6a, 5.6b and 5.6c, respectively. Results clearly depicts that the percentage adsorption of Cr^{6+} decreased when other cations were simultaneously present in the metal solution. Figure 5.6a shows that the Cr^{6+} adsorption is about 73% in the absence of other ions. However, the sorption capacity of Cr^{6+} decreased with increase in the concentration of other ions such as NH_4^+ and Ca^{2+}. At a concentration of 20 g/l of both NH_4^+ and Ca^{2+}, the removal of Cr^{6+} was about 55%. Figure 5.6b and 5.6c depicts that the addition of Ca^{2+} did not change the RB and MB dye sorption capacity of HTB. Nevertheless, the presence of low concentrations of both Na^+ and NH_4^+ slightly improved the RB and MB dye adsorption capacity onto HTB. These effects might be due to the ionic charge, ionic radii and chemical potential of each ion (Al-Ghouti *et al.,* 2010).

5.3.5 Effect of Binary System

A study to assess the change in metal and dye sorption capacity of HTB was conducted at various favourable pH conditions when these two were mixed together. An equal mixed binary concentration of 150 mg/l of metal and 150 mg/l of dye (each dye mixer separately) solution was used in this study. More than this proportion makes the precipitation of metal-dye complex. It was observed from Figure 5.7a and 5.7b that the adsorption of Cr^{6+} decreased from 94 to 37% and 87% to 6 % when pH of the binary solution ([150 mg/l of Cr^{6+} + 150 mg/l of RB dye] and [150 mg/l Cr^{6+} + 150 mg/l of MB dye]) increased from 2.0 to 3.5 (optimum pH) and 2.0 to 7 (optimum pH), respectively. Whereas the percentage of RB and MB dye adsorption increased from 30% to 71% (Figure 5.7a) and 37% to 100% (Figure 5.7b). Correspondingly, the unit adsorption capacity of Cr^{6+} decreased and MB dye increased when binary

solution pH increased from acid to basic pH. But the unit adsorption capacity of RB dye on HTB at pH 2.0, 2.5, 3.0 and 3.5 increased and thereafter at pH 3.76 decreased from 44.86, 71.85, 80.78 and 106.29 and 85.46 mg/g, respectively. The reasons are discussed already in the section 5.3.3. However, the overall sorption capacity of the adsorbent increased in binary system than that of single solution system.

5.3.6 Isotherm Studies

To optimize the design of an adsorption system for the adsorption of adsorbents, it is important to establish the most appropriate correlation for the equilibrium curves. Four isotherm equations namely Langmuir, Freundlich Temkin and Halsey isotherm models have been used to describe the equilibrium characteristics of Cr^{6+}, RB and MB dye adsorption onto HTB. Theoretical and mathematical relationships of each isotherm model are presented in Appendix 3. The plots of Langmuir (C_e/q_e versus C_e), Freundlich ($log\ C_e$ versus $log\ q_e$), Temkin ($ln\ C_e$ versus q_e) and Halsey ($ln\ C_e$ versus $ln\ q_e$) at different temperatures are shown in Figures 5.8a to 5.8c, Figures 5.9a to 5.9c, Figures 5.10a to 5.10c and Figures 5.11a to 5.11c, respectively for Cr^{6+}, RB and MB dye adsorption onto HTB. It can be observed from this figure that the data were fitted well by straight lines in all cases. The various isotherm model constants and regression coefficients obtained for Cr^{6+}, RB and MB dye at different temperatures are presented in Table 5.2. It can be observed from these figures based on regression coefficients (R^2) that the Langmuir data were well fitted by straight lines compared to all other three studied models. The Langmuir separation factor (R_L) indicates the isotherm shape and whether the adsorption is favourable or not. If $R_L = 0$, adsorption is irreversible; $0 < R_L < 1$, adsorption is favourable; $R_L = 1$ adsorption is linear and $R_L > 1$ adsorption is unfavourable. The R_L factor for different initial concentrations of Cr^{6+}, RB and MB dye adsorption onto HTB obtained in this work was in the range of $0 < R_L < 1$ and presented in Table 5.3. These values were in very good agreement with the reported values in the literature (Hameed and El-Khaiary, 2008). The monolayer adsorption capacity of Cr^{6+}, RB and MB dye on other adsorbents which are reported in the recent studies are presented in Appendix 4. Compare to these reported adsorbents HTB adsorbent shows the higher adsorption capacity even at higher range of concentration of Cr^{6+}, RB and MB dye.

5.3.7 Sorption Kinetics

In order to investigate the adsorption kinetics of Cr^{6+}, RB and MB dye onto HTB, two models such as pseudo-first order and pseudo-second-order models were used in this study. Theoretical and mathematical relationships of each kinetic model are presented in Appendix 5. The plots of *log* $(q_e - q_t)$ versus t and (t/q_t) versus t were used to determine the pseudo-first order and pseudo-second-order rate constants of K_{ad} and k', respectively for Cr^{6+} (Figures 5.12a and 5.12b) and RB dye (Figures 5.13a and 5.13b). The kinetic model that best fits the experimental data with high R^2 value (Table 5.4) for two models was the pseudo-second order model. Moreover, its calculated *qe* values were closely fitted with the experimental data. Thus, the pseudo-second-order kinetics was predominant, and that the overall rate of metal as well as dye adsorption process was largely controlled by the chemisorption process.

5.3.8 Sorption Thermodynamics

Thermodynamic parameters such as change in free energy ($\Delta G°$), enthalpy ($\Delta H°$) and entropy ($\Delta S°$) associated to the sorption process were obtained using the free energy and Van't Hoff equations that are presented in equations A5.1 and A5.2 of Appendix 5. The values of $\Delta H°$ and $\Delta S°$ were calculated from the slope and intercept of Van't Hoff plot between *ln* K_d versus *1/T* (Figure 5.14a, 5.14b and 5.14c) and are listed in Table 5.5a and 5.5b. $\Delta G°$ and distribution coefficient (K_d) are also presented in the Table 5.5a and 5.5b. The negative values of $\Delta G°$ increased with increase in temperatures. This indicates the spontaneous nature of the Cr^{6+}, RB and MB dye adsorption process. The positive $\Delta H°$ values of metals and dyes confirmed that the adsorption process was endothermic. The positive value of $\Delta S°$ showed the increased randomness at the solid-solution interface during adsorption.

5.3.9 Adsorption Mechanisms

The change in pH of the solution results in the formation of different ionic species and different adsorbent surface charge (Klika *et al*. 2004). Thus, it is necessary to identify the mechanism of Cr^{6+}, RB and MB dye uptake by the HTB adsorbent.

5.3.9.1 Adsorption Mechanism of Cr^{6+}

Two possible mechanisms such as direct and indirect reduction of Cr^{6+} to Cr^{3+} can be suggested for Cr^{6+} removal onto HTB. In first mechanism, Cr^{6+} is directly reduced to

Cr^{3+} by HTB surface electron-donor groups of the adsorbent and the reduced Cr^{3+} forms complexes with adsorbent or remains in the solution. But Cr^{3+} is not adsorbed by adsorbent at pH 2.0. But in second mechanism, the adsorption-coupled reduction of Cr^{6+} to Cr^{3+} occurred on the adsorbent site itself (Figure 5.15a). It consists of three steps; (i) the binding of anionic ($HCrO_4^-$) Cr^{6+} to the positively-charged groups present on the surface of the adsorbent, (ii) the reduction of adsorbed Cr^{6+} to Cr^{3+} takes place by adjacent electron-donor (CO and O–CH_3) groups of adsorbed sites and (iii) a part of surface reduced Cr^{3+} is released (Figure 5.15a) into the aqueous solution due to the electronic repulsion between the positively-charged groups of adsorbent and the surface bound Cr^{3+}. Similar behaviour was observed by Suksabye *et al.* (2007) and Sawalha *et al.* (2007).

To analyze the oxidation state of adsorbed chromium on the surface of HTB X-ray photoelectron spectroscopy (XPS) analysis was carried out for HTB after Cr^{6+} adsorption at 2Cr2p core region (Figure 5.16). The results of the spectra clearly depicts that the predominant peaks at 577.15 ($Cr2p_{3/2}$) and 586.65 ($Cr2p_{1/2}$) eV was corresponding to the Cr^{3+} oxidation state. This reveals that the bounded chromium on the HTB surface was mostly in trivalent form. Hence, at pH 2.0, the reduced Cr^{6+} is in Cr^{3+} form and it cannot be absorbed by adsorbent (Li *et al.,* 2008; Uysal *et al.,* 2007). When reaction pH increased further from 2.0 the Cr^{6+} adsorption coupled reduction was less, hence the Cr^{3+} fraction in the solution decreased steadily. Similar behaviour was observed by Dakiky *et al.* (2002) for both Cr^{6+} and Cr^{3+} removal using other adsorbents.

5.3.9.2 Adsorption Mechanism of RB and MB Dye

The possible mechanism of RB dye on HTB can be explained as follows: as pH decreased below 3.5, the excess H^+ ions neutralize (protonation) the HTB surface bearing $–OH^-$ groups and then it turns to $–OH_2^+$ site (Anandkumar and Mandal 2009; Chuah *et al.,* 2005). The positive charged surface sites (Figure 5.15a) of the sorbent do not favour for cationic dye sorption due to its electrostatic repulsion. At pH 3.5, both surface adsorption and pore diffusion dominates (Figure 5.15b) due to existence of monomeric form of RB molecules. Hence, maximum sorption capacity was observed at pH 3.5. Similar behaviour was observed at pH 3.45 by Guo *et al.* (2005) and Gad and El-Sayed (2009). When pH increased above 3.5, the zwitterionic form of

RB in water (Figures 5.15c and 5.15d) might increase the aggregation of RB dye to form larger molecules (dimer) and thus unable to enter into the pores. The greater aggregation of zwitterions (neutral) is due to the electrostatic interactions between the carboxyl and xanthene groups (Figure 5.15d). The aggregations of RB in water have been reported by Arbeloa and Ruizojeda (1982) and Mchedlov-Petrosyan (2004). Hence, at alkaline pH surface sorption only dominates the adsorption process. With increase in temperature the rate of diffusion of the Cr^{6+} and RB molecules across the external boundary layer as well as in the interior pores of HTB increases due to the decrease in the viscosity of the Cr^{6+} or RB solution. This impact might be also due to the enlargement of the pore size or the appearance of new adsorption active sites on the adsorbent surface because of the bond rupture (Figure 5.15d) while increasing the solution temperature (Couglin and Ezra, 1968).

At neutral and alkaline pH, MB dye molecules have positive net charge but HTB surface carrying net negative due to oxygen and hydroxyl groups. This opposite charge difference between dye molecules and HTB surface makes adsorption through strong electrostatic interaction. Therefore, at alkaline pH surface diffusion dominates the higher MB dye adsorption on HTB.

5.4 SUMMARY

This work presents some important phenomena associated with Cr^{6+}, rhodamine B and methylene blue adsorption using tannery residual biomass prepared by HCl activation methods. The adsorption was found to be strongly dependent on pH, initial adsorbate concentration and solution temperature. The maximum sorption capacity of Cr^{6+}, RB and MB dye was obtained at pH 2.0, 3.5 and 7.0, respectively. The presence of Ca^{2+}, Na^{+}, K^{+} and NH_4^{+} ions had no significant effect on RB and MB dye removal and but slightly affects the Cr^{6+} removal. The equilibrium data were best fitted by Langmuir isotherms than Freundlich, Temkin and Halsey isotherms. Halsey linear regression data showed heteroporosity (*i.e.*, macropore and micropore) of the HTB. The equilibrium sorption capacity of Cr^{6+}, RB and MB dye increased with increase in temperature from 30ºC to 50ºC. This indicates the adsorption process was endothermic. Pseudo-second-order kinetics was found to be the predominant mechanisms for both metal and dye adsorption onto HTB. The thermodynamic parameters associated with the adsorption process were also evaluated. The negative

value of $\Delta G°$ confirmed the spontaneous nature of both metal and dye sorption onto the HTB. The positive $\Delta H°$ values confirmed that the adsorption process was endothermic. The above result indicates that HTB could be employed as an efficient adsorbent for the removal of Cr^{6+}, RB and MB from the aqueous solution including industrial wastewater.

Chapter 5
Figures & Tables

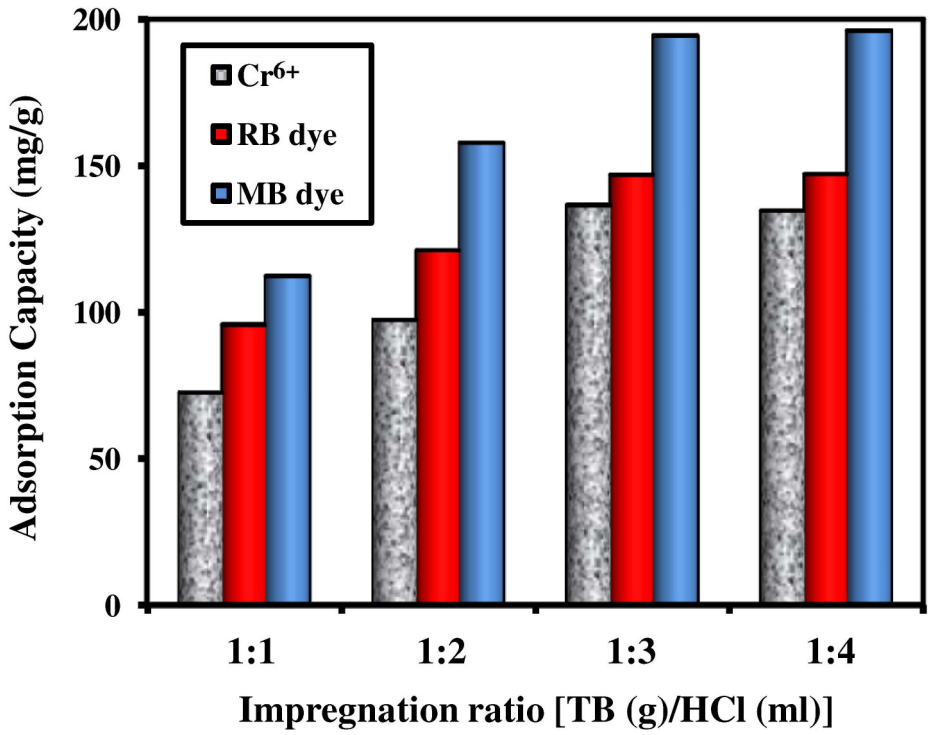

Figure 5.1 Effect of impregnation ratio on adsorption capacity of Cr^{6+}, RB and MB dye onto HTB (C_o = 200 mg/l; W = 0.05 g; V = 50 ml; t = 1440 min and T = 30°C)

(a)

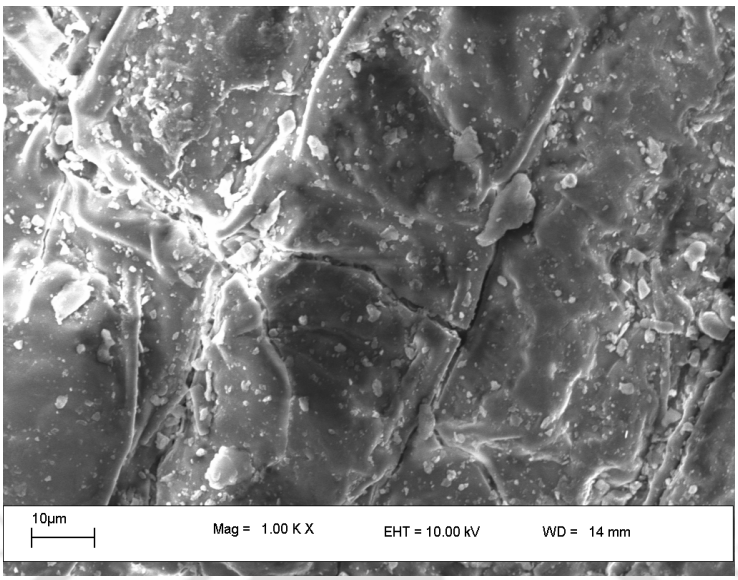

Figure 5.2a SEM picture of raw TB

(b)

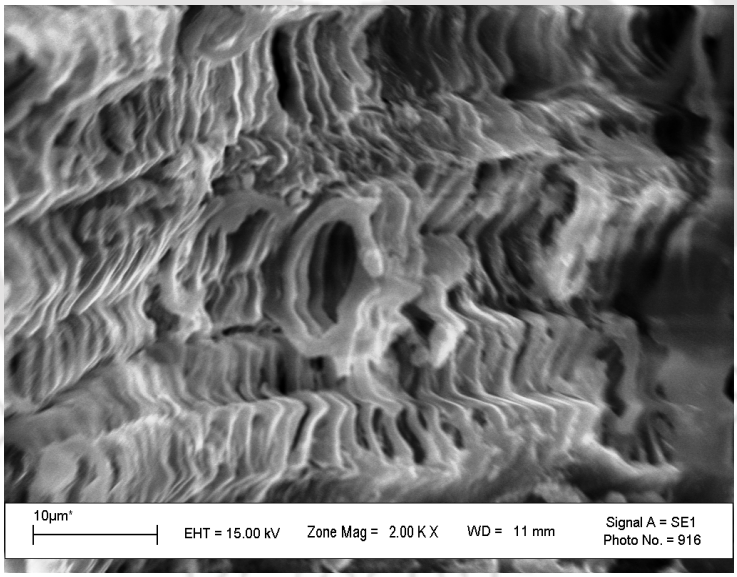

Figure 5.2b SEM picture of 1:3 (w/v) HCl treated TB

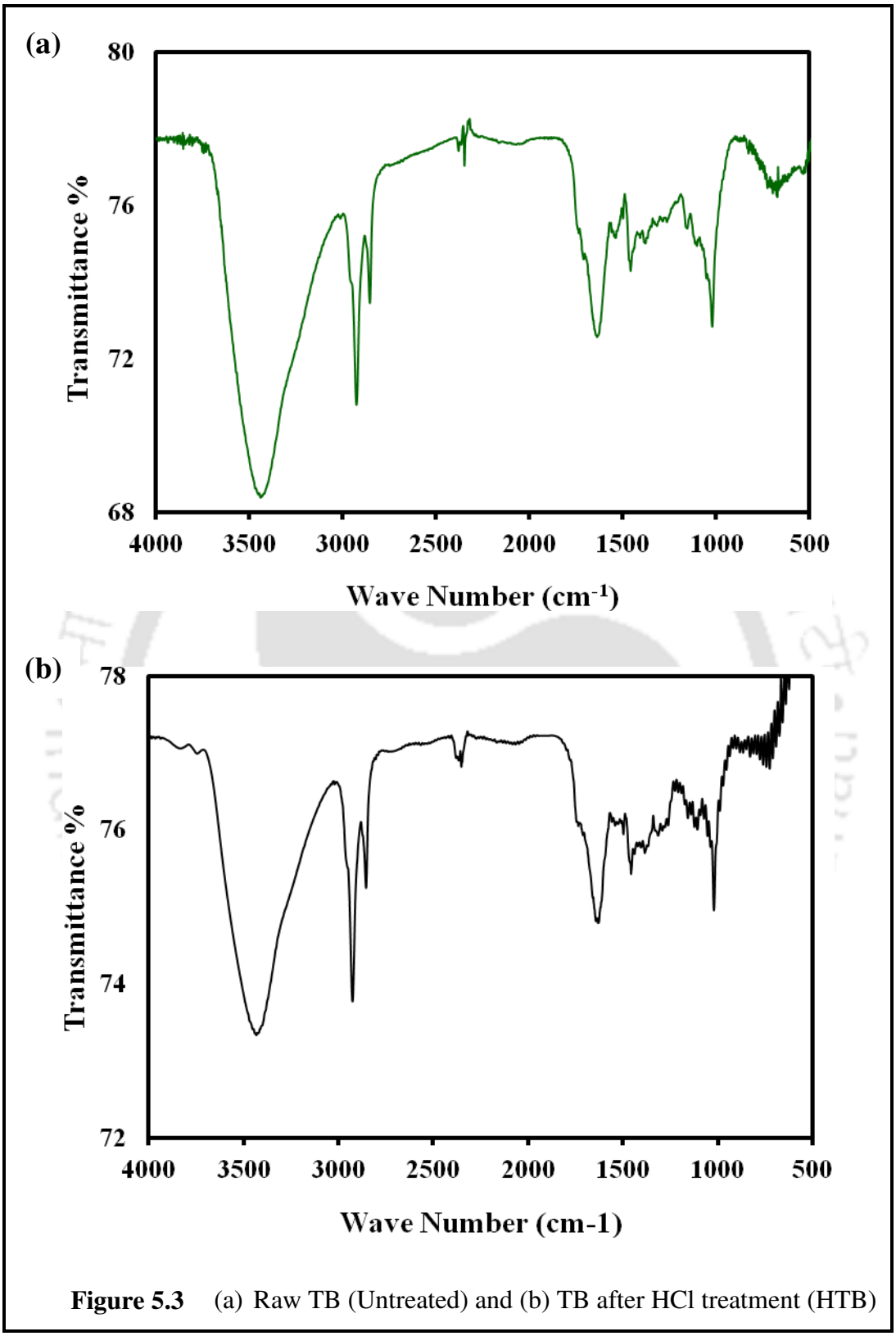

Figure 5.3 (a) Raw TB (Untreated) and (b) TB after HCl treatment (HTB)

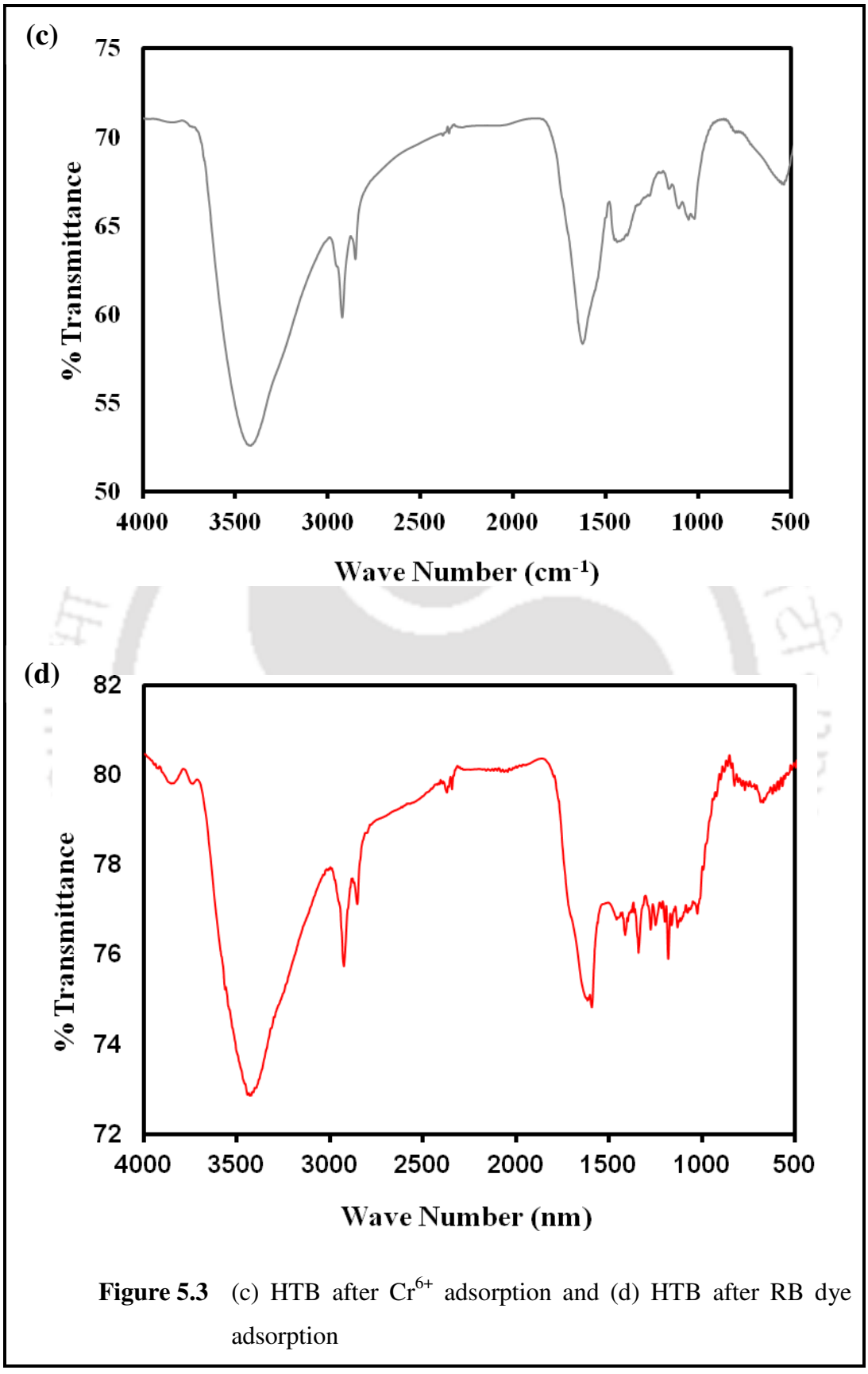

Figure 5.3 (c) HTB after Cr^{6+} adsorption and (d) HTB after RB dye adsorption

(a)

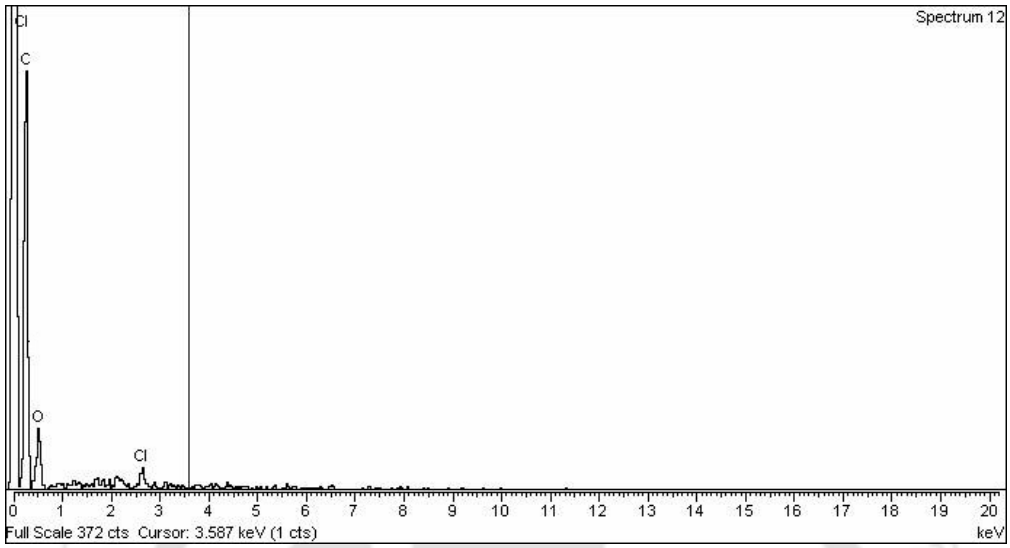

(b)

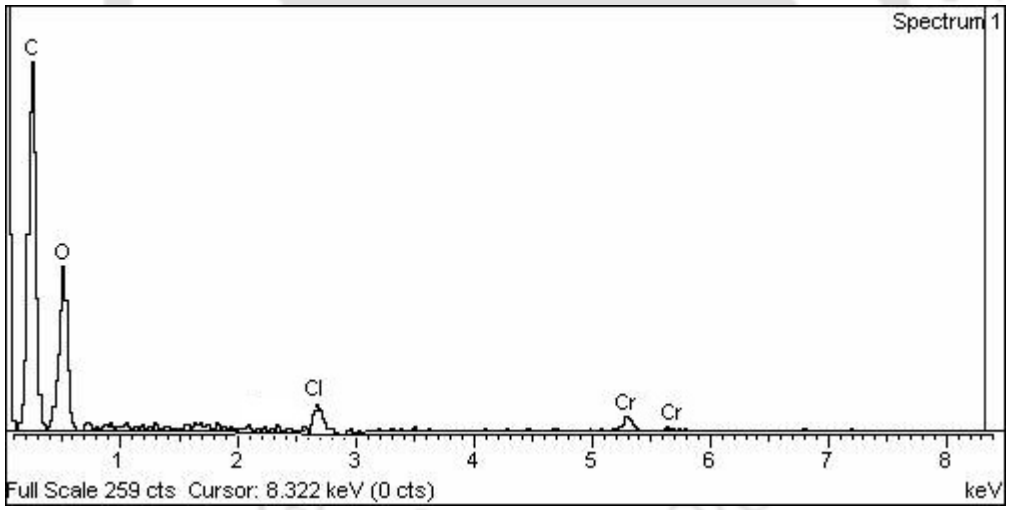

Figure 5.4 EDX spectra of HTB (a) before adsorption and (b) after Cr^{6+} adsorption

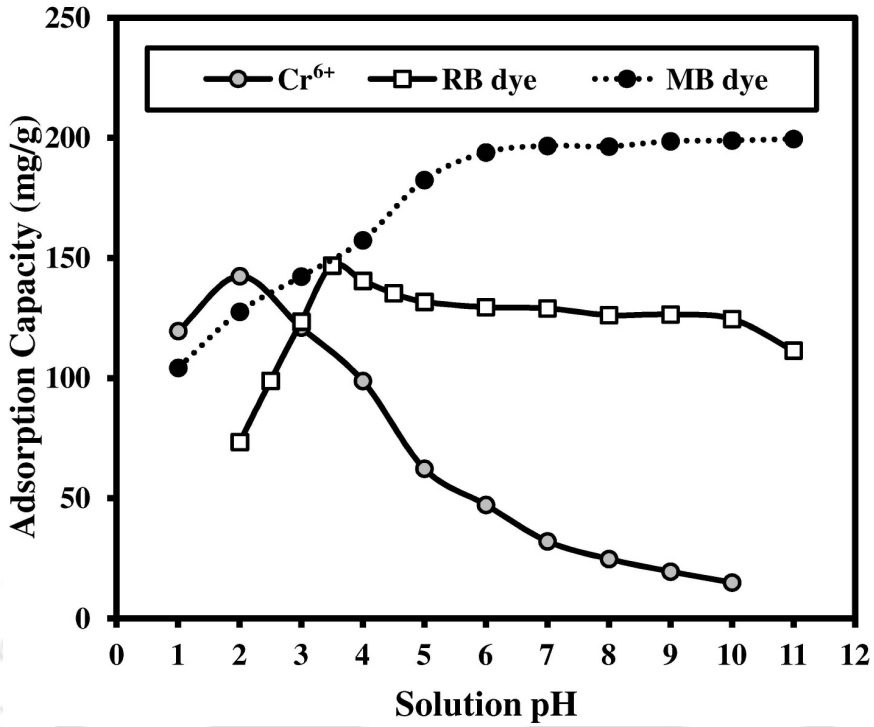

Figure 5.5 Effect of pH on sorption capacity of HTB: (C_o = 200 mg/l, W = 0.05 g, v = 50 ml, t = 1440 min and T = 30ºC)

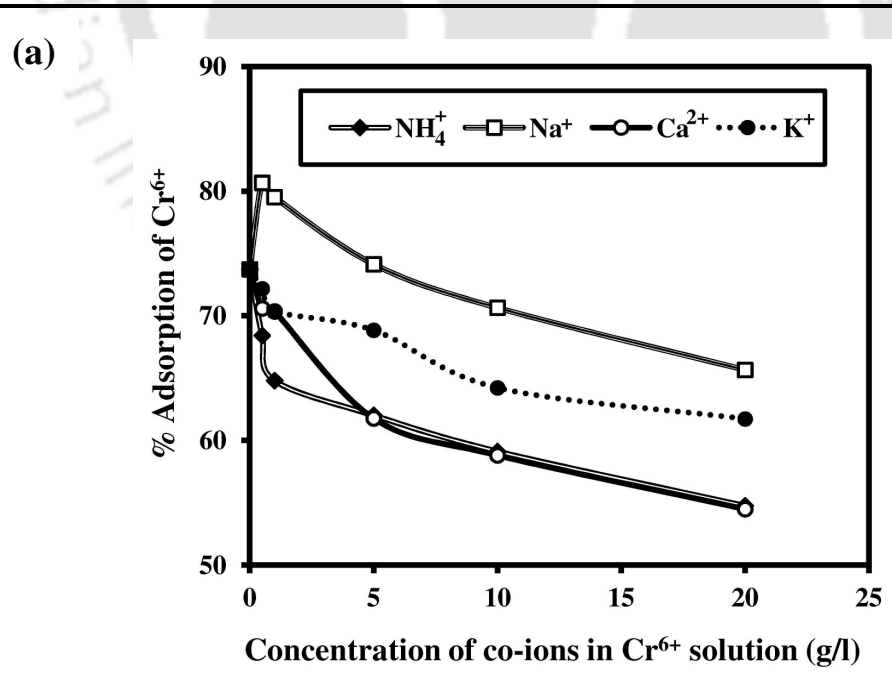

Figure 5.6 Effect of other co-ions on sorption of (a) Cr^{6+} onto HTB: (C_o = 200 mg/l; pH = 2.0; W = 0.05 g, V = 50 ml, t = 1440 min and T = 30ºC)

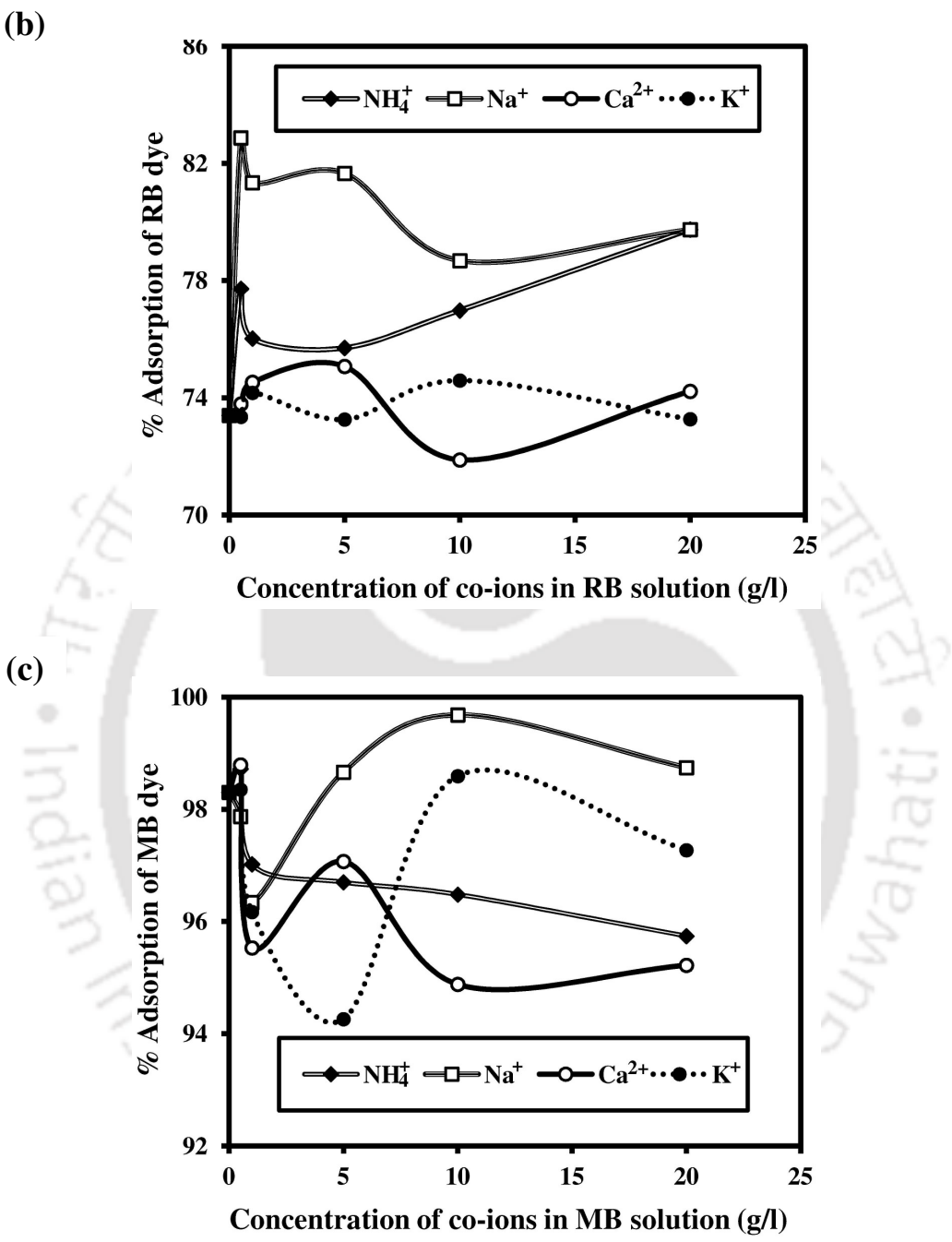

Figure 5.6 Effect of other co-ions on sorption of (b) RB and (c) MB dye onto HTB: (C_o = 200 mg/l; pH = 3.5 (RB) and 6.4 (MB); W = 0.05 g, V = 50 ml, t = 1440 min and T = 30ºC)

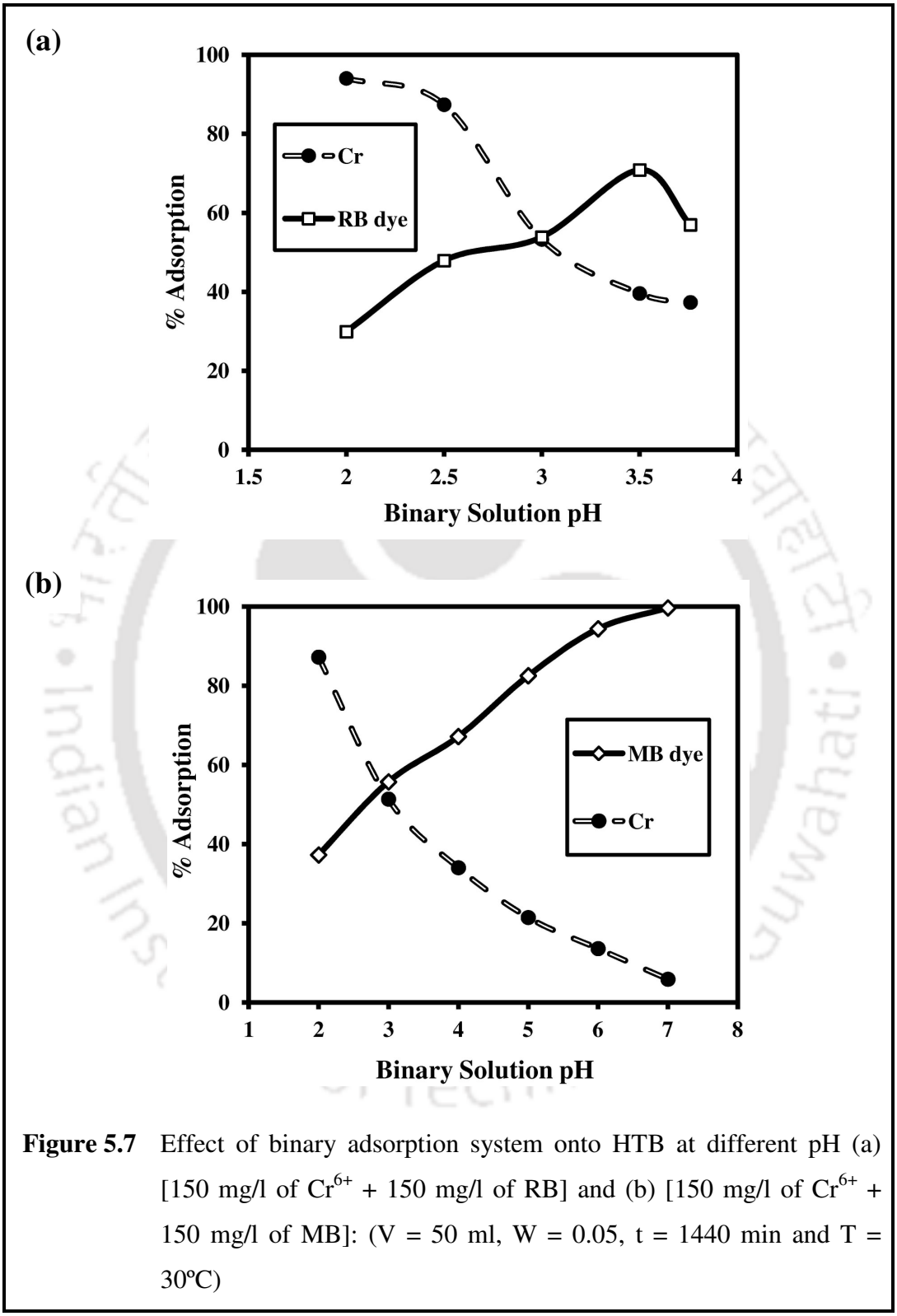

Figure 5.7 Effect of binary adsorption system onto HTB at different pH (a) [150 mg/l of Cr^{6+} + 150 mg/l of RB] and (b) [150 mg/l of Cr^{6+} + 150 mg/l of MB]: (V = 50 ml, W = 0.05, t = 1440 min and T = 30ºC)

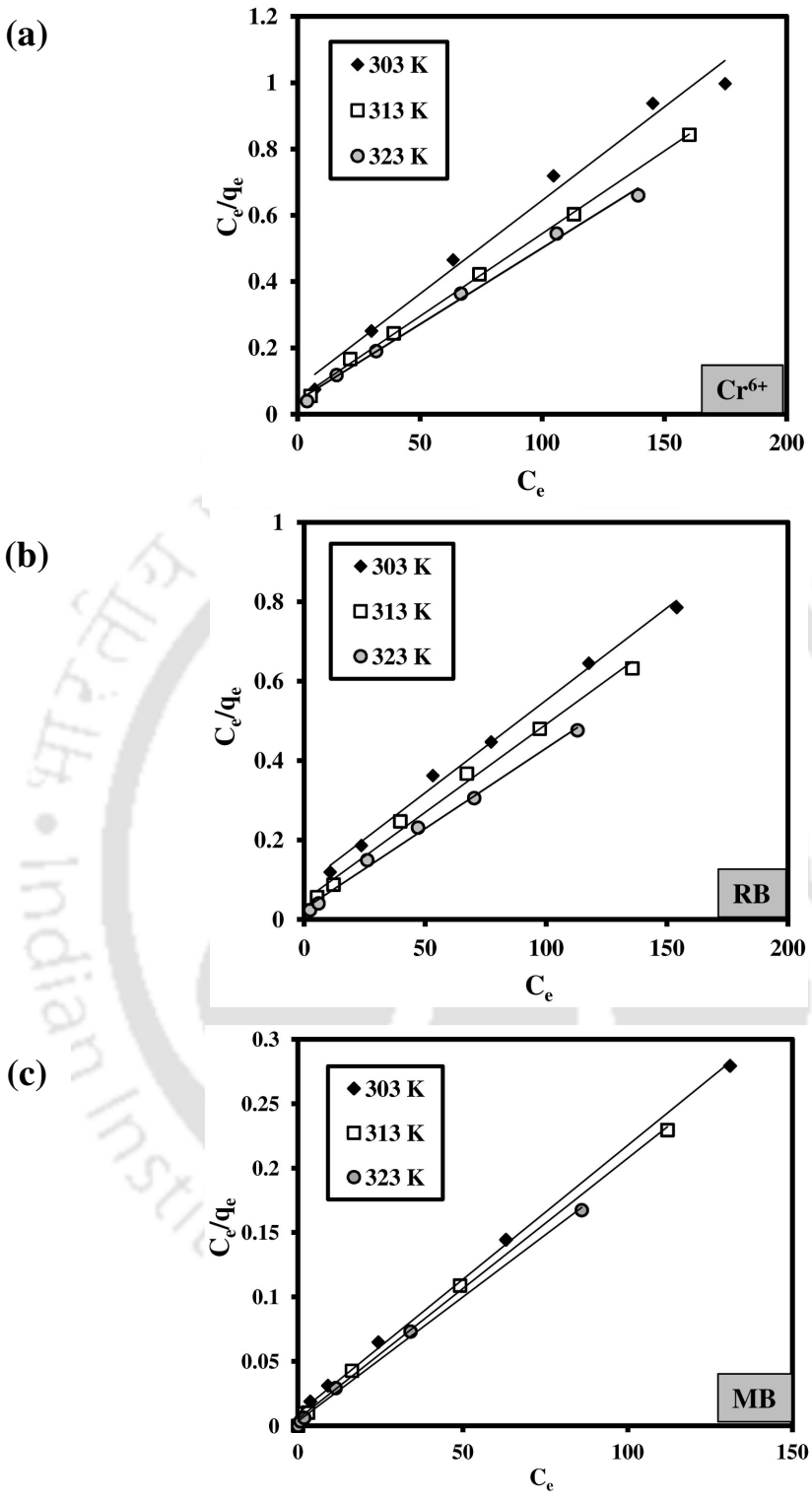

Figure 5.8 Langmuir isotherm plots for (a) Cr^{6+} (b) RB and (c) MB dye adsorption onto HTB at various temperature: (C_o = 200 mg/l each; pH = 2.0 (Cr^{6+}), 3.5 (RB) and 6.4 (MB); W = 0.05 g; V = 50 ml, t = 1440 min; and T = 30ºC)

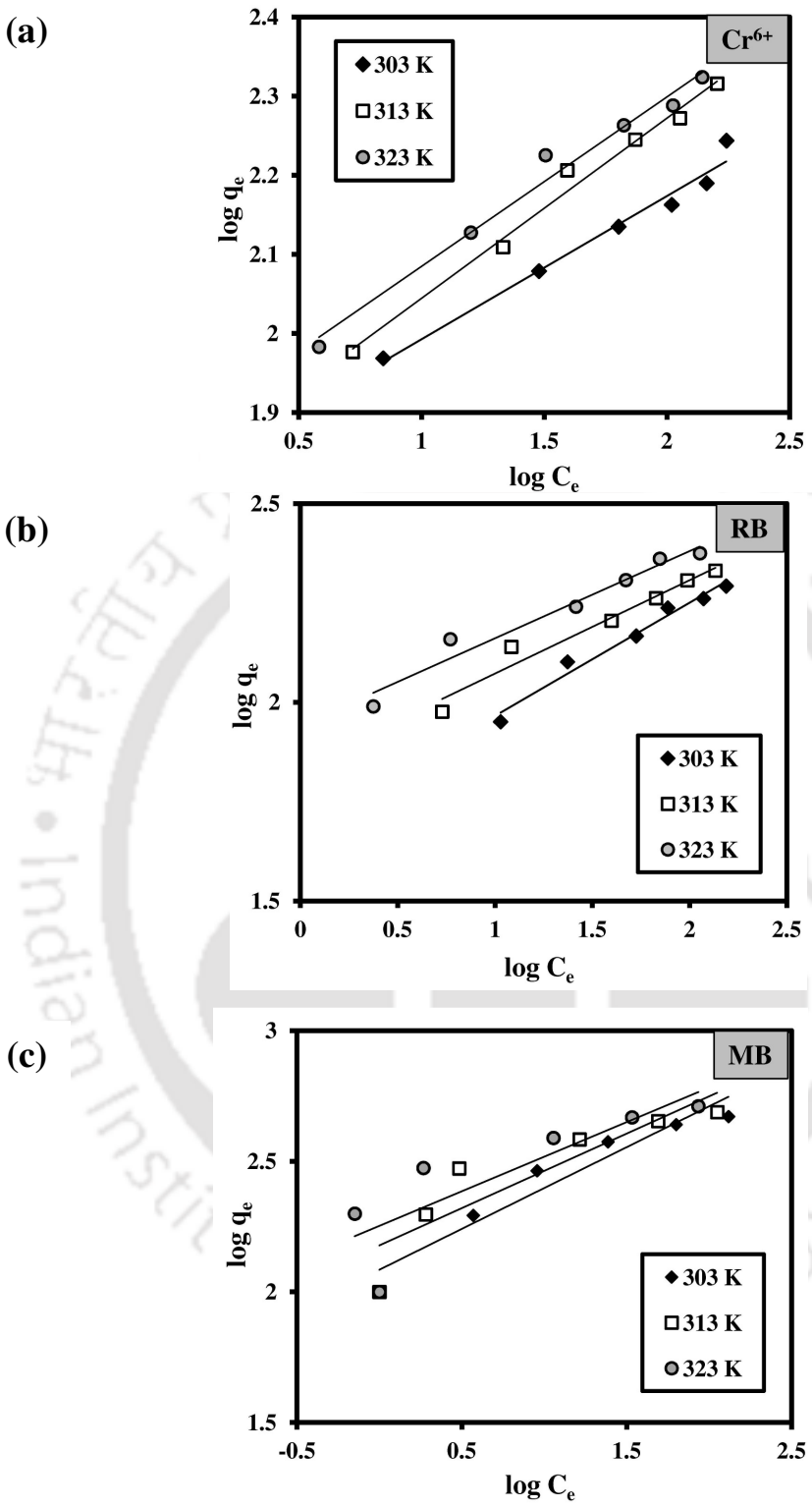

Figure 5.9 Freundlich isotherm plots for (a) Cr^{6+} (b) RB and (c) MB dye adsorption onto HTB at various temperature: (C_o = 200 mg/l each; pH = 2.0 (Cr^{6+}), 3.5 (RB) and 6.4 (MB); W = 0.05 g; V = 50 ml, t = 1440 min; and T = 30ºC)

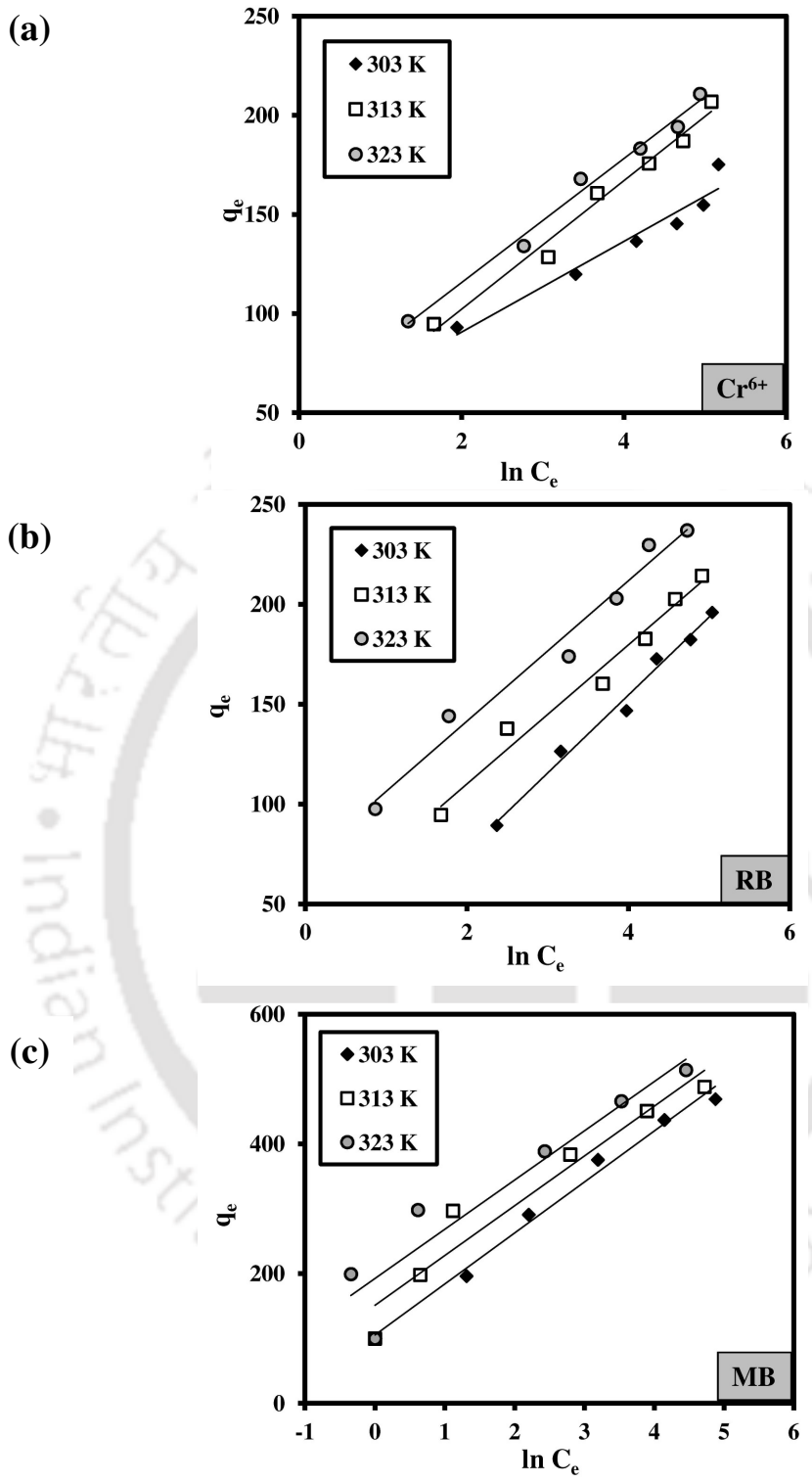

Figure 5.10 Temkin isotherm plots for (a) Cr^{6+} (b) RB and (c) MB dye adsorption onto HTB at various temperature: (C_o = 200 mg/l each; pH = 2.0 (Cr^{6+}), 3.5 (RB) and 6.4 (MB); W = 0.05 g; V = 50 ml, t = 1440 min; and T = 30ºC)

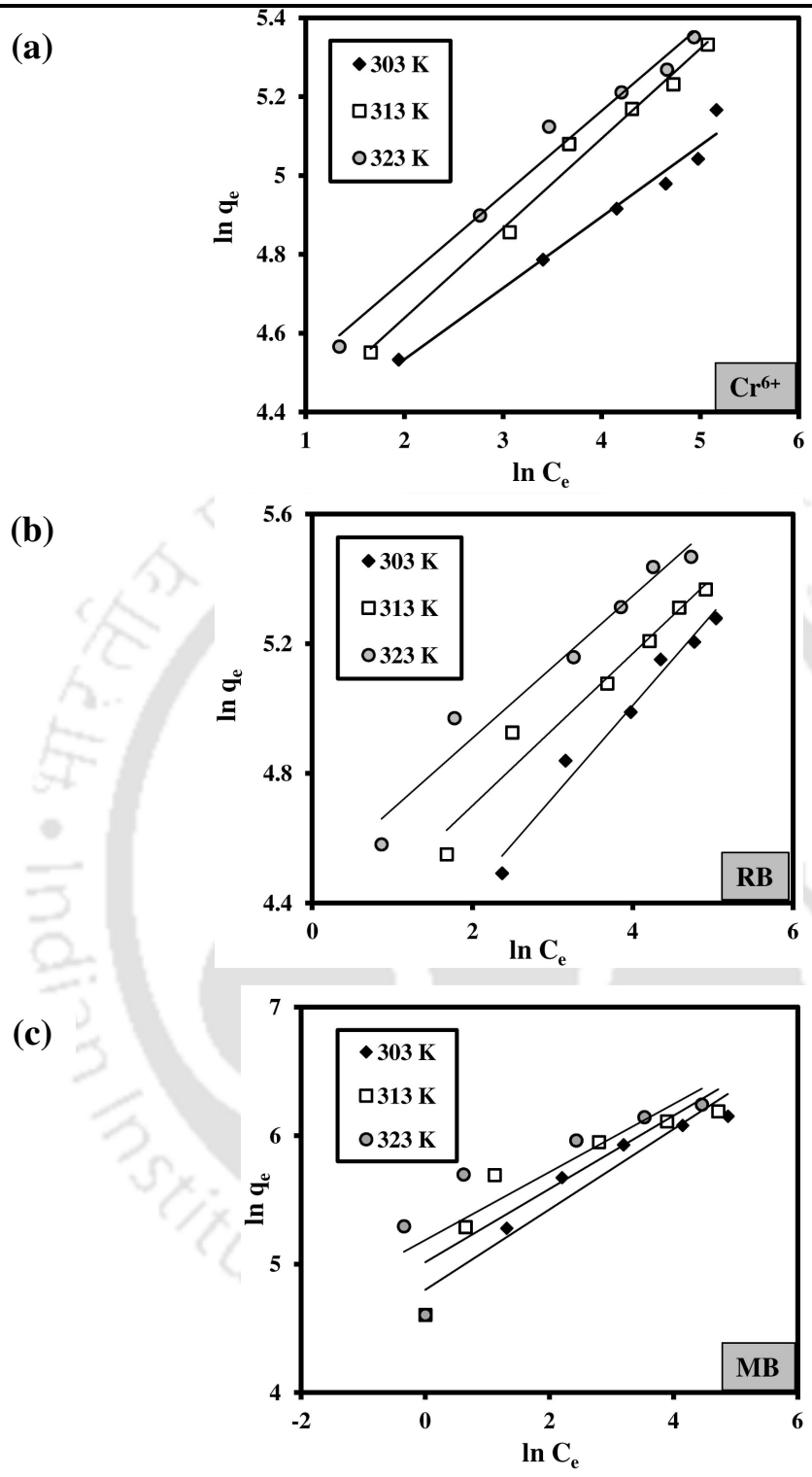

Figure 5.11 Halsey isotherm plots for (a) Cr^{6+} (b) RB and (c) MB dye adsorption onto HTB at various temperature: (C_o = 200 mg/l each; pH = 2.0 (Cr^{6+}), 3.5 (RB) and 6.4 (MB); W = 0.05 g; V = 50 ml, t = 1440 min; and T = 30ºC)

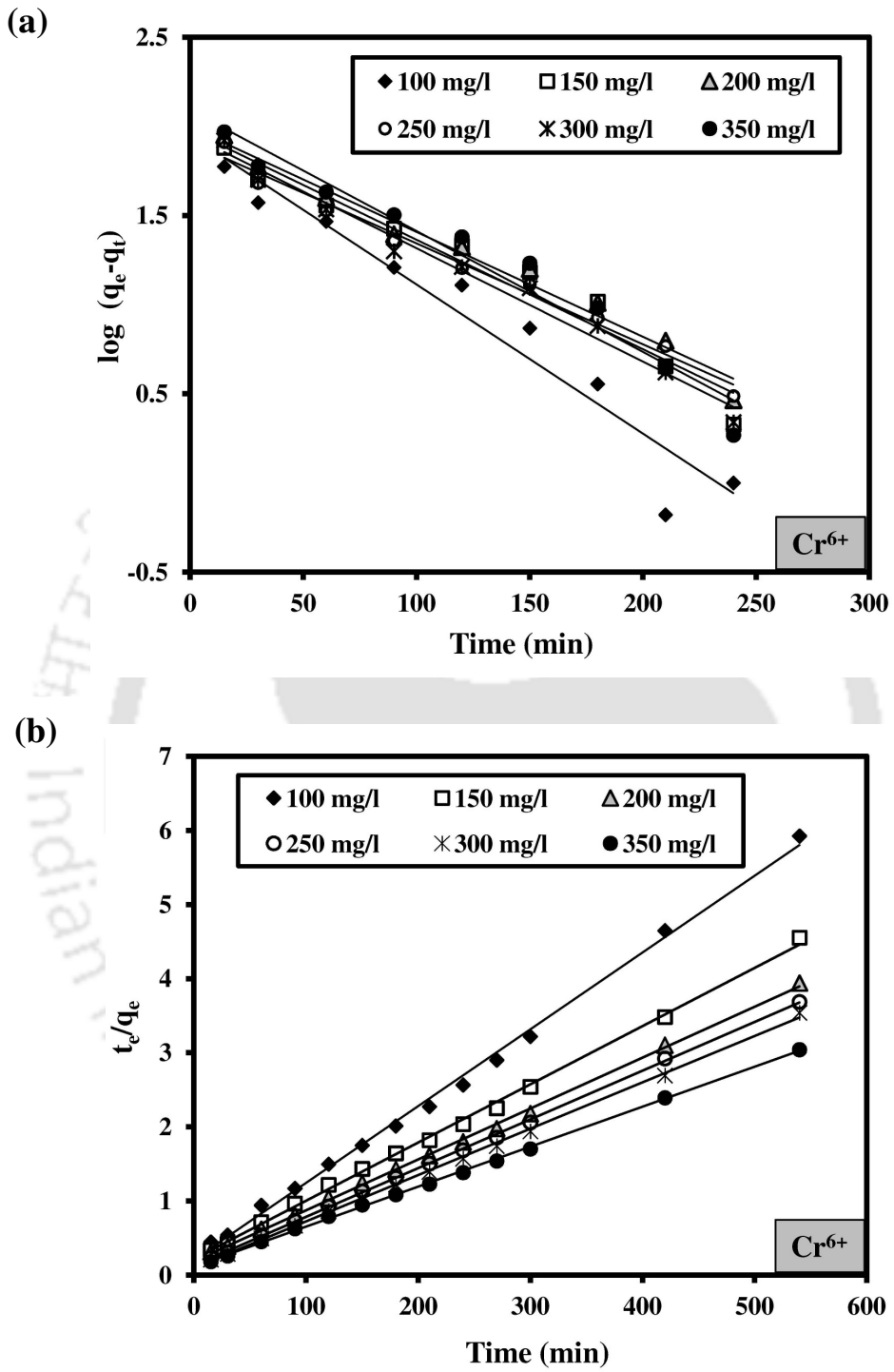

Figure 5.12 Kinetic plots of Cr^{6+} adsorption onto HTB (a) Pseudo-first-order model and (b) Pseudo-second-order model at 30°C

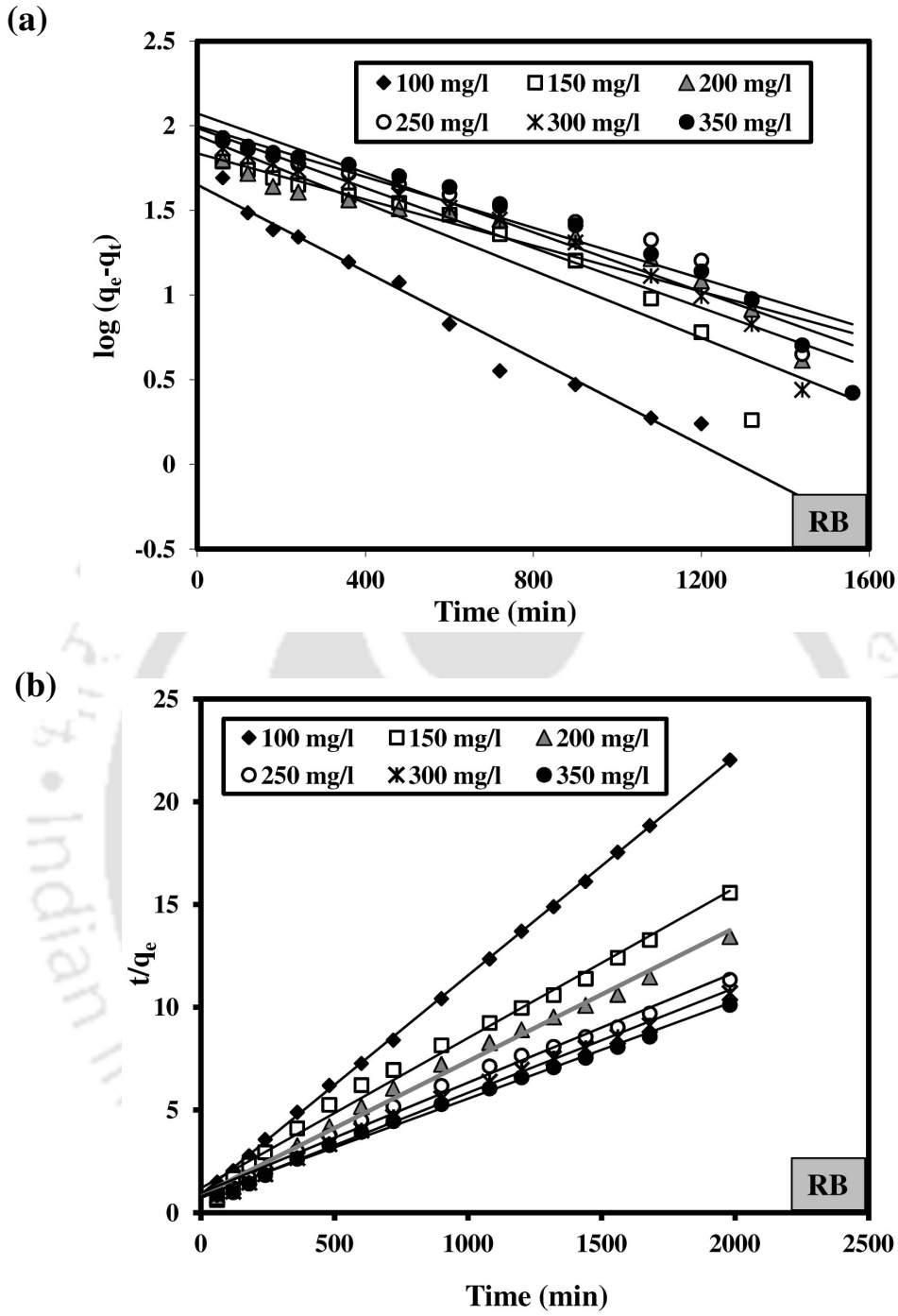

Figure 5.13 Kinetic plots of RB dye adsorption onto HTB (a) Pseudo-first-order model and (b) Pseudo-second-order model at 30°C

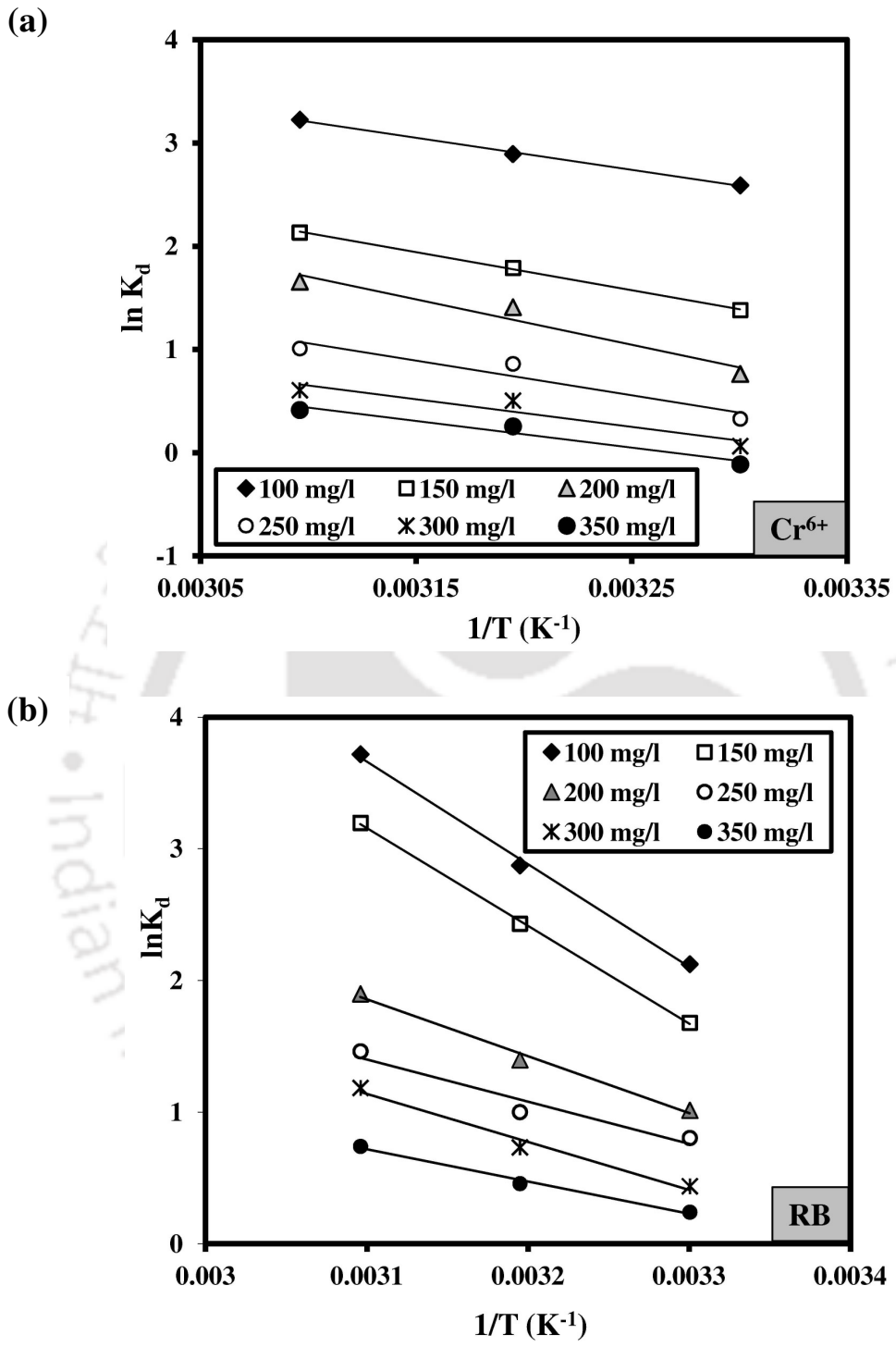

Figure 5.14 Van't Hoff equation plot for (a) Cr^{6+} and (b) RB dye adsorption at various concentrations.

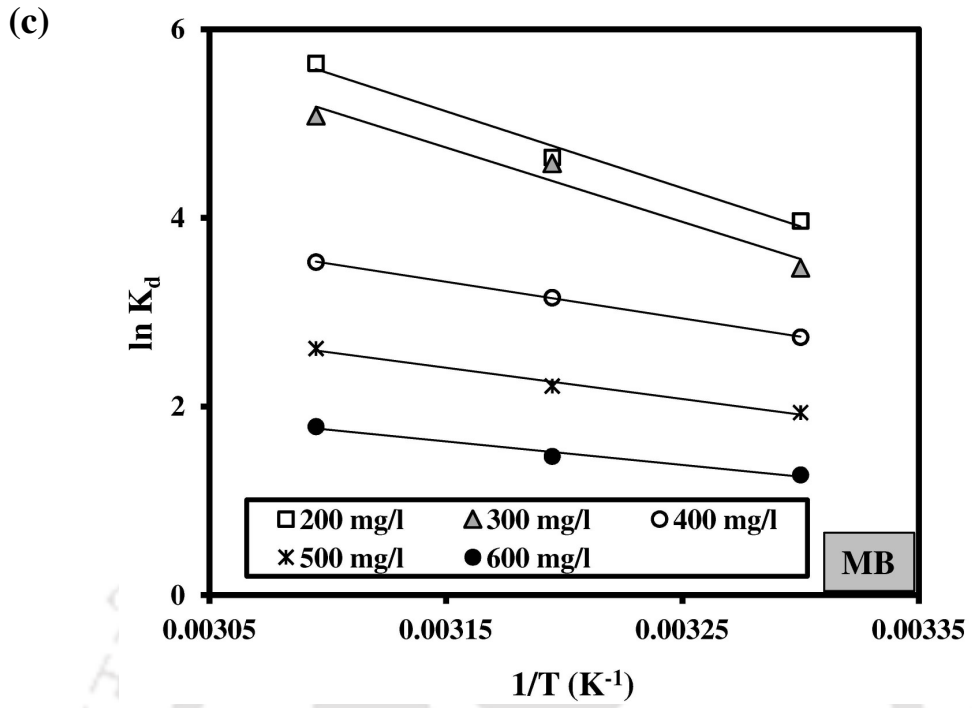

Figure 5.14 Van't Hoff equation plot for (c) MB dye adsorption at various concentrations.

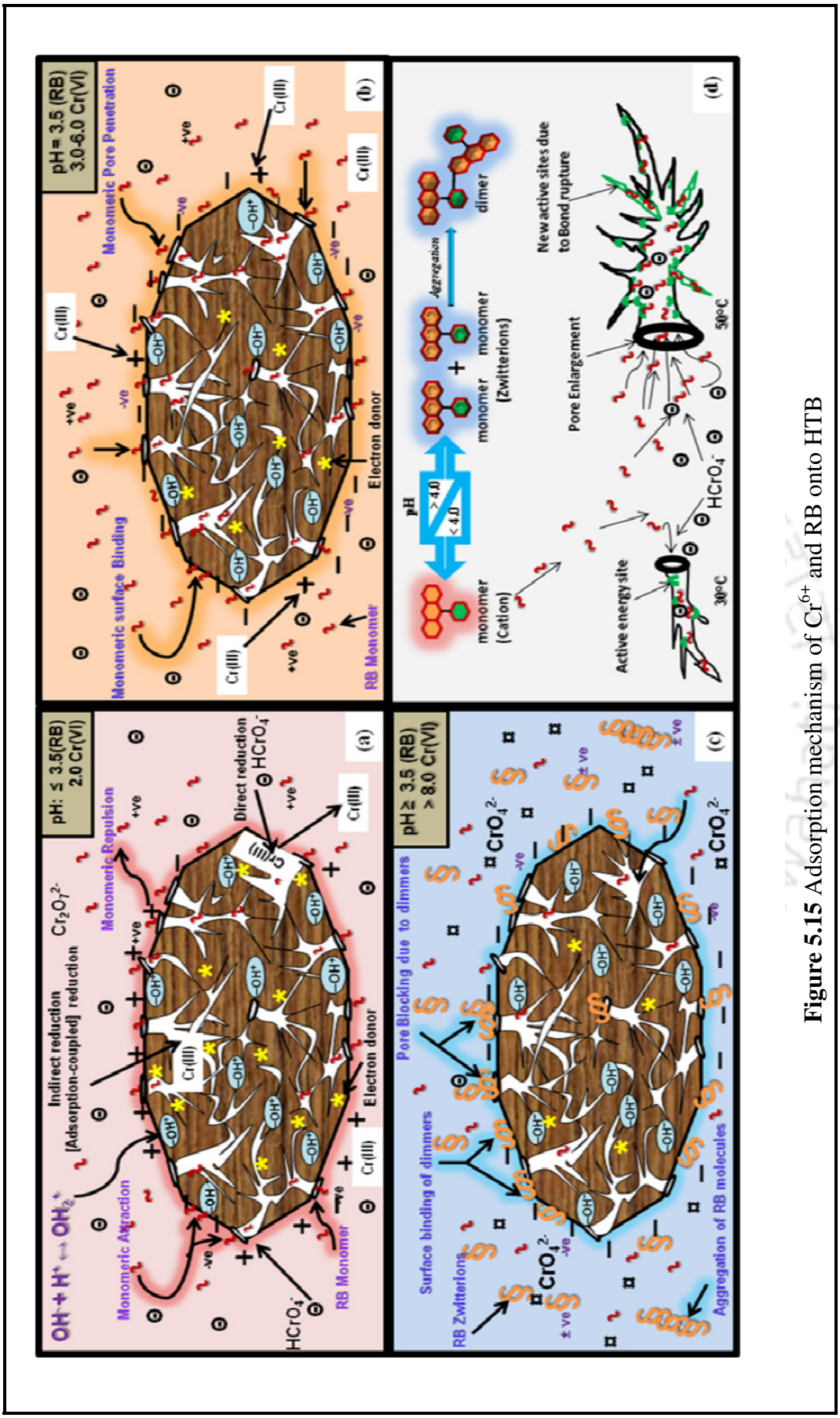

Figure 5.15 Adsorption mechanism of Cr^{6+} and RB onto HTB

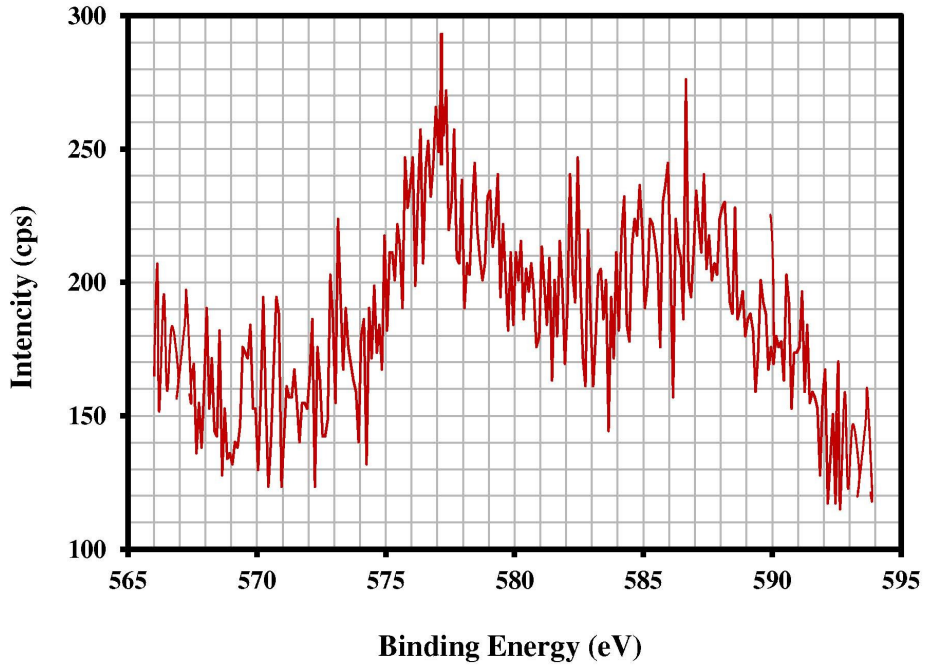

Figure 5.16 XPS spectra of HTB at Crp2 orbital core region

Table 5.1 Physical properties of HTB

Surface properties	HCl Treated TB (HTB)			
	Impregnation ratio [TB weight (g)/HCl volume (ml)]			
	1:1	1:2	1:3	1:4
BET surface area (m^2/g)	3.844	5.868	10.422	9.977
BET mono layer volume (cc/g)	0.8831	1.3481	2.3945	2.2922
Total pore volume (ml/g)	0.0289	0.0343	0.0508	0.0448
Langmuir surface area (m^2/g)	2.705	4.855	8.350	9.237
Langmuir monolayer volume (cc/g)	0.6215	1.1154	1.9184	2.1222

Table 5.2 Adsorption isotherm constants for adsorption of Cr^{6+}, RB and MB dye in single contaminant system onto HTB

Solution Temperature		Langmuir constants			Freundlich constants			Temkin constants			Halsey constants		
		Q_o (mg/g)	b (l/mg)	R^2	K_f (mg/g)	1/n	R^2	A (l/g)	B	R^2	K_h	-1/n	R^2
30°C	Cr^{6+}	177.3	0.0698	0.9918	66.85	0.1807	0.9881	7.066	22.89	0.9709	9.436×10^{-11}	0.1807	0.9881
	RB	212.8	0.0548	0.9952	48.01	0.2844	0.9746	1.037	38.98	0.9878	1.23×10^{-6}	0.2844	0.9872
	MB	480.8	0.2167	0.9974	121.5	0.3127	0.9285	3.821	78.62	0.9891	2.156×10^{-7}	0.3127	0.9285
40°C	Cr^{6+}	200.4	0.1090	0.9994	65.60	0.2275	0.9935	3.163	32.43	0.9917	1.034×10^{-8}	0.2275	0.9935
	RB	227.3	0.0911	0.9932	68.79	0.2347	0.9601	3.201	34.80	0.9767	1.48×10^{-8}	0.2345	0.9799
	MB	495.1	0.3811	0.9982	150.5	0.2852	0.8053	7.169	76.74	0.9363	2.318×10^{-8}	0.2852	0.8053
50°C	Cr^{6+}	217.4	0.1126	0.9977	74.25	0.2141	0.9907	5.477	31.25	0.9940	1.829×10^{-9}	0.2141	0.9907
	RB	250	0.1504	0.9943	87.44	0.2191	0.9613	7.580	35.15	0.9748	1.38×10^{-9}	0.2191	0.9805
	MB	518.1	0.5514	0.9977	178.8	0.2648	0.7216	12.67	75.84	0.8930	4.540×10^{-5}	0.2648	0.7216

Table 5.3a Langmuir separation factor (R_L) for Cr^{6+} and RB dye adsorption onto HTB at different temperatures

Initial concentration (mg/l)		R_L value		
		30 ºC	40 ºC	50 ºC
100	Cr^{6+}	0.1254	0.0840	0.0816
	RB	0.1544	0.0989	0.0624
150	Cr^{6+}	0.0872	0.0576	0.0559
	RB	0.1085	0.0682	0.0425
200	Cr^{6+}	0.0669	0.0439	0.0425
	RB	0.0836	0.0520	0.0322
250	Cr^{6+}	0.0542	0.0354	0.0343
	RB	0.0681	0.0421	0.0259
300	Cr^{6+}	0.0456	0.0297	0.0288
	RB	0.0574	0.0353	0.0217
350	Cr^{6+}	0.0394	0.0255	0.0247
	RB	0.0496	0.0304	0.0186

Table 5.3b Langmuir separation factor (R_L) for MB dye adsorption onto HTB at different temperatures

Initial concentration of MB dye (mg/l)	R_L value		
	30 ºC	40 ºC	50 ºC
100	0.0441	0.0256	0.0178
200	0.0226	0.0129	0.0089
300	0.0151	0.0087	0.0060
400	0.0114	0.0065	0.0045
500	0.0091	0.0052	0.0036
600	0.0076	0.0044	0.0030

Table 5.4 Kinetic constants for Cr^{6+} and RB adsorption onto HTB

Initial adsorbate concentration (mg/l)		Pseudo-first-order model				Pseudo-second-order model		
		$q_{e,exp}$ (mg/g)	k_{ad} (l/min)	$q_{e,cal}$ (mg/g)	R^2	k′ (g/mg/min) (1×10^{-4})	$q_{e,cal}$ (mg/g)	R^2
100	**Cr^{6+}**	93.03	0.0193	88.70	0.9390	5.16	96.15	0.9968
	RB	89.32	0.0030	49.78	0.9743	1.25	93.34	0.9998
150	**Cr^{6+}**	119.9	0.0141	94.93	0.9552	2.87	126.6	0.9981
	RB	126.4	0.0023	87.34	0.8983	0.449	137	0.9912
200	**Cr^{6+}**	136.5	0.0136	98.86	0.9773	2.53	144.9	0.9988
	RB	146.8	0.0016	68.64	0.9166	0.486	153.9	0.9926
250	**Cr^{6+}**	145.4	0.0131	80.91	0.9846	3.4	151.5	0.9995
	RB	172.7	0.0018	99.59	0.9229	0.303	185.2	0.9924
300	**Cr^{6+}**	154.8	0.0145	89.23	0.9818	3.8	161.3	0.9990
	RB	182.3	0.0021	96.81	0.9451	0.356	196.1	0.9967
350	**Cr^{6+}**	174.3	0.0157	122.8	0.9577	2.5	185.2	0.9993
	RB	196	0.0021	118.2	0.9360	0.277	212.8	0.9956

Table 5.5a Thermodynamic parameters for adsorption of Cr^{6+} and RB onto HTB

Initial RB concentration (mg/l)		$\Delta H°$ *(J/mol)*	$\Delta S°$ *(J/mol K)*	$-\Delta G°$ *(J/mol)*		
				30 °C	**40 °C**	**50 °C**
100	**Cr^{6+}**	25831	106.7	6526	7530	8476
	RB	64823	231.4	5350	7479	9770
150	**Cr^{6+}**	30615	112.6	3480	4660	5606
	RB	61741	217.6	4230	6327	8401
200	**Cr^{6+}**	36524	127.4	1925	3671	4356
	RB	35908	126.8	2557	3636	4990
250	**Cr^{6+}**	27872	95.21	829.7	2243	2655
	RB	26654	94.27	2027	2606	3843
300	**Cr^{6+}**	22205	74.25	162.1	1314	1594
	RB	30305	103.4	1103	1909	3113
350	**Cr^{6+}**	16806	55.60	6.998	667.1	1090
	RB	20308	68.92	607.5	1193	1947

Table 5.5b Thermodynamic parameters for adsorption of MB onto HTB

Concentration of MB dye	ΔS^o (J/mol K)	ΔH^o (J/mol)	$-\Delta G^o$ (J/mol)		
			30°C	40°C	50°C
200	255.6	67596	9998	12080	14814
300	246	65560	8742	11914	13352
400	129.4	32302	6890	8208	9278.
500	106.7	27521	4875	5770	6870
600	78.84	20733	3212	3829	4696

CHAPTER 6

ADSORPTION OF SELECTED CONTAMINANTS ON THERMOCHEMICALLY ACTIVATED TANNERY RESIDUAL BIOMASS

This chapter presents the adsorption studies of Cr^{6+}, o-cresol and rhodamine B using H_3PO_4 treated followed by thermal activated tannery residual biomass (TBAC). From the preliminary performance evaluation test, it has been found that Cr^{6+}, rhodamine B, methylene blue, o-cresol and phenol had high binding capacity with TBAC. However, in this chapter adsorption results of Cr^{6+}, o-cresol and rhodamine B dye only presented and discussed in detail for its possible usage in tanneries to solve its wastewater treatment problem through the recycling process of its own waste as a useful source.

6.1 INTRODUCTION

In the current scenario, tannery industry is one of the major places of generation of many liquid and solid based pollutants. It produces large amount of colored effluent and considerable amount of phenolic components such as phenols and cresols along with toxic metals (Liu *et al.,* 2010). The release of such effluents without proper treatment in ecosystem results the aesthetical and toxicological problems. Hexavalent chromium (Cr^{6+}), *o*-cresol and rhodamine B (RB) dye are widely used in many industries especially in tanneries. In this chapter, results of batch adsorption experiments which were carried out in single and binary contaminant systems of (Cr^{6+}), *o*-cresol and rhodamine B (RB) dye using high surface area TBAC are presented and discussed in detail. The significant parameters that influence the adsorption process such as solution pH, temperature, presence of other co-ions and effect of binary and ternary contaminant systems were monitored in this study to optimize the sorption process.

6.2 EXPERIMENTAL METHODS

6.2.1 Preparation of Synthetic Solution

A stock solution of Cr^{6+}, *o*-cresol and rhodamine B (RB) dye (1000 mg/l) was prepared by dissolving appropriate quantity of $K_2Cr_2O_7$, *o*-cresol (Merck, India) and RB dye (C.I. 45170, LOBA Chemie, India) in Millipore water, respectively. The stock solution was mixed thoroughly for 10 min at 180 rpm to obtain complete dissolution and then suitably diluted with water to get the required initial concentrations (50 to 300 mg/l of Cr^{6+} and 100 to 600 mg/l of *o*-cresol, and RB dye). The pH of the solution was adjusted using 0.1 N HCl or 0.1N NaOH before mixing the adsorbent. The pH of the solution was measured by pH meter (Eutech, model: 510).

6.2.2 Experimental Protocol

In order to study the nature of interaction of TBAC with Cr^{6+}, *o*-cresol and RB dye, initially the effect of pH on adsorption capacity was carried out under batch mode experiment. Then further experiments on the effect of other co-ions and solution temperature were conducted in single contaminant system using fixed doses (0.05 g per 50 ml) of TBAC at 180 rpm in an incubating shaker (LabTech, Model LSI-1005R) at optimum pH. The pH of each Cr^{6+}, *o*-cresol and RB dye solution was

adjusted using 1N HCl (or) 1N NaOH before mixing the adsorbent. After the adsorption of Cr^{6+}, *o*-cresol and RB dye, desorption experiments were carried out to check the regeneration possibilities of the TBAC using four desorption agents such as 0.1 M HNO_3, HCl, CH_3COOH and 0.01 M EDTA solutions at particular conditions.

Samples at predefined time intervals were withdrawn and the supernatant of Cr^{6+} solution was separated by filtration using Whatman filter paper no. 42. Final residual metal concentrations were directly measured by flame atomic absorption spectrophotometer (AAS) (Varian spectra, AA240) with an air–acetylene flame. Similarly, the supernatant of RB dye solutions were separated by centrifuging (5000 rpm) and the filtrate of dyes were analyzed for the residual dye concentrations using UV–visible spectrophotometer (Perkin-Elmer, model: Lambdas 45) at the maximum wavelength (λ_{max} = 555 nm) of the dyes. The final residual concentration of *o*-cresol was analyzed by HPLC (ProSTAR, Varian) equipped with a UV-vis detector and C18 column (particle size: 5 µm, length 15 cm, diameter 4.6 mm) at room temperature with a mobile phase of acetonitrile (80%): water (20%) at a flow rate of 0.8 ml/min. An aliquot of 20 µl of the sample was injected and analyzed using a UV-vis detector at a wavelength of 280 nm. Three replicates per sample were done and the average results are taken for calculation.

The methods of calculation of adsorption and desorption details are given in the Appendix 2.

6.2.3 Adsorbent Characterization

The surface texture and porosity of two different prospects of TB such as raw precursor and surface structure of H_3PO_4 treated followed by thermal activated TB was observed using Scanning electron microscopy (SEM) (Leo, 1430 vp, Carl Zeiss, German) characterisation. The morphological properties of TBAC were measured in Beckman-Coulter Surface area analyser (SA^{TM} 3100) using nitrogen adsorption/desorption isotherms at −196^{o}C. The samples were degassed using Helium at 200^{o}C for 2 h before measurement. The surface area was calculated using a multipoint Brunauer-Emmett-Teller (BET) model. To resolve the functional groups of TBAC, spectra analysis was recorded on a KBr translucent sample disk, which

contains 5% sample by weight, using a Fourier transform infrared spectrometer (FT-IR) (Perkin Elmer, PE-RXI) in the range of 500–4000 cm^{-1}.

6.3 RESULTS AND DISCUSSION

6.3.1 Characterization of Adsorbent

6.3.1.1 SEM Analysis

The SEM image of TB before and after activation is shown in Figures 6.1a and 6.1b. It can be seen from the Figure 6.1a that before to the activation (raw TB), TB had regular smooth surface in absence of pores, whereas Figure 6.1b (i.e. TB after activation) reveals the significant changes and well-developed pores on the surface of TB. The porous structure of TBAC is mainly attributed to the reaction of H_3PO_4 with TB cell wall functional groups at higher heat treatment.

6.3.1.2 BET Surface Area Analysis

The morphological properties such as surface area and pore volume of TBAC were measured using the BET surface area analyzer based on the nitrogen adsorption/desorption isotherms and pore size distribution of the TBAC. From the analysis, it was found that total BET surface area, mono layer volume and total pore volume of TBAC is 892 m^2/g, 204.58 ml/g and 0.4483 ml/g, respectively.

6.3.1.3 Fourier Transform Infrared (FT-IR) Analysis

The presence of functional groups depends on the treatment procedure of the sample. The FT-IR spectra of H_3PO_4 treated followed by thermal activated TB is shown in Figure 6.2 in wave length range of 500 to 4000 cm^{-1}. The band frequencies of TBAC at 3451, 2924, 2365, 1614, 1125 and 1015 cm^{-1} are the stretching vibrations of the hydroxyl (-OH) groups, symmetric vibrations of C–H predominantly aliphatic acids, amino groups ($–NH_2^+$ and $–NH^+$), COO and C=C groups, C–O stretch and stretching vibrations of C–O–C and $–OCH_3$ (indicative of lignin structure), respectively. The other bending vibrations less than 888 cm-1 are the fingerprint zone that indicates the presence of phosphate functional groups (Mohan and Sreelakshimi, 2008). It has been suggested that the oxidative treatment of TB adsorbent with H_3PO_4 would introduce more acidic C=O groups on the surface of adsorbent. This would enhance the electrostatic interaction between adsorbent surface groups and $HCrO_4^-$.

6.3.2 Effect of pH

Solution pH is one of the key factors that might control an adsorption process, since it influences the electrostatic interactions between the adsorbent and the adsorbate. Figure 6.3a shows the effect of initial pH on the adsorption capacity of Cr^{6+} using TBAC. It is clear front hr figure that the adsorption decreases with increase in pH from 2.0 to 10. The maximum removal occurred at pH 2.0 (60.98 mg/g). The higher removal of metal at acidic pH is attributed to the large amount of H^+ ions present in the solution. These excess H^+ ions first neutralize the hydroxyl and other negative functional groups and then it turns to the positively charged ($–OH_2^+$) functional groups through rapid protonation. This net positive sites enhanced the negative $HCrO_4^-$ ion adsorption (Uysal and Ar, 2007; Dakiky *et al.*, 2002).

$$OH_2^+ + HCrO_4^- \leftrightarrow OH_2^+(HCrO_4^-) \quad (6.1)$$

At alkaline pH, adsorbent surface carrying net negative charge due to the large availability of OH^- ions in the solution that repulse the negative chromate ion adsorption.

The adsorption of *o*-cresol was studied over a pH range between 2 and 10 by adding adequate amounts of 0.1 N NaOH or 0.1 N HCl diluted solutions to the initial unbuffered solution containing the *o*-cresol compound (Figure 6.3b). The amount adsorbed was found to be increased gradually from pH 2.0 to 6.0 (87.2 to 119.6 mg/g) and thereafter it gradually went down as the solution became more basic. This could be due to the increased solubility of cresol molecules at alkaline conditions, which results in greater affinity for the *o*-cresol molecules to remain in solution rather than to get adsorbed onto the carbon surface. The results confirm that *o*-cresol is preferentially adsorbed from its neutral form.

The adsorption capacity of RB dye as a function of pH was investigated over a pH range of 1 to 10 (Figure 6.3c). It is clear from the figure that adsorption of RB dye increases with increase in pH from 1 to 3.5 and thereafter slightly decreases. The maximum removal of RB dye at pH 3.5 was due to its monomeric form. This monomeric form of RB dye was enhanced by both pore diffusion and surface adsorption of TBAC. At alkaline pH the zwitter ionic form of dye structure enhanced

the formation of dimer and trimmers of RB and thus unable to enter inside the pores of the TBAC. Therefore, at alkaline pH surface diffusion only makes the dye binding with adsorbent surface. Therefore, all further experiments of Cr^{6+}, *o*-cresol and RB were conducted at optimum pH of 2.0, blank pH and 3.5, respectively.

6.3.3 Effect of Other Co-ions in Test Solution

The effect of various co-ions such as K^+, Na^+, NH_4^+ and Ca^{2+} on the adsorption capacity of Cr^{6+}, *o*-cresol and RB dye onto TBAC was studied. The initial concentration of co-ions in the test solution was varied (0.1, 0.5 1, 2 and 5 g/l) by keeping Cr^{6+} (100 mg/l), *o*-cresol (200 mg/l) and RB dye (200 mg/l) concentration constant in single component system. The presence of NH_4^+ and Ca^{2+} ions in the Cr^{6+} solution significantly reduces the adsorption capacity of Cr^{6+} at higher concentrations (1-5 g/l), but no major alteration in the adsorption capacity of Cr^{6+} was found when K^+, and Na^+ ions were simultaneously present in the Cr^{6+} solution. The adsorption capacity of RB dye was not affected by these co-ions. Whereas in *o*-cresol adsorption, NH_4^+ ions considerably enhanced the adsorption capacity of *o*-cresol on TBAC at their higher concentration and rest of the co-ions had no effect on *o*-cresol adsorption.

6.3.4 Adsorption Isotherm Studies

In order to analysis and optimize the design of adsorption process, the adsorption equilibrium experimental data for Cr^{6+}, *o*-cresol, RB dye adsorption onto the TBAC were analyzed using Langmuir, Freundlich, Temkin and Halsey isotherms. The theoretical details and mathematical equations of each isotherm model are given in the Appendix 3. The plots of (C_e/q_e versus C_e), ($log\ q_e$ versus $log\ C_e$), (q_e versus $ln\ C_e$) and ($ln\ q_e$ versus $ln\ C_e$) gives the equilibrium data fitting and the linear form of Langmuir (Figure 6.4a to 6.4c), Freundlich (Figure 6.5a-6.5c), Temkin (Figure 6.6a to 6.6c) and Halsey models (Figure 6.7a to 6.7c), respectively. The isotherm constants of Cr^{6+}, *o*-cresol and RB dye are given in (Tables 6.1a, 6.2a and 6.3a). Among the above four models, based on the linear correlation coefficients Langmuir model is fitted well than other three isotherm models. The sorption capacity of Cr^{6+}, *o*-cresol and RB dye onto TBAC is competitive in comparison with other recently reported adsorbents in the literature (refer Appendix 4). The separation factor (R_L) indicates the isotherm shape and whether the adsorption is favourable or not. If $R_L = 0$, adsorption is

irreversible; $0 < R_L < 1$, adsorption is favourable; $R_L = 1$ adsorption is linear and $R_L > 1$ adsorption is unfavourable. The R_L factor for various initial concentrations of Cr^{6+}, *o*-cresol and RB dye sorption on TBAC obtained in this work were in the range of $0 < R_L < 1$ and presented in Tables 6.1b, 6.2b and 6.3b.

6.3.5 Adsorption Kinetics

The sorption kinetics expressed by the correlation between the reaction time and adsorbate (Cr^{6+}, *o*-cresol and RB dye) uptake by TBAC for different initial Cr^{6+} (50-300 mg/l), *o*-cresol (100-600 mg/l) and RB dye (100-600 mg/l) concentrations are analyzed by pseudo-first order and pseudo-second-order kinetic models. The theoretical and mathematical details of each kinetic model are given in the Appendix 5. The plots of $log\ (q_e - q_t)$ versus t (Figures 6.8a, 6.9a and 6.10a) and (t/q_t) versus t (Figures 6.8b, 6.9b and 6.10b) for Cr^{6+}, *o*-cresol and RB dye adsorption were used to find out the rate constants of pseudo-first order and pseudo-second-order kinetic models. The results presented in Table 6.5 shows that pseudo second-order kinetics could describe the rate-controlling mechanism of Cr^{6+}, *o*-cresol and RB dye adsorption with extremely high correlation coefficients (R^2) (Reddad *et al.*, 2002). Nevertheless, R^2 value of pseudo first-order kinetics in Table 6.4 ranging of more than 0.94 for many cases is also acceptable to argue as a best fit, however this model fails to explain the adsorption saturation theoretically (experimental data fit) for all concentrations rather than pseudo second-order kinetics.

6.3.6 Adsorption Thermodynamics

The adsorption capacity of Cr^{6+}, *o*-cresol and RB dye onto TBAC was studied as a function of temperature ranging from 30ºC to 50ºC. It can be observed from the Tables 6.1a, 6.2a and 6.3a that the sorption capacity of Cr^{6+} and RB dye is increased with increase in temperature. However, for *o*-cresol adsorption, the adsorption capacity is decreased with increase in temperature. Thermodynamic parameters such as change in free energy ($\Delta G°$), enthalpy ($\Delta H°$) and entropy ($\Delta S°$) associated to the sorption process were obtained using the Van't Hoff equation. The theoretical details of adsorption thermodynamics are given in the Appendix 5. The values of $\Delta H°$ and $\Delta S°$ were calculated from the slope and intercept of Van't Hoff plot between $ln\ K_d$ versus $1/T$ (Figures 6.11a to 6.11c) and are listed in Table 6.5. The negative values of

ΔG^o increased with increase in temperatures indicate the spontaneous nature and the positive ΔH^o values confirmed that the Cr^{6+} and RB dye adsorption process was endothermic. The positive value of ΔS^o showed the increased randomness at the solid–solution interface during adsorption. However, the negative value of $\Delta H°$ of *o*-cresol indicates the exothermic nature of adsorption and the uptake of *o*-cresol is probably due to the physisorption effect.

6.3.7 Desorption Studies

After the equilibrium adsorption of 100, 200 and 200 mg/l of Cr^{6+}, *o*-cresol and RB dye per 0.05 g weight of TBAC, the metal, *o*-cresol and dye loaded carbons were separated and washed gently with little portions of distilled water to remove any unadsorbed species. The samples were then air-dried and agitated at 180 rpm with HCl (0.1 M), HNO_3 (0.1 M), CH_3COOH (0.1 M) and EDTA (0.01 M) solutions for a period of 5 hrs for Cr^{6+} and *o*-cresol, and 24 hr for RB dye. Afterwards the amounts of desorbed species were determined in the usual way which is given in the Appendix 2. Desorption results of different eluents are shown in Figure 6.12. The results show that desorption increases with increase in the acidity of the desorbing medium; desorption performance was higher for strong acids (HNO_3 and HCl) and low for weak acids (EDTA and CH_3COOH). HNO_3 gives the good desorption results than other acids for all three adsorbates.

6.3.8 Adsorption Mechanism

Adsorption mechanism of any adsorbent for a particular adsorbate is mainly depending upon the characteristics of both adsorbent as well adsorbate.

The most commonly reported mechanisms for metal ion sorption are ion exchange, electrostatic interaction, chelation, precipitation and complexation (Barrera *et al.*, 2006). However, for anions, electrostatic interaction plays an important role in allowing the approach of the ions to the adsorbent surface. To understand the Cr^{6+} mechanism, it is important to consider the speciation in the actual aqueous solution. As mentioned and discussed in the earlier chapters of this thesis, Cr^{6+} in aqueous media is in two anionic form such as $HCrO_4^-$ and $Cr_2O_7^{2-}$. At pH 2, the TBAC adsorbent surface is positively charged due to the protonation of excess H^+ ions in the solution, while the Cr^{6+}, metal ion, exists mostly as an anion leading to the

electrostatic attraction between adsorbent and adsorbate. The adsorbed Cr^{6+} on TBAC surface further involving in the adsorption-coupled reduction mechanism to create Cr^{3+} ions on the TBAC surface using the adjacent site electron donor groups of Cr^{6+} bounded site of TBAC surface (Anandkumar and Mandal, 2011). In TBAC, tannin content acted as electron donor and that reduces Cr^{6+} to Cr^{3+}. Similar, adsorption mechanism is reported elaborately in the chapter 5 for Cr^{6+} adsorption with HTB adsorbent.

The adsorption mechanisms of *o*-cresol and MB dye are similar to the mechanisms which are discussed in chapter 3 with BSAC adsorbent (see adsorption mechanisms in chapter 3).

6.4 SUMMARY

This chapter presents some important phenomena associated with Cr^{6+}, *o*-cresol and RB dye removal from aqueous solution using TBAC. The adsorption was found to be strongly dependent on pH and temperature of the solution. The FT-IR spectra revealed that the hydroxyl and amino cell wall functional group was the main binding site for Cr^{6+}. The adsorption capacity of *o*-cresol was enhanced by NH_4^+ ion when it was mixed with *o*-cresol. The adsorption behaviour of Cr^{6+}, *o*-cresol and RB dye onto TBAC matched well with Langmuir isotherm and pseudo-second-order kinetics model. The adsorption process was endothermic for Cr^{6+} and RB dye and exothermic for *o*-cresol.

Chapter 6
Figures & Tables

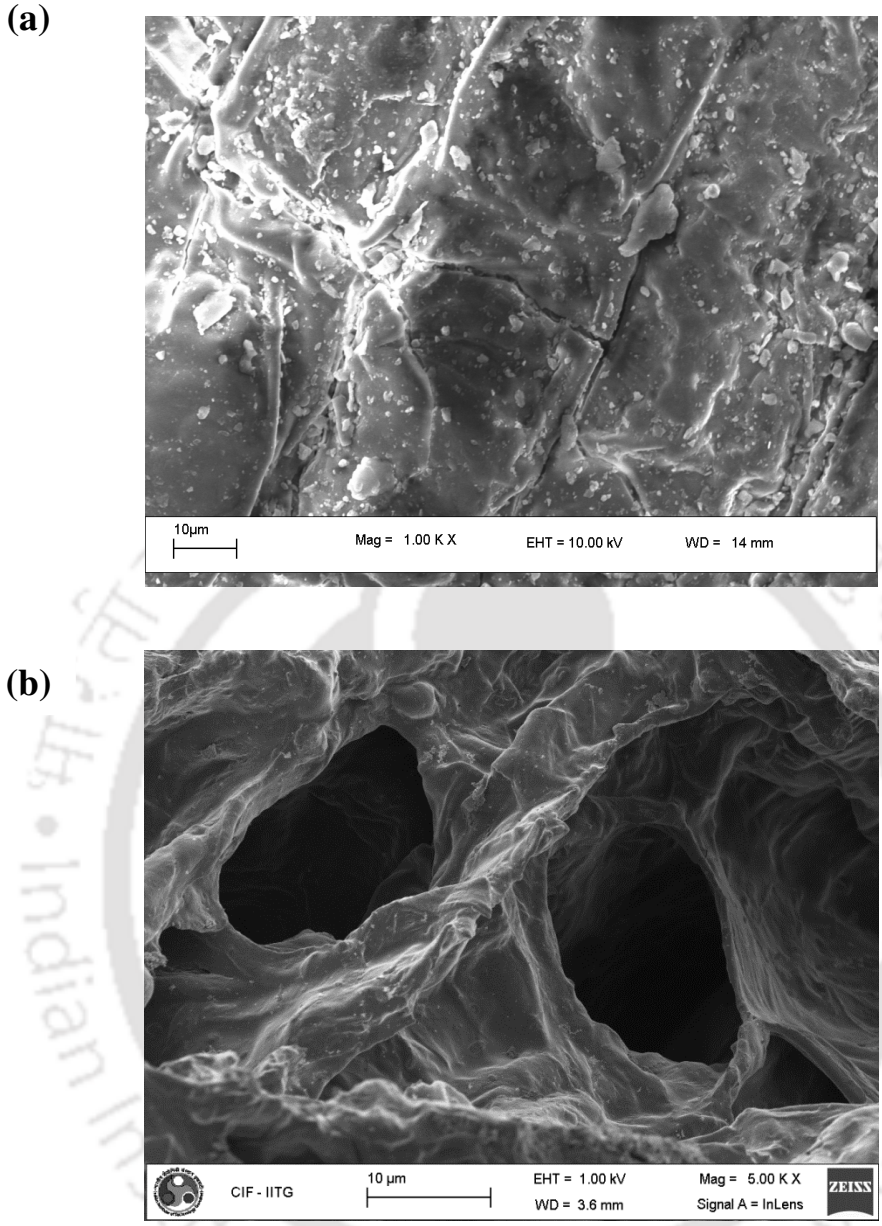

Figure 6.1 SEM picture of (a) raw TB (before activation) and (b) TB after activation (TRAC)

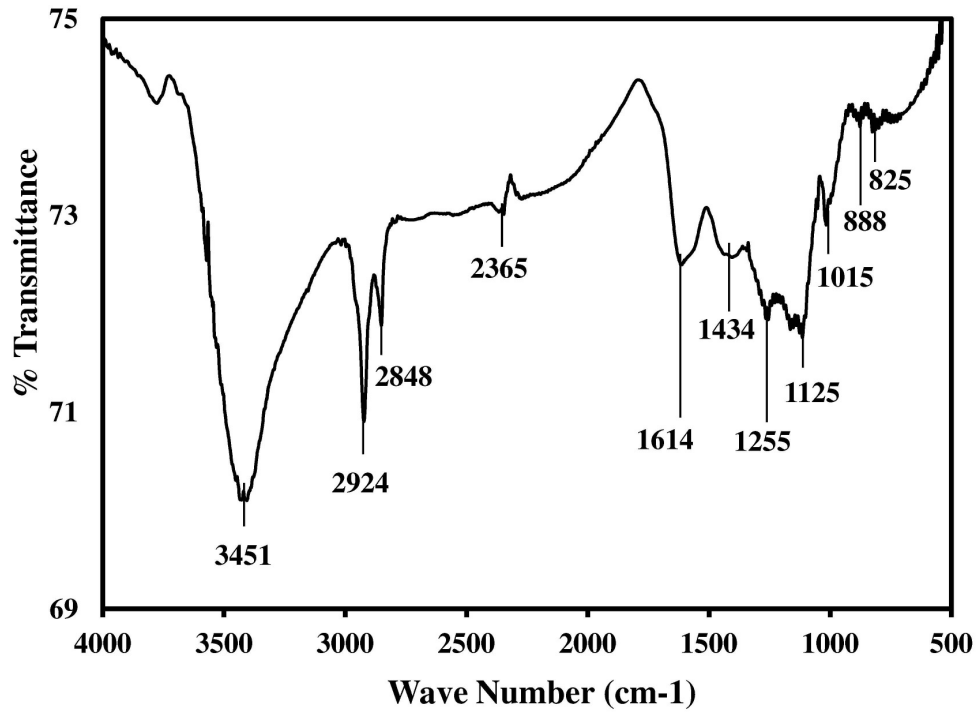

Figure 6.2 FT-IR spectra of TBAC (after thermochemical treatment)

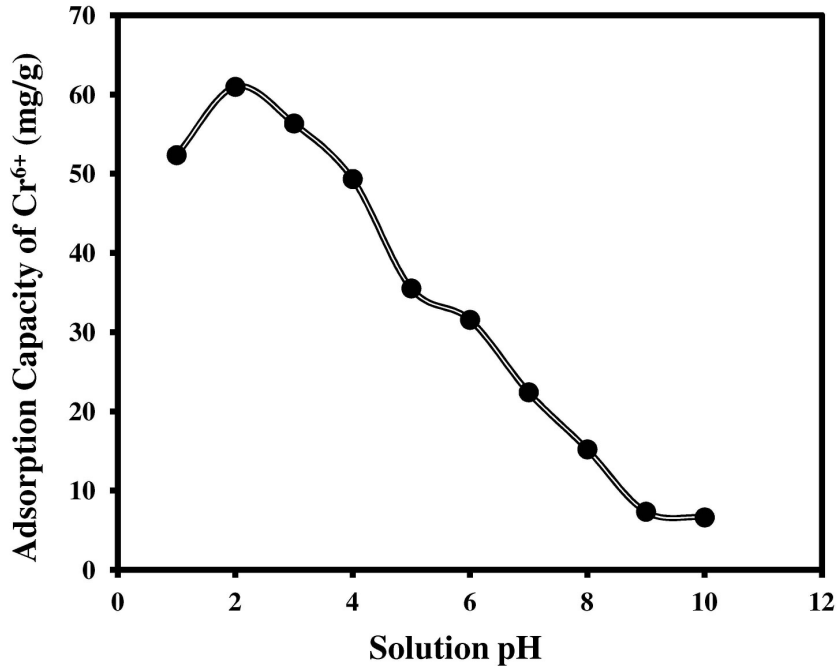

Figure 6.3a Effect of pH on adsorption capacity of Cr^{6+} (C_o = 100 mg/l T = 30°C, t = 360 min, W = 0.05 g TBAC, R = 180 rpm and V = 50 ml.

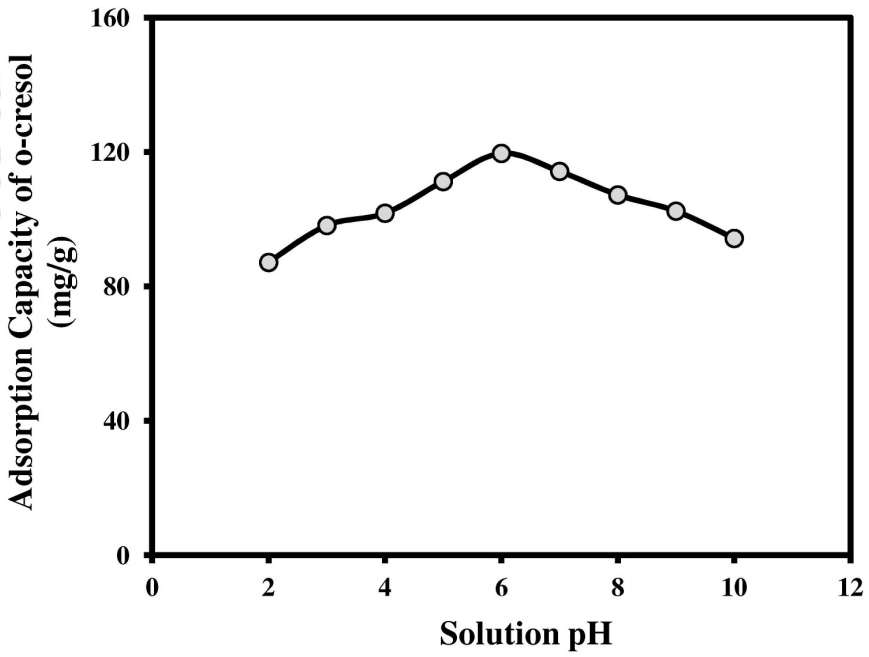

Figure 6.3b Effect of pH on adsorption capacity of *o*-cresol (C_o = 200 mg/l T = 30°C, t = 240 min, W = 0.05 g TBAC, R = 180 rpm and V = 50 ml.

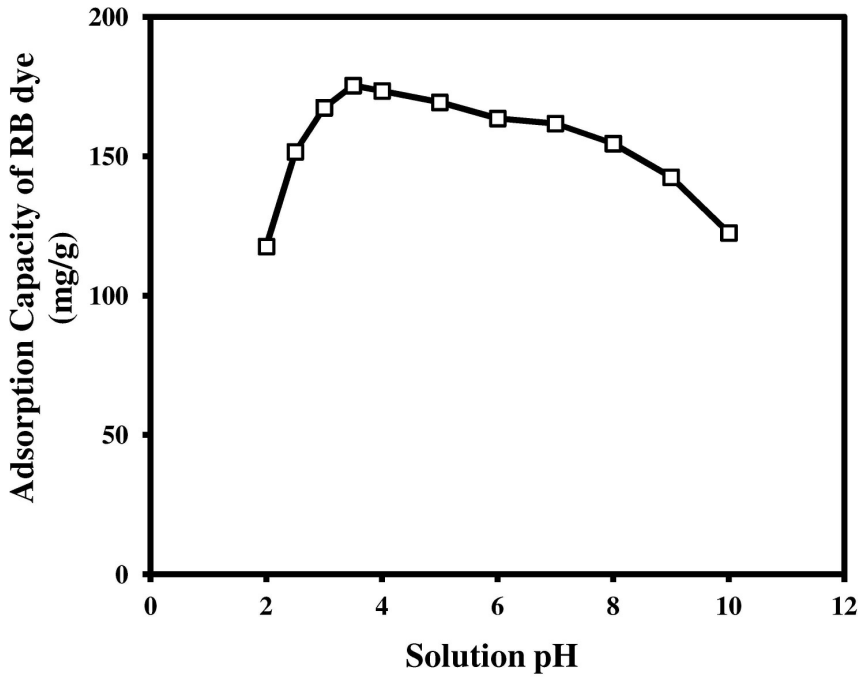

Figure 6.3c Effect of pH on adsorption capacity of RB dye (C_o = 200 mg/l T = 30^{o}C, t = 1440 min, W = 0.05 g TBAC, R = 180 rpm and V = 50 ml.

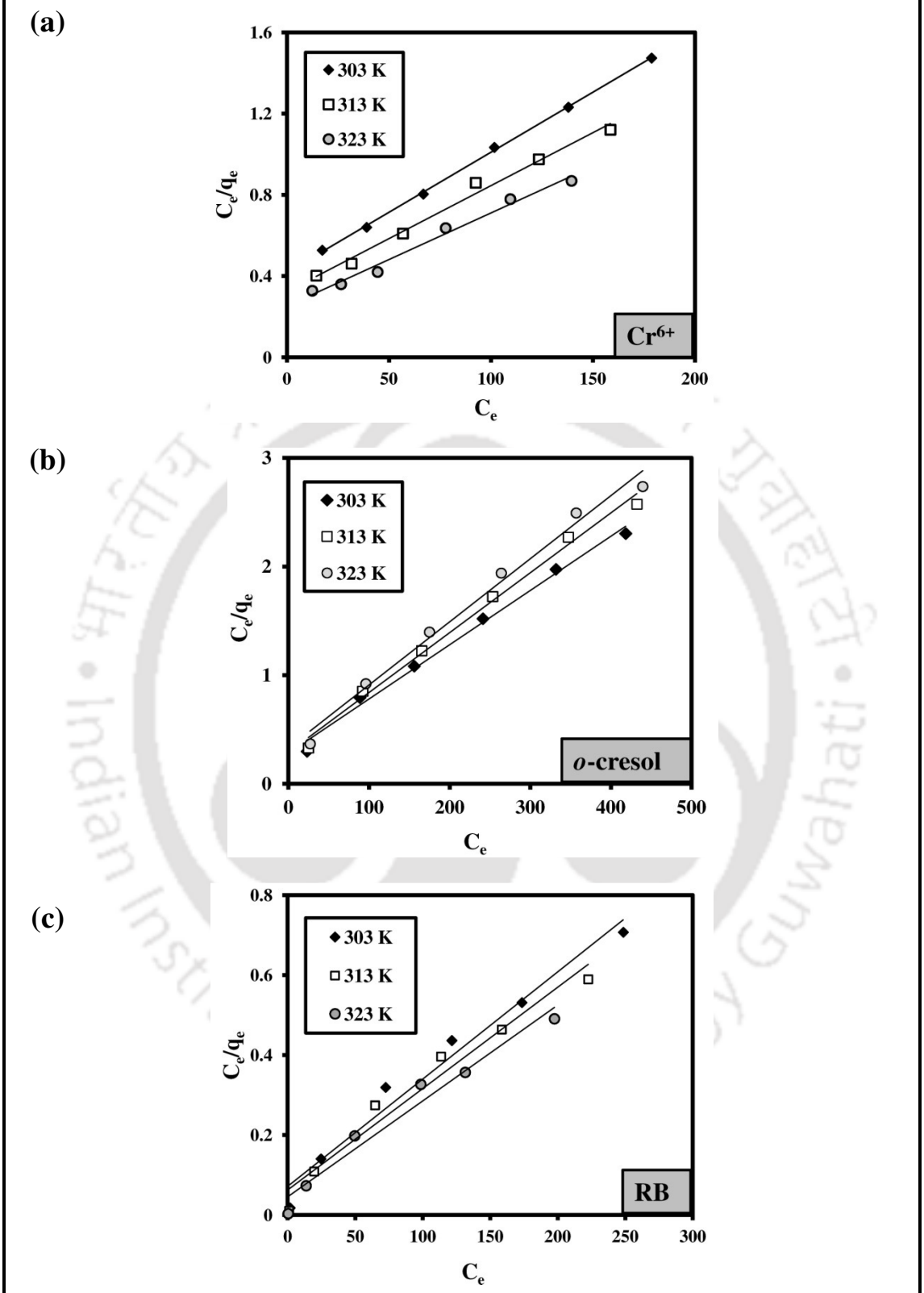

Figure 6.4 Langmuir isotherm plots of (a) Cr^{6+} (b) *o*-cresol and (c) RB dye onto TBAC

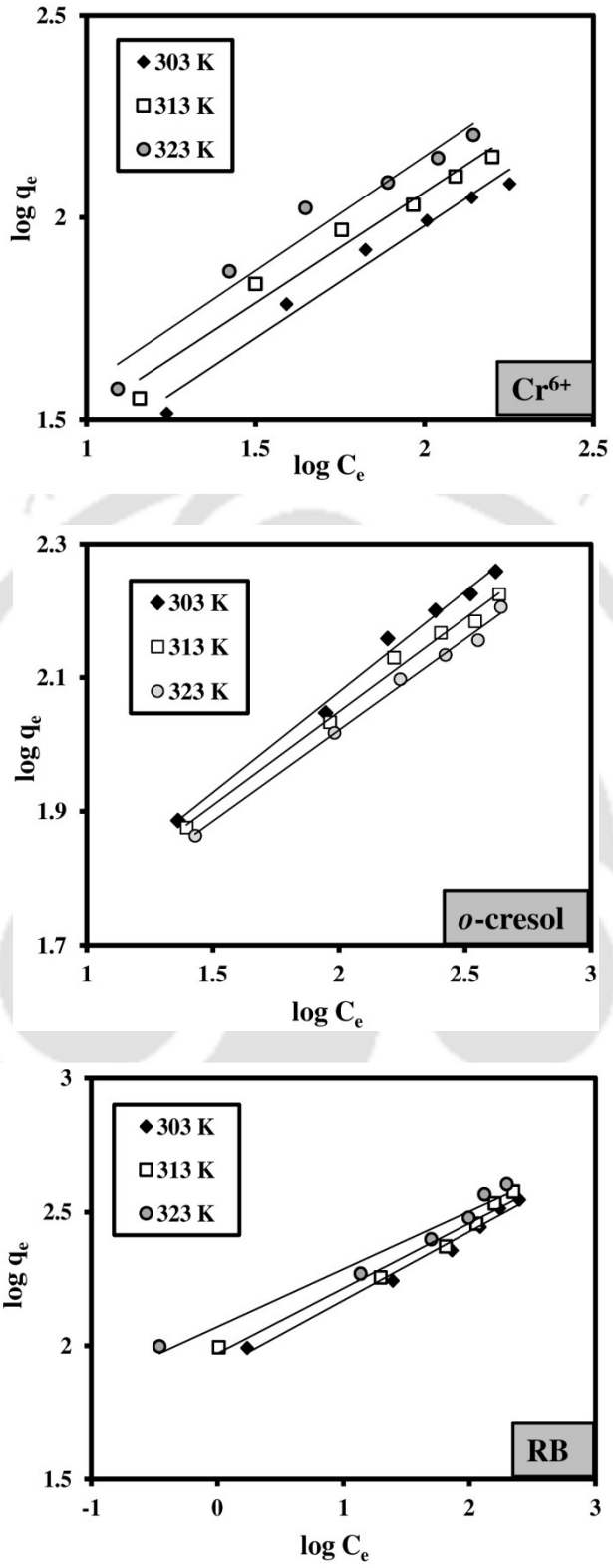

Figure 6.5 Freundlich isotherm plots of (a) Cr^{6+} (b) *o*-cresol and (c) RB dye onto TBAC

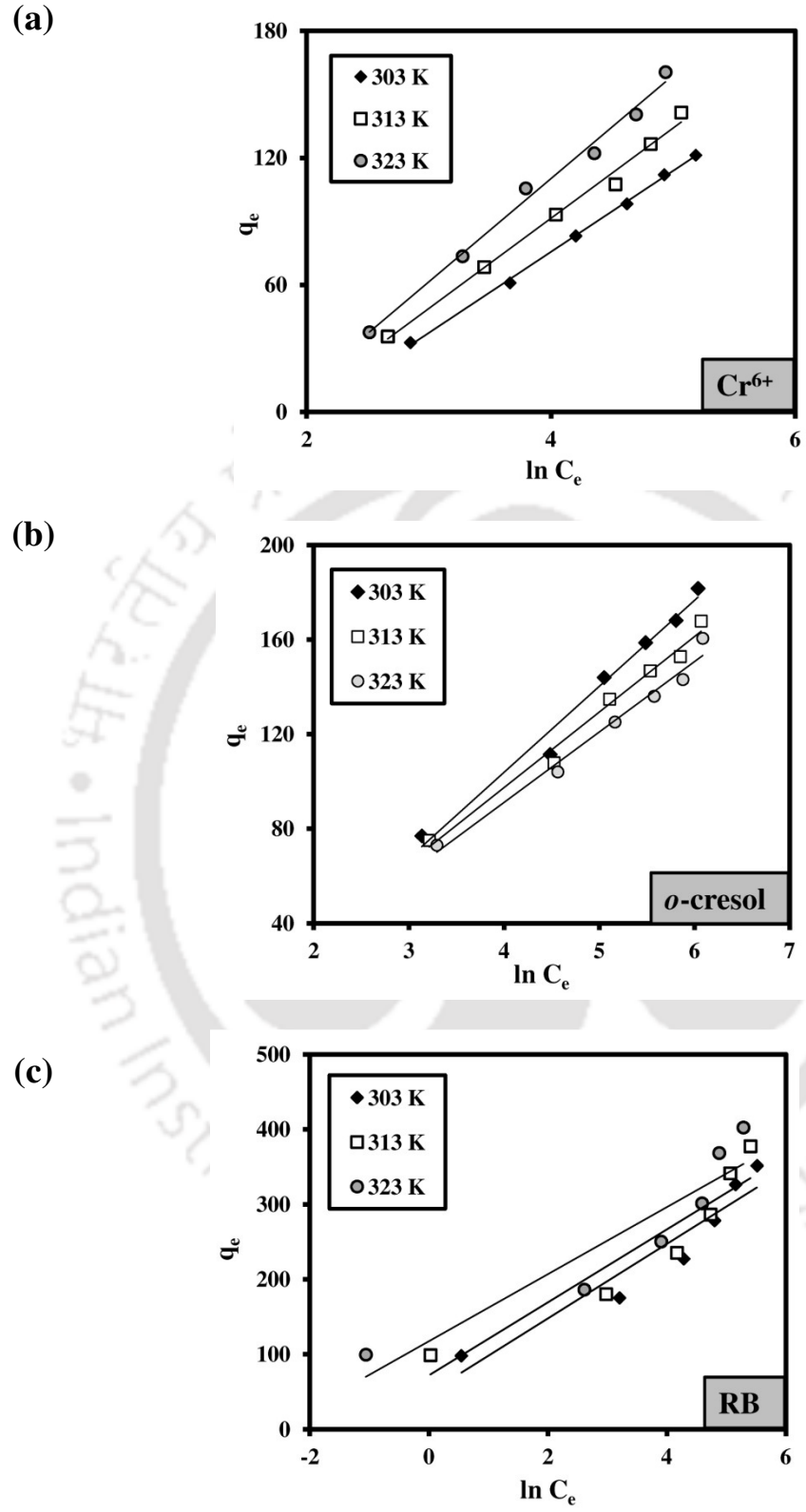

Figure 6.6 Temkin isotherm plots of (a) Cr^{6+} (b) *o*-cresol and (c) RB dye onto TBAC

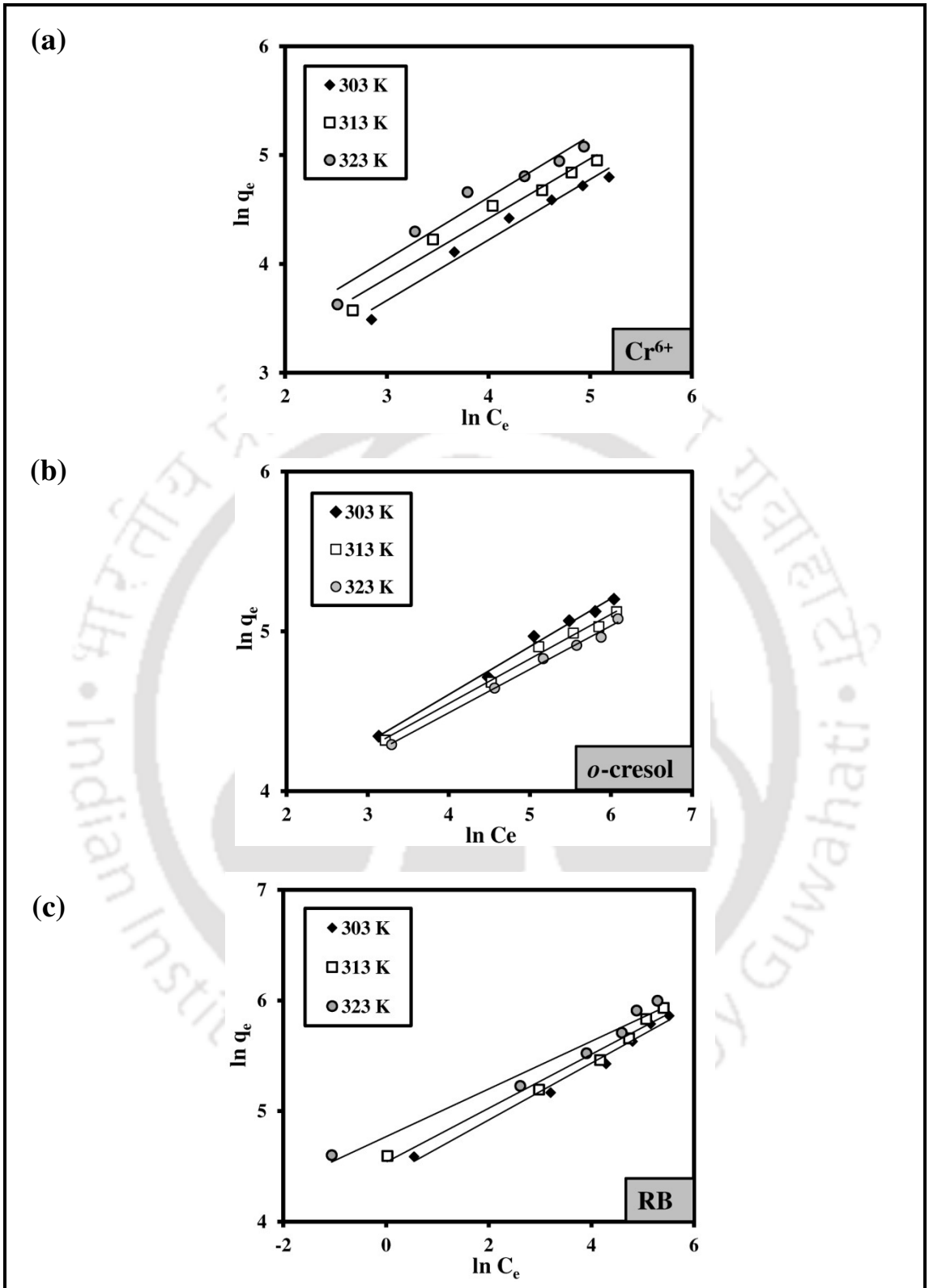

Figure 6.7 Halsey isotherm plots of (a) Cr^{6+} (b) *o*-cresol and (c) RB dye onto TBAC

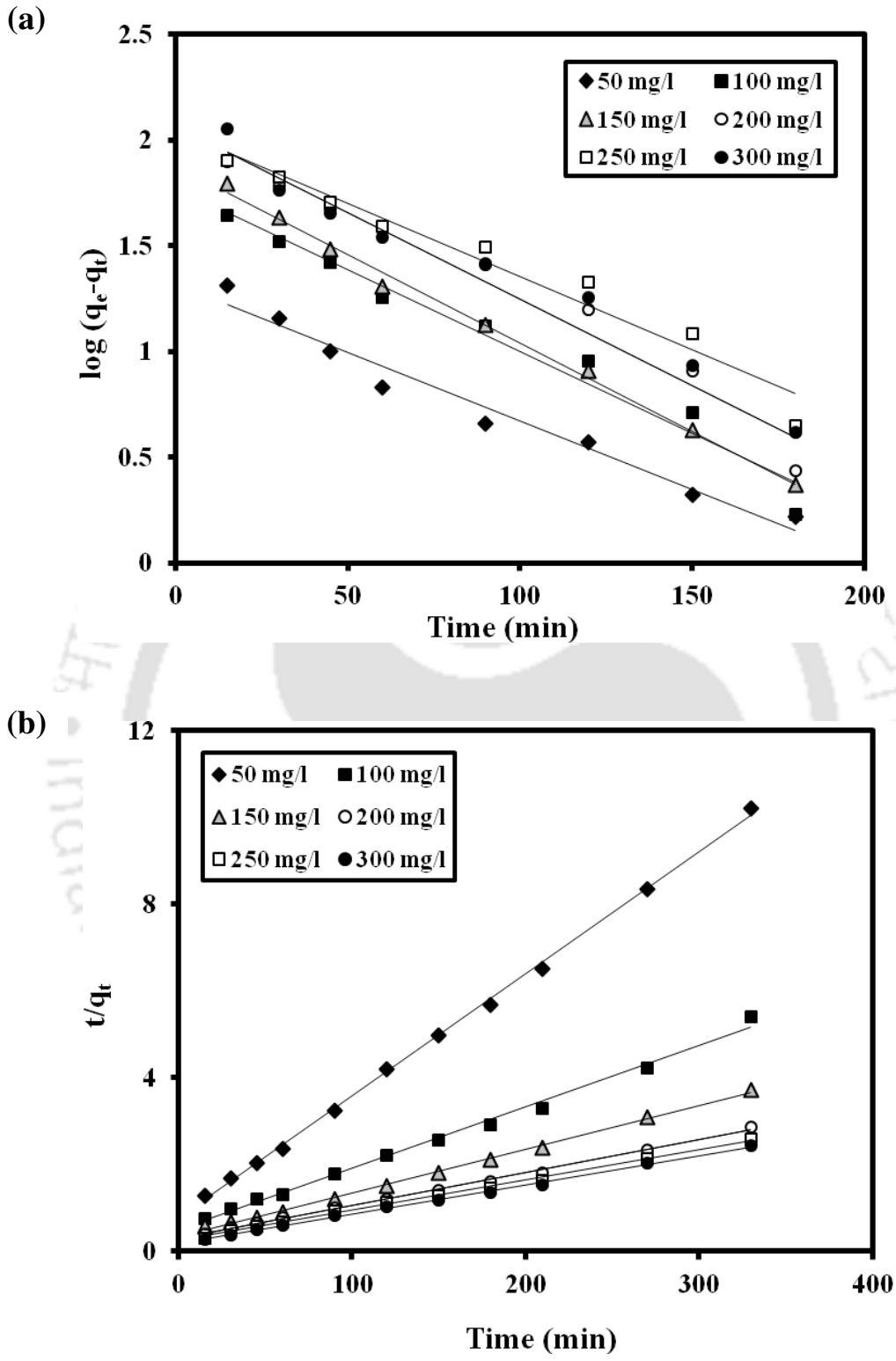

Figure 6.8 Kinetic plots of Cr^{6+} adsorption onto TBAC (a) pseudo-first-order and (b) pseudo-second-order

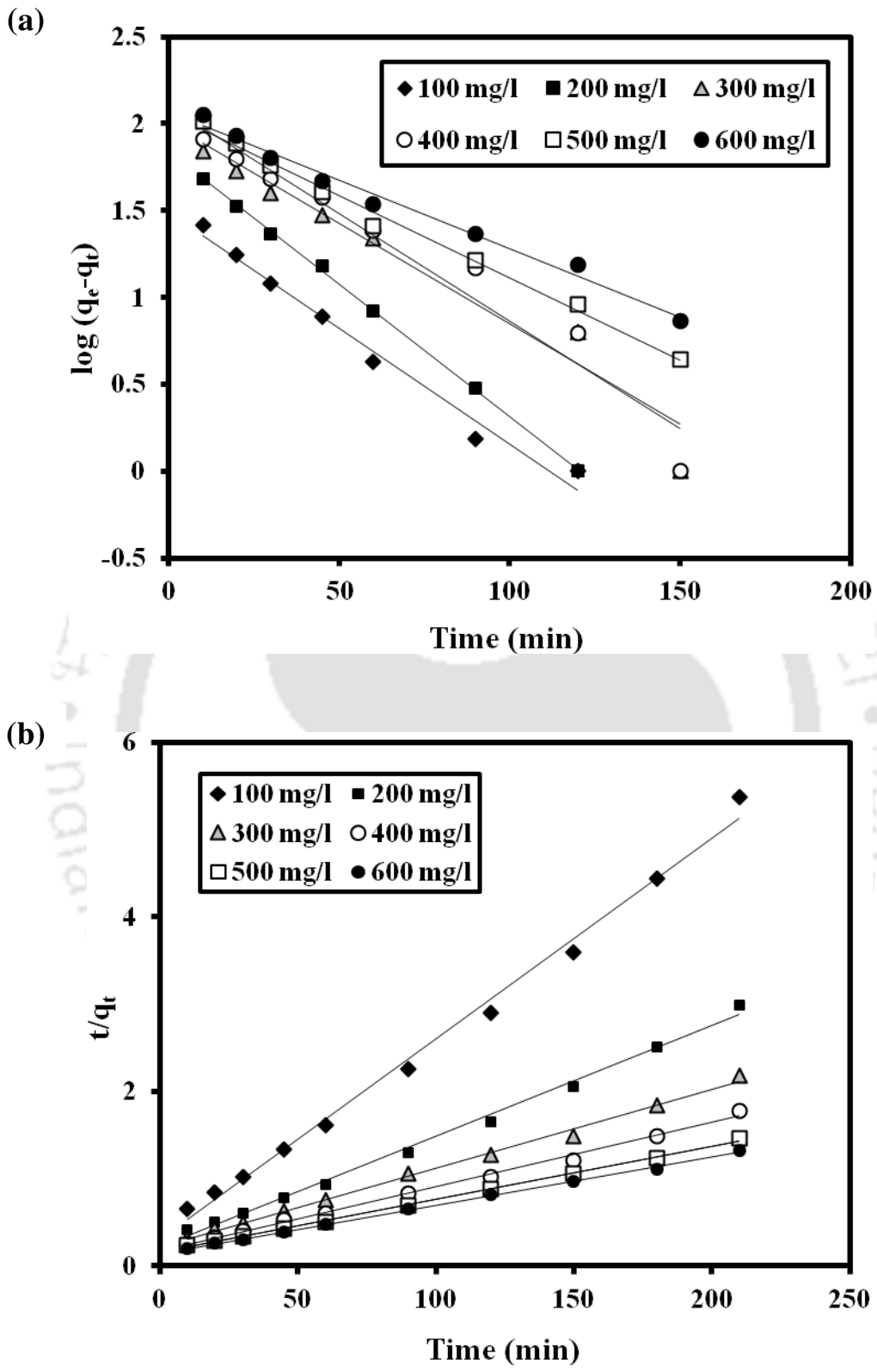

Figure 6.9 Kinetic plots of *o*-cresol adsorption onto TBAC (a) pseudo-first-order and (b) pseudo-second-order

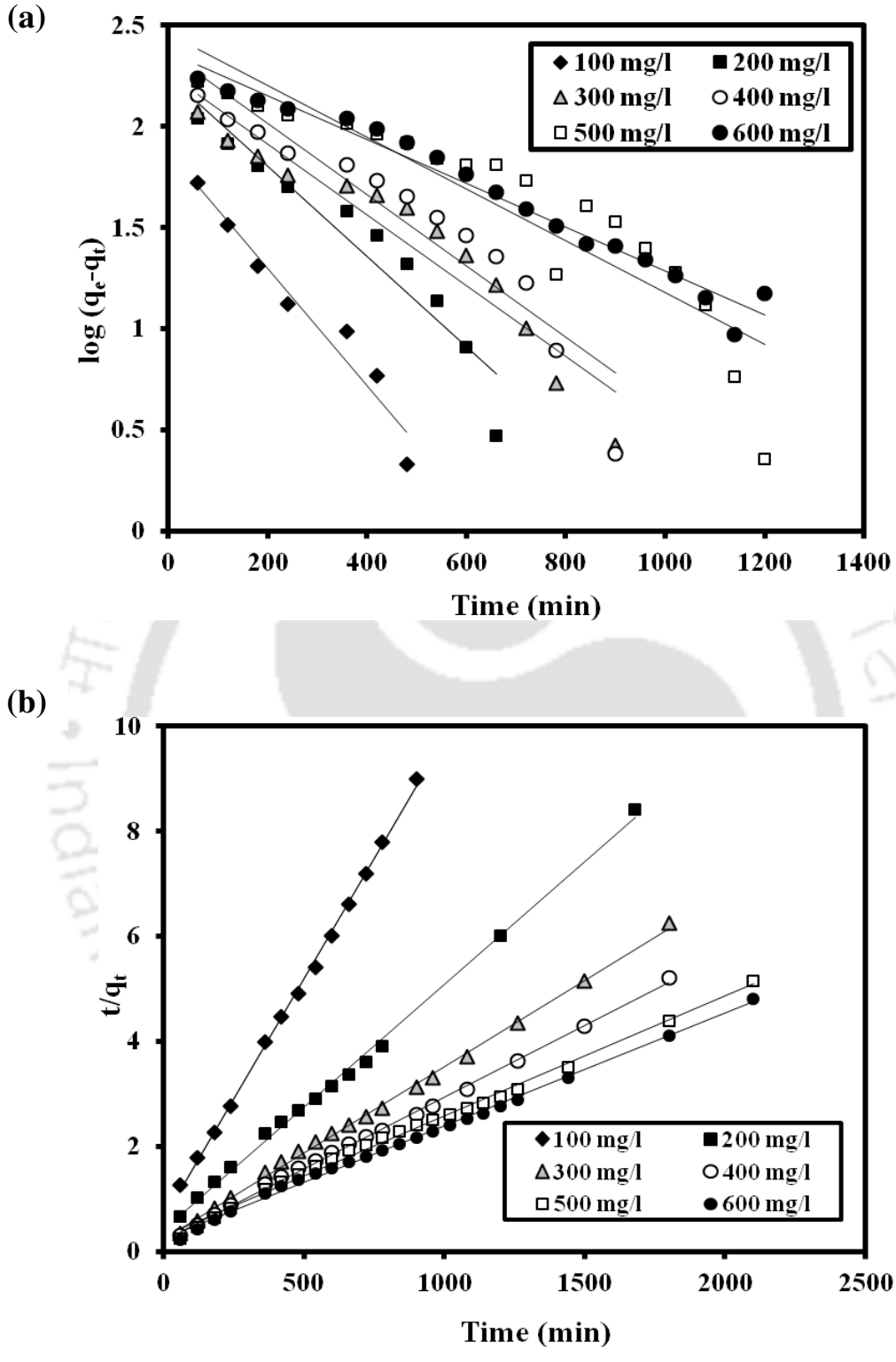

Figure 6.10 Kinetic plots of RB dye adsorption onto TBAC (a) pseudo-first-order and (b) pseudo-second-order

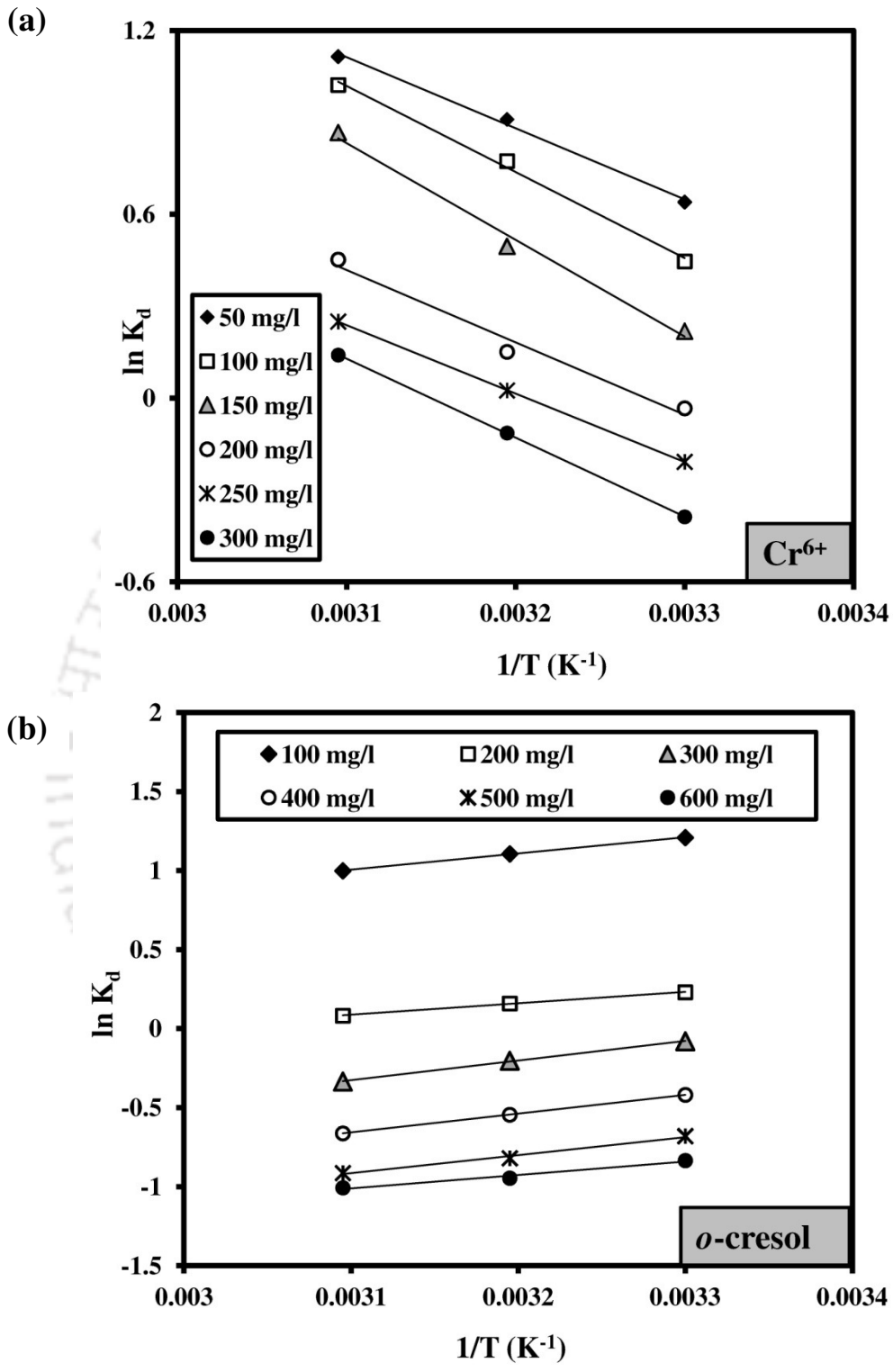

Figure 6.11 Van't Hoff plots of (a) Cr^{6+} and (b) *o*-cresol onto TBAC at various concentrations

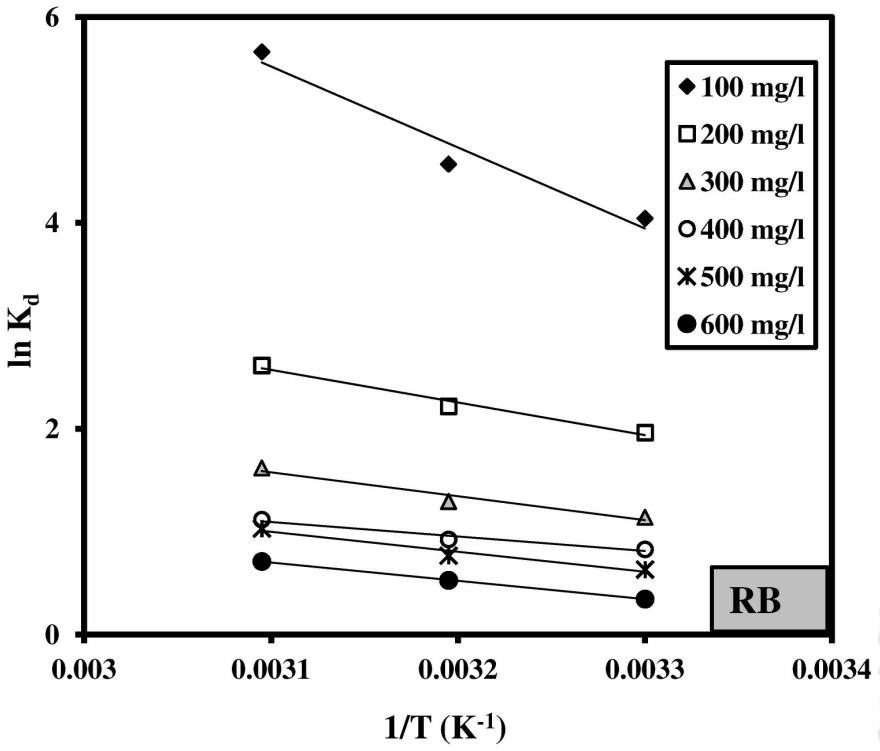

Figure 6.11 Van't Hoff plots of (c) RB dye adsorption onto TBAC at various concentrations

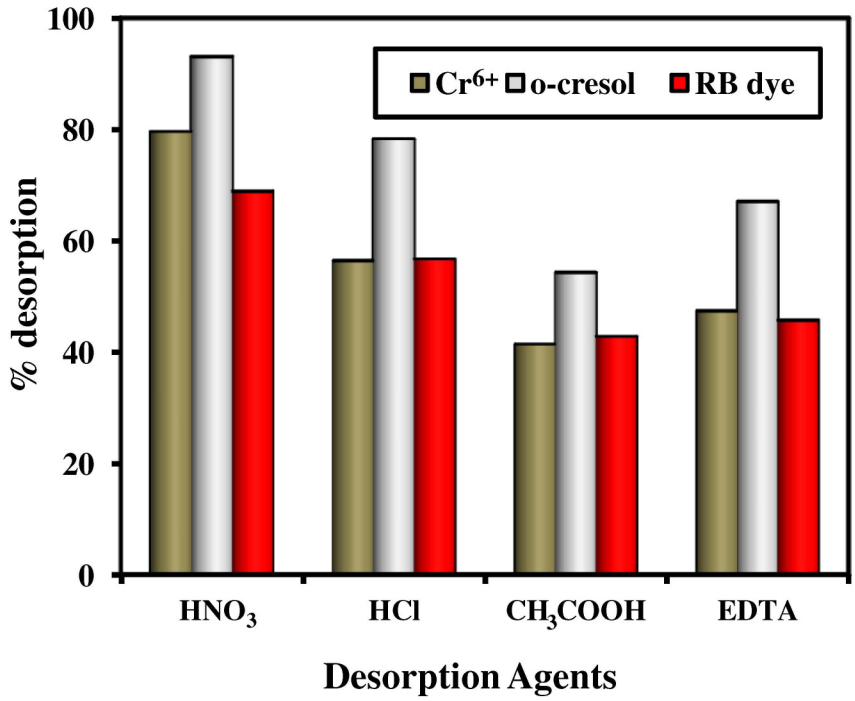

Figure 6.12 Desorption performance of Cr^{6+}, *o*-cresol and RB dye from TBAC (W = 0.1 g, V = 50 ml, T = 30°C, R = 180 rpm and t = 5 hr (Cr^{6+} and *o*-cresol) and 24 hr (RB dye).

Table 6.1a Isotherm constants of Cr^{6+} adsorption on TBAC

Isotherm Models	Solution Temperature		
	30°C	**40°C**	**50°C**
Langmuir constants			
Q_o (mg/g)	168.9	191.9	217.9
b (l/mg)	0.0142	0.0161	0.0182
R^2	0.9993	0.9889	0.9859
Freundlich constants			
K_f	7.362	9.185	10.42
1/n	0.5559	0.5496	0.5665
R^2	0.9754	0.9710	0.9547
Temkin constants			
A (l/g)	0.1319	0.1565	0.1757
B	38.25	42.64	48.73
R^2	0.9988	0.9916	0.9908
Halsey constants			
K_h	0.0276	0.0177	0.0159
-1/n	0.5559	0.5496	0.5665
R^2	0.9754	0.9710	0.9540

Table 6.1b Langmuir separation factor (R_L) for Cr^{6+} adsorption at different temperatures

Initial concentration of *o*-cresol (mg/l)	***R_L* values at different temperature**		
	30 ºC	**40 ºC**	**50 ºC**
50	0.5848	0.5540	0.5236
100	0.4132	0.3831	0.3546
150	0.3195	0.2928	0.2681
200	0.2604	0.2369	0.2155
250	0.2198	0.1990	0.1802
300	0.1901	0.1715	0.1548

Table 6.2a Isotherm constants of *o*-cresol adsorption on TBAC

Isotherm Models	Solution Temperature		
	30°C	**40°C**	**50°C**
Langmuir constants			
Q_o (mg/g)	200	181.8	172.4
b (l/mg)	0.0178	0.0189	0.0177
R^2	0.9922	0.9922	0.9874
Freundlich constants			
K_f	30.05	30.86	29.97
1/n	0.3001	0.2796	0.2723
R^2	0.9908	0.9913	0.9940
Temkin constants			
A (l/g)	0.3189	0.3871	0.3924
B	36.34	31.93	29.75
R^2	0.9817	0.9857	0.9799
Halsey constants			
K_h	1.189×10^{-5}	4.719×10^{-6}	3.774×10^{-6}
-1/n	0.3001	0.2796	0.2723
R^2	0.9908	0.9913	0.9940

Table 6.2b Langmuir separation factor (R_L) for *o*-cresol adsorption at different temperatures

Initial concentration of *o*-cresol (mg/l)	***R_L* values at different temperature**		
	30 ºC	**40 ºC**	**50 ºC**
100	0.3597	0.3460	0.3610
200	0.2193	0.2092	0.2203
300	0.1577	0.1499	0.1585
400	0.1232	0.1168	0.1238
500	0.1010	0.0957	0.1015
600	0.0856	0.0810	0.0861

Table 6.3a Isotherm constants of RB dye adsorption on TBAC

Isotherm Models	Solution Temperature		
	30°C	**40°C**	**50°C**
Langmuir constants			
Q_o (mg/g)	373.1	393.7	416.7
b (l/mg)	0.0374	0.0409	0.0531
R^2	0.9729	0.9634	0.9656
Freundlich constants			
K_f	81.77	93.41	117.7
1/n	0.2569	0.2438	0.2158
R^2	0.9850	0.9780	0.9697
Temkin constants			
A (l/g)	2.645	4.369	13.84
B	49.68	48.69	44.72
R^2	0.9104	0.8859	0.8638
Halsey constants			
K_h	3.592×10^{-8}	8.276×10^{-9}	2.54×10^{-10}
-1/n	0.2569	0.2438	0.2158
R^2	0.9850	0.9780	0.9697

Table 6.3b Langmuir separation factor (R_L) for RB dye adsorption at different temperatures

Initial concentration of o-cresol (mg/l)	***R_L* values at different temperature**		
	30 ºC	**40 ºC**	**50 ºC**
100	0.2109	0.1965	0.1585
200	0.1179	0.1089	0.0861
300	0.0818	0.0754	0.0591
400	0.0627	0.0576	0.0449
500	0.0508	0.0466	0.0363
600	0.0427	0.0392	0.0304

Table 6.4

Kinetic constants of Cr^{6+}, *o*-cresol and RB dye adsorption onto TBAC

Initial adsorbate concentration (mg/l)		Pseudo-first-order model				Pseudo-second-order model		
		$q_{e,\,exp}$ (mg/g)	k_{ad} (l/min)	$q_{e,\,cal}$ (mg/g)	R^2	k' (1 x 10^{-4}) (g/mg/min)	$q_{e,\,cal}$ (mg/g)	R^2
Cr^{6+}	50	32.74	0.0177	21.46	0.9636	11.89	34.71	0.9936
	100	60.98	0.0168	39.42	0.9754	6.328	67.29	0.9964
	150	83.16	0.0191	75.33	0.9944	4.396	92.85	0.9925
	200	98.34	0.0175	76.32	0.9656	2.753	103.8	0.9963
	250	112.1	0.0154	98.50	0.9541	2.467	117.7	0.9975
	300	121.3	0.0186	115.3	0.9666	3.252	131.1	0.9968
***o*-cresol**	100	77	0.0416	37.97	0.9857	23.53	81.68	0.9924
	200	111.5	0.0372	88.45	0.9995	9.924	115.7	0.9946
	300	144	0.0337	101.4	0.9455	4.736	146.5	0.9956
	400	158.7	0.0291	125.2	0.9543	3.734	164.7	0.9954
	500	168.1	0.0236	129.9	0.9757	3.625	175.7	0.9964
	600	181.6	0.0212	148.4	0.9762	3.423	185.2	0.9988
RB dye	100	98.28	0.0077	75.08	0.9557	1.643	105.3	0.9986
	200	175.4	0.0064	178.7	0.9258	0.7351	187	0.9943
	300	227.4	0.0051	183	0.9118	0.6454	237.6	0.9993
	400	278.5	0.0044	233.3	0.9013	0.4463	301.7	0.9922
	500	326.5	0.0032	294.5	0.8472	0.1835	332.9	0.9976
	600	351.5	0.0037	335.8	0.9101	0.2356	358.7	0.9974

Table 6.5

Thermodynamic parameters of Cr^{6+}, *o*-cresol and RB dye adsorption onto TBAC

Initial pollutant concentration (mg/l)		$\Delta S°$ *(J/mol K)*	$\Delta H°$ *(J/mol)*	$\Delta G°$ *(J/mol)*		
				30 ºC	**40 ºC**	**50 ºC**
Cr^{6+}	**50**	69.02	19280	-1613	-2369	-2930
	100	80.98	23388	-1124	-2013	-2686
	150	88.36	26265	-550.3	-1290	-2278
	200	64.38	19646	83.64	-393.3	-1188
	250	59.55	18571	523.85	-65.37	-656.8
	300	67.49	21426	976.5	296.3	-369.5
***o*-cresol**	**100**	-17.99	-8499	-3044	-2876	-2624
	200	-17.92	-6013	-579.9	-415.2	-215
	300	-34.67	-10311	201.3	528.3	878.2
	400	-36.12	-9890	1055	1417	1741
	500	-37	-9482	1713	2134	2400
	600	-30.11	-7002	2102	2461	2645
RB dye	**100**	248.7	65420	-10185	-11894	-14873
	200	103.2	26404	-4944	-5771	-6871
	300	72.94	19301	-2877	-3366	-4255
	400	45.34	11692	-2089	-2409	-2938
	500	58.22	16104	-1594	-1998	-2708
	600	51.73	14806	-873.2	-1375	-1870

CHAPTER 7

CONTINUOUS FLOW PACKED-BED STUDY FOR RHODAMINE B ADSORPTION BY THERMO-CHEMICALLY ACTIVATED BAEL SHELL

The entire analysis of the batch mode adsorption results reveals that BSAC has high potential to remove metals, phenols and cationic dyes. In this research work, cationic dyes such as rhodamine B and methylene blue are indentified as the highly removable adsorbates by BSAC among all other studied components. As a continuation of batch mode adsorption work, due to the work limitation and the commercial importance of the dye this chapter presents only the adsorption performance of BSAC with rhodamine B using continuous flow packed-bed column reactor. It also describes various experimental conditions and data fittings with available models.

7.1 INTRODUCTION

Batch adsorption experiments provide only fundamental information related with the RB dye adsorption performance of adsorbent. However, in most of the industrial wastewater treatment units, a continuous mode of operation is preferred. Batch reactors are very easy to use in the laboratory study, but less convenient for field applications. Moreover, accurate scale-up data for fixed bed systems cannot be obtained from the adsorption isotherms of batch results, so the practical applicability of the adsorbent should be ascertained in column operations. Adsorption on fixed bed columns presents numerous advantages. It is simple to operate, gives high yield and can be easily scaled up from a laboratory process. The breakthrough curve would be a step function for favourable separations in packed bed, i.e. there would be an instantaneous jump in the effluent concentration from zero to the feed concentration at the moment the column capacity is reached. Therefore, experimental data obtained from the laboratory scale packed-bed continuous flow column reactor could be suggested to design an adsorption column for industrial applications to handle the bulk quantity of wastewater.

7.2. ANALYSIS OF COLUMN DATA

7.2.1 Mathematical Analysis

The performance of the column bed is usually described through the concept of breakthrough curve, which is obtained by plotting throughput volume (V_{eff}) at any time (t) versus effluent dye concentration (C_t) at 't' time. Throughput volume was calculated using the following Equation (7.1).

$$V_{eff} = Ft_e \tag{7.1}$$

where *'F'* is the volumetric flow rate (ml/min) of influent dye solution. Generally, breakthrough is defined as phenomenon when concentration of effluent from column is reached about 1% to 5% of influent concentration. However, breakthrough concentration may vary on the basis of effluent discharge limit for specific pollutant. In this study, the breakthrough time was obtained for RB dye concentration of 1 mg/l (1%) considering the acceptable limit for dye discharge.

Exhaustion is usually considered when the effluent concentration remains same for long period close to influent concentration. In this study, exhaustion was considered when effluent dye concentration reached 95% of influent concentration. Area below the breakthrough curve represents mass of RB dye which is not removed (M_{ua}) and was calculated using Equation (7.2) (Sincero and Sincero, 2003):

$$M_{ua} = \sum \left[\frac{(V_{n+1} - V_n)(C_{n+1} + C_n)}{2} \right] \tag{7.2}$$

where V_n is the throughput volume at n^{th} reading (l), V_{n+1} the throughput volume at $(n + 1)^{th}$ reading (l), C_n is the effluent adsorbate concentration at n^{th} reading (mg/l) and C_{n+1} is the effluent adsorbate concentration at $(n + 1)^{th}$ reading (mg/l).

Influent adsorbate load (I) was calculated from throughput volume (V_{eff}) at column exhaustion and influent adsorbate concentration (Co) according to Equation (7.3).

$$I = V_{eff} C_o \tag{7.3}$$

Mass of adsorbate removed was calculated from difference of influent adsorbate load (I) and mass of adsorbate not removed (M_{us}) from Equation (7.4).

Mass of the adsorbate removed = $M_r(mg) = I - M_{ua}$ (7.4)

Adsorbate capacity by BSAC was calculated using Equation (7.5)

Adsorbate uptake by adsorbent $M_{ad} = \frac{M_r(mg)}{Adsorbent`mass'(g)}$ (7.5)

Total removal percentage of dye (column performance) with respect to flow volume can be also found from the ratio of total adsorbed quantity of dye to the total amount of dye sent to column given in Equation (7.6).

$$removal\% = \frac{M_r}{I} \times 100 \tag{7.6}$$

The mass transfer zone (Δt) is evaluated as the difference between the breakthrough time (t_b, time at which the dye concentration in the effluent reached 1% C_o = 1 mg/l)

and the exhaustion time (t_e, time at which the dye concentration in the effluent exceed 99% C_o = 99 mg/l) and given by Equation (7.7)

$$\Delta t = t_e - t_b \tag{7.7}$$

The critical bed height or height of the mass transfer zone (Z_m) which is related to bed height, breakthrough and exhaustion times and is determined using Equation (7.8).

$$Z_m = Z\left[1 - \frac{t_b}{t_e}\right] \tag{7.8}$$

As a continuation of previous batch work, the present study in this chapter is focused on evaluation of the performance of BSAC for RB dye removal from aqueous solution with the help of a lab scale packed-bed column. In order to study the behaviour of RB dye uptake of BSAC in fixed bed column reactor, continuous flow experiments were conducted as a function of three operating conditions such as feed flow rate, initial feed concentration of dye and column bed height. The experimental data were analysed using different kinetic models such as Bohart-Adams model, Thomas model, BDST model and Yoon Nelson model to find out the best model fit for design purpose.

7.2.2 Analysis of Breakthrough Curves

7.2.2.1 Bed Depth Service Time (BDST) model

The Bed Depth Service Time model which is a modified form of Bohart-Adams model (Tan *et al.*, 1993; Bohart and Adams, 1920; Muralidharan, 1994) and it was used to compare the uptake capacity of the adsorption columns. This model was derived based on the assumption that intra-particle diffusion and external mass transfer resistance are negligible and that the adsorption kinetics is controlled by surface chemical reaction between solute in the solution and the unused adsorbent. This model also serves as a useful tool for comparing the performance of columns operating under different process variables. In the fixed-bed systems, the main design criteria is to predict how long the adsorbent material will be able to sustain for removing a specified amount of adsorbate from influent solution before regeneration is needed. This period of time is called the service time of the bed. One of the most

allied models for adsorption of dyes on column studies is the bed depth service time (BDST) model based on Bohart-Adams equation. BDST is a simple and comprehensive model for predicting the relationship between bed height (Z), and service time (t). This BDST model was focused on the estimation of characteristic parameters such as the maximum adsorption capacity and kinetic constant. This model is used only for the description of the initial part of the break through curve i.e. up to the breakpoint or 10-50% of the saturation points. The Bohart-Adams equation can be represented as:

$$\ln\left(\frac{C_o}{C_b}-1\right)=\ln\left(\exp\left(\frac{KN_oZ}{\nu}\right)-1\right)-KC_ot \tag{7.9}$$

Thereafter, Hutchins (1973) modified the Bohart-Adams equation and proposed a linear relationship between the bed depth and service time, which requires only three fixed-bed tests to find out the necessary data and given by Eq. (7.10).

$$t_b=\frac{ZN_o}{C_o\nu}-\frac{1}{K_{ad}C_b}\left(\frac{C_o}{C_b}-1\right) \tag{7.10}$$

where t_b is service time at breakthrough point; N_o is dynamic bed capacity (mg/l), Z is the bed height of the column (cm), C_o is the initial concentration of solute in the liquid phase (mg/l), ν is linear flow rate (cm/hr), defined as the ratio of the volumetric flow rate F (cm^3/hr) to the cross-sectional area of the bed A_c (cm^2), K_{ad} is rate constant of adsorption (l mg^{-1} h^{-1}) and C_b is the breakthrough metal ion concentration (mg/l). Equation (7.10) can be rewritten in the form of a straight line.

$$t_b=m_xZ-C_x \tag{7.11}$$

$$C_x=\frac{1}{K_{ad}C_b}\ln\left(\frac{C_o}{C_b}-1\right) \tag{7.12}$$

where m_x is slope of BDST line ($m_x = N_o/C_o\nu$) and the intercept of this equation represents as Equation (7.12). N_o and K_{ad} can be evaluated from slope (m_x) and the intercept (C_x) of the plot of (t_b) versus Z, respectively.

7.2.2.2 Thomas Model

Thomas model is one of the most general and widely used models in the column performance theory. Thomas or reaction model assumes Langmuir kinetics of adsorption-desorption with no axial dispersion and is derived with the assumption that the rate driving force obeys second-order reversible reaction kinetics. Thomas model also assumes a constant separation factor but is applicable to either favourable or unfavourable isotherms. The expression developed by Thomas (Thomas, 1944), calculates the maximum solid phase concentration of the solute on the sorbent and the adsorption rate constant for a continuous adsorption process in the column. The breakthrough curves were analyzed by using the Thomas model through the following Equation. (7.13):

$$\frac{C_t}{C_o} = \frac{1}{1+\exp\left(\frac{k_{TH}}{F}\left(q_o M - C_o V_{eff}\right)\right)} \tag{7.13}$$

The linerized form of the Thomas model can be expressed as follows:

$$\ln\left(\frac{C_o}{C_t} - 1\right) = \frac{k_{TH} q_o M}{F} - k_{TH} C_o t \tag{7.14}$$

where the kinetic coefficient (K_{TH}) and the maximum adsorption capacity (q_o) can be determined from a plot of ln[(C_o/C)-1] against t at a given flow rate, bed height and initial dye concentration. C_o and C_t are dye ion concentrations (mg/l) in the influent and effluent, respectively, K_{TH} is the Thomas model rate constant (ml/mg min), F *is* the flow rate (l/ hr), q_o is the maximum solid-phase concentration of the solute (mg/g), M *is* the total mass of the adsorbent loaded in the column (g) and V_{eff} is the volume of dye solution passed through the column (l).

7.2.2.3 Yoon-Nelson Model

Yoon and Nelson (1984) have developed a relatively simple model. This model is based on the assumption that the rate of decrease in the probability of adsorption for each adsorbate molecule is proportional to the probability of adsorbate adsorption and the probability of adsorbate breakthrough on the adsorbent. The Yoon and Nelson model not only is less complicated than other models, but also requires no detailed

data concerning the characteristics of adsorbate, the type of adsorbent, and the physical properties of adsorption bed. The Yoon and Nelson equation regarding to a single component system is expressed as:

$$\frac{C_t}{C_o} = \frac{\exp\left(k_{YN}t - \tau k_{YN}\right)}{1+\exp\left(k_{YN}t - \tau k_{YN}\right)} \tag{7.15}$$

The linear form of Yoon-Nelson model can be expressed as:

$$\ln\left(\frac{C_t}{C_o - C}\right) = k_{YN}t - \tau k_{YN} \tag{7.16}$$

where K_{YN} is the rate constant (per min); τ is the time required for 50% adsorbate breakthrough (min) and t is the breakthrough (sampling) time (min). These values were determined from a plot of ln $C_t/(Co-C_t)$ versus sampling time (t) according to Eq. (7.16). If the theoretical model accurately characterizes the experimental data, this plot will result in a straight line with slope of K_{YN} and intercept τK_{YN}. The calculation of theoretical breakthrough curves for a single-component system requires the determination of the parameters K_{YN} and τ for the adsorbate.

7.3 EXPERIMENTAL METHODS

7.3.1 Experimental Setup

A schematic diagram of the reactor is shown in Figure 7.1. Packed bed column consists of a column of 1.1 cm diameter and 50 cm in height was used in the sorption studies for the removal of RB dye. Column was packed with known quantity of BSAC to obtain a predetermined bed height. To enable a uniform inlet flow of the dye solution into column, glass wool of 0.5 cm depth was placed at the bottom of the column just above the inlet point. Similarly, 0.5 cm height of the glass wool was tightly held on the top of the BSAC bed before the exit point to avoid the floating up and washed out of adsorbent from the column. The presence of air pockets within the packed BSAC caused channelling of influent dye solution and lowered the adsorption capacity of the bed (Ko *et al.*, 2000). To ensure the expulsions of the trapped air, BSAC packed column was fully wetted by filling with deionised water for 6-7 hr prior to starting of the experiments.

7.3.2 Experimental Protocol

An aqueous RB dye solution was pumped in an upward direction through the column reactor by peristaltic pump (Miclins, VSP-200-4C) at optimized pumping flow rate to get the particular outlet flow rate. Flow rate was cross-checked at the exit point of the column at regular time intervals to prevent and avoid the flow rate fluctuations. Experiments were conducted by using three different bed heights (10, 15 and 20 cm) with fixed flow rate and dye concentration, three different flow rates (5, 7 and 9 ml/min) with fixed bed depth and dye concentration, and three different dye concentration (100, 150 and 200 mg/l) with fixed bed height and flow rate of RB dye. The treated solution was collected from the top with the same flow rate of feed stream. The samples were collected at pre-determined time intervals and then centrifuged at 5000 rpm for 10 min. The concentrations of effluent (or) unabsorbed RB dye were measured using UV-spectrophotometer at particular wavelength (λ_{max} = 555 nm). The experiments were ended when the bed get saturated. During the experiment following precautions were taken: (a) bed was in vertical position, (b) no leakage of bed, in and out flow and (c) No stoppage of influent into the column until the experiment completed. The simple specification of this study is presented in the Table 7.1.

7.4 RESULTS AND DISCUSSION

7.4.1 Effect of Flow Rate

Based on the information from the batch studies, the pH of the influent solution was maintained at 3.5. To find out the effect of flow rate on the breakthrough curve, adsorption experiments were carried out by varying the flow rate between 5, 7 and 9 ml/min. In this process, the initial adsorbate concentrations, initial pH of the solution and bed height were maintained as 100 mg/l, 3.5 and 10 cm, respectively. The effect of flow rate on breakthrough performance at the above operating conditions is shown in Figure 7.2a. From the figure it was observed that the adsorption efficiency was higher at lower flow rate. This can be explained by the fact that at high flow rate, the diffusion process which controls the sorption becomes slow, and hence, the adsorbent needs more contact time to bond the dye efficiently. In other words, the residence time of the solute in the column is not large enough for adsorption equilibrium to be

reached at that flow rate, the dye solution leaves the column before equilibrium occurs. These breakthrough curves show the efficiency of the process kinetics.

It was also observed that the adsorbent gets saturated easily at higher flow rates. The uptake of dye decreased with increase in flow rate. The optimum uptake capacity for flow rate of 5, 7, and 9 ml/min was found to be 121.8, 115.6, and 113.2 mg/g respectively (Figure 7.2b). As shown in Figure 7.2b, the saturation occurred at 39.5, 26.9 and 20.9 h when the flow rates were 5, 7 and 9 ml/min, respectively.

7.4.2 Effect of Initial Adsorbate Concentration

Column experiments were carried out by varying the concentration of RB dye between 100 to 200 mg/l to determine the effect of adsorbate concentration on the performance of the breakthrough curve. During these experiments, other parameters like pH, bed height and flow rate were kept constant at 3.5, 10 cm and 5 ml/min respectively. The sorption breakthrough curve obtained for adsorbate concentrations of 100, 150 and 200 mg/l are given in Figure 7.3. The breakthrough time decreased with increase in inlet RB dye concentration as the binding sites became more quickly saturated. The equilibrium RB dye uptake and the total RB dye adsorbed were found to increase with increase in inlet RB dye concentration. The percentage of RB dye removal decreased with increase in adsorbate concentration. With increase in initial RB dye concentration from 100 to 200 mg/l, the adsorption capacity of RB dye was found to increase from 121.8 to 179.8 mg/g respectively. But the percentage removal of RB dye decreased when the inlet RB dye concentration was increased from 100 to 200 mg/l. The increase in adsorption capacity of the adsorbent might be due to the fact that high inlet RB dye concentration provides higher driving force for the transfer process to overcome the mass transfer resistance. As seen in Figure 7.3, for low inlet concentrations of RB dye, the breakthrough occurred late and surface of the adsorbent was saturated with RB dye after a long time whereas for higher RB dye concentration, the breakthrough occurred in a short period of time. The saturation time of adsorbent was decreases from 39.7 to 31.9 min (Figure 7.3) when the inlet RB dye concentration was increased from 100 to 200 mg/l. At lower inlet RB dye concentrations, the breakthroughs were flatter indicating a relatively wide mass transfer zone and film controlled process. On the contrary, the breakthrough curves were sharp at high inlet RB dye concentration, implying a relatively smaller mass transfer zone and intra-

particle diffusion controlled process. The same trend was also observed by other authors related to metal ion adsorption (Goel *et al.*, 2005).

7.4.3 Effect of Bed Height

In order to find out the effect of bed height on the breakthrough curve, the adsorbate solution having RB dye concentration of 100 mg/l, pH 3.5 and flow rate 5 ml/min was passed through the adsorption column by varying the bed height. Figure 7.4 presents the performance of breakthrough curves at bed heights of 10, 15 and 20 cm. It is evident from Figure 7.4 that the steepness of the breakthrough curve was a function of bed height. With increase in bed height, the throughput volume and bed saturation was increased which might be due to higher contact time. At a relatively lower contact time, the curve was steeper showing the faster exhaustion of the bed. The treated volume varied between 12 and 34.2 litres when the bed height was increased from 10 to 20 cm respectively. Similarly, RB dye adsorption uptakes were found to be 121.8, 127.9 and 140 mg/g when the bed heights were 10, 15 and 20 cm, respectively and the corresponding total RB dye adsorbed were 841, 1372 and 1878 mg, respectively. The increase in dye uptake capacity with the increase of bed height in the fixed bed column might be due to increased surface area of the adsorbent which provided more binding sites for the adsorption. The breakthrough time also increased with increase in bed height. The breakthrough curve followed a characteristic 'S' shape profile which was associated with adsorbate of smaller molecular diameter and simpler structure.

7.4.4 Application of Different Breakthrough Curves

Successful design of a continuous packed-bed column requires prediction of the concentration–time profile (or) breakthrough curve of effluent and the maximum uptake capacity of an adsorbent. In many cases, kinetics of adsorption in the column has been tested using Bohart-Adams model. However, various mathematical models can be used to describe and model fixed-bed adsorption process. Breakthrough curves obtained at different bed heights (Z) and flow rates (F) were analyzed using three mathematical models such as Bed depth service time (BDST), Thomas and Yoon–Nelson models.

7.4.4.1 Bed Depth Service Time (BDST) Model

The BDST adsorption model was applied to the experimental data to study the breakthrough behaviour of RB dye onto BSAC and to estimate the characteristic parameters, K and N_o from the model. Applying Equation (7.11) to the experimental data at different bed depths, inlet RB dye concentrations and flow rates, a linear relationship between (t_b) and Z was obtained for the relative concentration range up to exhaust. Figure 7.5 shows the plot of service time ($t_s = t_b$) and column bed depth of 10, 15 and 20 cm with the 100 mg/l of initial dye concentration and 5 ml/min flow rate. N_o and K_{ad} can be evaluated from slope (m_x) and the intercept (C_x) of the plot (Figure 7.5) of (t_b) versus Z, respectively. The respective values of K and N_o calculated from the slope and intercept of the linear plot are presented in Table 7.2. From the table it is evident that the maximum adsorption capacity N_o decreased with the increase in bed depth and increased with the increase in the initial RB dye concentration and flow rate. The values of the adsorption rate constants were influenced by initial concentration of dye and decreased with increase in concentration. BDST model provides a simple and comprehensive approach for evaluating adsorption column test, but its validity is limited in the range of conditions used (Bohart and Adams, 1920).

7.4.4.2 Thomas Model

The Thomas model was fitted to the column data to investigate the breakthrough behaviour of RB dye onto BSAC. Application of the Thomas model to the data in the concentration (C_t) range of 1 mg/ l < C_t < 0.95 C_o with respect to bed depth, initial RB dye concentration and flow rate helped in the determination of the Thomas' kinetic coefficients for this system. The coefficients were determined from the slope and intercepts obtained from the linear regression performed on each set of transformed data (ln [C_o/C_t –1] versus time). Analysis of the regression coefficients indicated that the regressed lines provided average fits to the experimental data with R^2 values ranging from 0.8830 to 0.8948 (Table 7.3). Table 7.3 also presents the values of k_{Th} and q_o. The bed capacity q_o decreased and the coefficient k_{Th} increased with increase in flow rates. On the other hand, with the increase in the initial RB dye concentration, the values of q_o increased and that of k_{Th} decreased. It is evident from Table 7.3 that the differences between the experimental and predicted values of bed capacity (q_o)

were very less at all the operating conditions studied. Thomas model plots for various operating parameters such as effect of flow rate, initial concentration and bed height are shown in the Figure 7.6a, 7.6b and 7.6c, respectively. It is clear from the model predicted normalized concentration values were in very good agreement with the experimental values at all RB dye concentrations at all operating conditions.

7.4.4.3 Yoon and Nelson Model

The simple Yoon–Nelson model was applied to investigate the breakthrough behaviour of RB dye onto BSAC in fixed bed. This model introduces the parameter τ, which shows the treatment time taken for C_t (effluent exit concentration) to be half the initial concentration (0.5 C_o). The values of the model parameters k_{YN} (rate constant) and τ were determined from the slope and intercepts of the linear plots of ln $[C_t/(C_o - C_t)]$ versus time (t) with respect to bed depth, initial RB dye concentration and flow rate and are presented in Table 7.4. The experimental data exhibited good fits to the model with linear regression coefficients ranging from 0.9788 to 0.9587 (Table 7.4). It is evident from the table that the experimental and the calculated τ-values are very close to each other indicating that the Yoon–Nelson model fits excellently to the experimental data with high correlation coefficients (R^2). Yoon and Nelson model plots for various operating parameters such as effect of flow rate, initial concentration and bed height are shown in the Figure 7.7a, 7.7b and 7.7c respectively. The results in the figures clearly indicate that the model proposed by Yoon–Nelson provided a very good correlation with the experimental normalized concentration values at all RB dye concentrations and at all operating conditions.

It is important to note that all the three models are mathematically equivalent in which a similar fitting equation can be obtained from Equations (7.12, 7.14 and 7.16). From the experimental results and model predicted values, the model proposed by Yoon-Nelson provided a very good correlation at studied flow rate, initial concentration of dye and bed height.

7.5 SUMMARY

The H_3PO_4 treated followed by thermal activated Bael shell activated carbon was found to be very effective adsorbent for the efficient removal of RB dye from aqueous solutions in the fixed-bed column reactor. The maximum removal of RB dye in a

packed-bed adsorption column was found to be 179.8 mg/g at pH 3.5, at an initial adsorbate concentration of 200 mg/l, flow rate of 5 ml/min and bed height of 10 cm. The effect of different adsorption parameters like flow rate, adsorbate concentration and adsorbent bed height on the removal of RB dye was studied. The percentage removal of RB dye was found to increase with increase in bed height but decrease with increase in both adsorbate concentration and flow rate. The reverse trend was observed for the RB dye adsorption capacity of the adsorbent. BDST, Thomas and Yoon-Nelson models were applied to the experimental data obtained from dynamic studies performed in the fixed bed column to predict the breakthrough curves and to determine the characteristic parameters of the column. Prominent and unique characteristic features of the respective models like service time (Hutchins BDST model), adsorption capacity (Thomas model) and time for 50% breakthrough (Yoon-Nelson model) were determined by using linear regression technique. The experimental and predicted unique characteristics of the models were compared. From the regression coefficient analysis, it was found that the experimental data well fitted to the Yoon-Nelson model. From these studies it was found that the BSAC adsorption capacity of the present adsorbate is high and comparable to other similar adsorbents reported in literatures.

Chapter 7
Figures & Tables

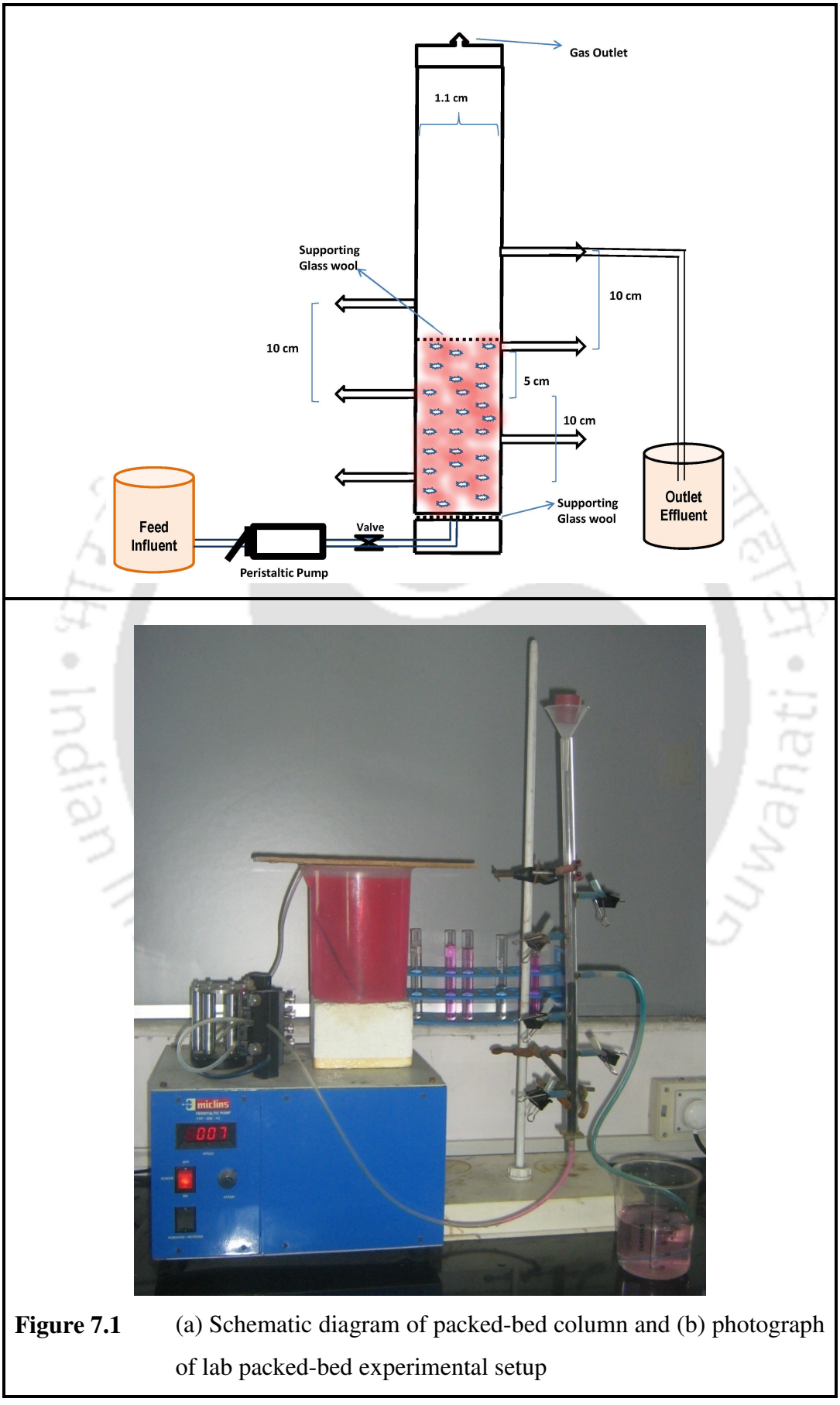

Figure 7.1 (a) Schematic diagram of packed-bed column and (b) photograph of lab packed-bed experimental setup

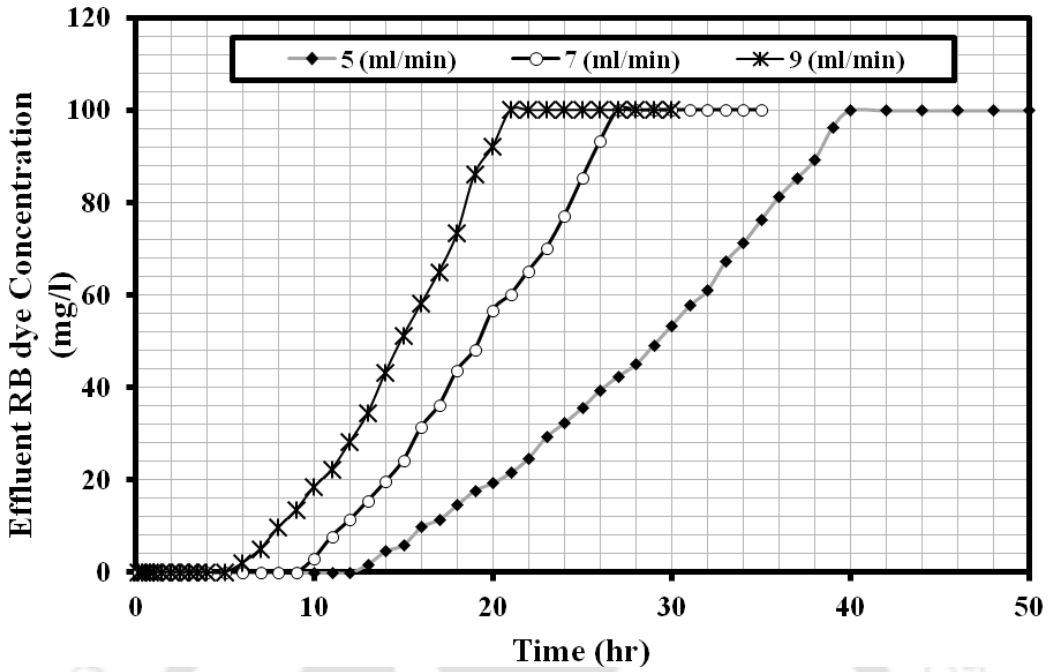

Figure 7.2a Effect of flow rate on RB dye adsorption (C_o = 100 mg/l, pH = 3.5, Bed Height = 10 cm)

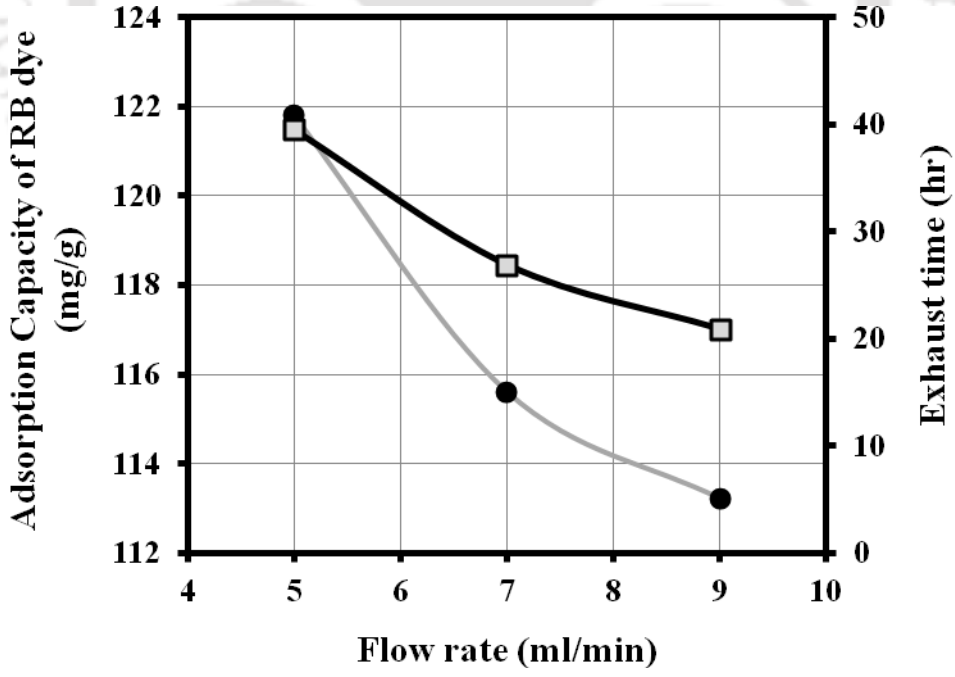

Figure 7.2b Effect of flow rate on RB dye adsorption capacity and Exhaust Time (C_o = 100 mg/l, pH = 3.5, Bed Height = 10 cm)

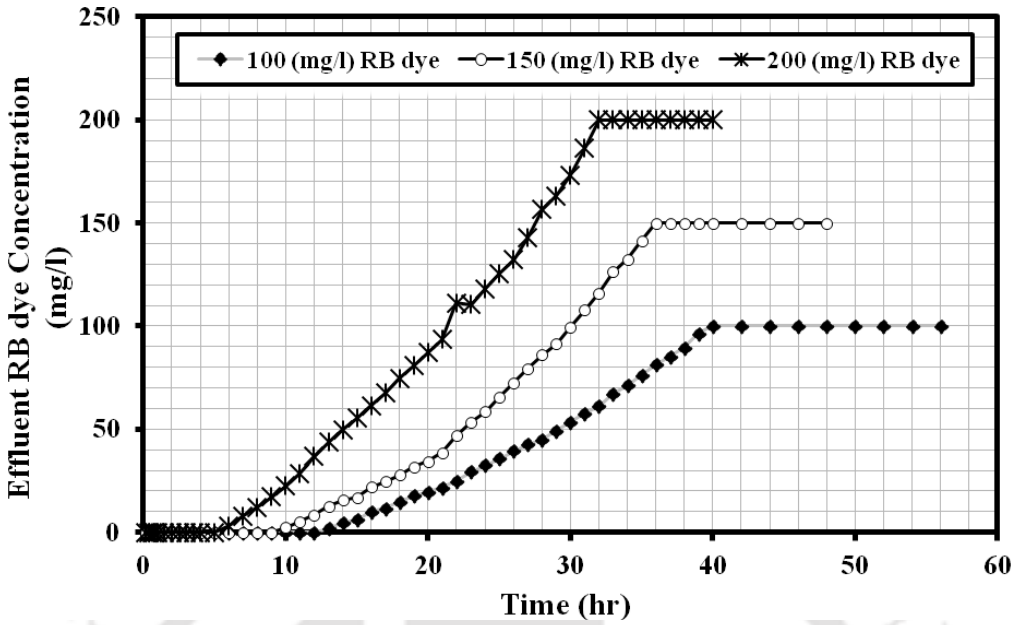

Figure 7.3 Effect of initial RB dye concentration on adsorption (F = 5 ml/min, pH = 3.5, Bed Height = 10 cm)

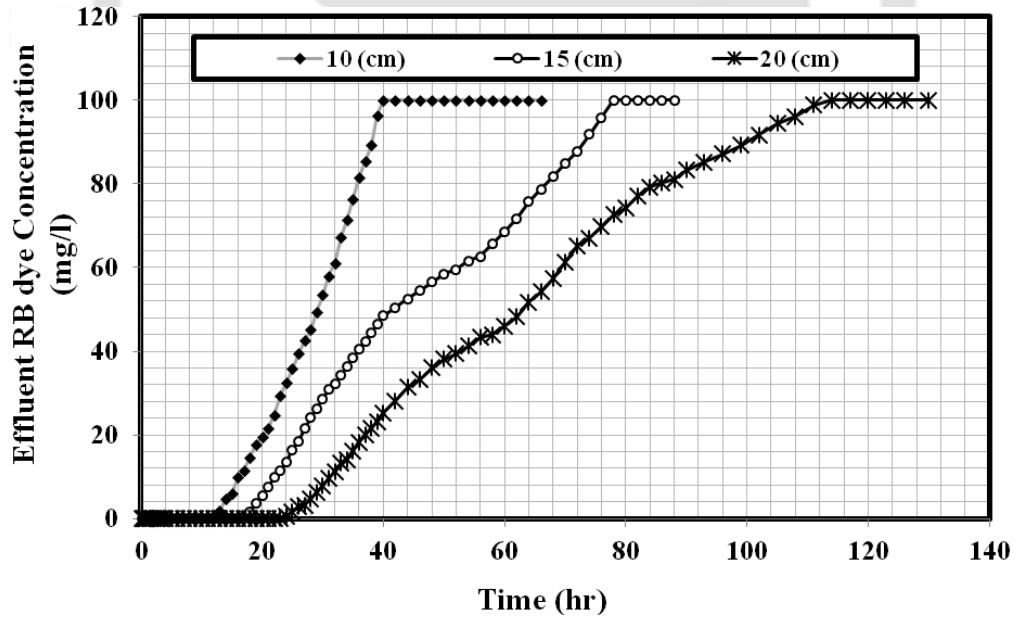

Figure 7.4 Effect of Bed Height on RB dye adsorption (F = 5 ml/min, pH = 3.5, C_o = 100 mg/l)

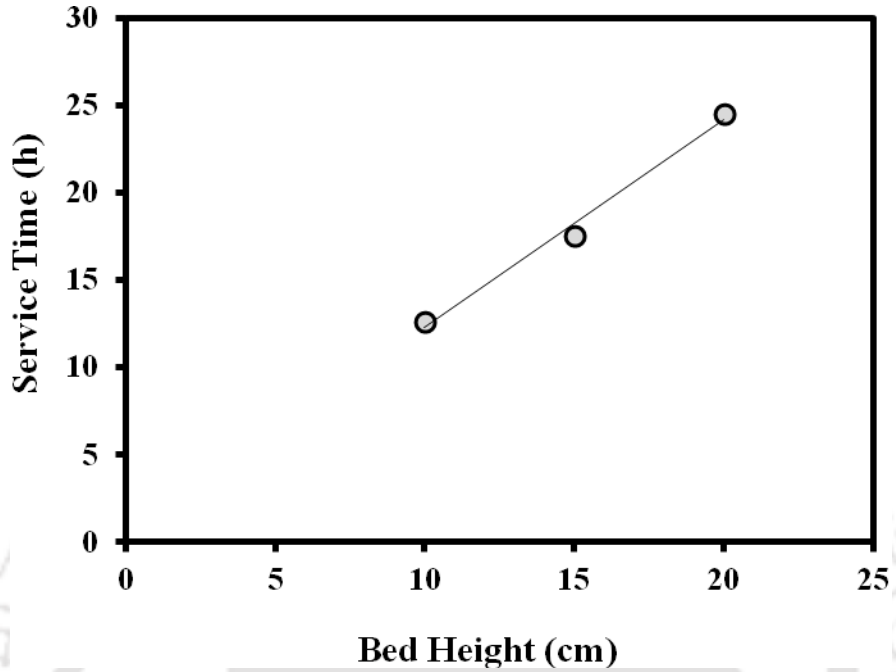

Figure 7.5 BDST model plot for RB dye adsorption (F = 5 ml/min, pH = 3.5, C_o = 100 mg/l)

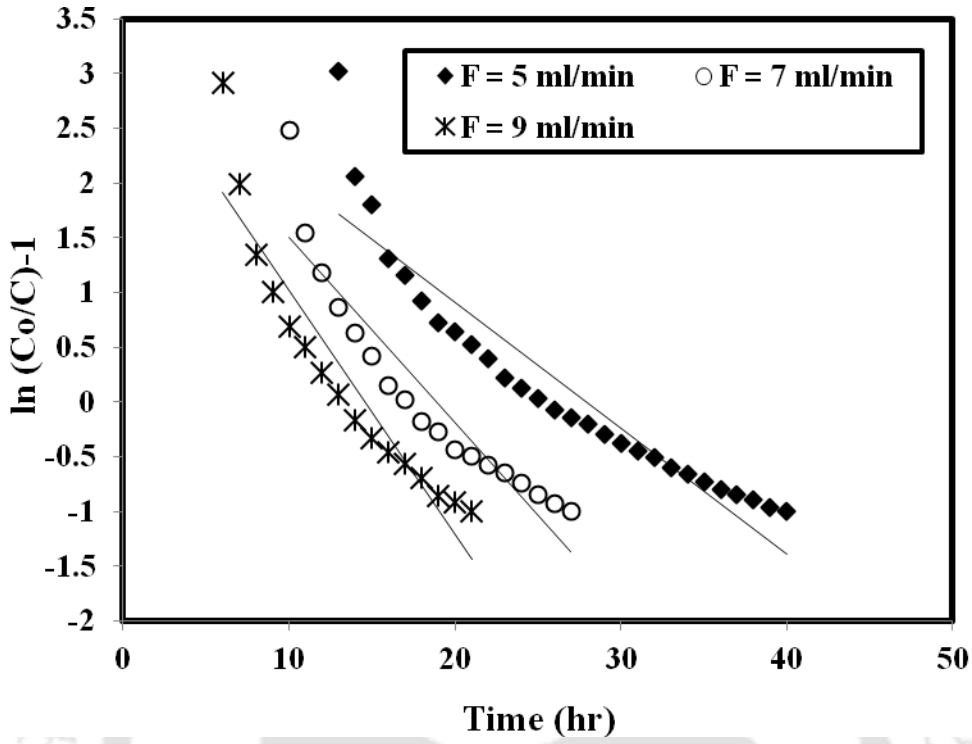

Figure 7.6a Effect of flow rate - Thomas model plot (C_o = 100 mg/l, Z = 10 cm and pH = 3.5)

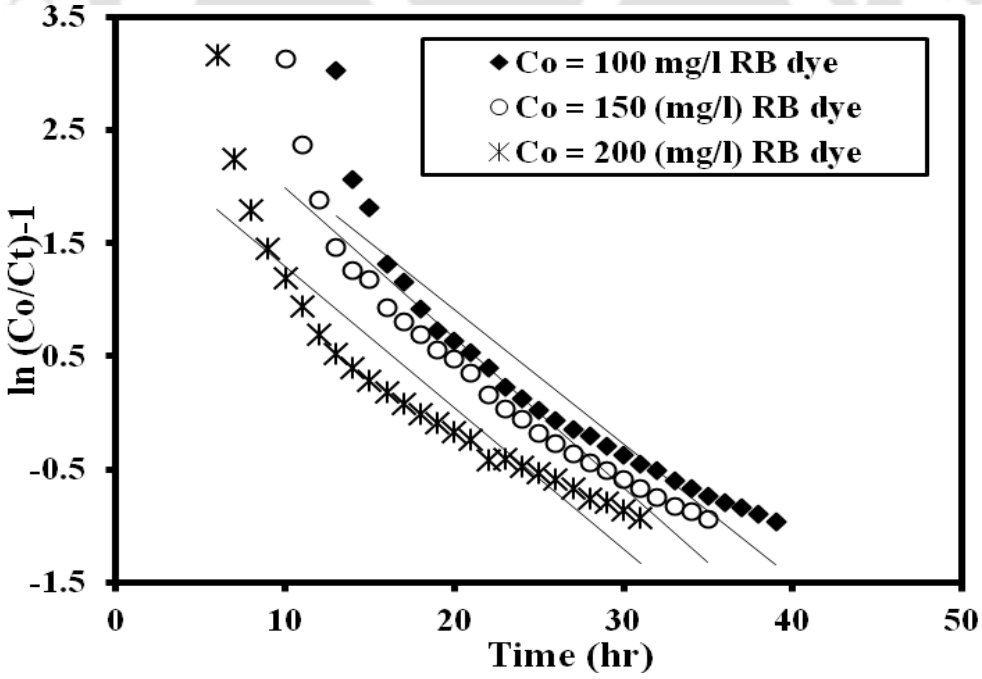

Figure 7.6b Effect of initial concentration - Thomas model plot (F = 5 ml/min, Z = 10 cm and pH = 3.5)

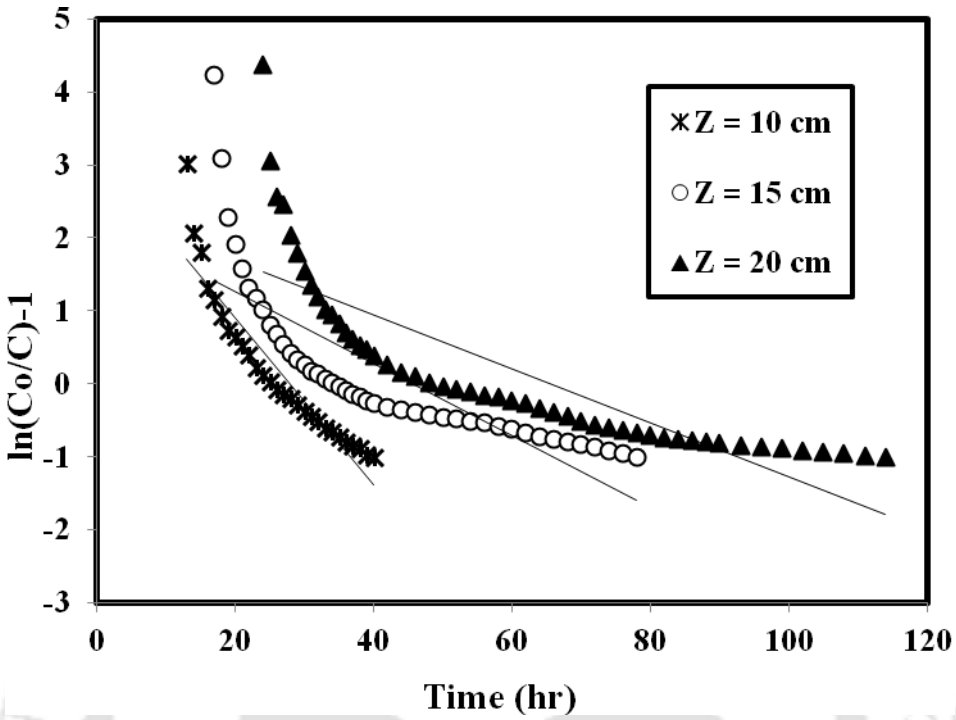

Figure 7.6c Effect of bed height - Thomas model plot (F = 5 ml/min, C_o = 100 mg/l and pH = 3.5)

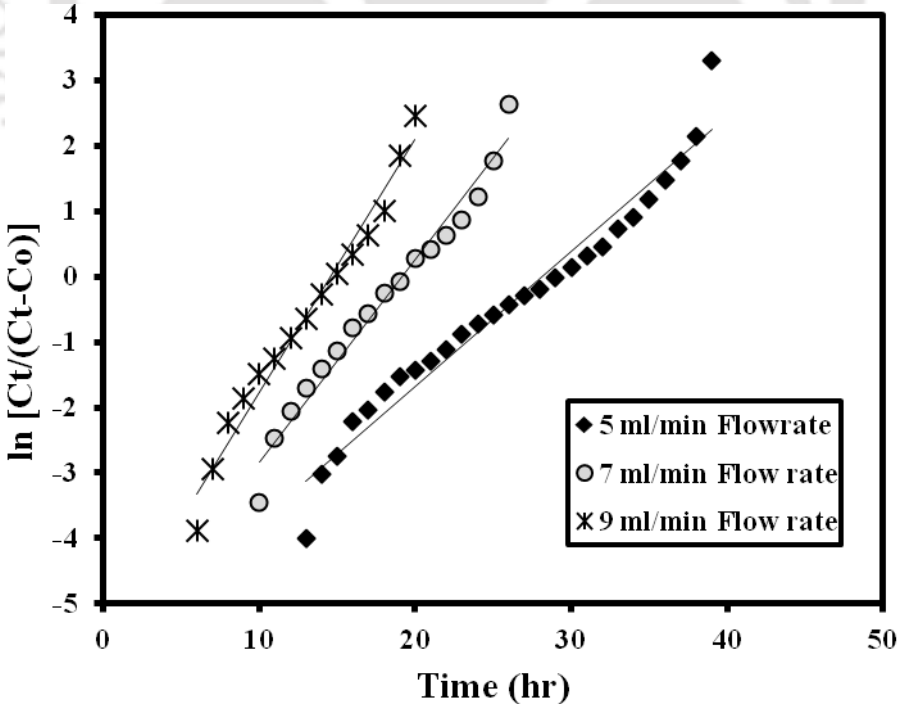

Figure 7.7a Effect of flow rate - Yoon and Nelson model plot (C_o = 100 mg/l, Z = 10 cm, pH = 3.5, pH = 3.5)

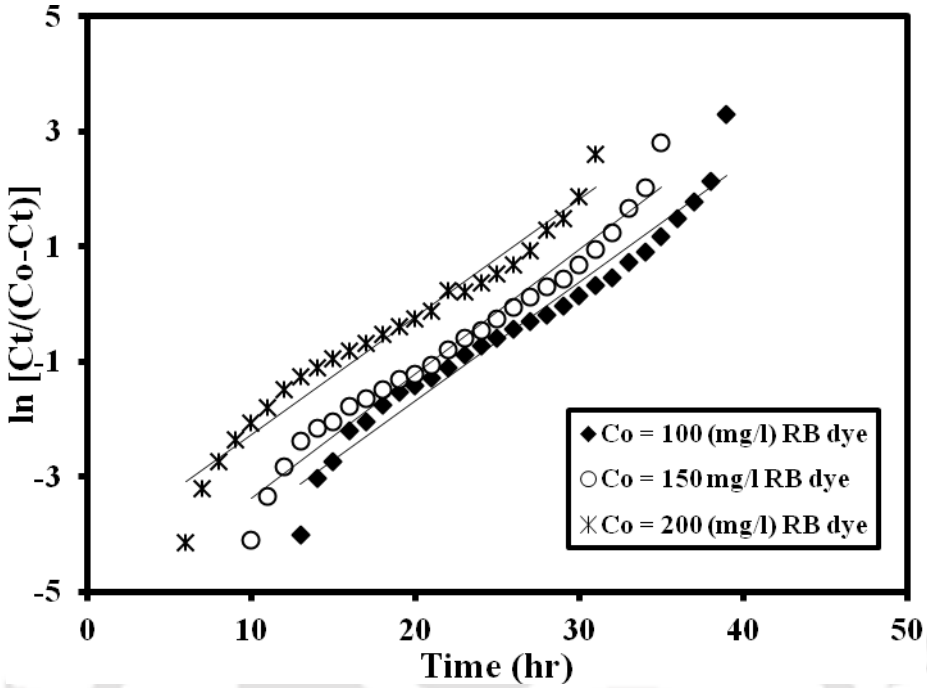

Figure 7.7b Effect of initial concentration - Yoon and Nelson model plot (F = 5 ml/min, Z = 10 cm and pH = 3.5)

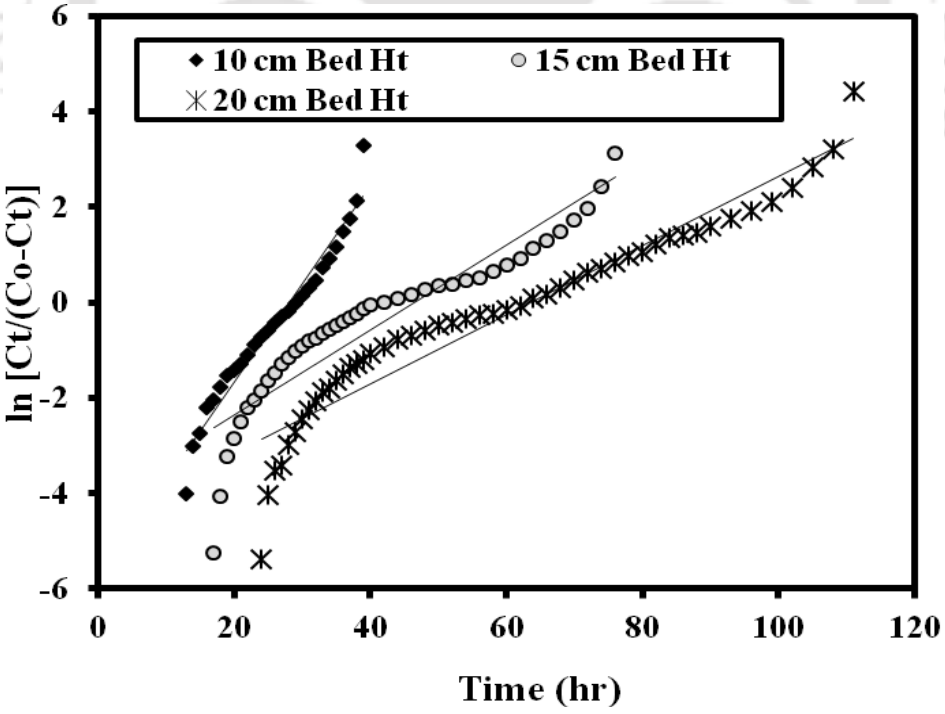

Figure 7.7c Effect of bed height - Yoon and Nelson model plot (F = 5 ml/min, C_o = 100 mg/l, pH = 3.5)

Table 7.1

Specifications of the packed-bed study

S. No	Parameters	Information
1.	**Adsorbent used**	BSAC (860 μm size)
2.	**Adsorbate concentration:**	Rhodamine B (RB) dye (100-200 mg/l)
3.	**Study temperature**	ambient temperature (24.3-25.4^{o}C)
4.	**Column details:**	Total height: 50 cm Internal diameter of column: 1.1 cm
5.	**Experimental conditions:**	**Flow rate used:** 5, 7 and 9 ml/min **Bed height used:** 10, 15 and 20 cm **Mass of bed:** 6.90, 10.49 and 13.42 g

Table 7.2

Different coefficients of BDST model

Concentration of dye, C_o (mg/l)	F (ml/min)	Z (cm)	N_o (mg/l)	$-K_a$ (l/ mg h)	R^2
100	5	10	3757	0.1313	0.9897
150	5	10	5635	0.0953	0.9897
200	5	10	7513	0.0756	0.9897
100	5	**10**	3757	0.1313	0.9897
100	5	**15**	2504	0.1313	0.9897
100	5	**20**	1878	0.1313	0.9897
100	**5**	10	3757	0.1313	0.9897
100	**7**	10	5259	0.1313	0.9897
100	**9**	10	6762	0.1313	0.9897

Note: C_b = assumed 1 mg/l

Table 7.3

Thomas model parameters

C_o (mg/l)	Z (cm)	F (ml/min)	K_{TH} (ml/min mg)	$q_{o,theo}$ (mg/g)	$q_{o,exp}$ (mg/g)	R^2
100	10	5	1.149×10^{-3}	121.1	121.8	0.8779
150	10	5	8.813×10^{-4}	163.3	164.4	0.9097
200	10	5	6.26×10^{-4}	176.7	179.8	0.8553
100	10	**5**	1.149×10^{-3}	121.1	121.8	0.8779
100	10	**7**	1.687×10^{-3}	114.8	115.6	0.8819
100	10	**9**	2.228×10^{-3}	113.9	113.2	0.8948
100	**10**	5	1.149×10^{-3}	121.1	121.8	0.8779
100	**15**	5	4.92×10^{-4}	130.5	127.9	0.966
100	**20**	5	3.69×10^{-4}	146.4	140	0.783

Table 7.4

Yoon and Nelson model parameters

C_o (mg/l)	F (ml/min)	Bed Height (cm)	K_{YN} (l/min)	τ (min)	$q_{o,exp}$ (mg/g)	$q_{o,theo}$ (mg/g)	R^2
100	5	10	0.2060	28.14	121.8	122.3	0.9778
150	5	10	0.2161	25.57	164.4	166.7	0.9705
200	5	10	0.2051	21.07	179.8	183.1	0.9587
100	5	**10**	0.2060	28.14	121.8	122.3	0.9778
100	5	**15**	0.0889	46.43	127.9	132.7	0.8598
100	5	**20**	0.0726	63.51	140	142	0.9170
100	**5**	10	0.2060	28.14	121.8	122.3	0.9778
100	**7**	10	0.3090	19.16	115.6	116.6	0.9721
100	**9**	10	0.3857	14.59	113.2	114.1	0.9760

CHAPTER 8

CONCLUSIONS AND RECOMMENDATION FOR FUTURE WORK

8.1 CONCLUSIONS

In this thesis, the possibilities to recycle two solid waste materials (Bael fruit shell and Tannery residual biomass) which are used in the ayurvedic and tannery industries as useful low-cost adsorbents to remove heavy metals, phenols and cationic dyes from wastewater in the single and multiple form with high efficiency have been discussed elaborately with the help of simple activation methods. Three types of activation methods such as thermal activation, chemical activation and thermochemical activation were employed to prepare high potential adsorbents. Initially, BET and ChemiSorb surface area analysis was carried out to optimize and identify the high surface area adsorbents in each activation method. Subsequently, preliminary performance evaluation test for various heavy metals, phenols and cationic dyes removal were carried out with the different optimized adsorbents.

High potential adsorbents to remove metals, phenols and dyes which are identified from the preliminary performance evaluation test are as follows:

(1) BSAC (H_3PO_4 with thermal activated bael shell)

(2) SBS (only H_2SO_4 activated bael shell)

(3) H-TRB (only HCl activated tannery residual biomass)

(4) TBAC (H_3PO_4 with thermal activated tannery residual biomass)

The maximum BET surface area obtained as 1954, 34.28, 10.42 and 892 m^2/g for BSAC, SBS, H-TRB and TBAC, respectively. After the activation, well developed honeycomb structured pores were observed on the surface of the adsorbents. Therefore, using the aforementioned four adsorbents the entire study to remove heavy metals and phenols and cationic dyes were carried out. Significant findings from this study are listed below.

8.1.1 Cr^{6+}, Sr^{2+}, phenol, *o*-cresol, RB and MB dye removal by BSAC:

- The maximum adsorption capacity of Cr^{6+}, phenol and RB dye was obtained at initial pH 2 (63.57 mg/g), blank (72.61mg/g) and 3.5 (199.74 mg/g), respectively. At lower pH 2.0 the surface of the activated carbon was more protonated and the competitive negative chromate ions ($HCrO_4^-$ and $Cr_2O_7^{2-}$) adsorption with positive surface ($-OH^+$) sites occurred through electrostatic interaction. At pH $\leq$ 3.5 RB molecules remain in monomeric form and thus dye molecule can easily enter into pore structure of the BSAC to enhance the pore diffusion. At pH above 3.5, zwitterionic form of RB in the water might increased the aggregation of RB (bigger molecule) to form the dimer and trimer molecules and thus unable to enter into the micro pore structure of the carbon.

- The maximum adsorption capacity of Sr^{6+}, *o*-cresol and MB dye was obtained at initial pH 6.7 (47.12 mg/g), 6-7 (132.54 mg/g) and 7 (193.81 mg/g), respectively. At alkaline pH, formation of metal precipitate reduced the Sr^{2+} adsorption efficiency. At alkaline pH, formation of metal precipitate, dye dissociation and repulsion of $C_6H_5O^-$ significantly reduced the Sr^{2+}, MB and *o*-cresol adsorption efficiency, respectively.

- The presence of NH_4^+, Ca^{2+}, F^-, and I^-, ions in Cr^{6+} solution significantly reduces the adsorption capacity of Cr^{6+} at higher concentrations, but no significant alteration in the adsorption capacity of Cr^{6+} was found when K^+, Na^+, and Cl^- ions were simultaneously present in the metal solution. The adsorption capacity of RB dye was not significantly affected by these co-ions. Whereas in phenol adsorption, NH_4^+ and NO_2^- ions considerably enhanced the

phenol adsorption on BSAC at their higher concentration and rest of the co-ions had no effect on phenol adsorption.

- The individual adsorption capacity of Cr^{6+}, Cr^{6+}, phenol, RB dye, Sr^{2+}, *o*-cresol and MB dye in their multi-contaminant system such as [(Cr^{6+} + RB dye) and (Cr^{6+} + phenol + RB dye)], (phenol + Cr^{6+}), [(RB dye + Cr^{6+}) and (RB dye + phenol)], [(Sr^{2+} + MB dye) and (Sr^{2+} + *o*-cresol + MB dye)], (*o*-cresol + Sr^{2+}) and [(MB dye + Sr^{2+}) and (MB dye + *o*-cresol)] decreased while compared to their single system.

- Among the four tested isotherm models (Langmuir, Freundlich, Temkin and Halsey), based on the linear correlation coefficients, equilibrium data fitted satisfactorily with the Langmuir model and monolayer sorption capacity obtained as 222.2-271, 304-256.41 and 434.8-471.70 mg/g for Cr^{6+}, phenol and RB dye at 30-50ºC, respectively. However, Langmuir and Freundlich models were fitted for Sr^{2+} (113.38-106.49 mg/g), *o*-cresol (243.31-233.10 mg/g) and MB dye (476.19-510.20 mg/g) adsorption onto BSAC at 30-50ºC. More over BSAC is competitive in comparison with other recently literature reported and commercially available adsorbents for Cr^{6+}, Sr^{2+}, phenol, *o*-cresol, MB and RB dye.

- The positive $\Delta H°$ values confirmed that the Cr^{6+}, MB and RB dye adsorption process was endothermic. However, the negative value of $\Delta H°$ for Sr^{2+}, phenol and o-cresol adsorption indicates the exothermic nature of adsorption and uptake of Sr^{2+}, phenol and o-cresol is probably due to the physisorption effect.

- Cr^{6+} removal by BSAC at pH 2.0 occurred through direct and indirect reduction mechanism of Cr^{6+} to Cr^{3+}. The intermolecular binding (ion–dipole) mechanism was suggested for Sr^{6+} removal. But both pore diffusion and surface diffusion mechanism were responsible for MB and RB dye adsorption.

8.1.2 Pb^{2+}, Ni^{2+}, Sr^{2+}, MB and RB dye removal by SBS adsorbent:

- The maximum adsorption capacities of Pb^{2+}, Ni^{2+} and Sr^{2+} was obtained at pH 5.2 (82.9 mg/g), 5.8 (54.89 mg/g) and 6.8 (72.95 mg/g), respectively. At pH

>6 and pH >7, Pb^{2+} and Ni^{2+} and Sr^{2+} ions were precipitated as insoluble hydroxides that causes the reduction of adsorption. Maximum adsorption capacities of MB and RB dye was observed at pH 6-8 (82.9 mg/g) and 3.5-4 (54.89 mg/g), respectively. The slight reduction of MB and RB dye adsorption at pH >8 was due to the competitive adsorption of OH^- ions and dye.

- Adsorption sorption capacity of Pb^{2+}, Ni^{2+} and Sr^{2+} decreased with increase in the concentration of other ions such as K^+, Na^+, NH_4^+ and Ca^{2+} from 0.5 to 20 g/l. However, adsorption capacity of MB and RB dye did not change significantly when these ions were simultaneously present in the solution.

- The individual adsorption capacity of Pb^{2+}, Ni^{2+} and Sr^{2+} decreased in their binary [(Pb^{2+}+Ni^{2+}), (Pb^{2+}+Sr^{2+}) and (Ni^{2+}+Sr^{2+}) and ternary (Pb^{2+}+Ni^{2+}+Sr^{2+})] system at every concentration range while compared with their single metal adsorption and the behaviour was antagonistic. However, in the binary system, the overall unit metal adsorption capacity of adsorbent (combined sorption capacity of two metals) increased as compared with the single metal system.

- Among the four tested isotherm models, based on the linear correlation coefficients, equilibrium data fitted well with the Langmuir model and monolayer sorption capacity obtained as 122.70-117.25, 70.18-72.25 and 86.73-78.74 mg/g for Pb^{2+}, Ni^{2+} and Sr^{2+} at 30-50ºC, respectively. However, Langmuir and Freundlich models were fitted for MB (196.1-256.41 mg/g) and RB dye (221.24-255.75 mg/g) adsorption onto SBS at 30-50ºC. As observed, the Cr^{6+}, Sr^{2+}, phenol, *o*-cresol, MB and RB dye sorption capacity of SBS is competitive in comparison with other reported adsorbents in the literature. In addition, the SBS can remove the toxic Pb^{2+}, Ni^{2+} and Sr^{2+} ions in single, binary and ternary metal system with high efficiency.

- The negative $\Delta H°$ values confirmed that the Pb^{2+} and Sr^{2+} metal adsorption process was exothermic. However, the positive value of $\Delta H°$ for Ni^{2+}, MB and RB dye adsorption indicates the endothermic nature of adsorption. Pseudo-second-order rate equation could describe the single metal system with

extremely high correlation coefficients (R^2) highlighting the rate controlling mechanism.

- Two possible metal binding mechanisms such as intermolecular binding (ion–dipole) of Pb^{2+} and Sr^{2+} and intermolecular binding coupled with intra-molecular binding of Ni^{2+} was suggested with cellulosic and lignin molecules.

8.1.3 Cr^{6+}, MB and RB dye removal by HTB adsorbent:

- The maximum removal of Cr^{6+}, MB and RB dye occurred at initial pH 2.0 (142.45), 6-7 (196.63 mg/g) and 3.5 (146.8), respectively.

- The percentage adsorption of Cr^{6+} decreased when other co-ions such as Na^+, Ca^{2+}, and NH_4^+ were present in the metal solution and but no significant impact was found on the adsorption of both dyes.

- Langmuir isotherm model best fitted the experimental data with high R^2 value rather than other three studied models for Cr^{6+}, MB and RB dye adsorption onto HTB. Monolayer sorption capacity obtained as 177.3-217.4, 480.8-518.1 and 212.8-250 mg/g for Cr^{6+}, MB and RB dye adsorption at 30-50ºC, respectively.

- The kinetic model that best fits the experimental data with high R^2 value for two models was the pseudo-second order model. Moreover, its calculated theoretical values of Cr^{6+}, MB and RB dye adsorption were closely fitted with the experimental data. Thus, the pseudo-second-order kinetics was predominant, and that the overall rate of metal as well as dye adsorption process was largely controlled by the chemisorption process.

- The negative values of ΔG° increased with increase in temperatures. This indicates the spontaneous nature of the adsorption process. The positive ΔH° values confirmed that the Cr^{6+}, MB and RB dye adsorption process was endothermic. The positive value of ΔS^o showed the increased randomness at the solid–solution interface during adsorption.

- Two possible mechanisms such as direct and indirect reduction of Cr^{6+} to Cr^{3+} were identified for Cr^{6+} removal with the help of XPS analysis. Monomeric pore diffusion and the surface diffusion mechanisms were suggested for RB and MB dye adsorption.

8.1.4 Cr^{6+}, *o*-cresol and RB dye removal by TBAC adsorbent:

- The maximum removal of Cr^{6+} (100 mg/l), *o*-cresol (200 mg/l) and RB dye (200 mg/l) was occurred at initial pH 2.0 (60.98), 6-7 (196.6 mg/g) and 3.5 (175.4), respectively.

- The presence of NH_4^+, Ca^{2+}, F^-, and I^-, ions in Cr^{6+} solution considerably reduced the adsorption capacity of Cr^{6+} at higher concentrations, but no significant change in the adsorption capacity of Cr^{6+} was found when K^+, Na^+, and Cl^- ions were simultaneously present in the metal solution. The adsorption capacity of RB dye was not considerably affected by these co-ions. Whereas in *o*-cresol adsorption, NH_4^+ and NO_2^- ions slightly enhanced the *o*-cresol adsorption on TBAC at their higher concentration and rest of the co-ions had no effect on phenol adsorption.

- The individual adsorption capacity of Cr^{6+}, *o*-cresol and RB dye in their multi-contaminant system decreased when compared to their single system.

- Langmuir and Freundlich model fitted well than other three analysed isotherm models. The monolayer adsorption capacity obtained as 168.4-217.7, 200.4-172.1 and 373.1-416.7 mg/g for Cr^{6+}, *o*-cresol and RB dye adsorption at 30-50ºC, respectively. The sorption capacity of Cr^{6+}, *o*-cresol and RB dye onto TBAC is competitive in comparison with other recently literature reported. Furthermore, the TBAC simultaneously can remove the toxic Cr^{6+}, *o*-cresol and RB dye in multi-contaminant system with high efficiency.

- Pseudo second-order adsorption kinetics could describe the rate-controlling mechanism of Cr^{6+}, *o*-cresol and RB dye with extremely high correlation coefficients (R^2) compared to pseudo first-order kinetics.

- The positive ΔH^{o} values of Cr^{6+} and RB dye showed that the adsorption process was endothermic and the negative value of ΔH° for *o*-cresol adsorption indicated the exothermic nature of adsorption.

- The binding mechanism of Cr^{6+} is principally based on ionic equilibrium between Cr^{6+} and Cr^{3+}. Cr^{6+} removal by TBAC at pH 2.0 occurred through direct and indirect reduction mechanism of Cr^{6+} to Cr^{3+}. The *o*-cresol had many possible interactions with TBAC such as hydrophobic effect and ion-dipole interaction, electron donor-acceptor interaction and hydrogen bonding, electrostatic interaction and π-π interactions. The monomeric form of RB molecules at pH 3.5 enhances both pore diffusion and surface adsorption.

8.1.5 Packed-bed study for RB dye removal by BSAC:

- From the results of packed-bed study of RB dye adsorption by BSAC, it was found that the experimental data were well fitted to the Yoon-Nelson model using regression coefficient analysis. The maximum removal of RB dye was found to be 179.8 mg/g at pH 3.5, at an initial adsorbate concentration of 200 mg/l, flow rate of 5 ml/min and bed height of 10 cm.

In this work, thermal activated BS and TB having maximum BET surface area of 25.81 m^2/g (1.5 hr at 300°C) and 21.26 m^2/g (1.5 hr at 400°C), respectively and low adsorption capacity with studied metals, phenols and dyes. The chemical activated (KOH, HCl, H_2SO_4 and H_3PO_4) BS and TB having the surface area of (13.44, 6.871, 34.28 and 12.62 m^2/g) and (12.61, 10.42, 21.35 and 9.327 m^2/g). The maximum BET surface area of (KOH + thermal), (HCl + thermal), (H_2SO_4 + thermal) and (H_3PO_4 + thermal) activated BS was 39.73, 322.2, 26.37 and 1954 m^2/g at their optimum impregnation ratio, activation temperature and time. But the thermochemically activated TB [(KOH + thermal), (HCl + thermal), (H_2SO_4 + thermal) and (H_3PO_4 + thermal)] surface area was quite low [23.52, 26.37, 17.61 and 892.6 m^2/g] compared with thermochemically activated BS.

The Cr^{6+} adsorption capacity was very high for BSAC (222.2 mg/g), HTB (177.3 mg/g) and TBAC (168.9 mg/g) when compared to all other synthesized adsorbents. The maximum adsorption capacity of Pb^{2+}, Ni^{2+} and Sr^{2+} was 122.7, 70.18 and 113.4

mg/g, respectively for SBS. The maximum removal of phenol (304 mg/g) and *o*-cresol (243.3 mg/g) was obtained using BSAC. The RB and MB dye adsorption affinity order was found as [BSAC (434.8 mg/g) > TBAC (373.1 mg/g) > SBS (221.2 mg/g) and > HTB (212.8 mg/g)] and [HTB (480.8 mg/g) > BSAC (476.2 mg/g) and > SBS (330 mg/g)], respectively. The obtained results demonstrated that BSAC having the maximum BET surface area (1954 m^2/g) and adsorption capacities with most of the studied adsorbates when compared with all other synthesized adsorbents.

The results from this work indicate that BSAC (H_3PO_4 with thermal activated bael shell), TBAC (H_3PO_4 with thermal activated tannery residual biomass), HCl modified TB (HTB) could be employed as a very good low-cost adsorbent for the removal of both Cr^{6+}, phenol, *o*-cresol, MB and RB dyes in single and multiple form from the aqueous solution including tannery wastewater. Besides, SBS (only H_3PO_4 treated bael shell) can also be suggested for the removal other heavy metals such as Pb^{2+}, Ni^{2+} and Sr^{2+} from the aqueous solution with high efficiency compared to the literature and commercially available adsorbents in single and multiple form. Finally, we strongly suggest that tannery residual biomass and waste bael fruit shell could be recycled as efficient adsorbents to remove toxic heavy metals, phenols and cationic dyes which are used in the industries especially in tanneries.

8.2 RECOMMENDATION FOR FUTURE WORK

Based on the findings of the present investigation, the following suggestions are made for future studies:

1) Studies with real industrial wastewater to evaluate and optimize continuous packed-bed study for commercial application.
2) Estimation of kinetic and thermodynamic parameters in multi-contaminant system and the identification of mechanisms in multi-contaminant system.
3) To carry out pilot scale column study with objective of removing multi-contaminants effectively.
4) Study on removal of other unexplored industrially important heavy metal ions, dyes and other phenolic compounds in batch and column mode with the synthesized adsorbents.
5) Desorption properties of synthesized adsorbents at various temperatures and the reusable capacities with the targeted pollutant.

REFERENCES

Agrawal, A., Pal, C. and Sahu, K.K. Extractive Removal of Chromium(VI) from Industrial Waste Solution. *Journal of Hazardous Materials,* 159 **(2008)** 458–464.

Ahmaruzzaman, M. A review on the utilization of fly ash. *Progress in Energy and Combustion Science,* 36 **(2010)** 327–363.

Ahmaruzzaman, M. Adsorption of phenolic components on low-cost adsorbents- A review. *Advances in Colloidal and Interface Science,* 36 **(2010)** 327–363.

Ahmaruzzaman, M. and Sharma, D.K. Adsorption of phenols from wastewater. *Journal of Colloid and Interface Science,* 287 **(2005)** 14–24.

Ahmadpoura, A., Zabihi, M., Tahmasbi, M. and Bastami, T.R. Effect of adsorbents and chemical treatments on the removal of strontium from aqueous solutions. *Journal of Hazardous Materials,* 182 **(2010)** 552–556.

Aksu, Z. and Tezer, S. Biosorption of reactive dyes on the green alga *Chlorella vulgaris*. *Process Biochemistry,* 40 **(2005)** 1347–1361.

Aksu, Z., Kutsal, T., Gun, S., Haciosmanoglu, N. and Gholaminejad, M. Investigation of biosorption of Cu(II), Ni(II) and Cr(VI) ions to activated sludge bacteria. *Environmental Technology,* 12 **(1991)** 915–21.

Aksu, Z. Application of biosorption for the removal of organic pollutants: a review. *Process Biochemistry,* 40 **(2005)** 997–1026.

Aksu, Z. and Gonen, F. Bio sorption of phenol immobilized activated sludge in a continuous packed bed: prediction of breakthrough curves. *Process Biochemistry,* 39 **(2004)** 599–613.

Aksu, Z. and Tezer, S. Equilibrium and kinetic modelling of biosorption of Remazol Black B by R. arrhizus in a batch system: effect of temperature. *Process Biochemistry*, 36 **(2000)** 431–439.

Al-Asheh, S., Banat, F. and Abu-Aitah, L. Adsorption of phenol using different types of activated bentonites. *Separation and Purification Technology,* 33 **(2003)** 1–10.

Al-Asheh, S. and Duvnjak, Z. Sorption of cadmium and other heavy metals by pine bark. *Journal of Hazardous Materials,* 56 **(1997)** 35–51.

Al-Ghouti, M.A. Li, J., Salamh, Y., Al-Laqtah, N., Walker, G. and Ahmad, M.N.M. Adsorption mechanisms of removing heavy metals and dyes from aqueous solution using date pits solid adsorbent. *Journal of Hazardous Materials,* 176 **(2010)** 510–520.

Allen, S.J., Gan, Q., Matthews, R., Pauline A. and Johnson, P.A. Comparison of optimised isotherm models for basic dye adsorption by kudzu. *Bioresource Technology,* 88 **(2003)** 143–152.

Al-Rub, F.A.A., El-Naas, M.H., Benyahia, F. and Ashour, I. Biosorption of nickel on blank alginate beads, free and immobilized algal cells. *Process Biochemistry,* 39 **(2004)** 1767–1773.

Alnaizy, R. and Akgerman, A. Advanced oxidation of phenolic compounds. *Advances in Environmental Research,* 4 **(2000)** 233–244.

Amarasinghe, B.M.W.P.K. and Williams, **R.A.** Tea waste as a low cost adsorbent for the removal of Cu and Pb from wastewater. *Chemical Engineering Journal,* 132 **(2007)** 299–309.

Anandkumar, J. and Mandal, B. Single, Binary and Ternary Metal Adsorption Using Acid-Treated *Aegle marmelos* Correa Shell: Kinetic, Mechanistic and Thermodynamic Studies. *Asia-Pacific Journal of Chemical Engineering*, **(2012)** *doi: 10.1002/apj.1612*.

Anandkumar, J. and Mandal, B. Removal of Cr(VI) from aqueous solution using Bael fruit *(Aegle marmelos correa)* shell as an adsorbent. *Journal of Hazardous Materials,* 168 **(2009)** 633–640.

Anandkumar, J. and **Mandal, B**. Adsorption of Chromium (VI) and Rhodamine B by Surface Modified Tannery Waste: Kinetic, Mechanistic and Thermodynamic Studies. *Journal of Hazardous Materials,* 186 **(2011)** 1088–1096.

Annadurai, G., Juang, R. and Lee, D. Use of cellulose-based wastes for adsorption of dyes from aqueous solutions. *Journal of Hazardous Materials,* 92 **(2002)** 263–274.

Anon., Heavy Metal Removal by Try starch xanthate. *Product Finishing,* 31 **(1978)** 72–74.

Arbeloa, L. and Ojeda, P.R. Dimeric States of Rhodamine B. *Chemical Physics Letters,* 87 **(1982)** 6.

Archibald, F. and Roy, B. Production of marganic chelates by laccase from the lignin degrading fungus Trametes versicolor. *Applied and Environmental Microbiology,* 58 **(1992)** 1496–1499.

Aygun, A., Yenisoy-Karakas, S. and Duman, I. Production of granular activated carbon from fruit stones and nutshells and evaluation of their physical, chemical and adsorption properties. *Microporous Mesoporous Mater,* 66 **(2003)** 189–195.

Argun, M.E. and Dursun, S. A new approach to modification of natural adsorbent for heavy metal adsorption. *Bioresource Technology,* 99 **(2008)** 2516–2527.

Azam, T., Din, M., Hameed, B.H. and Ahmad, A.L. Batch adsorption of phenol onto physiochemical-activated coconut shell. *Journal of Hazardous Materials,* 161 **(2009)** 1522–1529.

Bahnemann, D.W. Photocatalytic water treatment: solar energy applications. *Solar Energy,* 77 **(2004)** 445–459.

Bai, J., Wen, J.P., Li, H.M. and Jiang Y. Kinetic modeling of growth and biodegradation of phenol and *m*-cresol using *Alcaligenes faecalis*. *Process Biochemistry,* 42 **(2007)** 510–517.

Banat, I.M., McMullan, G., Meehan, C., Kirby, N., Nigam, P., Smyth, W.F. and Marchant, R. Microbial decolorization of textile dyes present in textile industries effluueunt. In: *Proceedings of the Industrial Waste Technical Conference*, Indianapolis, USA **(1999)** 1–16.

Banat, I.M., Nigam, P., McMullan, G., Marchant, R. and Singh, D. The isolation of thermophilic bacterial cultures capable of textile dyes decolorization. *Environment International,* 23 **(1997)** 547–551.

Banat I.M., Nigam P., Singh D. and Marchant R. Microbial decolourization of textile-dye containing effluents: a review. *Bioresource Technology,* 58 **(1996)** 217–227.

Banat, F.A. and Al-Asheh, S. Biosorption of phenol by chicken feathers, *Environmental Engineering and Policy,* 2 **(2000)** 85-90.

Baral, S.S. Adsorption of Hexavalent Chromium from Aqueous Solution using Various Adsorbents. Ph.D Thesis, National Institute of Technology, Rourkela, India, **2007**.

Baral, S.S., Das, S.N. and Rath, P. Hexavalent chromium removal from aqueous solution by adsorption on treated sawdust. *Biochemical Engineering Journal,* 31 **(2006)** 216–222.

Barr, D.P. and Aust, S.D. Mechanisms white rot fungi use to degrade pollutants. *Environmental Science & Technology,* 28 **(1994)** 320–328.

Barrera, H. Nunez, F.U., Bilyeu, B. and Diaz, C.B. Removal of chromium and toxic ions presents inmine drainage by *Ectodermis of Opuntia*. *Journal of Hazardous Materials,* B136 **(2006)** 846–853.

Bhat, R.V. and Mathur, P. Changing scenario of food colours in India. *Current Science,* 74 **(1998)** 198–202.

Bhatnagar, A. and Jain, A.K. A comparative adsorption study with different industrial wastes as adsorbents for the removal of cationic dyes from water. Journal of Colloidal Interface Science, 281 **(2005)** 49-55.

Bohart, G.S. and Adams, E.O. Some aspects of the behaviour of charcoal with respect to chlorine. *Journal of the American Chemical Society,* 43 **(1920)** 545–523.

Boeniger, M.F. Carcinogenicity of Azo Dyes Derived From Benzidine, Department of Health and Human Services (NIOSH), Cincinnati (**1980)** Pub. No. 8-119.

Boudenne, J., Cercleir, O., Galéa, J. and Van Der Vlist, E. Electrochemical oxidation of aqueous phenol at a carbon black slurry electrode. *Applied Catalysis A: General,* 143 **(1996)** 185-202.

Briglia, M., Nurmiaho-Lassila, E.L., Vallini, G. and Salkinoja-Salonen, M.S. The survival of the pentachlorophenol-degrading *Rhodococcus chlorophenolicus* PCPol and *Flavobacterium* sp. in natural soil. *Biodegradation,* 1 **(1990)** 273–281.

Brillas, E., Sauleda, R. and Casado, J. Degradation of 4-chlorophenol by anodic oxidation, electro-Fenton, photo electro-Fenton and peroxicoagulation processes. *Journal of the Electrochemical Society,* 145 **(1998)** 2253–2262.

Buscaa, G., Berardinelli, S., Resini, C. and Arrighib, L. Technologies for the removal of phenol from fluid streams: A short review of recent developments. *Journal of Hazardous Materials,* 160 **(2008)** 265–288.

Calleja, G., Serna, J. and Rodríguez, J. Kinetics of adsorption of phenolic compounds from wastewater onto activated carbon. *Carbon,* 31 **(1993)** 691–697.

Carliell, C.M., Barclay, S.J. and Buckley, C.A. Treatment of exhausted reactive dye bath e.uent using anaerobic digestion: laboratory and full scale trials. *Water S.A.,* 22 **(1996)** 225–233.

Case, O.P. Metallic recovery from wastewaters utilising cementation, EPA-270/2-74-008, U.S. Washington DC **(1974).**

Chegrouche, S., Mellah, A. and Barkat, M. Removal of strontium from aqueous solutions by adsorption onto activated carbon: kinetic and thermodynamic studies. *Desalination,* 235 **(2009)** 306–318.

Chiron, N., Guilet, R. and Deydier, E. Adsorption of Cu(II) and Pb(II) onto a grafted silica: isotherms and kinetic models. *Water Research,* 37 **(2003)** 3079–3086.

Choong, T.S.Y., Chuah, T.G., Robiah, Y., Koay, F.L.G. and Azni, I. Arsenic toxicity, health hazards and removal techniques from water: an overview. *Desalination,* 217 **(2007)** 139–166.

Choy, K.K.H., McKay, G. and Porter, J.F. Sorption of acid dyes from effluent using activated carbon. *Resources*, *Conservation and Recycling,* 27 **(1999)** 57–71.

Chu, H.C. and Chen, K.M. Reuse of activated sludge biomass: I. Removal of basic dyes from wastewater by biomass. *Process Biochemistry,* 37 **(2002)** 595–600.

Chuah, T.G., Jumasiah, A., Azni, I., Katayon, S. and Choong, S.Y.T. Rice Husk as a Potentially Low-Cost Biosorbent for Heavy Metal and Dye Removal: an Overview. *Desalination,* 175 **(2005)** 305–316.

Chung, T.P., Tseng, H.Y. and Juang, R.S. Mass transfer and intermediate detection for phenol degradation in immobilized pseudomonas putida systems. *Process Biochemistry,* 38 **(2003)** 1497–1507.

Clarke, E.A. and Anliker, R. Organic dyes and pigments. In: Handbook of environmental chemistry, anthropogenic compounds, part A. New York: Springer-Verlag, 3 **(1980)** 181–215.

Connell, D.W., Birkinshaw, C. and O'Dwyer, T.F. Heavy metal adsorbents prepared from the modification of cellulose: A review. *Bioresource Technology*, 99 **(2008)** 6709–6724.

Connell, D.W. and Miller, G.J. *Chemistry and Ecotoxicology of Pollution*. John Wiley & Sons, NY **(1984)**.

Costan, G., Bermingham, N., Blaise, C. and Ferard, J.F. Potential eco–toxic effect probe (PEEP); a novel index to assess and compare the toxic potential of industrial effluents. *Environmental toxicology,* 8 **(1993)** 115–140.

Cook, S.M.F. and Linden, D.R. Use of rhodamine WT to facilitate dilution and analysis of atrazine samples in short-term transport studies. *Journal of Environmental Quality,* 26 **(1997)** 1438–1441.

Couglin, R.W. and Ezra, F.S. Role of surface acidity in the adsorption of organic pollutants on the surface. *Environmental Science and Technology,* 2 **(1968)** 291–297.

Crini, G. Recent developments in polysaccharide-based materials used as adsorbents in wastewater treatment. *Progress in Polymer Science,* 30 **(2005)** 38–70.

Cruz C.C.V., Costa A.C.A., Henriques C.A. and Luna, A.S. Kinetic modeling and equilibrium studies during cadmium biosorption by dead *Sargassum* sp. biomass. *Bioresource Technology,* 91 **(2004)** 249-257

Dabrowski, A. Adsorption from theory to practice. *Advances in Colloidal and Interface Science,* 93 **(2001)** 135–224.

Da Costa, A.C.A. An emerging biotechnology for metal containing waste water treatment. *Série Tecnologia Ambiental* 17, MCT-CNPq-CETEM, 100 p.

Dakiky, M., Khamis, M., Manassra, A. and Mer'eb, **M.** Selective adsorption of chromium(VI) in industrial wastewater using low-cost abundantly available adsorbents. *Advances in Environmental Research,* 6 **(2002)** 533–540.

Daneshvar, N., Aleboyeh, A. and Khataee, A.R. The evaluation of electrical energy per order (E_{Eo}) for photooxidative decolorization of four textile dye solutions by the kinetic model. *Chemosphere,* 59 **(2005)** 761–767.

Daneshvar, N., Salari, D. and Aber, S. Chromium adsorption and Cr(VI) reduction to trivalent chromium in aqueous solutions by soya cake. *Journal of Hazardous Materials,* B94 **(2002)** 49–61.

Dargaville, T.R., Guerzoni, F.N., Looney, M.G. and Solomon D.H. The adsorption of multinuclear phenolic compounds on activated carbon. *Journal of Colloid and Interface Science,* 182 **(1996)** 17-25.

Demirbas, E., Kobya, M. and Sulak, M.T. Adsorption kinetics of a basic dye from aqueous solutions onto apricot stone activated carbon. *Bioresource Technology,* 99 **(2008)** 5368–5373.

Demirbas, A., Pehlivan, E., Gode, F., Altun, T. and Arslan, G. Adsorption of Cu(II), Zn(II), Ni(II), Pb(II), and Cd(II) from aqueous solution on Amberlite IR-120 synthetic resin. *Journal of Colloidal and Interface Science,* 282 **(2005)** 20–25.

Demiral, H., Demiral, I., Tumsek, F. and Karabacakoglu, **B.** Adsorption of chromium (VI) from aqueous solution by activated carbon derived from olive bagasse and applicability of different adsorption models. *Chemical Engineering Journal,* 144 **(2008)** 188–196.

Dikusar, A.I., Molin, A.I., Simashkevich, A.V., Sherban, D.A. and Yakubu, H. Electrochemical synthesis of Cd-Te semiconductor films by cathodic deposition from aqueous solutions. *Journal of Electrochemical Machining of Materials,* 4 **(1992)** 51–55.

Dizge, N., Keskinler, B. and Barlas, H. Sorption of Ni(II) ions from aqueous solution by Lewatit cation exchange resin. *Journal of Hazardous Materials,* 167 **(2009)** 915–926.

Dubey, S.P. and Gopal, K. Adsorption of chromium(VI) on low cost adsorbents derived from agricultural waste material: a comparative study. *Journal of Hazardous Materials,* 145 **(2007)** 465–470.

El-Qada, E.N., Allen, S.J. and Walker, G.M. Adsorption of basic dyes from aqueous solution onto activated carbons. *Chemical Engineering Journal,* 135 **(2008)** 174–184.

El-Hendawy, A.A. Variation in the FTIR spectra of a biomass under impregnation, carbonization and oxidation conditions. *Journal of Analytical and Applied Pyrolysis*, 75 **(2006)** 159–166.

Ergican, E., Gecol, H. and Fuchs, A. The effect of co-occurring inorganic solutes on the removal of arsenic (V) from water using cationic surfactant micelles and an ultrafiltration membrane. *Desalination,* 181 **(2005)** 9–26.

Fahim, N.F., Barsoum, B.N., Eid, A.E. and Khalil, M.S. Removal of Chromium (III) from Tannery Wastewater Using Activated Carbon from Sugar Industrial Waste. *Journal of Hazardous Materials,* B136 **(2006)** 303–309.

Farajzadeh, M.A. and Monji, A.B. Adsorption characteristics of wheat bran towards heavy metal cations. *Separation and Purification Technology,* 38 **(2004)** 197–207.

Feng, W., Wen, J., Liu, C., Yuan, Q., Jia, X. and Sun, Y. Modeling of local dynamic behavior of phenol degradation in an internal loop airlift bioreactor by yeast *Candida tropicalis*. *Biotechnology Bioengineering,* 97 **(2007)** 251–264.

Field, M.S., Wilhelm, R.G., Quinlan, J.F. and Aley, T.J. An assessment of the potential adverse properties of fluorescent tracer dyes used for groundwater tracing. *Environmental Monitoring and Assessment,* 38 **(1995)** 75–97.

Figueira, M.M., Volesky, B., Ciminelli, V.S.T. and Roddick, F.A. Biosorption of metals in brown seaweed biomass. *Water Research,* 34 **(2000)** 196–204.

Fox, M.A. and. Dulay, M.T. Heterogeneous photo catalysis. *Chemical Reviews,* 93 **(1993)** 341–357.

Freundlich, H. Colloid and Capillary Chemistry. Methuen, London. **(1926).**

Fu, Y. and Viraraghavan, T. Dye biosorption sites in Aspergillus niger. *Bioresource Technology,* 82 **(2002)** 139–145.

Fu, Y. and Viraraghavan, T. Fungal decolourization of wastewaters: a review. *Bioresource Technology,* 79 **(2001)** 251–262.

Fu, Y. and Viraraghavan, T. Removal of C.I. Acid Blue 29 from an aqueous solution by Aspergillus niger. *American Association of Textile Chemists and Colourists magazine,* 1 **(2001)** 36–40.

Gad, H.M.H. and El-Sayed, A. Activated carbon from agricultural by-products for the removal of Rhodamine-B from aqueous solution. *Journal of Hazardous Materials,* 168 **(2009)** 1070–1081.

Gang, D., Banerji, S.K. and Clevenger, T.E. Chromium(VI) removal by modified PVP-coated silica gel. *Practice Periodical of Hazardous, Toxic, and Radioactive Waste Management,* 4 **(2000)** 105–110.

Gahr, F., Hermanutz, F. and Opperman, W. Ozonation-an important technique to comply with new German law for textile wastewater treatment. *Water Science and Technology,* 30 **(1994)** 255–263.

Garg, U.K., Kaur, M.P., Garg, V.K. and Sud, D. Removal of hexavalent chromium from aqueous solution by agricultural waste biomass. *Journal of Hazardous Materials,* 140 **(2007)** 60–68.

Garg V.K., Kumar R and Gupta R. Removal of malachite green dye from aqueous solution by adsorption using agro-industry waste: a case study of Prosopis cineraria. *Dyes and Pigments,* 62 **(2004)** 1–10.

Garg, V.K., Amita, M., Kumar, R. and Gupta, R. Basic dye (methylene blue) removal from simulated wastewater by adsorption using Indian Rosewood sawdust: a timber industry waste. *Dyes and Pigments,* 63 **(2004)** 243–250.

Garcı´a, G.I., Pen˜a, P.R. J., Venceslada, J.L. B., Martı´n, A. M., Santos, M.A. M. and Go´mez, E.R. Removal of phenol compounds from olive mill wastewater using *Phanerochaete chrysosporium, Aspergillus niger, Aspergillus terreus* and *Geotrichum candidum*. *Process Biochemistry,* 35 **(2000)** 751–758.

Gerçel, Ö., Özcan, A., Özcan, A.S. and Gerçel, H.F. Preparation of activated carbon from a renewable bio-plant of *Euphorbia rigida* by H_2SO_4 activation and its adsorption behaviour in aqueous solutions. *Applied Surface Science,* 253 **(2007)** 4843–4852.

Giirses, A., Bayrakqeken, S. and Giilaboglu, M.S. Adsorption of o-cresol romaqueous solution on coal. *Colloids and Surfaces,* 64 **(1992)** 7–I3.

Girgis, B.S., Nasser, A.A. and Hendawy, E. Porosity development in activated carbons obtained from date pits under chemical activation with phosphoric acid. *Microporous Mesoporous Mater,* 52 **(2002)** 105–117.

Girods, P., Dufour, A., Fierro, V., Rogaume, Y., Rogaume, C., Zoulalian, A. and Celzardc, A. Activated Carbons Prepared from Wood Particleboard Wastes: Characterisation and Phenol Adsorption Capacities. *Journal of Hazardous Materials,* 166 **(2009)** 491–501.

Glaze, W., Lay, Y. and Kang, J. Advanced oxidation processes. A kinetic model for the oxidation of 1,2-dibromo-3-chloropropane in water by the combination of hydrogen peroxide and UV radiation. *Industrial and Engineering Chemistry Research,* 34 **(1995)** 2314–2323.

Goel, P.K. Water Pollution Causes, Effects and Control. *New age international publishers*, New Delhi, India **(1997)**.

Goel, J., Kadirvelu, K., Rajagopal, C. and Garg, V.K. Removal of lead(II) by adsorption using treated granular activated carbon: Batch and column studies. *Journal of Hazardous Materials,* 125 **(2005)** 211-220.

Groffman, A., Peterson, S. and Brookins, D. Removing lead from wastewater using zeolite. *Water Environment and Technology,* 4 **(1992)** 54–59.

Guaratini, C.C.I. and Zanoni, M.V B. Textile dyes. Química Nova, 23 **(2000)** 71–78.

Guittonneau, S., Glaze, W., Duguet, J. and Wable, O. Characterization of natural waters for potential to oxidize organic pollutants with ozone. *Proceedings of 10th Ozone World Congress*, Zürich, Switzerland **(1991)**.

Guo, Y., Zhao, J., Zhang, H., Yang, S., Qi, J., Wang, Z. and Xu, H. Use of rice husk-based porous carbon for adsorption of Rhodamine B from aqueous solutions. *Dyes and Pigments,* 66 **(2005)** 123–128.

Gupta, V.K., Jain, C.K., Ali, I., Sharma, M. and Saini, V.K. Removal of cadmium and nickel from wastewater using bagasse fly ash a sugar industry waste. *Water Research,* 37 **(2003)** 4038–4044.

Gupta, S. and Babu, B.V. Removal of toxic metal Cr(VI) from aqueous solutions using sawdust as adsorbent: equilibrium, kinetics and regeneration studies. *Chemical Engineering Journal,* 150 **(2009)** 352–365.

Gupta, V.K., Suhas, I.A. and Mohan, D. Equilibrium uptake and sorption dynamics for the removal of a basic dye (basic red) using low-cost adsorbents. *Journal of Colloidal Interface Science,* 265 **(2003)** 257–264.

Gupta, G.S., Shukla, S.P., Prasad, G. and Singh, V.N. China clay as an adsorbent for dye house wastewater. *Environmental Technology,* 13 **(1992)** 925–936.

Gupta, G.S., Prasad, G. and Singh, V.H. Removal of chrome dye from aqueous solutions by mixed adsorbents: fly ash and coal. *Water Research,* 24 **(1990)** 45–50.

Gupta, M.P. and Bhattacharrya, P.K. Studies on colour removal from bleach plant effluent of a craft pulp mill. *Journal of Chemical Technology & Biotechnology,* 35B **(1985)** 23–32.

Gündogan, R., Acemioglu, B. and Alma, M.H. Copper (II) adsorption from aqueous solution by herbaceous peat. *Journal of Colloid and Interface Science,* 269 **(2004)** 303–309.

G¨urbo˘ga, G. and Tel, H. Preparation of TiO_2–SiO_2 mixed gel spheres for strontium adsorption. *Journal of Hazardous Materials,* B120 **(2005)** 135–142.

Gürses, A., Karaca, S., Dogar, C., Bayrak, R., Acikyildiz, M. and Yalcin, M. Determination of adsorptive properties of clay/water system: methylene blue sorption. *Journal of Colloidal Interface Science,* 269 **(2004)** 310–314.

Hadjara, H., Hamdib, B. and Aniac, C.O. Adsorption of P-cresol on novel diatomite/carbon composites. *Journal of Hazardous Materials,* 188 **(2011)** 304–310.

Hamadi, N. K., Chen, X.D., Farid, M.M. and Lu, M.G.Q. Adsorption kinetics for the removal of chromium (VI) from aqueous solutions by adsorbents derived from used tyres and saw dust. *Chemical Engineering Journal,* 84 **(2001)** 95–105.

Hameed, B.H. and El-Khaiary, M.I. Sorption Kinetics and Isotherm Studies of a Cationic Dye Using Agricultural Waste: Broad Been Peels. *Journal of Hazardous Materials,* 154 **(2008)** 639–648.

Hameed, B.H., Ahmad, A.L. and Latiff, K.N.A. Adsorption of basic dye (methylene blue) onto activated carbon prepared from rattan sawdust. *Dyes and Pigments,* 75 **(2007)** 143–149.

Hameed, B.H. and Rahman, A.A. Removal of phenol from aqueous solutions by adsorption onto activated carbon prepared from biomass material. *Journal of Hazardous Materials,* 160 **(2008)** 576–581.

Hassenklo¨ver, T., Predehl, S., Pilli, J., Ledwolorz, J., Assmann, M. and Bickmeyer, U. Bromophenols, both present in marine organisms and industrial flame retardants, disturb cellular Ca2 signaling in neuroendocrine cells (PC12). *Aquatic Toxicology,* 76 **(2006)** 37–45.

Herrero, R., Lodeiro, P., Rey-Castro, C., Vilarino, T. and Sastre de Vicente, M.E. Removal of inorganic mercury from aqueous solutions by biomass of the marine macroalga *Cystoseira baccata*. *Water Research,* 39 **(2005)** 3199–3210.

Herrmann, J.M., Duchamp, C., Karkmaz, M., Hoai, B.T., Lachheb, H., Puzenat, E. and Guillard. C Environmental green chemistry as defined by photocatalysis. *Journal of Hazardous Materials,* 146 **(2007)** 624–629.

Hill, G.A. and Robinsin, C.W. Substrate inhibition kinetics:phenol degrdation by *Pseudomonas putida. Biotechnology and Bioengineering,* 179 **(1975)** 1599–1615.

Hincapié, M., Maldonado, M.I., Oller, I., Gernjak, W., Sánchez-Pérez, J.A., Ballesteros, M.M. and Malato, S. Solar photocatalytic degradation and detoxification of EU priority substances. *Catalysis Today,* 101 **(2005)** 230-210.

Ho, Y.S. and Mckay, G. A. comparison of chemisorption kinetic models applied to pollutant removal on various sorbents. *Process Safety and Environmental Protection,* 76B **(1998)** 332–340.

Ho, Y.S. and McKay G. Batch lead(II) removal from aqueous solution by peat: equilibrium and kinetics. *Process Safety and Environmental Protection,* 77 **(1999)** 165–73.

Ho, Y.S. Removal of copper ions from aqueous solution by tree fern. *Water Research,* 37 **(2003)** 2323–30.

Hoffmann, M.R., Martin, S.T., Choi, W. and Bahnemann, D.W. Environmental Applications of semiconductor catalysis. *Chemical Reviews,* 95(1) **(1995)** 69–96.

Holan, Z.R. and Volesky, B. Accumulation of cadmium, lead and nickel by fungal and wood biosorbents. *Applied Biochemistry and Biotechnology,* 53 **(1995)** 133–146.

Holan, Z.R. and Volesky, B. Biosorption of lead and nickel by biomass of marine algae. *Biotechnology and Bioengineering,* 43 **(1994)** 1001–1009.

Hosono, M., Arai, H., Aizawa, M., Yamamoto, I., Shimizu, K. and Sugiyama, M. Decoloration and degradation of azo dye in aqueous solution of supersaturated with oxygen by irradiation of high-energy electron beams. *Applied Radiation and Isotopes*, 44 **(1993)** 1199–1203.

Hosseini, M., Mertens, S.F.L., Ghorbani, M. and Arshadi, M.R. Asymmetrical Schiff bases as inhibitors of mild steel corrosion in sulphuric acid media. *Materials Chemistry and Physics,* 78 **(2003)** 800–808.

Howe, P.D., Dobson, S. and Malcolm, H.M. 2,4,6-Tribromophenol and Other Simple Brominated Phenols. *World Health Organization*, Geneva **(2005)**.

Hsu, T.C. and Chiang, C.S. Activated sludge treatment of dispersed dye factory wastewater. *Journal of Environmental Science and Health, Part A: Toxic/Hazardous Substances and Environmental Engineering,* 32 **(1997)** 1921–1932.

Hu, Z., Lei, L., Li, Y. and Ni, Y. Chromium adsorption on high-performance activated carbons from aqueous solution. *Separation and Purification Technology,* 31 **(2003)** 13–18.

Hu T.L. Sorption of reactive dyes by Aeromonas biomass. *Water Science and Technology,* 26 **(1992)** 357–366.

Hussain, A., Kumar P. and Mehrotra, I. Treatment of phenolic wastewater in UASB reactor: Effect of nitrogen and phosphorous. *Bioresource Technology,* 99 **(2008)** 8497–8503.

Hutchins R A. New method simplifies design of activated carbon systems, *Chemical Engineering,* 80 **(1973)** 133-138.

Inbaraj, B.S. and Sulochana, N. Mercury adsorption on a carbon sorbent derived from fruit shell of *Terminalia catappa. Journal of Hazardous Materials,* B133 **(2006)** 283–290.

Ince, N.H. and Gonenc, D.T. Treatability of a textile azo dye by UV/H_2O_2. *Environmental Technology,* 18 **(1997)** 179–185.

Ivanov, K., Gruber, E., Schempp, W. and Kirov, D. Possibilities of using zeolite as filler and carrier for dyestuffs in paper. *Das Papier,* 50 **(1996)** 456–46.

Jeon, C. and Ho¨ll, W.H. Chemical modification of chitosan an equilibrium study for mercury ion removal. *Water Research,* 37 **(2003)** 4770–4780.

Ju, D.J., Byun, I.G., Park, JJ., Lee, C.H., Ahn, G.H. and Park, T.J. Biosorption of a reactive dye (Rhodamine-B) from an aqueous solution using dried biomass of activated sludge. *Bioresource Technology,* 99 **(2008)** 7971–7975.

Juang R.S., Tseng R.L., Wu F.C. and Lee S.H. Adsorption behavior of reactive dyes from aqueous solutions on chitosan. *Journal of Chemical Technology & Biotechnology,* 70 **(1997)** 391–399.

Kabadasil, I., Tünay, O. and Orhon, D. Wastewater control and management in a leather tanning district. *Water Science and Technology,* 40 **(1999)** 261–267.

Kadirvelu, K., Kavipriya, M., Karthika, C., Vennilamani, N. and Pattabhi, S. Mercury (II) adsorption by activated carbon made from sago waste. *Carbon,* 42 **(2004)** 745–752.

Kadirvelu, K., Kavipriya, M., Karthika, C., Radhika, M., Vennilamani, N. and Pattabhi, S. Utilization of various agricultural wastes for activated carbon preparation and application for the removal of dyes and metal ions from aqueous solutions. *Bioresource Technology,* 81 **(2003)** 129–132.

Kadirvelu, K., Karthika, C., Vennilamani, N. and Pattabhi, S. Activated carbon from industrial solid waste as an adsorbent for the removal of Rhodamine-B from aqueous solution: kinetic and equilibrium studies. *Chemosphere,* 60 **(2005)** 1009–1017.

Kadirvelu, K. Preparation and characterization of activated carbon, from coir pith and its application to metal bearing wastewater. Ph.D. Thesis, Bharathiar University, Coimbatore, India. **(1998).**

Kandaha M.I. and Meunier, J. Removal of nickel ions from water by multi-walled carbon nanotubes. *Journal of Hazardous Materials,* 146 **(2007)** 283–288.

Kanamadi, R.D., Ahalya, N. and Ramachandra, T.V. Biosorption of Heavy Metals by Low cost Adsorbents, Technical Report : 112 December **2006**.

Kannan, N. and Sundaram, M.M. Kinetics and mechanism of removal of methylene blue by adsorption on various carbon-a comparative study. *Dyes and Pigments,* 51 **(2001)** 25–40.

Kar, S., Swaminathan, T. and Baradarajan, A. Biodegradation of phenol and cresol isomer mixtures by *Arthrobacter*. *World Journal of Microbiology and Biotechnology,* 13 **(1997)** 659–663.

Karcher, S., Kornmuller, A. and Jekel, M. Removal of reactive dyes by sorption/complexation with cucurbituril. *Water Science and Technology,* 40 **(1999)** 425–433.

Karthikeyan, T., Rajgopal, S. and Miranda, L.R. Chromium(VI) adsorption from aqueous solution by *Hevea Brasilinesis* sawdust activated carbon. *Journal of Hazardous Materials,* 124 **(2005)** 192–199.

Kavitha, D. and Namasivayam, C. Experimental and kinetic studies on methylene blue adsorption by coir pith carbon. *Bioresource Technology,* 98 **(2007)** 14–21.

Kawai, T. and Tsutsumi, K. Adsorption Characteristics of Surfactants and Phenol on Modified Zeolites from Their Aqueous Solutions. *Colloid Poly. Sci*. 273 **(1995)** 787-792.

Keith, L. and Telliard, W. Priority pollutants: I-a perspective view. *Environmental Science & Technology,* 13 **(1979)** 416–423.

Kennedy, L.J., Judith, J., Vijaya B., Sekaran, G. and Kayalvizhi, K. Equilibrium, kinetic and thermodynamic studies on the adsorption of *m*-cresol onto micro-and mesoporous carbon. *Journal of Hazardous Materials,* 149 **(2007)** 134–143.

Kennish, M.J. *Ecology of Estuaries: Anthropogenic Effects*. Boca Raton: CRC press **(1992)**.

Khattri, S.D. and Singh, M.K. Colour removal from synthetic dye wastewater using a bioadsorbent. *Water*, *Air*, & *Soil Pollution,* 120 **(2000)** 283–294.

Kidak, R. and Ince, N.H. Ultrasonic destruction of phenol and substituted phenols: A review of current research. *Ultrasonics Sonochemistry,* 13 **(2006)** 195–199.

Kim, J.H., Oh, K.K., Lee, S.T., Kim, S.W. and Hong, S.I. Biodegradation of phenol and chlorophenols with defined mixed culture in shake-flasks and a packed bed reactor. *Process Biochemistry,* 37 **(2002)** 1367–1373.

Klika, Z., Weissmannova, H., ˇCapkova, P. and Pospiˇsil, M. The Rhodamine B intercalation of montmorillonite. *Journal of Colloidal and Interface Science,* 275 **(2004)** 243–250.

Kirby, N. Bioremediation of textile industry wastewater by white rot fungi. D.Phil Thesis, University of Ulster, Coleraine, UK. **(1999).**

Krishnan, K.A. and Anirudhan, T.S. Kinetic and equilibrium modelling of Cobalt(II) adsorption onto bagasse pith based sulphurised activated carbon. *Chemical Engineering Journal,* 137 **(2008)** 257–264.

Knapp, J.S. and Newby, P.S. The microbiological decolorization of an industrial effluent containing a diazo-linked chromophore. Water Res. 7 **(1995)** 1807–1809.

Krishnan, A.K. and Anirudhan, T.S. Kinetic and equilibrium modelling of Cobalt(II) adsorption onto bagasse pith based sulphurised activated carbon. *Chemical Engineering Journal,* 137 **(2008)** 257–264.

Kross, B.C., Nicholson, H.F. and Ogilvie, L.K. Methods development study for measuring pesticide exposure to golf course workers using video imaging techniques. *Applied Occupational and Environmental Hygiene,* 11 **(1996)** 1346–1351.

Ku, Y. and Lee, K. Removal of Phenols from Aqueous Solution by XAD-4 Resin. *Journal of Hazardous Materials*, B80 **(2000)** 59–68.

Kumar, M.N.V.R., Sridhari, T.R., Bhavani, K.D. and Dutta, P.K. Trends in color removal from textile mill effluents. *Colorage,* 40 **(1998)** 25–34.

Kumaran, P. and Paruchuri, Y.L. Kinetics of phenol biotransformation. *Water Research,* 31 **(1996)** 11–22.

Kulshreshtha, S.N. A Global Outlook for Water Resources to the Year 2025. *Water Resources Management,* 12 **(1998)** 167–184.

Kumar, A., Kumar, S. and Kumar, S. Biodegradation kinetics of phenol and catechol using *Pseudomonas putida* MTCC 1194. *Biochemical Engineering Journal,* 22 **(2005)** 151–159.

Kun-She, L., Chnoong-Kheng, L. and Bee-Foong, T. Quaternised wood as sorbent for reactive dyes. *Applied Biochemistry and Biotechnology*, 87 **(2000)** 233–245.

Kurniawan, A., Chan, G.Y.S., Lo, W-H. and Babel, S. Physico-chemical treatment techniques for wastewater laden with heavy metals. *Chemical Engineering Journal,* 118 **(2006)** 83-98.

Lagergren, S. Zur theorie der sogenannten adsorption gelöster stoffe. Kungliga Svenska Vetenskapsakademiens, Handlingar, Band 24 **(1898)** 1–39.

Lalhruaitluanga, H., Jayaram, K., Prasad, M.N.V. and Kumar, K.K. Lead(II) adsorption from aqueous solutions by raw and activated charcoals of Melocanna baccifera Roxburgh (bamboo)–A comparative study. *Journal of Hazardous Materials,* 175 **(2010)** 311–318.

Langmuir, I. The adsorption of gases on plane surfaces of glass, mica and platinum. *Journal of the American Chemical Society,* 40 **(1918)** 1361–1403.

Lata, H., Garg, V.K. and Guta, R.K. Removal of basic dye from aqueous solution using *Parthenium hysterophorus*: An agricultural waste. *Dyes and Pigments,* 74 **(2007)** 653–658.

Legrini, O., Oliveros, E. and Braun, A.M. Photochemical processes for water treatment. *Chemical Reviews*, 93 **(1993)** 671–698.

Leyva, E., Moctezuma, E, Ruíz, M. G. and Torres-Martínez, L. Photo degradation of phenol and 4-chlorophenol by BaO–LiO_2–TiO_2 catalysts. *Catalysis Today,* 40 **(1998)** 367–376.

Li, H., Li, Z., Liu, T., Xiao, X., Peng, Z. and Deng, L. A novel technology for biosorption and recovery hexavalent chromium in wastewater by bio-functional magnetic beads. *Bioresource Technology,* 99 **(2008)** 6271–6279.

Li, J.K. and Humphrey, A. E. Kinetic and fluorometric behavior of a phenol fermentation. *Biotechnology Letters,* 11 **(1989)** 177–182.

Li, J., Lin, Q., Zhang, X. and Yan, Y. Kinetic parameters and mechanisms of the batch biosorption of Cr(VI) and Cr(III) onto Leersia hexandra Swartz biomass. *Journal of Colloid and Interface Science,* 333 **(2009)** 71–77.

Li, Q., Liu, H., Liu, T., Guo, M., Qing, B., Ye, X. and Wu, Z. Strontium and calcium ion adsorption by molecularly imprinted hybrid gel. *Chemical Engineering Journal,* 157 **(2010)** 401–407.

Liao, D., Zheng, W., Li, X., Yang, Q., Yue, X., Guo, L. and Zeng, G. Removal of lead(II) from aqueous solutions using carbonate hydroxyapatite extracted from eggshell waste. *Journal of Hazardous Materials,* 177 **(2010)** 126–130.

Lin, S.H. and Juang, R.S. Adsorption of phenol and its derivatives from water using synthetic resins and low-cost natural adsorbents: A review. *Journal of Environmental Management,* 90 **(2009)** 1336–1349.

Liu, Q., Zheng, T., Wang, P. Jiang, J. and Li, N. Adsorption Isotherm, Kinetic and Mechanism Studies of Some Substituted Phenols on Activated Carbon Fibers. *Chemical Engineering Journal,* 157 **(2010)** 348–356.

Lin, S.H. and Lin, C.M. Treatment of textile waste effluents by ozonation and chemical coagulation. *Water Research,* 27 **(1993)** 1743–1748.

Liversidge, R.M., Lloyd, G.J., Wase, D.A.J. and Forster, C.F. Removal of basic blue 41 dye from aqueous solution by linseed cake. *Process Biochemistry,* 32 **(1997)** 473–477.

Lonergan, G. White-rot-fungi-an environmental panacea? *Environmental Bio-technology,* 2 **(1992)** 214–217.

Lyubchik, S. I., Lyubchik, A. I., Galushko, O. L., Tikhonova, L. P., Vital, J., Fonseca, I. M. and Lyubchik, S. B. Kinetics and thermodynamics of the Cr(III) adsorption on the activated carbon from co-mingled wastes. *Colloids and Surfaces A: Physicochemical and Engineering Aspects,* 242 **(2004)** 151–158.

Mahamadi, C. and Nharingo, T. Competitive adsorption of Pb^{2+}, Cd^{2+} and Zn^{2+} ions onto *Eichhornia crassipes* in binary and ternary systems. *Bioresource Technology,* 101 **(2010)** 859–864.

Mall, I.D. and Upadhyay, S.N. Studies on Treatment of Basic Dyes Bearing Wastewater by Adsorptive Treatment Using Flyash. *Indian Journal of Environmental Health,* 40 **(1998)** 177–188.

Malik, R., Ramteke, D.S. and Wate, S.R. Adsorption of malachite green on ground net shell waste based powdered activated carbon. *Waste Management,* 27 **(2007)** 1129-1138.

Matheickal, J.T. Yu, Q. and Woodburn, G.M. Biosorption of Cadmium(II) from aqueous solutions by pre-treated biomass of marine alga *DurvillAea potatorum*. *Water Research,* 33 **(1999)** 335–342.

Mathur, N., Krishnatrey, R., Sharma, S., Pathak, S. and Sharma, K.P. Certain haematological responses in Swiss albino mice following exposure to textile dye wastewater. *Journal of Environmental Biology,* 24 **(2003)** 161–164.

McGeorge, L. J., Louis, J. B., Atherholt, T. B. and McGarrity, G. J. Mutagenicity analyses of industrial effluent: Results and considerations for integration into water pollution control programs.-In: Short-Term Bioassays in the Analysis of Complex

Environmental Mixtures IV (eds M. D. Waters et al.). Plenum Press, New York **(1985)**.

Mchedlov-Petrosyan, N.O. and Kholin, Y.V. Aggregation of Rhodamine B in Water. *Russian Journal of Applied* Chemistry, 77 **(2004)** 414–422.

Mckay, G. Waste colour removal from textile effluents. *American Dyestuff Reporter,* 68 **(1979)** 29–36.

McKay, G., Otterburn, M.S. and Sweeney, A.G. Fullers earth and fired clay as adsorbents for dyestuffs-equilibrium and rate studies. *Water*, *Air*, & *Soil Pollution,* 24 **(1985)** 147–161.

Meena, A.K., Kadirvelu, K., Mishra, G.K., Chitra, R. and Nagar, P.N. Adsorptive removal of heavy metals from aqueous solution by treated saw dust (*Acacia Arabica*). *Journal of Hazardous Materials,* 150 **(2009)** 604–611.

Messina, P.V. **and Schulz, P.C.** Adsorption of reactive dyes on titania-silica mesoporous materials. Journal of Colloidal and Interface Science, 299 **(2006)** 305-320.

Metcalf and Eddy. Inc Wastewater engineering: Treatment, disposal and reuse. 4th eds. Tata-McGraw-Hill, New Delhi, India. **(2003).**

Minero, C., Pelizzetti, C., Piccini, P. and Vinceti, M. Photo catalyzed transformation of nitrobenzene on TiO_2 and ZnO. *Chemosphere,* 28 **(1994)** 1229–1244.

Mishra, G. and Tripathy, M. A critical review of the treatment for decolourization of textile effluent. *Colourage,* 40 **(1993)** 35–38.

Mittal, A.K. and Gupta, S.K., Biosorption of cationic dyes by dead macro fungus Fomitopsis carnea: batch studies. *Water Science and Technology,* 34 **(1996)** 157–181.

Mock, W.I. Cucurbituril. *Topics in Current Chemistry,* 175 **(1995)** 1–24.

Mohamed, M.M. Acid dye removal: comparison of surfactant modified mesoporous FSM-16 with activated carbon derived from rice husk. *Journal of Colloidal and Interface Science,* 272 **(2004)** 28–34.

Mohan, D. and Singh, K.P. Single and multi-component adsorption of cadmium and zinc using activated carbon derived from bagasse-an agricultural waste. *Water Research*, 36 **(2002)** 2304–2318.

Mohan, S. and Sreelakshmi, G. Fixed bed column study for heavy metal removal using phosphate treated rice husk. *Journal of Hazardous Materials,* 153 **(2008)** 75–82.

Mohanty, K., Jha, M., Meikap, B.C. and Biswas, M.N. Removal of Chromium(VI) from Dilute Aqueous Solutions by Activated Carbon Developed from *Terminalia Arjuna* Nuts Activated with Zinc Chloride. *Chemical Engineering Science,* 60 **(2005)** 3049–3059.

Mollaei, M., Abdollahpour, S., Atashgahi, S., Abbasi, H., Masoomi, F., Rad, I., Sahebghadam, A., Lotfi, Zahiri, H.S., Vali, H. and Noghabi, K.A. Enhanced phenol degradation by *Pseudomonas* sp. SA01: Gaining insight into the novel single and hybrid immobilizations. *Journal of Hazardous Materials,* 175 **(2010)** 284–292.

Monteiro, A.A.M.G., Boaventura, R.A.R. and Rodrigues, A.E. Phenol biodegradation by *Pseudomonas putida* DSM 548 in a batch reactor. *Biochemical Engineering Journal,* 6 **(2000)** 45–49.

Morgan-Sagastume, J.M., Jimenez, B. and Noyola, A. Tracer studies in a laboratory and pilot scale UASB reactor. *Environmental Technology,* 18 **(1997)** 817–826.

Moran C., Hall M.E. and Howell R.C. Effects of sewage treatment on textile effluent. *Journal of Society of Dyers and Colourists,* 11 **(1997)** 272–274.

Murialdo, S.E., Fenoglio, R., Haure P.M. and González, J.F. Degradation of phenol and chlorophenols by mixed and pure cultures. *Water SA,* 2 **(2003)** 457–463.

Mukherjee, S., Kumar, S., Misra, A.K. and Fan, M. Removal of phenols from water environment by activated carbon, bagasse ash and wood charcoal. *Chemical Engineering Journal,* 129 **(2007)** 133–142.

Naas, H., Shaheen Al-Muhtaseb, A. and Makhlouf, S. Biodegradation of phenol by *Pseudomonas putida* immobilized in polyvinyl alcohol (PVA) gel. *Journal of Hazardous Materials,* 164 **(2009)** 720–725.

Naimo, T.J. A review of the effects of heavy metals on freshwater mussels, *Ecotoxicology,* 4 **(1995)** 341 – 362.

Nalawade P.M., Kamble J.R., Late A.M., Solunke K.R. and Mule M.B. Studies on integrated use of tannery wastewater, municipal solid waste and fly ash amended

compost on vegetable growth. *International Journal of Agriculture Sciences,* 1 **(2009)** 55-58.

Namasivayam, C. and Kavitha, D. Removal of Congo Red from water by adsorption onto activated carbon prepared from coir pith, an agricultural solid waste. *Dyes and Pigments,* 54 **(2002)** 47–58.

Namasivayam, C., Radhika, R. and Suba, S. Uptake of dyes by a promising locally available agricultural solid waste: coir pith. *Waste Management,* 21 **(2001)** 381–387.

Namasivayam, C., Kadirvelu, K. and Kumuthu, M. Removal of direct red and acid brilliant blue by adsorption on to banana pith. *Bioresource Technology,* 64 **(1998)** 77–79.

Ngah, W.S.W. and Fatinathan, S. Adsorption characterization of Pb(II) and Cu(II) ions onto chitosan-tripolyphosphate beads: Kinetic, equilibrium and thermodynamic studies. *Journal of Environmental Management,* 91 **(2010)** 958–969.

Nigam, P. and Marchant, R. Selection of the substratum for composing biofilm system of textile decolourizing bacteria. *Biotechnology Letters,* 17 **(1995)** 993–996.

Nigam, P., Banat, I.M., Singh, D. and Marchant, R. Microbial process for the decolorization of textile e.uent containing azo, diazo and reactive dyes. *Process Biochemistry,* 31 **(1996)** 435–442.

Noeline, B.F., Manohar, B.F. and Anirudhan, T.S. Kinetic and equilibrium modelling of Lead(II) sorption from water and wastewater by polymerized banana stem in a batch reactor. *Separation and Purification Technology,* 45**(2005)** 131–140.

Nuhoglu, A. and Yalcin, B. Modeling of phenol removal in a batch reactor. *Process Biochemistry,* 40 **(2005)** 1233–1239.

Ogawa, T. and Yatome, C. Biodegradation of azo dyes in multistage rotating biological contractor immobilized by assimilating bacteria. *Bulletin of Environmental Contamination and Toxicology,* 44 **(1990)** 561–566.

Ogutveren, U.B., Gonen, N. and Koparal, S. Removal of dye stuffs from waste water: electrocoagulation of acilan blau using soluble anode. *Journal of Environmental Science and Health*, *Part A. Toxic / Hazardous Substances and Environmental Engineering,* 27 **(1992)** 1237–1247.

Ogutveren, U.B. and Kaparal, S. Colour removal from textile effluents by electrochemical destruction. *Journal of Environmental Science and Health*, *Part A. Toxic / Hazardous Substances and Environmental Engineering,* 29 **(1994)** 1–16.

Okieimen, J.F.E., Sogbaike, C.E. and Ebhoaye, J.E. Removal of cadmium and copper ions from aqueous solution with cellulose graft copolymers. *Separation and Purification Technology,* 44 **(2005)** 85–89.

Oladoja, N.A., Ololade, I.A., Idiaghe, J.A. and Egbon, E.E. Equilibrium Isotherm Analysis of the Sorption of Congo Red by Palm Kernel Coat. *Central European Journal of Chemistry,* 7 **(2009)** 760–768.

O'Mahony, T., Guibal, E. and. Tobin J.M. Reactive dye biosorption by Rhizopus arrhizus biomass. *Enzyme and Microbial Technology,* 31 **(2002)** 456–463.

O'Neill, C., Hawkes, F.R., Esteves, S.R.R., Hawkes, D.L. and Wilcox, S.J. Anaerobic and aerobic treatment of a simulated textile effluent. *Journal of Chemical Technology & Biotechnology,* 74 **(1999)** 993–999.

Orhon, D., Sözen, S., Görgün, E., Cokgör, E. and Artan, N. Technological aspects of wastewater management in coastal tourist areas. *Water Science and Technology,* 39 **(1999)** 177–184.

Ozer, A. and Dursun, G. Removal of methylene blue from aqueous solution by dehydrated wheat bran carbon. *Journal of Hazardous Materials,* 146 **(2007)** 262–269.

Ozer, D., Dursun, G.A. and Ozer, A. Methylene blue adsorption from aqueous solution by dehydrated peanut hull. *Journal of Hazardous Materials,* 144 **(2007)** 171–179.

Papachristodoulou, C.A., Assimakopoulos, P.A. and Gangas, N-H.J. Strontium Adsorption Properties of an Aluminum-Pillared Montmorillonite Carrying Carboxylate Functional Groups. *Journal of Colloidal and Interface Science,* 245 **(2002)** 32–39.

Park, D., Lim, S.R., Yun, Y.S. and Park, J.M. Reliable evidences that the removal mechanism of hexavalent chromium by natural biomaterials is adsorption-coupled reduction. *Chemosphere,* 70 **(2007)** 298–305.

Pak, D. and Chang, W. Decolorizing dye wastewater with low temperature catalytic oxidation. *Water Science and Technology,* 40 **(1999)** 115–121.

Park, D., Yun, Y.S., Jo, J.H. and Park, J.M. Mechanism of hexavalent chromium removal by dead fungal biomass of *Aspergillus niger. Water Research,* 39 **(2005)** 533–540.

Patterson, J.W. Wastewater Treatment Technology. *Ann Arbor Science Publishers,* Michigan (**1975).**

Pelegrini, R., Peralto-Zamora, P., de Andrade, A.R., Reyers, J. and Duran, N. Electrochemically assisted photocatalytic degradation of reactive dyes. *Applied Catalysis B*: *Environmental,* 22 **(1999)** 83–90.

Peralto-Zamora, P., Kunz, A., Gomez de Morales, S., Pelegrini, R., de Capos Moleiro, P., Reyes, J. and Duran, N. Degradation of reactive dyes I. A comparative study of ozonation, enzymatic and photochemical processes. *Chemosphere,* 38 **(1999)** 835–852.

Perineau, F., Molinier, J. and Gaset, A. Adsorption of ionic dyes onto charred plant-material. *Journal of Chemical Technology & Biotechnology,* 32 **(1982)** 749–758.

Peyton, G. and Glaze, W. Destruction of pollutants in water with ozone in combination with ultraviolet radiation. 3. Photolysis of aqueous ozone. *Environmental Science and Technology,* 229 **(1988)** 761–767.

Polman, A. and Brekenridge, C.R. Biomass-mediated binding and recovery of textile dyes from waste effluents. *Textile Chemist and Colorist,* 28 **(1996)** 31–35.

Poots, V.J.P. and Mckay, J.J. The removal of acid dye from effluent using natural adsorbents-I peat. *Water Research,* 10 **(1976)** 1061–1066.

Prakasham, R.S., Merrie, J.S., Sheela, R., Saswathi, N. and Ramakrishna, S.V. Biosorption of chromium (VI) by free and immobilized *Rhizopus arrhizus*. *Environmental Pollution,* 104 **(1999)** 421–427.

Przepiórski, J. Enhanced adsorption of phenol from water by ammoniatreate activated carbon. *Journal of Hazardous materials,* 135 **(2006)** 453–456.

Pyrzynska, K. The elevation of carbon nanotubes as a sorbent for dicamba herbicide. Journal of separation science, 29 (2006) 2241-44.

Raghavacharya, C. Colour removal from industrial effluents -a comparative review of available technologies. *Chemical Engineering World,* 32 **(1997)** 53–54.

Rajeshwarisivaraj, and Subburam, V. Activated parthenium carbon as an adsorbent for the removal of dyes and heavy metal ions from aqueous solution. *Bioresource Technology,* 85 **(2002)** 205–206.

Rao, K.V.K. Inhibition of DNA synthesis in primary rat hepatocyte cultures by malachite green: a new liver tumor promoter. *Toxicological letters,* 81 **(1995)** 107–113.

Reddad, Z., Gerente, C., Andres, Y. and Cloirec, P.L. Adsorption of several metal ions onto a low-cost biosorbent: kinetic and equilibrium studies. *Environmental Science Technology,* 36 **(2002)** 2067–2073.

Reddy, C.A. The potential for white rot fungi in the treatment of pollutants. *Current Opinion in Biotechnology,* 6 **(1995)** 320–328.

Rhee, G.Y., Bush, B., Bethoney, C.M., Denucci, A., Oh, H.M. and Sokol, R.C. Anaerobic dechlorination of Aroclor 1242 as effected by some environmental conditions. *Environmental Toxicology and Chemistry,* 12 **(2003)** 1033–1039.

Ricordel, S., Taha, S., Cisse, I. and Dorange, G. Heavy metals removal by adsorption onto peanut husks carbon: characterization, kinetic study and modeling. *Separation and Purification Technology,* 24 **(2001)** 389–401.

Robert, D. and Malato, S. Solar photocatalysis: a clean process for water detoxification. *The Science of The Total Environment,* 291 **(2002)** 85–97.

Robinson T., Mcmullan G., Marchant R. and Nigam P. Remediation of dyes in textile effluent: a critical review on current treatment technologies with a proposed alternative. *Bioresource Technology,* 77 **(2001)** 247–255.

Robinson, T., Chandran, B. and Nigam, P. Effect of pretreatments of three wastes residues, wheat straw, corn cobs and barley husks on dye adsorption. *Bioresource Technology,* 85 **(2002)** 119–124.

Rodriguez, G.V., Youssef, C.B. and Vilanova, J.W. Two-step modeling of the biodegradation of phenol by an acclimated activated sludge. *Chemical Engineering Journal,* 117 **(2006)** 245–252.

Royer, B., Cardoso, N.F., Lima, E.C., Vaghetti, J.C.P., Simon, N.M., Calvete, T. and Veses, R.C. Applications of Brazilian-pine fruit shell in natural and carbonized forms as adsorbents to removal of methylene blue from aqueous solutions-Kinetics and equilibrium study. *Journal of Hazardous Materials,* 164 **(2009)** 1213–1222.

Saeed, A., Akhter, W.M. and Iqbal, M. Removal and recovery of heavy metals from aqueous solution using papaya wood as a new biosorbent. *Separation and Purification Technology,* 45 **(2005)** 25–31.

Santos, V.L.D., Monteiro, A.D.S., Braga, D.T. and Santoro, M.M. Phenol degradation by *Aureobasidium pullulans* FE13 isolated from industrial effluents. *Journal of Hazardous Materials,* 161 **(2009)** 1413–1420.

Sawalha, M.F., Peraita-Videa, J.R., Saupe, G.B., Dokken, K.M. and Gardea-Torresdey, J.L. Using FTIR to corroborate the identity of functional groups involved in the binding of Cd and Cr to saltbush (*Atriplex canescens*) biomass. *Chemosphere,* 66 **(2007)** 1424–1430.

Saygideger, S., Gulnaz, O., Istifli, E.S. and Yucel, N. Adsorption of Cd(II), Cu(II) and Ni(II) ions by Lemna minor L.: Effect of physicochemical environment. *Journal of Hazardous Materials,* B126 **(2005)** 96–104.

Sayler, G.S., Nelson, J.D., Jr. and Colwell, R.R. Role of Bacteria in bioaccumulation of mercury in the Oyster Crassostrea virginica. *Applied Microbiology,* 30 **(1975)** 91–96.

Schuler, C.A., Anthony R.G. and Ohlendorf, H.M. Selenium in Wetlands and Waterfowl Foods and Kesterson Reservoir, California. *Archives of Environmental Contamination and Toxicology,* 29 **(1984)** 845-853.

Scarpi, C., Ninci, F., Centini, M. and Anselmi, C. High-performance liquid chromatography determination of dir Schuler. *Archives of Environmental Contamination and Toxicology,* 29 **(1998)** 845–853.

Schliephake, K. and Lonergan, G.T. Laccase variation during dye decolourisation in a 200 L packed-bed bioreactor. *Biotechnology Letters,* 18 **(1996)** 881–886.

Sekar, M., Sakthi, V. and Rengaraj, S. Kinetics and equilibrium adsorption study of lead(II) onto activated carbon prepared from coconut shell. *Journal of Colloid and Interface Science,* 279 **(2004)** 307–313.

Serrano, E.G., Cordero, T., Mirasol, J.R., Cotoruelo, L. and Rodriguez, J.J. Removal of water pollutants with activated carbons prepared from H_3PO_4 activation of lignin from Kraft black liquors. *Water Research,* 38 **(2004)** 3043–3050.

Shaul, G.M., Holdsworth, T.J., Dempsey, C.R. and Dostal, K.A. Fate of water soluble azo dyes in the activated sludge process. *Chemosphere,* 22 **(1991)** 107–119.

Sheng, P.X., Ting, Y., Chen, J.P. and Hong, L. Sorption of lead, copper, cadmium, zinc, and nickel by marine algal biomass: characterization of biosorptive capacity and investigation of mechanisms. *Journal of Colloid and Interface Science,* 275 **(2004)** 131–141.

Shore, J. Advances in direct dyes, *Indian Journal of Fiber and Textile Research*, 21 (1996) 1-29.

Shourian, M., Noghabi, K.A., Zahiri, H.S., Bagheri, T., Karballaei, G., Mollaei, M., Rad, I., Ahadi, S., Raheb, J. and Abbasi, H. Efficient phenol degradation by a newly characterized *Pseudomonas* sp. SA01 isolated from pharmaceutical wastewaters. *Desalination,* 246 **(2009)** 577–594.

Shukla, A., Zhang, Y.H, Dubey, P., Margrave, J.L. and Shukla, S.S. The role of sawdust in the removal of unwanted materials from water. *Journal of Hazardous Materials,* B95 **(2002)** 137–152.

Shukla, S.P. and Gupta, G.S. Toxic effects of omega chrome red ME and its treatment by adsorption. *Ecotoxicology and Environmental Safety,* 24 **(1992)** 155–163.

Sikaily, A.E., Nemr, A.E., Khaled, A. and Abdelwehab, O. Removal of toxic chromium from wastewater using green alga Ulva lactuca and its activated carbon. *Journal of Hazardous Materials,* 148 **(2007)** 216–228.

Sincero, A.P. and Sincero, G.A. Physical-Chemical Treatment of Water and Wastewater, *IWA Publishing,* **(2003).**

Singh, V.N., Mishra, G. and Panday, K.K. Removal of congo red by wallastonite. *Indian journal of technology,* 22 **(1984)** 70–71.

Singh, R.K., Kumar, S., Kumar, S. and Kumar, A. Development of parthenium based activated carbon and its utilization for adsorptive removal of *p*-cresol from aqueous solution, *Journal of Hazardous Materials,* 155 **(2008)** 523–535.

Singh, K.K., Talat, M. and Hasan, S.H. Removal of lead from aqueous solutions by agricultural waste maize bran. *Bioresource Technology,* 97 **(2006)** 2124–2130.

Slokar, Y.M. and Le Marechal, A.M. Methods of decoloration of textile wastewaters. *Dyes and Pigments,* 37 **(1997)** 335–356.

Sokolowska-Gajda, J., Freeman, H.S. and Reife, A. Synthetic dyes based on environmental considerations: 2. Iron complexed formazan dyes. *Dyes and Pigments,* 30 **(1996)** 1–20.

Sorensen, B.L. and Wakeman, R.J. Filtration characterization and specific surface area measurement of activated sludge by rhodamine B adsorption. *Water Research,* 30 **(1996)** 115–121.

Srivastava, S.J., Singh, N.D., Srivastava, A.K. and Sinha, R. Acute toxicity of malachite green and its effects on certain blood parameters of a catfish, Heteropneustes fossilis. *Aquatic Toxicology,* 31 **(1995)** 241–247.

Srivastava, V.C., Swamy, M.M., Mall, I.D., Prasad, B. and Mishra, I.M. Adsorptive removal of phenol by bagasse fly ash and activated carbon: equilibrium, kinetics and thermodynamics. *Colloids and Surfaces A: Physicochemical and Engineering Aspects,* 272 **(2006)** 89–104.

Srivastava, V.C., Mall, I.D. and Mishra, I.M. Equilibrium modelling of single and binary adsorption of cadmium and nickel onto bagasse fly ash, *Chemical. Engineering Journal*, 117 **(2006)** 79–91.

Subramanyam, B. and Das, A. Study of the Adsorption of Phenol by Two Soils Based on Kinetic and Isotherm Modeling Analyses. *Desalination,* 249 **(2009)** 914–921.

Suksabye, P., Thiravetyan, P., Nakbanpote, W. and Chayabutra, **S.** Chromium removal from electroplating wastewater by coir pith. *Journal of Hazardous Materials,* 141 **(2007)** 637–644.

Sumathi, S. and. Manju, B.S. Uptake of reactive textile dyes by Aspergillus foetidus. *Enzyme and Microbial Technology,* 27 **(2000)** 347–352.

Sureshkumar, M.V. and Namasivayam, C. Adsorption behavior of Direct Red 12B and Rhodamine B from water onto surfactant-modified coconut coir pith. *Colloids and Surface A: Physicochemical Engineering Aspects,* 317 **(2008)** 277–283.

Tan, I.A.W., Hameed, B.H. and Ahmed, A.L. Equilibrium and kinetic studies on basic dye adsorption by oil palm fibre activated carbon. *Chemical Engineering Journal,* 127 **(2007)** 111–119.

Tare, V., Jawed, M. and Iyengar, L. Application of xanthates in heavy metal removal. *Indian Association of Water Pollution Control Technology Annual,* 15 **(1988)** 88–94.

Thomas, H.C. Heterogeneous ion exchange in a flowing system. *Journal of the American Chemical Society,* 66 **(1944)** 1664–1666.

Thomas, D.J., Li, J., Waters, S.B., Xing, W., Adair, B.M., Drobna, Z., Devesa, V. and Styblo, M. Arsenic (+3 oxidation state) methyltransferase and the methylation of arsenicals. *Experimental Biology and Medicine (Maywood),* 232 **(2007)** 3–13.

Thurston, C.F. The structure and function of fungal laccases. *Microbiology,* 140 **(1994)** 19–26.

Tsai, S.Y. and Juang, R.S. Biodegradation of phenol and sodium Salicylate mixtures by suspended *Pseudomonas Putida* CCRC 14365. *Journal of Hazardous Materials,* 138 **(2006)** 125–132.

Tsezos, M. and Bell, J.P. Comparison of the biosorption and desorption of hazardous organic pollutants by live and dead biomass. *Water Research,* 23 **(1989)** 561–568.

Tsuda, S., Murakami, M., Matsusaka, N., Kano, K., Taniguchi, K. and Sasaki, Y.F. DNA damage induced by red food dyes orally administered to pregnant and male mice. *Toxicological Science,* 61 **(2001)** 92-99.

Tsunomori, F. and Ushiki, H. Pore Size Effect on Diffusion Coefficient of Rhodamine B in PNIPA Gel. *Phy. Lett. A*, 258 **(1999)** 171–176.

Tunali, S., Kiran, I. and Akar, T. Chromium(VI) biosorption characteristics of Neurospora crassa fungal biomass. *Minerals Engineering,* 18 **(2005)** 681–689.

Tünay, O., Kabdasli, I., Ohron, D. and Cansever, G. Use and minimalization of water in leather tanning processes. *Water Science and Technology,* 40 **(1999)** 237–244.

Tziotzis, G., Teliou, M., Kaltsouni, V., Lyberatos, G. and Vayenas, D.V. Biological phenol removal using suspended growth and packed bed reactors. *Biochemical Engineering Journal,* 26 **(2005)** 65–71.

Ucun, H., Bayhan, Y.K., Kayab, Y., Cakici, A. and Algurb, O.K. Biosorption of lead (II) from aqueous solution by cone biomass of *Pinus sylvestris*. *Desalination,* 154 **(2003)** 233–238.

Uhnáková, B., Petrˇícˇková, A., Biedermann, D., Homolka, L., Vejvoda, V., Bednárˇ, P., Papoušková, B., Šulc, M. and Martínková, L. Biodegradation of brominated aromatics by cultures and laccase of *Trametes versicolor*. *Chemosphere,* 76 **(2009)** 826–832.

Uysal, M. and Ar, I. Removal of Cr(VI) from industrial wastewaters by adsorption Part I: determination of optimum condition. *Journal of Hazardous Materials,* 149 **(2007)** 482–491.

Vasu, A.E. Removal of Phenol and *O*-Cresol by Adsorption onto Activated Carbon. *E-Journal of Chemistry,* 5 **(2008)** 224–232.

Vázquez, I., Rodríguez-Iglesias, J., Marañón, E., Castrillón L. and Álvarez, M. Removal of residual phenols from coke wastewater by adsorption. *Journal of Hazardous materials,* 147 **(2007)** 395–400.

Venkateswaralu, P., Ratnan, M.V., Rao, D.S. and Rao, M.V. Removal of chromium from an aqueous solution using *Azadirachta indica* (neem) leaf powder as an adsorbent. *International Journal of Physical Sciences,* 2 **(2007)** 188–195.

Villaescusa, I., Fiol, N., MartInez, M., Miralles, N., Poch, J. and Serarols, J. Removal of copper and nickel ions from aqueous solutions by grape stalks wastes. *Water Research,* 38 **(2004)** 992–1002.

Wagner, R.W. and Lindsey, J.S. Boron-dipyrromethane dyes for incorporation in synthetic multi-pigment light-harvesting arrays. *Pure and Applied Chemistry,* 68 **(1996)** 1373–1380.

Wang, D.S., Sun, W., Xu, Y., Tang, H.X. and Gregory, J. Speciation stability of inorganic polymer flocculant-PACI. *Colloidal Surface A: Physicochemical and Engineering Aspects,* 243 **(2004)** 1-10.

Waranusantigul, P., Pokethitiyook, P., Kruatrachue, M. and Upatham, E.S. Kinetics of basic dye (methylene blue) biosorption by giant duckweed (*Spirodela polyrrhiza*). *Environmental Pollution,* 125 **(2003)** 385–392.

Wieland, E., Tits, J., Kunz, D. and Dähn, R. Strontium Uptake by Cementitious Materials. *Environmental Science and Technology,* 42 **(2008)** 403–409.

Willmott, N., Guthrie, J. and Nelson, G. The biotechnology approach to colour removal from textile effluent. *Journal of the Society of Dyers and Colourists,* 114 **(1998)** 38–41.

Wollmann. Water Resources. National Academy of Sciences, National Research Council, Washington DC **(1962)** Publication No. 100-B.

Wrobel, D., Boguta, A. and Ion, R.M. Mixtures of synthetic organic dyes in a photoelectronic cell. *Journal of Photochemistry and Photobiology A: Chemistry,* 138 **(2001)** 7–22.

Xu, Y. and Lebrun, R.E. Treatment of textile dye plant effluent by nano-filtration membrane. *Separation Science Technology,* 34 **(1999)** 2501–2519.

Xu, Y. and R.E. Lebrun, Investigation of the solute separation by charged nanofiltration membrane: effect of pH, ionic strengh and solute type. *Journal of Membrane Science,* 158 **(1999)** 93–104.

Villaescusa, I., Fiola, N., Martinezb, M., Miralles, N., Pochc, J. and Serarolsc, J. Removal of copper and nickel ions from aqueous solutions by grape stalks wastes. *Water Research,* 38 **(2004)** 992–1002.

Viraraghavan, T., Alfaro, F. and de. M. Adsorption of phenol from bv wastewater by peat, fly ash and bentonite. *Journal of Hazardous materials,* 57 **(1998)** 59–70.

Yan, J., Jianping, W., Bai, J., Daoquan, W. and Zongding, H. Phenol biodegradation by the yeast *Candida tropicalis* in the presence of *m*-cresol. *Biochemical Engineering Journal,* 29 **(2006)** 227–23.

Yang, Y.Q., Wyatt, D.T. and Bahorsky, M. Decolorization of dyes using UV/H_2O_2 photochemical oxidation. *Textile Chemist and Colorist,* 30 **(1998)** 27–35.

Yardim, M. F., Budinova, T., Ekinci, E., Petrov, N., Razvigorova, M. and Minkova, V. Removal of mercury (II) from aqueous solution by activated carbon obtained from furfural. *Chemosphere,* 52 **(2003)** 835–841.

Yoon, Y.H. and Nelson J.H. Application of gas adsorption kinetics. I. A theoretical model for respirator cartridge service time. *American Industrial Hygiene Association Journal,* 45 **(1984)** 509–516.

Yu, J., Li, B., Sun, X., Yuan, J. and Chi, R. Polymer modified biomass of baker's yeast for enhancement adsorption of methylene blue, Rhodamine B and basic magenta. *Journal of Hazardous Materials,* 168 **(2009)** 1147–1154.

Zeroual, Y., Moutaouakkil, A., Dzairi, F.Z., Talbi, M., Chung, P.U., Lee, K. and Blaghen, M. Biosorption of mercury from aqueous solution by *Ulva lactuca* biomass. *Bioresource Technology,* 90 **(2003)** 349–351.

Zissi, W., Lyberatus, G. and Pavlou, S. Biodegradation of paminoazobenzene by Bacillus subtilis under aerobic conditions. *Journal* of *Industrial Microbiology and Biotechnology,* 19 **(1997)** 49–55.

Zollinger, H. Azo dyes and pigments. Colour chemistry-synthesis, properties and applications of organic dyes and pigments. New York: VCH, **(1993)** 92–100.

Zollinger, H. Color Chemistry: Syntheses, Properties, and Applications of Organic Dyes and Pigments. New York: Wiley–VCH, **(2003)** 92–100.

APPENDIX 1

ILLUSTRATIONS

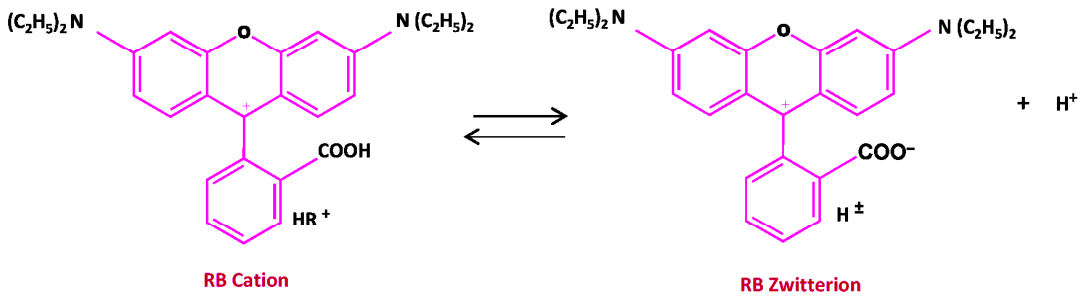

Figure A1.1 Chemical Structure of Rhodamine B (RB) dye

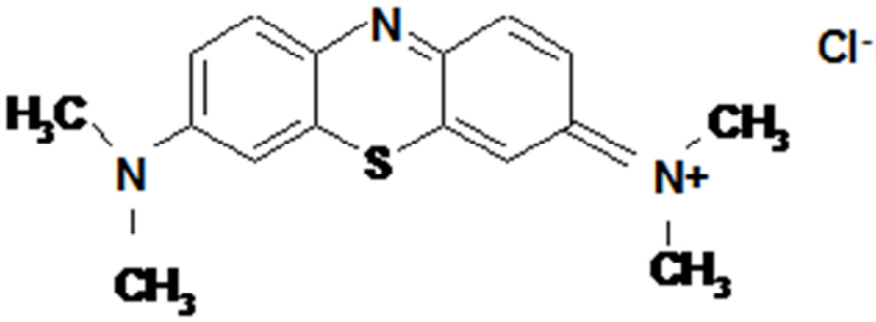

Figure A1.2 Chemical Structure of Methylene Blue (MB) dye

APPENDIX 2

A2.1 ADSORPTION CALCULATIONS

To estimate the percentage removal of (metal or dye or phenol) from aqueous solution the following equation was used:

$$\% \text{ Adsorption} = \frac{C_o - C_f}{C_o} \times 100 \qquad \text{(A2.1)}$$

Metal or dye or phenol uptake (q_e) at equilibrium time was calculated by mass balance expression:

$$W\ (q_e - q_o)\ =\ V\ (C_o - C_e) \qquad \text{(A2.2)}$$

When $q_o = 0$ equation (A2.2) becomes equivalent to

$$q_e = \frac{(C_o - C_e)\ V}{1000\ W} \qquad \text{(A2.3)}$$

where q_e (mg/g) is the amount of (metal or dye or phenol) adsorbed, C_o is the initial (metal or dye or phenol) concentration (mg/l), C_f and C_e are the final residual concentrations of (metal or dye or phenol) (mg/l) after adsorption at time 't' and at equilibrium time, respectively. 'V' is the volume of aqueous solution (ml) and 'W' is the adsorbent weight (g).

A2.2 DESORPTION CALCULATIONS

After desorption, the eluted metal (or) dye (or) phenol per gram of adsorbent (q_{des}) from the concentration of metal (or) dye (or) phenol desorbed (C_{des}) in the solution was calculated by following equation.

$$q_{des} = C_{des}\ \frac{V}{W} \qquad \text{(A2.4)}$$

where 'V' is the volume of the solution of eluent used in Liters and 'W' is weight of the adsorbent in grams. Percentage desorption was acquired by comparing metal (or) dye (or) phenol desorbed (q_{des}) to the metal (or) dye (or) phenol adsorbed (q). Desorption % is calculated using the following equation.

$$\% \ desorption \ = \ \frac{q_{des}}{q} \times 100 \qquad \text{(A2.5)}$$

A2.3 EXPERIMENTAL PROTOCOL

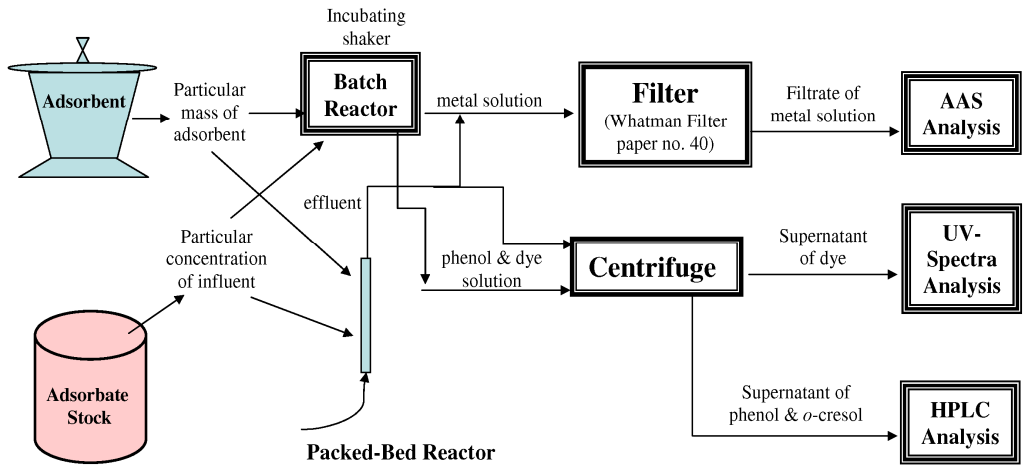

Figure A2.1 Adsorption protocol of batch and packed-bed adsorption study

APPENDIX 3

ISOTHERM MODELS

In this thesis, four isotherm models are used such as Langmuir, Freundlich, Temkin and Halsey to find out the best model fitting with equilibrium experimental data and those are discussed below:

A3.1 Langmuir Isotherm

The Langmuir equation was chosen to estimate the maximum adsorption capacity corresponding to the complete monolayer coverage on homogenous adsorbent surface without any interaction between adsorbed ions.

Langmuir equation is commonly represented as

$$q_e = \left(\frac{Q_o b C_e}{1 + b C_e} \right) \tag{A3.1}$$

$$\frac{C_e}{q_e} = \left(\frac{1}{Q_o b} \right) + \left(\frac{C_e}{Q_o} \right) \text{ (linear form)} \tag{A3.2}$$

where q_e is the amount of adsorbate adsorbed per unit mass of adsorbent (mg/g), C_e is the equilibrium concentration of adsorbate ions (mg/l), Q_o is a measure of adsorption capacity of adsorbent (mg/g), b is the Langmuir constant which is a measure of energy of adsorption (l/mg). The essential Langmuir separation factor or equilibrium constant (R_L) is represented by:

$$R_L = \left(\frac{1}{1 + b C_o} \right) \tag{A3.3}$$

where C_o is the initial concentration of adsorbate (mg/l) and b is the Langmuir constant which indicates the nature of adsorption. The separation factor (R_L) indicates the isotherm shape and whether the adsorption is favourable or not. If $R_L = 0$, adsorption is irreversible; $0 < R_L < 1$, adsorption is favourable; $R_L = 1$ adsorption is linear and $R_L > 1$ adsorption is unfavourable.

A3.2 Freundlich Isotherm

The Freundlich empirical equation was chosen to describe the exponential distribution of active centres, characteristic of heterogeneous surface and infinite surface coverage.

Freundlich equation is commonly represented by:

$$q_e = KC_e^{1/n} \quad \text{(A3.4)}$$

$$\log q_e = \log K + \frac{1}{n}\log C_e \text{ (linear form)} \quad \text{(A3.5)}$$

where K is the measure of adsorption capacity and $1/n$ adsorption intensity. The plot between $log\ q_e$ against $log\ C_e$ is show the isotherm data fitting of Freundlich model. Slope and intercept gives the values of $1/n$ and K. The value of $1/n$ is less than 1 indicates a favourability of adsorption. The Freundlich equation frequently gives an adequate description of adsorption data over a restricted range of concentration, even though it is not based on the theoretical background. Apart from homogenous surface, the Freundlich equation is also suitable for a highly heterogonous surface and an adsorption isotherm lacking a plateau, indicating a multi-layer adsorption.

A3.3 Temkin Isotherm

Temkin isotherm model assumes that the heat of adsorption of all the molecules in the layer would decrease linearly with coverage due to adsorbate/adsorbent interactions (Hameed and El-Khaiary *et al.,* 2008). The linerized form of Temkin isotherm is commonly represented by:

$$q_e = B \ln A + B \ln C_e \quad \text{(A3.6)}$$

where RT/b = B, R is the universal gas constant (8. 314 J/mol K) and T (K) is the absolute temperature. The constant B is related to the heat of adsorption; A is the equilibrium binding constant (l/g) corresponding to the binding energy. A plot of q_e versus $ln\ C_e$ yields a linear line of adsorbate adsorption. The good linear fitting by higher correlation coefficients indicates interaction between the adsorbate and the adsorbent.

A3.4 Halsey Isotherm

The Halsey isotherm model is suitable for multilayer adsorption. The linerized form of Halsey isotherm is commonly represented by:

$$\ln q_e = \left[\frac{1}{n}\ln K_h\right] - \frac{1}{n}\ln C_e \qquad \text{(A3.7)}$$

where k_h and $1/n$ are the Halsey isotherm constant and exponent, respectively. The plot of $ln\ q_e$ versus $ln\ C_e$ gives the equilibrium data fitting and the linear form of Halsey model. The good fitting of the Halsey isotherm equations indicates the heteroporosity (*i.e.*, macropore and micropore) of the adsorbent (Oladoja *et al.*, 2009).

APPENDIX 4

Mono layer adsorption capacities of literature studied adsorbents are tabulated in this appendix.

Table A4.1 Cr^{6+} adsorption capacity of literature reported adsorbents

Adsorbents	Q_o (mg/g)	Initial Cr^{6+} concentration (mg/l)	pH	References
CSC CAC Nitric-oxidized CSC	2.18 4.72 10.88	25	6.0 6.0 4.0	Babel and Kurniawan, 2004
Coconut tree sawdust	3.46	20	3.0	Selvi *et al.*, 2001
Olive cake Sawdust Cactus	33.44 15.82 7.082	100	2.0	Dakiky *et al.*, 2002
Terminalia arjuna nuts activated carbon Sawdust of Sal tree activated carbon Tamirind hull activated carbon	28.4 9.55 85.91	10 - 30	1.0	Mohanty *et al.*, 2005
Sawdust of Sal tree activated carbon	9.55	40	3.5	Baral *et al.*, 2006
Jatropha oil cake Maize corn cob Sugarcane bagasse	0.82 0.28 0.63	5 - 500	2.0	Garg *et al.*, 2007
Tamarind hull activated carbon	85.91	25 - 75	2.0	Verma *et al.*, 2006
GNH – AC SGNH - AC	7.0 11.34	50	3.0	Lata *et al.*, 2008
Neem leaf powder	7.43	25 - 125	7.0	Venkateswaralu *et al.*, 2007
Leersia hexandra Swartz biomass	2.45	5-25	2.0	Gupta and Babu, 2009
Ulva lactuca alga and its activated carbon	10.6 & 112.4	5-50 & 75-250	1.0	Li *et al.*, 2009
Pine needles Eucalyptus bark Coconut husk fibres	5.36 45.0 29.0	100 250 80	2.0 2.0 2.1	Sikaily *et al.*, 2007

Table A4.2 Monolayer adsorption capacity (Q_o) of RB on various literature reported adsorbents

Adsorbents	Q_o (mg/g)	pH	References
Bagasse pith activated carbon	93.1-103.6	3.5	Dubey and Gopal, 2007
H_2SO_4 acid activated sludge	7.181	6.5	Ju *et al.*, 2008
Carbonaceous industrial waste	91.1	5.5	Boeniger, 2004
Sago waste carbon	16.2	5.7	Kadirvelu *et al.*, 2005
Treated parthenium biomass	59.2	7.0	Yu *et al.*, 2009
Surfactant modified coconut coir pith	14.9-16.45	9.2	
Activated carbon	400	-	
Modified parthenium biomass	18.5	7.0	
Zeolite	37.8	-	
Unburned carbon	46.5	-	
Fly ash	4.5	-	
Industrial solid waste	16.1	5.7	
Carbonaceous adsorbent	82.8	-	
Coir pith	2.6	-	
Modified biomass of bakers yeast	267.4	6.5	
Bagasse pith activated carbon	263.6	-	Gad and El-Sayed, 2009
Surfactant modified coir pith	14.9-16.5	6.0	Sureshkumar and Namasivayam, 2008
Industrial wastes	91.1-83.3	-	Bhatnagar and Jain, 2005
DTAB + TiO2	18.2	-	Messina and Schulz, 2006
DDAB +TiO2	21.56		
HTAB	22.03		
DDAB	37.84		

Table A4. 3 MB dye adsorption capacity (Q_o) of literature reported adsorbents

Sorbents	Q_o (mg/g)	Process condition	Activation	Reference
Dehydrated Wheat bran	122–222.2	C_o: 50–500 mg/l, T:25–45ºC, pH: 2.5	H_2SO_4 impregnated	Ozer and Dursun, 2007
Dehydrated peanut hull	108.6–161.3	C_o: 100–500 mg/l, T: 25–45ºC, pH: 3.5	H_2SO_4 impregnated	Ozer *et al.*, 2007
Coir pith carbon	5.87	C_o: 10–40 mg/l, T: 35ºC, pH: 6.9	activated at 700 ºC	Kavitha and Namasivayam, 2007
Bamboo dust AC Groundnut shell AC	143.2 164.90	C_o: 100–400 mg/l, T: 30ºC, pH: 7.4	carbonised at 300 ºC and steam digested at 700 ºC followed by 120ºC for 1h in an air oven.	Tan *et al.*, 2008
Marine seaweed Paper sludge Poplar saw dust Lemon peel	5.23 35.18 4.89 29	C_o: 5–100 mg/l, T: 27, pH: 7	80 ºC drying for 14 h	Hameed *et al.*, 2007
Euphorbia rigida H_2SO_4 AC	109.98	C_o: 100–400 mg/l	sorbent impregnated with 50% H_2SO_4 for 24 + carbonization at 850 ºC for 30 min	Gercel *et al.*, 2007
Almond AC Walnut AC Hazelnut shell AC apricot stones AC	1.33, 3.53, 8.82 4.11	C_o: 300 mg/l	dried at 110ºC for 24 h + $ZnCl_2$ (30 wt.%) dehydrated at 103 ºC for 6–10–18–24 h and activated at 750–800–850 ºC for 2 h in presence of N_2 (40 ml min^{-1} flow rate).	Demirbas *et al.*, 2008
PAC1 PAC2 Commercial F400	380 588 476	C_o: 100–800 mg/l T: 20ºC, pH: 11	activated at 1050ºC with steam concentration of 120 kg steam/kg carbon	El-Qada *et al.*, 2008
(i) H_2SO_4 activated (ii) H_3PO_4 activated *Parthenium hysterophorus*	39.68 88.49	C_o: 50–250 mg/l, T: 26ºC, pH: 7.0	(i) 1:1.5 weight ratio (acid: sorbent) 120 ºC for 24 h and 24 h hot oven drying. (ii) 2:1 (acid volume: sorbent weight) 300 ºC and 24 h hot oven drying.	Lata *et al.*, 2007

Table A4.4 Monolayer adsorption capacities (Q_o) of Pb^{2+}, Ni^{2+} and Sr^{2+} on various adsorbents from literature

Metal	Adsorbents	Q_o (mg/g)	References
Pb^{2+}	Chitosan-tripolyphosphate beads	57.33	Ngah and Fatinathan, 2010
	Penicillium simplicissimum	76.90	Lalhruaitluanga and Jayaram, 2010
	M. baccifera activated charcoal	53.76	
	M. baccifera raw charcoal	10.66	
	Crushed concrete fines	37.0	
	Cephalosporium aphidicola	36.91	
	Mustard husk	30.48	
	Caulerpa lentillifera	28.7	
	Coconut shell activated carbon	21.88	
	Powder activated carbon	20.7	
	Carbonate hydroxyapatite	94.3	
	Wheat bran	87	Liao *et al.*, 2010
	Calcium hydroxyapatite	85	
Ni^{2+}	Blank alginate beads	25.6	Al-Rub *et al.*, 2004
	Free dead algal cells	13.9	
	Immobilized dead algal cells	31.3	
	Amberlite IR-120 synthetic resin	10.673	Demirbas and Pehlivan, 2005
	Grape stalks wastes	10.67	Villaescusa *et al.*, 2004
	Bagasse fly ash	6.45	Srivastava *et al.*, 2006
Sr^{2+}	Imprinted hybrid gel	77.12-84.12	Li *et al.*, 2010
	Aluminum-pillared montmorillonite	30.45-49.46	Papachristodoulou *et al.*, 2002
	Almond green hull	116.30	Ahmadpoura *et al.*, 2010
	TiO_2–SiO_2 mixed gel spheres	54.64	G¨urbo˘ga, *et al.*, 2005
	Granular activated carbon	44.42	Chegrouche *et al.*, 2009

Table A4.5 Monolayer adsorption capacity (Q_o) of phenols on various literature reported adsorbents

Adsorbent	Qo (mg/g)	References
Phenol		
Rattan sawdust based activated carbon	149.25	Hammed and Rahman, 2008
Activated coal	1.481	
Granular activated carbon	165.8	
Sugarcane bagasse fly ash	23.83	
Activated carbon-commercial (ACC)	30.22	
Activated carbon-Laboratory grade	24.64	
Powdered activated carbon (Filtrasorb)	206	Banat and Al-Asheh, 2000
Powdered activated carbon from apricot stone shells	32-120	
Chicken feathers	19.5	
Organo-clay ($HDPY^+$-Smectite)	99	
Polymeric adsorbent	40	
Carbonized polymers	90	
CNTs	15.9	Lin and Juang, 2009
F400-Air	96	
F400-N_2	75.5	
APET	184	
CCM200 (carbon crogel)	140	
Activated sewage sludge	29.46	Ahmaruzzaman, 2008
Residual coal treated with H_3PO_4	142.8	
Residual coal	45.45	
Commercail activated carbon	322	
Cresol		
Coal FA (*o*-cresol)	85.4-96.4	Ahmaruzzaman, 2008
Wood FA (*m*-cresol)	34.5	
Wood FA (*p*-cresol)	52.5	
Granular activated carbon (*o*-cresol)	64.19	Vasu, 2008

APPENDIX 5

A5.1 KINETIC MODELS

According to the first- and second-order dependences of driving force on its rate (dqt/dt) in an adsorption process two kinetic models such as pseudo-first-order equation (also known as Lagergren's equation) and the pseudo-second-order equation are used in this research work to find out the best model fitting with experimental data and those are discussed below:

A5.1.1 Pseudo-First-Order Kinetics

The pseudo first-order model assumes that the rate of adsorption is proportional to the number of free adsorption sites. The following equation expresses the adsorption rate according to the pseudo-first-order equation (Lagergren, 1898):

$$\frac{dq_t}{dt} = k_{ad}(q_e - q_t) \qquad \text{(A5.1)}$$

After integration by applying the conditions $q_t = 0$ at $t = 0$ and $q_t = q_t$ at $t = t$ equation (A5.1) becomes

$$\log(q_e - q_t) = \log q_e - \frac{K_{ad}}{2.303}t \qquad \text{(A5.2)}$$

where q_e is the amount of adsorbate adsorbed at equilibrium per unit weight of adsorbent (mg/g), q_t is the amount of solute adsorbed at '*t*' time (mg/g), t is the agitation time (min) and K_{ad} (l/min) is the adsorption equilibrium rate constant of pseudo-first-order reaction (min^{-1}). The slope and intercept of plot of *log* $(q_e - q_t)$ against't' is used to determine the first-order rate constant K_{ad}.

A5.1.2 Pseudo-First-Order Kinetics

The pseudo second-order kinetic model relies on the assumption that the rate-limiting step may be adsorption, involving valence forces through the sharing or exchanging of electrons between adsorbent and adsorbate. The following represents the second-

order equation for describing an adsorption process (Ho, 1995; Ho and McKay, 1999):

$$\frac{dq_t}{dt} = k'(q_e - q_t)^2 \qquad \text{(A5.3)}$$

where *k'* is the second-order rate constant (g/(mmol min)). After integrating equation (A5.3), we have

$$\frac{t}{q_t} = \left(\frac{1}{k' q_e^2}\right) + \frac{t}{q_e} \qquad \text{(A5.4)}$$

where, *q*e (mg/g) and *qt* (mg/g) are the amount of adsorbate adsorbed at equilibrium and at time *t* (min), respectively, *k*' (g/mg/min) is the pseudo second-order rate constant. The straight line plots of *t*/*qt* versus *t* were used to determine the amount of adsorbate adsorbed and the rate constant, which can be obtained from the slope and intercept of plots, respectively.

A5.2 ADSORPTION THERMODYNAMICS

Thermodynamic parameters such as change in free energy ($\Delta G°$), enthalpy ($\Delta H°$) and entropy ($\Delta S°$) associated to the sorption process were obtained using the following equation:

$$\ln K_d = \frac{\Delta S°}{R} - \frac{\Delta H°}{RT} \qquad \text{(A5.5)}$$

where *R* is the universal gas constant (8.314 J/K mol), *T* is the absolute solution temperature (ºC) and K_d is the distribution coefficient. The values of $\Delta H°$ and $\Delta S°$ are calculated from the slope and intercept of Van't Hoff plot between *ln* K_d versus *1/T*. $\Delta G°$ and K_d were calculated by using the relation below:

$$\Delta G° = -RT \ln K_d \qquad \text{(A5.6)}$$

$$K_d = \frac{C_{Ae}}{C_e} \qquad \text{(A5.7)}$$

where C_{Ae} is amount of the adsorbate adsorbed at equilibrium (mg/l) and C_e is retained concentration of adsorbate in solution at equilibrium (mg/l). The negative values of $\Delta G°$ will indicate the spontaneous nature of the adsorption process. The positive and negative values $\Delta H°$ will reveal whether the adsorption process is endothermic or exothermic. The positive value of $\Delta S°$ will show randomness at the solid-solution interface during adsorption.